AN INVESTIGATION OF THE MATCHED LAYER IN A TURBULENT BOUNDARY LAYER WITH ZERO PRESSURE GRADIENT

A THESIS
SUBMITTED TO
THE FACULTY OF THE GRADUATE SCHOOL OF
THE STATE UNIVERSITY OF NEW YORK AT BUFFALO
IN PARTIAL FULFILLMENT OF THE REQUIREMENTS
FOR THE DEGREE OF
MASTER OF SCIENCE

By
Pierre KNECHT

Department of Mechanical and Aerospace Engineering
State University of New York at Buffalo

September, 1990.

This work is dedicated
to my parents, my brother
and Sandra.

Acknowledgement

I would like to take this opportunity to thank my thesis advisor, Professor William K. GEORGE, for his excellent guidance and patience throughout the course of this research. Without his consistent encouragement, it would have been impossible for me to have completed this work.

I would also like to express my gratitude to Professor Ching Shi LIU for his excellent remarks and suggestions.

Finally, I am highly grateful to Professor Gerard UNTERNAEHRER, of ENSICA, and Professor Roger MAYNE, of UB, who made possible this exchange program between the "Ecole Nationale Superieure d'Ingenieurs de Constructions Aeronautiques", and the Department of Mechanical and Aerospace Engineering of the State University of New York at Buffalo.

Contents

List of Figures (in Appendix)

A.1 GENERAL FIGURES

A.2 VELOCITY PROFILES

A.3 VELOCITY DERIVATIVE REPRESENTATION

Pg. 126: Fig. 3.1.1.1 *Outer variables*:

Smith & Walker. Rth = 5680, 18340, 37190, 44750.

Pg. 127: Fig. 3.1.1.2.03 *Outer variables*:

Smith & Walker. Rth = 5680.

Pg. 128: Fig. 3.1.1.2.06 *Outer variables*:

Smith & Walker. Rth = 18340.

Pg. 129: Fig. 3.1.1.2.10 *Outer variables*:

Smith & Walker. Rth = 37190.

Pg. 130: Fig. 3.1.1.2.13 *Outer variables*:

Smith & Walker. Rth = 44750.

Pg. 131: Fig. 3.1.2.1 *Outer variables*:

Purtell et al.. Rth = 1340, 1840, 3480, 5100.

Pg. 132: Fig. 3.1.2.2.05 *Outer variables*:

Purtell et al.. Rth = 1340.

Pg. 133: Fig. 3.1.2.2.07 *Outer variables*:

Purtell et al.. Rth = 1840.

Pg. 134: Fig. 3.1.2.2.09 *Outer variables*:

Purtell et al.. Rth = 3480.

Pg. 135: Fig. 3.1.2.2.11 *Outer variables*:

Purtell et al.. Rth = 5100.

Pg. 136: Fig. 3.2.1.1 *Inner variables*:

Smith & Walker. Rth = 5680, 18340, 37190, 44750.

Pg. 137: Fig. 3.2.1.2.03 *Inner variables*:

Smith & Walker. Rth = 5680.

Pg. 138: Fig. 3.2.1.2.06 *Inner variables*:

Smith & Walker. Rth = 18340.

Pg. 139: Fig. 3.2.1.2.10 *Inner variables*:

Smith & Walker. Rth = 37190.

Pg. 140: Fig. 3.2.1.2.13 *Inner variables*:

Smith & Walker. Rth = 44750.

Pg. 141: Fig. 3.2.2.1 *Inner variables*:

Purtell et al.. Rth = 1840, 3480, 5100.

Pg. 142: Fig. 3.2.2.2.05 *Inner variables*:

Purtell et al.. Rth = 1340.

Pg. 143: Fig. 3.2.2.2.07 *Inner variables*:

Purtell et al.. Rth = 1840.

Pg. 144: Fig. 3.2.2.2.09 *Inner variables*:

Purtell et al.. Rth = 3480.

Pg. 145: Fig. 3.2.2.2.11 *Inner variables*:

Purtell et al.. Rth = 5100.

A.4 BOUNDARY LAYER PARAMETERS, X-DEPENDENCE AND FRICTION COEFFICIENT

Verification of COLES' results

Verification of the power law results, with the full expressions derived for the boundary layer parameters, x-dependence and friction coefficient:

Pg. 169: Fig. 4.3.1.1.1 *Displacement thickness*:

Smith and Walker. x = 15.75 in, 27.75 in, 39.75 in, 51.75 in.

Pg. 170: Fig. 4.3.2.1.1 *Momentum thickness*:

Smith and Walker. x = 15.75 in, 27.75 in, 39.75 in, 51.75 in.

Pg. 171: Fig. 4.3.3.1.1 *Shape factor*:

Smith and Walker. x = 15.75 in, 27.75 in, 39.75 in, 51.75 in.

Pg. 172: Fig. 4.3.4.1.1 *Friction coefficient in local variable*:

Smith and Walker. x = 15.75 in, 27.75 in, 39.75 in, 51.75 in.

Pg. 173: Fig. 4.3.5.1.1 *X dependence*:

Smith and Walker.

Pg. 174: Fig. 4.3.6.1.1 *Friction coefficient as a function of x*:

Smith and Walker (53 points).

Verification of the power law, with only the linear term

Abstract

Since the work of MILLIKAN (1938), it is well known that scaling the velocity in the outer region in a "Velocity Defect" form and the velocity in the inner region in the "Law of the Wall" form yields a logarithmic profile for the matched region.

The derivation is strongly based on the so-called "MILLIKAN's argument", which enables to derive the velocity profile in the matched layer by matching the velocity derivatives. This argument has been presented in a mathematical form by GILL (1968). However, none of the assumptions of the so-called GILL's theorem have been verified so far. Secondly, MILLIKAN's theory is strongly based on the "Velocity Defect" or "Reynolds' number Similarity" form of the velocity in the outer region. In this work, the consequences and the consistency of a "Strict Similarity" assumption for the outer region are examined.

A new concept is introduced, *the Asymptotic Invariance Principle*, so that MILLIKAN's argument is not needed. By this mean, it is showed that a Strict Similarity assumption yields a power law for the matched region, whereas a logarithmic form for the velocity in the matched region is deduced from a Velocity Defect form for the outer flow.

Also, by two different derivations, (i) by cutting the boundary layer into three regions, inner, matched and outer regions, and (ii) by using a composite form for the velocity, the same expressions are derived for the displacement and momentum thickness. The momentum integral yields expressions for the x dependence and friction coefficient.

Experimental data of SCHULTZ & GRUNOW (1941), WIEGHARDT & TILLMANN (1944), KLEBANOFF & DIEHL (1951), SMITH & WALKER (1958) and PURTELL et al. (1981) are examined. It is seen that in a boundary layer there are both a logarithmic region and a power law region. The remaining question is which one dominates the flow at high Reynolds' numbers. It is shown for the experimental data available that the velocity, the velocity derivative and the friction coefficient representations do not exclude the power law or the log law. In fact, at low Reynolds' numbers, PURTELL's data seems to show stronger support for a power law behavior in the matched layer. At higher Reynolds' numbers, the experimental errors, due to the total pressure probe technique used in SMITH & WALKER, prevent us from drawing any definite conclusions.

Although major errors in the velocity measurements exist, the effect on the integrated parameters should be reduced. The displacement and momentum thicknesses of this set of data seems however to indicate that the expressions derived for the boundary layer parameters are not accurate past their first order. Incidentally, the same experimental data is also shown not to collapse with the results obtained by COLES (1956) for the boundary layer thicknesses. It has been concluded that the experimental data available do not corroborate with either one of the theories to a satisfactory degree.

It is thought that a finer structure exist in the turbulent boundary layer so that the use of a composite form for the velocity, and, more generally, the concept of inner and outer regions, as they are commonly accepted, may be questioned.

This work also points out the crude need to update the experimental data using a hot wire technique in the same range of moderate and high Reynolds' numbers as SMITH & WALKER's set of experiments.

INTRODUCTION

Dimensional analysis constitutes one of the major tool in fluids mechanics and turbulence research. Often however, deductive schemes, such as the Π theorem, do not yield a single solution. Researchers have then to rely on intuition and design experiments that will eliminate one or the other solution.

MILLIKAN (1938) considered that the boundary layer is made up of two regions that have different physics: the inner region, which can be described by the Law of the Wall, and the outer region that can be described by the Velocity Defect expression. Both regions are overlapping, constituting a "matched region". MILLIKAN derived that the velocity in the matched region profile is to be described by a logarithmic law.

GEORGE (1989) showed that using the Π Theorem yields two different scaling possibilities for the velocity in the outer region of a boundary layer, i.e. a Velocity Defect form and a Strict Similarity form. Since the work of Van KARMAN, the latter has been disregarded unanimously. In this work, we will attempt to investigate the consequences and the consistency of a Strict Similarity scaling form for the velocity in the outer region.

Chapter 1 MATCHED LAYER: THE CLASSICAL VIEW

1.1 MILLIKAN'S PIPES AND CHANNELS DERIVATION (1938)

Before we see the derivation of the so-called log-law as it is commonly derived presently, and as it has first been derived by MILLIKAN (1938), let us first see contemporary accepted theories. Note that among them, the PRANDTL and Van KARMAN results gave the same expression for the velocity profile as MILLIKAN's derivation. Interestingly enough, MILLIKAN presented these previous theories as "alternative special cases of [his] formulae".

1.1.1 Strict Similarity — Reynolds' Number Similarity

MILLIKAN adopted the Velocity Defect in a form that has been presented by Van KARMAN (1930), the so-called "Reynolds' number Similarity", sometimes called the "Velocity Defect Law". It had been shown in previous work that a strict non-dimensional expression of the velocity in the following form is dependent on the Reynolds' number:

$$\frac{U}{U_{cl}} = F_2(\overline{y}) \tag{1.1.1}$$

where the velocity scale, U_{cl}, is the center-line velocity and $\overline{y}$ the non-dimensional distance from the wall is given by:

$$\overline{y} = \frac{y}{h} \tag{1.1.2}$$

h being the half width of the pipe or channel. It is possible to obtain empirically a reasonable representation of F_2 over the entire channel or pipe by a power law:

$$F_2(\overline{y}) \sim (\overline{y})^{\frac{1}{n}} \tag{1.1.3}$$

But n is found to vary with the Reynolds' number from one-third to one tenth, see SCHLICHTING (1968) for further information.

Because of this Reynolds' number dependence, Van KARMAN (1930) looked for a velocity profile expression independent of the Reynolds' number. He showed on experimental grounds that:

$$\frac{U - U_{cl}}{u_\tau} = F(\overline{y}) \tag{1.1.4}$$

is the proper similarity form, where u_τ is the friction velocity defined by:

$$u_\tau = \sqrt{\nu \left(\frac{\partial u}{\partial y}\right)_{y=0}} \tag{1.1.5}$$

This expression is not only found to be independent of the Reynolds' number of the flow but is also independent of the wall roughness (see for instance HAMA, 1954). Although Van KARMAN is generally credited with proposing equation 1.1.4, it was first suggested by STANTON (1914).

It is interesting to note that for:

$$\overline{y} = 1: \quad F(\overline{y}) = 0 \tag{1.1.6}$$

and for:

$$\overline{y} = 0: \quad F(\overline{y}) = \frac{U_{cl}}{u_\tau} \tag{1.1.7}$$

Thus, the origin point for $F(\overline{y})$ depends on the Reynolds' number if the friction velocity is not proportional to the center line velocity, which it is not. However, this dependence can not be seen in a velocity profile in cartesian coordinates. Later, for boundary layer flow, semi-logarithmic plots of the velocity profile will give birth to the wake function similarity (CLAUSER, 1956; COLES, 1956).

1.1.2 The Law of the Wall

Using dimensional analysis, PRANDTL derived that close to the wall the velocity has the following form:

$$\frac{U}{u_\tau} = f\left(\frac{y u_\tau}{\nu}\right) \tag{1.1.8}$$

Indeed, the proper scale for the viscous region is the friction velocity, u_τ, a length scale, η, can be formed from the viscosity and the velocity scale with:

$$\frac{\eta u_\tau}{\nu} = 1 \tag{1.1.9}$$

1.1.3 Van KARMAN and PRANDTL theories.

Both theories have in common that:

(i) they are based on closures model for the Reynolds Stress involving a *mixing length* concept,
(ii) they are to be valid for the whole width of the channel or the pipe,
(iii) they lead to a logarithmic law for the velocity profile.

Van KARMAN (1930 a, b) derived that the velocity profile is given by:

$$\frac{U_{cl}-U}{u_\tau}=\frac{1}{\chi}\left(\ln\left(1-\sqrt{1-\overline{y}}\right)+\sqrt{1-\overline{y}}\right) \tag{1.1.10}$$

assuming that the Reynolds' stress is given by:

$$\tau_t=-\frac{\overline{uv}}{\rho}=l^2\left|\frac{dU}{dy}\right|\frac{dU}{dy} \tag{1.1.11}$$

where the mixing length, l, is given by:

$$l=\chi\left|\frac{\frac{dU}{dy}}{\frac{d^2U}{dy^2}}\right| \tag{1.1.12}$$

and where χ is to be known as Van KARMAN's constant.

Later, PRANDTL (1932) assuming that the mixing length is proportional to the wall distance, y:

$$l=\chi y \tag{1.1.13}$$

obtained by integration of the Reynolds' stress:

$$\frac{U}{u_\tau}=\frac{1}{\chi}\ln y+B \tag{1.1.14}$$

so that:

$$\frac{U_{cl}}{u_\tau}=\frac{1}{\chi}\ln h+B \tag{1.1.15}$$

or, if we write it in a velocity defect form:

$$\frac{U_{cl}-U}{u_\tau}=-\frac{1}{\chi}\ln\overline{y} \tag{1.1.16}$$

1.1.4 MILLIKAN's Theory

MILLIKAN's theory is based on the following original assumptions. Close to the wall the flow can be described by the "Law of the Wall". In this region, viscosity and roughness are the basic parameters that govern the flow. However, far away from the wall, the flow is to be described by the "Velocity Defect Law", so that there exist a region, a *matched layer*, where both laws are valid. As a result, MILLIKAN matches the velocity derivatives[1] of both regions to obtain a law valid in that matched layer.

From 1.1.8:

$$\frac{1}{u_\tau}\frac{dU}{dy} = \frac{1}{\eta}\frac{df}{dy_+}(y_+) \tag{1.1.17}$$

where:

$$y_+ = \frac{y}{\eta} = \frac{u_\tau y}{\nu} \tag{1.1.18}$$

From 1.1.4:

$$\frac{1}{u_\tau}\frac{dU}{dy} = \frac{1}{h}\frac{dF}{d\overline{y}}(\overline{y}) \tag{1.1.19}$$

Multiplying 1.1.17, 1.1.19 by y yields:

$$y_+\frac{df}{dy_+}(y_+) = \overline{y}\,\frac{dF}{d\overline{y}}(\overline{y}) \tag{1.1.20}$$

Now, if we assume that both sides are independent[2] and hence equal to a constant:

$$y_+\frac{df}{dy_+}(y_+) = \overline{y}\,\frac{dF}{d\overline{y}}(\overline{y}) = \frac{1}{\chi} \tag{1.1.21}$$

we find by integration:

$$\frac{U}{u_\tau} = \frac{1}{\chi}\ln(y_+) + d \tag{1.1.22}$$

or introducing U_{cl}:

$$\frac{U - U_{cl}}{u_\tau} = \frac{1}{\chi}\ln(\overline{y}) + D \tag{1.1.23}$$

---

1 It is interesting to note that only the derivatives of the velocity are to be matched and not the velocity itself.

2 Most authors, TENNEKES and LUMLEY, PANTON,... state that both sides of 1.1.20 are independent since both non-dimensionized length, $y_+, \overline{y}$, are "independent" at infinite Reynolds' numbers. Note however that $y_+, \overline{y}$ are obviously related to each other by $\mathcal{R}_*$. We will present in a further section a rigorous derivation of MILLIKAN's argument, see GILL (1968).

From 1.1.22 and 1.1.23, we have:

$$\frac{U_{cl}}{u_\tau} = \frac{1}{\chi}\ln(\Re_*) + d - D \tag{1.1.24}$$

where $\Re_*$ is defined as the ratio of outer to inner length scales:

$$\Re_* = \frac{h}{\eta} \tag{1.1.25}$$

We can rewrite this equation as:

$$\sqrt{\frac{2}{c_f}} = \frac{1}{\chi}\ln\Re_* + d - D \tag{1.1.26}$$

or using different notations:

$$\frac{1}{\varepsilon} = \frac{1}{\chi}\ln\varepsilon\Re_\delta \quad + d - D \tag{1.1.27}$$

where $\Re_\delta$ is the Reynolds' number given by:

$$\Re_\delta = \frac{U_\infty \delta}{\nu} \tag{1.1.28}$$

and ε is defined as the inner to outer velocity ratio:

$$\varepsilon = \sqrt{\frac{c_f}{2}} = \frac{u_\tau}{U_\infty} \tag{1.1.29}$$

Experimentalists sometimes consider that this problem has 4 unknowns (χ, d, D, u_*), and work only on the velocity profile. However, equation 1.1.24 reduces the number of equation to 3. In fact, the friction velocity, u_τ , may be determined independently from experimental measurements. Therefore, the present author will make a distinction between the friction velocity, u_*, determined from logarithmic results, and the actual friction velocity, u_τ, given from the shear stress at the wall, since the latter is not dependent on the validity of any theory but is only dependent on the experimental measurements.

1.2 RESULTS FROM THE AVERAGED NAVIER-STOKES EQUATIONS FOR PIPES

Because one can find simple expressions for the governing equations of the fluid motion in pipes, it is worth to investigate that type of flow and gain some insight that may be useful for the boundary layers case. As we will see, this case enables valuable simplifications to the equations of motion, simplifications that have been used in singular perturbation methods. Nevertheless, one should never forget that pipe flows are different in their features and physics from boundary layers flow.

Since we can assume a parallel mean flow for pipe and channel, the equations of motion are, see TENNEKES and LUMLEY (1972):

$$0 = \frac{1}{\rho}\frac{\partial P}{\partial x} - \frac{d\,\overline{uv}}{dy} - \nu\frac{d^2U}{dy^2} \tag{1.2.30}$$

$$0 = -\frac{1}{\rho}\frac{\partial P}{\partial y} - \frac{d\,\overline{v^2}}{dy} \tag{1.2.31}$$

The y-momentum equation can be integrated:

$$\frac{P(x,y)}{\rho} + \overline{v^2}(x,y) = \frac{P_0(x)}{\rho} \tag{1.2.32}$$

but, since we assume that all velocity derivatives are independent with respect to the streamwise coordinate, we have:

$$\frac{\partial P}{\partial x} = \frac{dP_0}{dx} = const \tag{1.2.33}$$

The x-momentum equation can therefore be integrated with respect to y:

$$0 = -\frac{y}{\varrho}\frac{dP_o}{dx} - \overline{uv} + \nu\frac{dU}{dy} - u_\tau^2 \tag{1.2.34}$$

where u_τ is the friction velocity. In addition, the total shear stress $(\rho\,\overline{uv} + \mu\frac{dU}{dy})$ must be zero in the middle of the channel or pipe, because of symmetry reasons, therefore:

$$u_\tau^2 = -\frac{h}{\rho}\frac{dP_o}{dx} \tag{1.2.35}$$

The same result follows also from a force balance on the pipe. The momentum equation may therefore be written:

$$\frac{1}{u_\tau^2}\left(-\overline{uv}+\nu\frac{dU}{dy}\right)=\left(1-\frac{y}{h}\right) \tag{1.2.36}$$

Now, let us write these equations in both regions of interest, i.e., the near-wall region and the outer region. At the wall, $y=0$, the Reynolds' stress is zero:

$$\frac{1}{u_\tau^2}\left(\nu\frac{dU}{dy}\right)=1 \tag{1.2.37}$$

At the center-line, $y=h$, the viscous stress is zero:

$$\frac{1}{u_\tau^2}\left(-\overline{uv}\right)=\left(1-\frac{y}{h}\right) \tag{1.2.38}$$

A dimensional analysis is done to have both Reynolds' stress and mean velocities in the previous equations. The parameters of the flow are: $U_{cl}, h, \nu, \frac{dP_o}{dx}$ or U_{cl}, h, ν, u_τ. *Close to the wall*, we expect viscosity, as well as the friction velocity to be important, therefore, the parameters that govern the flow near the wall are: ν, u_τ. So we write equation 1.2.36 as:

$$\left(-\left(\frac{\overline{uv}}{u_\tau^2}\right)+\frac{d\left(\frac{U}{u_\tau}\right)}{dy_+}\right)=\left(1-\frac{1}{\Re_*}y_+\right) \tag{1.2.39}$$

Far away from the wall we can neglect the viscous stress, therefore the important parameters seem to be: $U_{cl}, h, \frac{1}{\rho}\frac{dP_0}{dx}$. Note that u_τ enter the problem indirectly[3] through the pressure gradient. Commonly, see for instance TENNEKES and LUMLEY, u_τ is taken as the proper scale for the velocity, and u_τ^2 is taken as the proper scale for the Reynolds' stress, so that equation 1.2.36 becomes:

$$\left(-\left(\frac{\overline{uv}}{u_\tau^2}\right)+\frac{1}{\Re_*}\frac{d\left(\frac{U}{u_\tau}\right)}{d\xi}\right)=(1-\overline{y}) \tag{1.2.40}$$

[3] From this point of view, the boundary layer has a different dimensional analysis for the outer flow.

1.3 GILL's THEOREM

MILLIKAN's theory was the starting point of a new mathematical concept, the asymptotic expansions matching processes, which we shall refer to in further chapters. However, "MILLIKAN's argument", i.e., the matching of the velocity derivatives, is from a mathematical point of view fragile. GILL (1968) reformulated the problem and MILLIKAN's argument in a rigorous way. It is interesting to point out that his three assumptions, although used to derive[4] second order asymptotic expansions, were, to our knowledge, never studied experimentally[5].

The problem is to describe the mean flow at high Reynolds' numbers, i.e., to describe the asymptotic behavior of U as $\Re_* \to \infty$. Let us introduce the non-dimensional velocity:

$$w = w(\Re_*, \overline{y}) = \frac{U}{u_\tau} \tag{1.3.41}$$

and the velocity at the center-line:

$$W(\Re_*) = \frac{U_{cl}}{u_\tau} = w(\Re_*, 1) \tag{1.3.42}$$

Equating the velocity derivatives in both forms, yields (1.1.20). GILL (1968) showed that when the left and right-hand side of (1.1.20) is asymptotically of a certain higher order, the classical laws are obtained.

Theorem:

Given that:

(i) $\exists\lambda$, a positive constant, and a differentiable function, $f(y_+)$, satisfying:

$$f(0) = 0 \tag{1.3.43}$$

and for $0 \leq y_+ \leq \Re_*^\lambda$:

$$\frac{dw}{dy_+} = f'(y_-) + o\left(\Re_*^{-\lambda}\right) \quad as \ \Re_* \to \infty \tag{1.3.44}$$

(ii) $\exists\sigma$, a positive constant, and a differentiable function, $F(\overline{y})$, satisfying:

$$F(1) = 0 \tag{1.3.45}$$

---

[4] See FENDEL (1972) and AFZAL (1976).

[5] Perhaps, because the Turbulence Community may not have yet accepted GILL's theorem.

and for $\Re_*^{-\sigma} \leq \overline{y} \leq 1$:

$$\frac{dw}{d\overline{y}} = F'(\overline{y}) + O(1) \quad as \ \Re_* \to \infty \tag{1.3.46}$$

(iii) the constants, λ, σ, can be chosen so that:

$$1 - \sigma = \lambda \tag{1.3.47}$$

Then, there exist finite constants A, B, C, such that as $\Re_* \to \infty$:

$$W = C \ln(\Re_*) + A + o(1) \tag{1.3.48}$$

$$w = C \ln(y_+) + B + o(1) \tag{1.3.49}$$

for any $y_+(\Re_*)$ such that as $\Re_* \to \infty$:

$$y_+ \to \infty \ \ and \ \ \overline{y} = \left(\Re_*^{-1} y_+\right) \to 0 \tag{1.3.50}$$

1.4 MILLIKAN'S ARGUMENT EXTENDED TO TURBULENT BOUNDARY LAYERS

In the fifties, MILLIKAN's argument was extended to turbulent boundary layers. CLAUSER (1954, 1956) and COLES (1956), conducting slightly different approaches ended with similar expressions for the boundary layer parameters ratios. It seems to us that COLES' results, at least as far as the experimental data computations is concerned, is more precise than CLAUSER's. It is mentioned that CLAUSER's work is strongly based on the Velocity Defect form of the velocity valid for the whole width of the boundary layer, whereas the wake function analysis by COLES is based on empirical grounds.

1.4.1 CLAUSER's Analysis (1954, 1956)

CLAUSER (1956) extended the log law to turbulent boundary layers. Although he does not follow MILLIKAN's argument, he obtains[6] the same expressions as MILLIKAN being valid for turbulent boundary layers.

[6] By a mathematical more overlooked argument.

He assumed that the inner form is given by the universal Law of the Wall:

$$\frac{U}{u_\tau} = f\left(\frac{y u_\tau}{\nu}\right) = f\left(\Re_* \frac{y}{\delta}\right) \tag{1.4.51}$$

and that the law governing the motion in the outer region is given by the Reynolds' number Similarity Law:

$$\frac{U - U_\infty}{u_\tau} = F\left(\frac{y}{\delta}\right) \tag{1.4.52}$$

So that CLAUSER gets the traditional logarithmic velocity profile:

$$\frac{U}{u_\tau} = \frac{1}{\chi} \ln\left(\Re_* \frac{y}{\delta}\right) + d \tag{1.4.53}$$

$$\frac{U - U_\infty}{u_\tau} = \frac{1}{\chi} \ln\left(\Re_* \frac{y}{\delta}\right) + D \tag{1.4.54}$$

And, again, the skin friction is given by the difference of the two previous equations:

$$\sqrt{\frac{2}{c_f}} = \frac{U_\infty}{u_\tau} = \frac{1}{\chi} \ln\left(\Re_\delta \sqrt{\frac{2}{c_f}}\right) + d - D \tag{1.4.55}$$

$$\frac{1}{\varepsilon} = \frac{1}{\chi} \ln(\Re_*) + d - D \tag{1.4.56}$$

CLAUSER finds, from the a survey of the data available, that the constants are:

$$\chi = \frac{ln(10)}{5.6} = .41 \tag{1.4.57}$$

$$d = 4.9 \tag{1.4.58}$$

$$D = -2.5 \tag{1.4.59}$$

What is original is that CLAUSER (1954) showed experimentally that the deviation from the logarithmic law, in both the inner and the outer region, obeys

a similarity law in their own respectively non-dimensionalized variables, even in positive pressure gradient:

$$\frac{U}{u_*} = \left[\frac{1}{\chi}\ln\left(\Re_*\frac{y}{\delta}\right) + c\right] + h\left(\Pi, \frac{y}{\delta}\right) \tag{1.4.60}$$

where Π is a profile parameter that account for the Reynolds' number and/or pressure gradient effects. It is commonly referred to as the form parameter, h being the wake function. CLAUSER made a representation of the deviation from the logarithmic line both in the outer and in the inner[7] region available. However, he did not explore all the consequences of that result.

Secondly, CLAUSER derived expressions for the boundary layer parameters. The crucial aspect of CLAUSER's theory is that it is entirely a strict application of the Reynolds' number Similarity Law. He therefore does not take into account his results for the wake function, dependent on the Reynolds' number and pressure gradient, and avoids the Law of the Wall physics[8]. Nevertheless, this assumption yields consistent results, since the inner region plays a less important influence than the outer region on the coefficient determination.

Since the ratio of the various thicknesses depend upon the skin friction coefficient, CLAUSER (1956) formed a thickness parameter, Δ defined by:

$$\Delta = \delta\int_0^\infty \frac{U_\infty - U}{u_*} d\left(\frac{y}{\delta}\right) \tag{1.4.61}$$

Introducing, the displacement thickness,

$$\delta^* = \int_0^\infty \left(1 - \frac{U}{U_\infty}\right) dy \tag{1.4.62}$$

and the momentum thickness,

$$\theta = \int_0^\infty \frac{U}{U_\infty}\left(1 - \frac{U}{U_\infty}\right) dy \tag{1.4.63}$$

---

7 It seems that, in CLAUSER's paper (1956), the inner deviation from the logarithmic line has a wrong behavior for $y_+ < 5$, since it is supposed to reach $d = -4.9$ as $y_+ \to 0$.

8 He uses however the Law of the Wall to derive the logarithmic velocity profile.

he showed that:

$$\frac{\delta^*}{\Delta} = \sqrt{\frac{c_f}{2}} = \varepsilon \tag{1.4.64}$$

$$\frac{\theta}{\Delta} = \varepsilon(1 - G\varepsilon) \tag{1.4.65}$$

where

$$G = \int_0^\infty \left(\frac{U_\infty - U}{u_*}\right)^2 d\left(\frac{y}{\Delta}\right) \tag{1.4.66}$$

The inverse of the shape factor is then given by:

$$\frac{1}{H} = \frac{\theta}{\delta^*} = 1 - G\varepsilon \tag{1.4.67}$$

A strict application of the Reynolds' number Similarity Law allows us to calculate the two constants from the experimental data[9]:

$$\frac{\Delta}{\delta} = \int_0^\infty \frac{U_\infty - U}{u_*} d\left(\frac{y}{\delta}\right) = 3.6 \tag{1.4.68}$$

$$G = \int_0^\infty \left(\frac{U_\infty - U}{u_*}\right)^2 d\left(\frac{y}{\Delta}\right) = 6.8 \tag{1.4.69}$$

Finally, we will mention CLAUSER's derivation for the shear distribution. Again, assuming that the whole profile is in a Reynolds' number Similarity form:

$$\frac{U - U_\infty}{u_*} = -f'(\overline{y}) \tag{1.4.70}$$

and that the Reynolds' stress is also in a similarity form:

$$\frac{\tau_t}{\tau_w} = g(\overline{y}) \tag{1.4.71}$$

[9] CLAUSER does not mention how the value of G was obtained, by using the velocity profiles or the boundary layer parameters profiles, or both.

where τ_w is the wall shear stress and $\overline{y}$ is given by:

$$\overline{y} = \frac{y}{\delta} \tag{1.4.72}$$

CLAUSER (1956) obtained from the continuity equation:

$$\frac{V}{u_\tau} = \frac{d\delta}{dx}\left(f - \overline{y}\frac{df}{d\overline{y}}\right), \quad f(0) = 0 \tag{1.4.73}$$

And substituting in the boundary layer equation:

$$U\frac{\partial U}{\partial x} + V\frac{\partial U}{\partial y} = \frac{1}{\rho}\frac{\partial \tau}{\partial y} \tag{1.4.74}$$

he gets the following equation:

$$\frac{d\delta}{dx}(x)\left[\frac{1}{\varepsilon(x)}\,\overline{y}\,f''(\overline{y}) - ff''(\overline{y})\right] = h'(\overline{y}) \tag{1.4.75}$$

which by integration yields the shear distribution:

$$h(\overline{y}) = \frac{d\delta}{dx}\left(\left[-ff' + \int_{\infty}^{\overline{y}} f'^2(\zeta)\,d\zeta\right](\overline{y}) + \frac{1}{\varepsilon(x)}\left[\overline{y}\,f' - f + f(\infty)\right](\overline{y})\right) \tag{1.4.76}$$

The Velocity Defect assumption allows the two expressions in brackets to be "universal functions", the shear distribution is proportional to the boundary layer thickness and is a linear expression of the ratio of the free stream velocity to the friction velocity:

$$\frac{1}{\varepsilon} = \frac{U_\infty}{u_\tau} \tag{1.4.77}$$

1.4.2 COLES' Analysis (1956)

Pursuing CLAUSER's work on the similarity form of the wake function, COLES (1956) showed empirically that 1.4.60 can be more specifically expressed as:

$$\frac{U}{u_*} = \left[\frac{1}{\chi}\ln\left(\Re_*\frac{y}{\ell}\right) + d\right] + \frac{\Pi}{\chi}\,w\left(\frac{y}{\delta}\right) \tag{1.4.78}$$

COLES normalized the wake component in 1.4.78, by:

$$w(0) = 0 \tag{1.4.79}$$

$$\int_0^2 \left(\frac{y}{\xi}\right) dw = \int_0^1 w d\left(\frac{y}{\delta}\right) = 1 \tag{1.4.80}$$

giving:

$$w(1) = 2 \tag{1.4.81}$$

The parameter Π which is a distance characteristic of the deviation from the logarithmic line is found to be related to the skin coefficient by:

$$\varepsilon = \frac{1}{\chi} \ln(\Re_*) + d + \frac{2\Pi}{\chi} \tag{1.4.82}$$

COLES (1962, p. 56) tabulated the form parameter, Π, for different values of $\Re_\theta$. It interesting to note that for $\Re_\theta > 5500$, Π stays constant at a value of:

$$\Pi = 0.55 \tag{1.4.83}$$

For lower Reynolds' numbers. the form parameter, Π, varies. Based on the experiments of WIEGHARDT (1944), COLES gives a zero value for Π for a Reynolds' number of $\Re_\theta = 425$. Using 1.4.78, He finds that the form parameter, Π, is related to the displacement thickness and the momentum thickness by the following relations:

$$\frac{\delta^*}{\delta} = \frac{(1+\Pi)}{\chi} \varepsilon \tag{1.4.84}$$

$$\frac{\delta^* - \theta}{\delta} = 2\frac{\left(1 + \alpha\Pi + \beta\Pi^2\right)}{\chi^2} \varepsilon^2 \tag{1.4.85}$$

where α, β are constants of order unity given by:

$$\alpha = 2 + \int_0^1 w\left(\frac{y}{\delta}\right) \ln\left(\frac{y}{\delta}\right) d\frac{y}{\delta} \approx 1.600 \tag{1.4.86}$$

$$\beta = \frac{1}{2}\int_0^1 w^2\left(\frac{y}{\delta}\right) d\frac{y}{\delta} \approx .761 \tag{1.4.87}$$

To conclude, let us rewrite the different thickness ratio, using compact notations:

$$\frac{\delta^*}{\delta} = \frac{\Pi_1}{\chi}\epsilon \tag{1.4.88}$$

$$\frac{\theta}{\delta} = \frac{\Pi_1}{\chi}\epsilon - \frac{2\Pi_2}{\chi^2}\epsilon^2 \tag{1.4.89}$$

$$\frac{1}{H} = 1 - \frac{2\Pi_2}{\Pi_1\chi}\epsilon \tag{1.4.90}$$

where the constants are given by:

$$\frac{\Pi_1}{\chi} = \frac{(1+\Pi)}{\chi} \tag{1.4.91}$$

$$2\frac{\Pi_2}{\chi\Pi_1} = \frac{(1+\alpha\Pi+\beta\Pi^2)}{\chi(1+\Pi)} \tag{1.4.92}$$

which, for $\Re_\theta > 5500$ are equal to:

$$\frac{\Pi_1}{\chi} = 3.78 \tag{1.4.93}$$

$$2\frac{\Pi_2}{\chi\Pi_1} = 6.641 \tag{1.4.94}$$

As mentioned in the introduction of this section, the boundary parameters ratio have the same expressions, the different constants found by COLES (1956) are also close to CLAUSER's constants.

We note that in latter work, COLES (1968a) chose an analytical form for the wake function in the form:

$$w\left(\frac{y}{\delta}\right) = 2\sin^2\left(\frac{\pi}{2}\frac{y}{\delta}\right) \tag{1.4.95}$$

and obtains the following results:

$$\frac{\delta^*}{\delta} = \frac{(1+\Pi)}{\chi}\epsilon \tag{1.4.96}$$

$$\frac{\delta^* - \theta}{\delta} = 2\left(1 + \left(1 + \frac{1}{\pi}\mathrm{Si}(\Pi)\right)\Pi + \frac{3}{2}\Pi^2\right)\frac{\epsilon^2}{\chi^2} \qquad (1.4.97)$$

where

$$\mathrm{Si}(x) = \int_0^x \frac{\sin u}{u}\,du = -x\int_0^1 \ln y \cos(xy)\,dy \qquad (1.4.98)$$

COLES (1968a) note that the velocity expressed as in 1.4.78, where the wake function is given by 1.4.95, has an abrupt change at the outer edge of the layer. Indeed, the theoretical slope $\frac{\delta}{u_\tau}\frac{du}{dy}$ changes from $1/\chi$ to 0, which " constitutes an obvious deficiency".

1.5 CONCLUSION

To conclude this chapter, let us see the four basic ideas on which MILLIKAN's theory rests:

(i) **Law of the Wall** for the inner flow,

(ii) **Reynolds' number Similarity** for the outer flow,

(iii) **Existence of a Matched Region,**

(iv) **GILL's Theorem** that makes MILLIKAN's argument legitimate.

Chapter 2 SOME CRITICAL REFLECTIONS

2.1 THE LAW OF THE WALL — FRICTION COEFFICIENT MEASUREMENTS

See A.1, Fig. 1.1.1 and 1.1.2.

The Law of the Wall has not been questioned as it has been stated in the previous chapter. To check the Law of the Wall, experimentalists either refer to the log region in inner variables, or plot the linear leading term close to the wall, valid for pipes and boundary layers:

$$\frac{U}{u_\tau} \simeq \frac{yu_\tau}{\nu} \tag{2.1.99}$$

Experimentalists have different ways of determining the friction velocity, u_τ: (i) by *measuring the skin friction directly*, by using a floating-element device, or a PRESTON tubes, (ii) by *determining the wall slope*, by measuring the velocity down to the wall, (iii) by *computing the momentum loss*, by computing the derivative of the momentum thickness in a boundary layer, or measuring streamwise static pressures in a pipe, (iv) by what is known as the *CLAUSER plot method*, i.e., fitting the data in the log region.

All of the above methods have their drawbacks and advantages: (i) *Measuring he skin friction directly* supposes that one is able to achieve a good calibration or the measurement device, and therefore relies more or less on some other nethod for the calibration. Often used and less expensive than the skin friction alance, the PRESTON tube, although a skin friction measuring device, measures elocity in the inner and/or matched layer and is therefore subject to the theoretical odelization of the different layers. The major experimental problems in a RESTON tube calibration, given an undisturbed flow of high quality are to etermine the static pressure which would exist in the absence of the probe and to inimize any non-local disturbances to the mean flow when the probe is present. ese problems have received careful attention in PATEL (1965) work. (ii) *A all slope method* would be extremely useful, unfortunately, for boundary layers, is extremely difficult to measure the velocity in the inner region, because the limitations of the measurement device (wall-hot wire interaction, lack

of precision of the laser technique, etc.). Interestingly enough to this respect, CLAUSER (1956) plots pipe flow experiment points down to the wall, which may be questionable. (iii) *Computing the momentum derivative* can also be done and is done, usually as a checking procedure. This method relies on the velocity measurements. Moreover, if one wants to compute the momentum loss for a given flow, one has to measure the velocity profile very regularly along the downstream axis, which, for calibration purposes, can not always be done. More often done is the computation of the derivative of the momentum thickness in a batch-wise fashion, using different flow results. This assumes that there is no initial condition effects. (iv) *CLAUSER's method* is based on the log law results, results that are questioned here.

KLINE et al. (1967) show clearly that the way of determining the friction velocity is crucial, and yields different results especially in a pressure gradient flow. KLINE et al. argued that CLAUSER (1956) determined Van KARMAN's constant and the y-intercept of the log law from LAUFER's (1954) pipe data, but only from $y_- > 70$. They further argued that if CLAUSER had employed LAUFER's channel data, the two methods of determining the friction velocity would have given the same results.

It seems to us that both methods, the CLAUSER plot and the wall slope method do not give the same results in general. In fact, we see in KLINE et al. that there is no order in the way the different profile separate from each other when plotted in variables based on the friction velocity, u_τ, determined by a wall slope method. For that reason, we object to the actual computed values of u_τ in KLINE et al. Clearly, a small error in the friction coefficient, u_τ, gives a random scatter in the log-region... and thereby explains the attraction of the CLAUSER plot method.

2.2 LOW REYNOLDS' NUMBER EFFECTS

There are few people who challenge COLE's hypothesis and results for the wake function. However, an important area of controversy is the behavior of turbulent flow at low-Reynolds' number. Indeed, the flow is turbulent in the sense that the fluctuations have a significant energy and a strong effect on the mean velocity through the Reynolds' stress they generate. On the other hand, the range of scales is not sufficient enough for many widely-used theoretical arguments, which are based on the separation of large and small scales. To this respect,

COLES (1968a) and SPALART (1988) notices that the theories have been unable so far to predict the universal Van KARMAN's —and KOLMOGOROFF's— constant(s). Low Reynolds' number experiments do not tend to support the universal character of χ and d, as well as the behavior of the form parameter Π. SIMPSON (1970), SPALART (1988) and PHILLIPS (1990) find a Reynolds' number dependence for Van KARMAN's constant, χ. Furthermore, PHILLIPS (1990) obtains results for the form parameter, Π. On the other hand, we will mention in the next chapter PURTELL et al. (1981), who believe that χ and d are not altered for low Reynolds' numbers.

2.2.1 SIMPSON (1970)

SIMPSON (1970) finds that the Van KARMAN's constant is decreasing for low Reynolds' number and he proposes:

$$\chi = \begin{cases} 0.40 \left(\frac{\Re_\theta}{6000.}\right)^{-\frac{1}{8}} & for\ \Re_\theta < 6000. \\ 0.40 & for\ \Re_\theta > 6000. \end{cases} \qquad (2.2.100)$$

to model empirically that variation. Let us note that SIMPSON uses measurements taken in the outer region, and does not go down to the wall.

2.2.2 SPALART (1988)

See A.1, Fig. 1.2.

SPALART (1988) simulated numerically a turbulent boundary layer on a flat plate with zero pressure gradient for four Reynolds' numbers ranging from $\Re_\theta = 225$ to $\Re_\theta = 1410$. Because of the nature of his work, he encounters low Reynolds' number effects. Interesting for us, he compares the mean velocity profile with experimental data and the theoretical log-law. More interesting, he, apparently the first, plots the velocity derivatives:

$$y_+ \frac{du_+}{dy_+} = g(y_+) \qquad (2.2.101)$$

which enables seeing the logarithmic region and measuring Van KARMAN's constant by seeking the minimum of the previously defined function, g. In other words, this procedure amounts to seeking the inflection point of the velocity profile and determine Van KARMAN's constant, χ, and the y-intercept of the log-law, d. He notices that this procedure is sensitive to the noise and may therefore not

be suitable to experimental data. On the other hand, his simulation shows a low level of noise. He therefore prefers this method to the questionable "CLAUSER plot method".

SPALART notices that at the lowest Reynolds number, $\Re_\theta = 300$, the region of local minimum of the g function is narrow and appears to get somewhat wider as the Reynolds' number increases. Moreover, the Van KARMAN's constant, the local minimum value, is seen to vary with the Reynolds' number. SPALART gives two possible explanations, preferring however the second one:
(i) this phenomena may be reminiscent of SIMPSON interpretation, i.e., at low Reynolds' numbers, there is a log region but Van KARMAN's constant varies. He compares his value to SIMPSON's expression and finds that his values for Van KARMAN's constant (0.32, 0.38 and 0.40) are not as far away from the traditional Van KARMAN's constant (0.41) as the one given by SIMPSON's (0.28, 0.31 and 0.34).
(ii) the log layer, because of the very narrow region and the variable Van KARMAN's constant does not exist at low values of Reynolds' number and appears for $\Re_\theta = 1410$.

2.2.3 PHILLIPS (1990)

PHILLIPS (1990) objects to COLES (1956) results at low Reynolds' number and has an interesting theory. According to COLES (1956), based on WIEGHARDT (1944) experiment, $\Pi = 0$ for $\Re_\theta = 425$. We note that COLES (1968a) recognizes that the very use of the logarithmic profile in evaluating the displacement and momentum thickness leads to some scatter at low Reynolds' numbers.[10].

Seemingly, PHILLIPS (1990) derives that:

$$\chi c = 2 \tag{2.2.103}$$

He is therefore able to derive two solutions for Π, one positive and the other negative. He quotes SMITS et al. (1983) who found a logarithmic region for a Reynolds number of $\Re_\theta = 365$, indeed, PHILLIPS derives that the form parameter, Π, is zero for $\Re_\theta \approx 70$.

[10] He proposes to correct the displacement expression 1.4.84 by reducing the Reynolds' number based on the displacement thickness by 65:

$$\frac{\Re_{\delta^*} - 65}{\Re_\delta} = (1 + \Pi)\frac{c}{\chi} \tag{2.2.102}$$

2.3 THE MESOLAYER: AN ALTERNATIVE TO THE TRADITIONAL MATCHED LAYER (LONG, 1981)

LONG et al. (1981) proposed an alternative to the classical logarithmic theory. In fact, he rejects the overlap process and finds that a new region, the mesolayer, exists. Let us try to shed some light on that theory.

According to LONG et al., in the classical theory, the viscosity is unimportant in the outer region, whereas in the inner region, the outer scale is unimportant, so that in the matched layer both viscosity and outer scale are unimportant. LONG et al., on the contrary, argue that, as we move from the inner region to outer region the outer scale is becoming important and the viscosity is becoming unimportant. Therefore, in the transition region, both viscosity and outer scale are important[11]. To illustrate this point, LONG et al. give the example of mathematicians carrying out singular perturbation methods to derive second order behavior in the matched region using the Reynolds' number, $\Re_*$, as a perturbation parameter in their expansion. This perturbation parameter involves both the outer scale, viscosity and the friction velocity that can be seen as a combination of outer scale and viscosity effects. Going further, LONG et al. argue that contrary to the classical theory, the Reynolds' stress in the overlap region is heavily influenced by viscosity. In fact, they find apparently that the maximum of the Reynolds stress lies on the following curve:

$$y_+ = 1.89\Re_*^{\frac{1}{2}} \tag{2.3.104}$$

Interesting for us, LONG et al. derive expressions for pipes and turbulent boundary layer at zero incidence and obtains[12] a log-law for pipe flow in the mesolayer and a power law for boundary layer flow. On physical ground, it is argued that:

$$\varepsilon = \frac{1}{A_0}(\Re_x)^{-\frac{s}{1-s}} \tag{2.3.105}$$

and

$$\Re_* = \frac{1}{B_0}(\Re_x)^{-\frac{1-2s}{1-s}} \tag{2.3.106}$$

[11] The present writer notes that if one follows MILLIKAN's argument, the physics involved in the matched layer is not used in the matching process, once both inner and outer laws have been defined.

[12] The full details of the derivation have not been provided.

Using the data of SMITH & WALKER, SCHULTZ & GRUNOW and WIEGHARDT, it is found that:

$$A_0 = 11.86 \tag{2.3.107}$$

$$B_0 = 0.0301 \tag{2.3.108}$$

$$s = 0.0635 \tag{2.3.109}$$

2.4 THE POWER LAW: AN ALTERNATIVE TO THE LOG LAW (GEORGE, 1989)

GEORGE (1988, 1989) rejects, for boundary layer, the velocity-defect in a "Reynolds Similarity" form, and thus writes it in a strict similarity form:

$$\frac{U_\infty - U}{U_\infty} = F\left(\frac{y}{\delta}\right) \tag{2.4.110}$$

Indeed, he argues that the friction velocity is not the proper outer velocity scale, and takes the free stream velocity, U_∞, as outer scale, on the ground that the overlap layer should include both viscosity and inertia effects. Assuming that:

$$\frac{u_\tau}{U_\infty} = A\left(\frac{\eta}{\delta}\right)^\gamma \tag{2.4.111}$$

he derives that at infinite Reynolds' number, the velocity profile in the matched layer is given by a power law, i.e., in inner variables:

$$\frac{U}{u_\tau} = \frac{C}{A}\left(\frac{y}{\eta}\right)^\gamma \tag{2.4.112}$$

and in outer variables:

$$\frac{U}{U_\infty} = C\left(\frac{y}{\delta}\right)^\gamma \tag{2.4.113}$$

Note that the matching of 2.4.112 and 2.4.113 recovers 2.4.111 thereby demonstrating the consistency of the derivation. A few remarks need to be made:

(i) From a physical point of view, the derivation is highly dependent on two assumptions, 2.4.110 and 2.4.111. Both relations need to be verified experimentally. Indeed, since Van KARMAN's work (1930), most experiments are interpreted as supporting the Reynolds' number Similarity Law.

(ii) From an experimental point of view, it is well known that, fitting the velocity profile with a power law, leads to a power that is dependent on the Reynolds' number. It should be noted that experimentalists unaware of the asymptotic expansions matching concept, have previously determined the exponent by fitting the whole profile. On the other hand, GEORGE (1989) suggest that the exponent, γ, is characteristic of the matched layer at infinite Reynolds' numbers. Therefore, one needs to find γ from large Reynolds' number experiments, and be sure that the data reflect the true asymptotic behavior.

(iii) From a mathematical point of view, 2.4.111 is given *a priori* whereas it should be an important deduction. Note however that this assumption yields consistent results[13].

2.5 FRICTION COEFFICIENT EMPIRICAL FORMULAE

There has been numerous attempts to give empirical friction coefficient laws, MONIN and YAGLOM (1972) have a good summary of those. Let us just point out some of them.

If one assume the " one-seventh law", valid for moderate Reynolds' numbers, one may obtain, see SCHILCHTING (1960), BLASIUS' expression:

$$c_f = 0.0576\ (\Re_x)^{-\frac{1}{5}} \tag{2.5.114}$$

which gives a good description of the friction coefficient measurements in the range: $5.\ 10^5 < \Re_x < 10^7$. But, for larger Reynolds' numbers, the velocity profile shows an increasing power. As a consequence, the power in the friction law is also increasing. Up to a Reynolds' number of $\Re_x = 10^9$, good agreement with the data is obtained with FALKNER's (1943) expression:

$$c_f = 0.0262\ (\Re_x)^{-\frac{1}{7}} \tag{2.5.115}$$

[13] Indeed in the next chapter, it will be seen that 2.4.111 can be derived from a Strict Similarity assumption using the *Asymptotic Invariance Principle.*

Before we close this section, let us give LUDWIEG-TILLMANN's (1949) formula which is often used by COLES as a comparison to his expression:

$$c_f = .246\, 10^{-0.678\, H}\, \Re_\theta^{-.268} \qquad (2.5.116)$$

This expression is interesting in the fact that it uses the shape factor and the Reynolds' number based on the momentum thickness. Moreover, it gives a explicit soluble form for each of its variable as function of the other two.

2.6 MATCHED ASYMPTOTIC EXPANSIONS

A number of efforts, TENNEKES (1968), YAJNIK (1970), MELLOR (1971), BUSH and FENDELL (1972), (1973), (1974), AFZAL and YAJNIK (1973), AFZAL (1976), LUND and BUSH (1980), have been made to extend the classical theory to higher orders. In this section, we will attempt to review some aspects of this work.

We already have seen that equating velocity derivatives involves a ratio of inner and outer length scales which is the Reynolds' number, $\Re_*$. It is important to note that this number is the only parameter that enters the description of the flow, see 1.2.39 and 1.2.40 for pipe flow, the usual Reynolds' number based on the outer scale or the outer velocity scale only appears in the influence it has on $\Re_*$. It is therefore the (only) perturbation parameter if one applies a perturbation method to the flow.

Often to achieve that goal, one needs a "closure" concept, either a closure model, to the first or the second order, or MILLIKAN's argument. This is especially true for boundary layer flow (for pipe, more simple governing equations enable some deductions for the inner and outer expansions). Indeed, YAJNIK (1970) assumes that:

$$\frac{du_-}{dy_-} \sim \frac{1}{y_+} \qquad (2.6.117)$$

... what should indeed be a major deduction.

MELLOR's (1971) approach differs from the traditional approach, indeed he considers three region: (i) the viscous region, (ii) the defect layer, what is most often called the outer region, (iii) the inviscid region, which, argues MELLOR, is a part of the total problem and has therefore to be taken into consideration.

He obtains a logarithmic law for the outer asymptote of the viscous layer or the inner asymptote of the defect layer. Moreover, one may also recognize COLES' law of the wake as the Velocity Defect from which the common asymptote has been subtracted. Apparently, MELLOR could only obtain the first order with this procedure.

BUSH and FENDELL (1972), (1973), (1974) adopt closure models to find the higher orders: eddy viscosity model in channel and boundary layer flow (1972), (1974), or energy conservation in channel flow (1973). Later, using eddy viscosity model, LUND et al. (1980) generalize the POISEUILLE flow results to COUETTE-POISEUILLE flow. Interesting is the fact that they conclude that the conventional eddy diffusivity closures are inadequate for this type of flow.

FENDELL (1972) follows MILLIKAN and matches the velocity derivative to derive second order expressions for pipe flow and turbulent boundary layers.

AZFAL and YAJNIK (1973), considering essentially pipe and channel flow, assume the general form of the inner and outer expansions of the laminar and Reynolds' stress, in the outer region:

$$U_{ou} = U_1(\overline{y}) + \epsilon U_2(\overline{y}) + \epsilon^2 U_3(\overline{y}) + \ldots \qquad (2.6.118)$$

$$T_{ou} = T_1(\overline{y}) + \epsilon T_1(\overline{y}) + \epsilon^2 T_3(\overline{y}) + \ldots \qquad (2.6.119)$$

in the inner region:

$$u_{in} = u_1(y_+) + \epsilon u_2(y_+) + \epsilon^2 u_3(y_+) + \ldots \qquad (2.6.120)$$

$$t_{in} = t_1(y_+) - \epsilon t_2(y_+) + \epsilon^2 t_3(y_+) + \ldots \qquad (2.6.121)$$

where the perturbation parameter is given by:

$$\epsilon = \frac{1}{\Re_*} \qquad (2.6.122)$$

We will note in lower case the non-dimensionalized velocity and Reynolds' stress, and in capitals the non-dimensionalized velocity and Reynolds' stress. For instance, in the outer region:

$$U_{ou} = \frac{U_\infty - U}{u_\tau} \qquad (2.6.123)$$

$$T_{ou} = \frac{1}{\rho}\frac{\overline{uv}}{u_\tau^2} \tag{2.6.124}$$

and in the inner region:

$$u_{in} = \frac{U}{u_\tau} \tag{2.6.125}$$

$$t_{in} = \frac{1}{\rho}\frac{\overline{uv}}{u_\tau^2} \tag{2.6.126}$$

Afzal et al. match the Reynolds' stress deducing afterward the velocity, which gives in the inner region:

$$u_1 = b_1 \ln(1 + y_+) + \lambda_1(y_+) \tag{2.6.127}$$

$$u_2 = a_2 y_+ + b_2 \ln(1 + y_+) + \lambda_2(y_+) \tag{2.6.128}$$

The constants in the previous equations are:

$$\lambda_n(y_+) = \int_0^{y_+} \left(t_n - 2y_+\delta_{1,n} + \delta_{2,n} + \frac{b_n}{1+y_+} \right) dy_+ \tag{2.6.129}$$

where $\delta_{i,j}$ is the Kronecker delta. The integrals are bounded as $y_+ \to \infty$
outer variables, the velocity is given by:

$$U_1 = b_1 \ln(\overline{y}) + \Lambda_1(\overline{y}) \tag{2.6.130}$$

$$U_2 = -\frac{c_1}{\overline{y}} + b_2 \ln(\overline{y}) + \Lambda_2(\overline{y}) \tag{2.6.131}$$

re, Λ_n is given by:

$$(\overline{y}) = U_n\left(\frac{1}{2}\right) + 2c_1\delta_{2,n} + a_n\left(\overline{y} - \frac{1}{2}\right) - \int_{\frac{1}{2}}^{\overline{y}} \left(T_n - \frac{c_1}{(\overline{y})^2}\delta_{2,n} - \frac{b_n}{\overline{y} - a_n} \right) d\overline{y} \tag{2.6.132}$$

Matching the mean velocity, AFZAL et al. get:

$$\frac{u_\tau}{\chi}\ln\epsilon = (1+\epsilon(-\chi b_2)+...)$$
$$-u_\tau\left((\Lambda_1(0)-\lambda_1(\infty))+\epsilon(\Lambda_2(0)-\lambda_2(\infty)-\chi b_2(\Lambda_1(0)-\lambda_1(\infty)))+...\right) \tag{2.6.133}$$

where:

$$\chi = \frac{1}{b_1} \tag{2.6.134}$$

On the other hand, AZFAL (1976), following MILLIKAN and FENDELL, matches the velocity derivative and deduces the Reynolds' stress. The interesting point is that he uses MILLIKAN's argument, in fact GILL's theorem, to get both the first order and the second order:

$$y_+\frac{\partial u_1}{\partial y_+}+\epsilon y_+\frac{\partial u_2}{\partial y_+}+O(\epsilon^2)\approx\overline{y}\frac{\partial U_1}{\partial\overline{y}}+\epsilon\overline{y}\frac{\partial U_2}{\partial\overline{y}}+O(\epsilon^2) \tag{2.6.135}$$

To the first order, the classical MILLIKAN form is obtained:

$$y_+\frac{\partial u_1}{\partial y_+}+O(\epsilon)\approx\overline{y}\frac{\partial U_1}{\partial\overline{y}}+O(\epsilon) \tag{2.6.136}$$

Finally, AFZAL obtains, as $y_+\to\infty$:

$$u_{in}=\left(A_1\ln(y_+)+b_1+\frac{b_2}{y_+}+...\right)$$
$$+\epsilon(B_2y_++A_2\ln(y_+)+d_1+...)+O(\epsilon^2) \tag{2.6.137}$$

and as $\overline{y}\to 0$:

$$U_{ou}=(A_1\ln(\overline{y})+B_1+B_2\overline{y}+...)$$
$$+\epsilon\left(-\frac{b_2}{\overline{y}}+A_2\ln(\overline{y})+D_1+...\right)+O(\epsilon^2) \tag{2.6.138}$$

As in MILLIKAN's derivation, the skin friction law is obtained by subtracting the outer form of the expansion in the matched region from the inner form of the expansion in the matched region.

Chapter 3 ASYMPTOTIC INVARIANCE PRINCIPLE (A.I.P.)

3.1 ASYMPTOTIC INVARIANCE PRINCIPLE

To see more precisely what is involved in the derivation of the matched layer we will derive here the log law in the matched layer assuming a Reynolds' number Similarity form for the outer region. We do not consider MILLIKAN's argument since GILL's assumptions have not been studied experimentally.

The *Asymptotic Invariant Principle (A.I.P.)* is introduced and used to derive the leading term in the matched region assuming a Velocity Defect or a Strict Similarity form. It is clear that one needs more assumptions relevant to the problem considered if one wants to get second order terms. In doing so, the *Asymptotic Invariance Principle* might be useful.

By *Asymptotic Invariant Principle (A.I.P.)*, we mean that:

1. The velocity forms of both regions are **"matched"**[14].
2. We derive that "matched" expression of the velocity with respect to the **perturbation parameter.**
3. We derive that "matched" expression of the velocity with respect to an **intermediate matching process type of variables** characteristic of the matched region:

$$y_\varrho = \varrho(\epsilon)\,\overline{y} = \varrho(\epsilon)\,\epsilon y_+ \tag{3.1.139}$$

where ϵ is the perturbation parameter, given here by:

$$\epsilon = \frac{1}{\Re_*} \tag{3.1.140}$$

The following derivations are appropriate for boundary layers with or without pressure gradient, but may be extended to pipes or channels. We obtain a necessary condition for this process which practically gives an expression for the friction coefficient[15].

[14] Equate would mathematically be more correct.

[15] We can recover, if we assume a Reynolds' number Similarity, the logarithmic result for the friction coefficient or GEORGE's *a priori* assumption if a Strict Similarity assumption is made.

3.2 A. I. P. APPLIED TO A VELOCITY DEFECT

Let us consider a boundary layer on a flat plate, and express the velocity form in the outer region as:

$$U(\epsilon, \overline{y}) = U_0(\epsilon) + U_1(\epsilon)\ F_1(\overline{y}) + ... \tag{3.2.141}$$

and in the inner region:

$$U(\epsilon, y_+) = u_1(\epsilon)\, f_1(y_+) + ... \tag{3.2.142}$$

The different scales are, see for instance FENDELL (1972):

$$U_0 = U_\infty \tag{3.2.143}$$

$$U_1 = u_\tau \tag{3.2.144}$$

$$u_1 = u_\tau \tag{3.2.145}$$

Following AFZAL (1976), the higher order velocities may be given as power of the perturbation parameter, but, as we mentioned previously, only the first order terms are considered in this work.
The non-dimensionalized length variables are for the outer region:

$$\overline{y} = \frac{y}{\delta} \tag{3.2.146}$$

and for the inner region:

$$y_+ = \frac{y}{\eta} \tag{3.2.147}$$

where the length scales are δ, the boundary layer thickness, and η, given by:

$$\frac{\eta u_\tau}{\nu} = 1 \tag{3.2.148}$$

The perturbation parameter is given by the ratio of inner to outer scales:

$$\epsilon = \frac{\eta}{\delta} \tag{3.2.149}$$

Using an intermediate matching process type of variable[16], y_ϱ, characteristic of the matched region, see COLE (1968), we consider the velocity form in the matched layer associated with the limit:

$$\epsilon \to 0, \quad at \quad y_\varrho = \varrho(\epsilon)\,\overline{y} = \varrho(\epsilon)\,\epsilon\, y_+, \quad fixed \tag{3.2.150}$$

where:

$$ord(\epsilon) \leq ord(\varrho) \leq 1 \quad or \quad \left(\frac{\varrho}{\epsilon} \underset{\epsilon \to 0}{\to} \infty \; and \; \varrho \underset{\epsilon \to 0}{\to} 0\right) \tag{3.2.151}$$

Let us note that the different velocity and length scales have for a boundary layer on a flat plate an x dependence. As a matter of fact, the perturbation parameter for a given flow can be determined as a function of x and vice versa. The relationship may be given by an expression relating the friction coefficient to the Reynolds' number based on x. To achieve a perturbation method, the perturbation parameter is considered to be constant. In a boundary layer, the perturbation parameter, $\epsilon = 1/\Re_*$, as we move downstream decreases and tends to zero monotonically. Naturally, the perturbation factor varies, and naturally the velocity in the matched region reaches its asymptotic expansion. We argue[17] that it is possible to derive with respect to the perturbation parameter, and match the derivatives obtained for both regions.

From 3.2.142, and 3.2.141, we get to the first order:

$$u_1(\epsilon)\, f_1\left(\frac{\varrho(\epsilon)}{\epsilon} y_m\right) = U_0(\epsilon) + U_1(\epsilon)\, F_1(\varrho(\epsilon)\, y_\varrho) \tag{3.2.152}$$

We derive equation 3.2.152 with respect to y_ϱ:

$$u_1(\epsilon)\, \frac{\varrho(\epsilon)}{\epsilon}\, f_1'\left(\frac{\varrho(\epsilon)}{\epsilon} y_\varrho\right) = U_1(\epsilon)\, \varrho(\epsilon)\, F_1'\,(y_\varrho \varrho(\epsilon)) \tag{3.2.153}$$

We derive 3.2.152 with respect to ϵ:

$$\begin{aligned} &u_1'(\epsilon)\, f_1\left(\frac{\varrho(\epsilon)}{\epsilon} y_\varrho\right) + u_1(\epsilon)\, \frac{\varrho'\epsilon - \varrho}{\epsilon^2}(\epsilon)\, y_\varrho f_1'\left(\frac{\varrho(\epsilon)}{\epsilon} y_\varrho\right) \\ &= U_0'(\epsilon) + U_1' F_1(\varrho(\epsilon)\, y_\varrho) + U_1(\epsilon)\, \varrho'(\epsilon)\, y_\varrho F_1'(\varrho(\epsilon)\, y_\varrho) \end{aligned} \tag{3.2.154}$$

[16] This following derivation without the use of the matched variable, y_ϱ, leads to a contradiction, which seems natural considering the matching process theory.

[17] Note that we do not argue on mathematical grounds.

considering 3.2.153, 3.2.154 simplifies to:

$$u_1'(\epsilon)\, f_1\left(\frac{\varrho(\epsilon)}{\epsilon}y_\varrho\right) - u_1(\epsilon)\frac{1}{\epsilon}\left(\frac{\varrho(\epsilon)}{\epsilon}y_\varrho\right) f_1'\left(\frac{\varrho(\epsilon)}{\epsilon}y_\varrho\right) = U_0'(\epsilon) + U_1'(\epsilon)\, F_1(\varrho(\epsilon)\, y_\varrho) \tag{3.2.155}$$

which simplifies when applying 3.2.152:

$$u_1'(\epsilon)\, f_1\left(\frac{\varrho(\epsilon)}{\epsilon}y_\varrho\right) - u_1(\epsilon)\frac{1}{\epsilon}\left(\frac{\varrho(\epsilon)}{\epsilon}y_\varrho\right) f_1'\left(\frac{\varrho(\epsilon)}{\epsilon}y_\varrho\right) = U_0'(\epsilon) + \frac{U_1'}{U_1}(\epsilon)\left(u_1(\epsilon) f_1\left(\frac{\varrho(\epsilon)}{\epsilon}y_\varrho\right) - U_0(\epsilon)\right) \tag{3.2.156}$$

or

$$\left(\frac{u_1'}{u_1} - \frac{U_1'}{U_1}u_1\right)(\epsilon)\, f_1\left(\frac{\varrho(\epsilon)}{\epsilon}y_\varrho\right) - \frac{1}{\epsilon}\left(\frac{\varrho(\epsilon)}{\epsilon}y_\varrho\right) f_1'\left(\frac{\varrho(\epsilon)}{\epsilon}y_\varrho\right) = \left(\frac{U_0'}{u_1} - \frac{U_1'U_0}{U_1u_1}\right)(\epsilon) \tag{3.2.157}$$

finally:

$$y_+ f'(y_+) - \frac{1}{\epsilon}\left(\frac{u_1'}{u_1} - \frac{U_1'}{U_1}u_1\right)(\epsilon)\, f(y_+) + \frac{1}{\epsilon}\left(\frac{U_0'}{u_1} - \frac{U_1'U_0}{U_1u_1}\right)(\epsilon) = 0 \tag{3.2.158}$$

By assumption, the asymptotic profile, $f_1(y_+)$, cannot depend on x, therefore the x-dependent coefficients are proportional to each other. So that, 3.2.158 becomes

$$y_- f'(y_+) - \gamma_1 f(y_+) - \frac{1}{\chi_i} = 0 \tag{3.2.159}$$

where the constants are defined by:

$$\left(\frac{u_1'}{u_1} - \frac{U_1'}{U_1}\right)(\epsilon) = \gamma_1\frac{1}{\epsilon} \tag{3.2.160}$$

and

$$\left(\frac{U_0'}{u_1} - \frac{U_1'U_0}{U_1u_1}\right)(\epsilon) = -\frac{1}{\chi_i}\frac{1}{\epsilon} \tag{3.2.161}$$

We can integrate the right hand side of 3.2.160, and get:

$$\frac{u_1}{U_1}(\epsilon) = A_1 \epsilon^{\gamma_1} \tag{3.2.162}$$

Using 3.2.162, 3.2.161 can be written:

$$\left(\frac{U_0' U_1 - U_1' U_0}{U_1^2}\right)(\epsilon) = -\frac{A_1}{\chi_i}\ \epsilon^{\gamma_1 - 1} \tag{3.2.163}$$

which can also be integrated:

$$\frac{U_0}{U_1}(\epsilon) = \begin{cases} -\frac{A_1}{\chi_i}\ln(\epsilon) + E_1 & if\ \gamma_1 = 0 \\ -\frac{A_1}{\chi_i \gamma_1}\epsilon^{\gamma_1} + A_2 & else \end{cases} \tag{3.2.164}$$

In outer variables, 3.2.154 and 3.2.153 also yield:

$$\begin{aligned} &\frac{u_1'}{u_1}(\epsilon)\left(U_0(\epsilon) + U_1(\epsilon) F_1(\varrho(\epsilon) y_\varrho)\right) - U_1(\epsilon)\frac{1}{\epsilon}(\varrho(\epsilon) y_\varrho) F_1'(\varrho(\epsilon) y_\varrho) \\ &\qquad = U_0'(\epsilon) + U_1'(\epsilon) F_1(\varrho(\epsilon) y_\varrho) \end{aligned} \tag{3.2.165}$$

or

$$\begin{aligned} &-\varrho(\epsilon) y_\varrho F_1'(\varrho(\epsilon) y_\varrho) + \epsilon\left(\frac{u_1'}{u_1} - \frac{U_1'}{U_1}\right)(\epsilon) F_1(\varrho(\epsilon) y_\varrho) + \\ &\qquad = \epsilon\left(\frac{U_0'}{U_1} - \frac{U_0}{U_1}\frac{u_1'}{u_1}\right)(\epsilon) \end{aligned} \tag{3.2.166}$$

which gives finally:

$$\overline{y} F_1'(\overline{y}) - \epsilon\left(\frac{u_1'}{u_1} - \frac{U_1'}{U_1}\right)(\epsilon) F_1(\overline{y}) - \epsilon\left(\frac{U_0'}{U_1} - \frac{U_0}{U_1}\frac{u_1'}{u_1}\right)(\epsilon) = 0 \tag{3.2.167}$$

or expressed with the proper constants:

$$\overline{y} F_1'(\overline{y}) - \gamma_1 F_1(\overline{y}) - \frac{1}{\chi_o} = 0 \tag{3.2.168}$$

where

$$\frac{1}{\chi_o} = -\epsilon\left(\frac{U_0'}{U_1} - \frac{U_0}{U_1}\frac{u_1'}{u_1}\right)(\epsilon) = \frac{u_1}{U_1}\frac{1}{\chi_i} \tag{3.2.169}$$

We choose to find our solutions by considering two cases depending on the existence of γ_1.

First case: $\gamma_1 = 0$:
We have:

$$u_1 = U_1 \tag{3.2.170}$$

and

$$\frac{1}{\chi_i} = \frac{1}{\chi_o} = \frac{1}{\chi} \tag{3.2.171}$$

where $\frac{1}{\chi}$ is given by:

$$\frac{U_0}{u_1}(\epsilon) = -\frac{1}{\chi}\ln(\epsilon) + E_1 \tag{3.2.172}$$

The equations for the profile are:

$$y_+ f_1'(y_+) - \frac{1}{\chi} = 0 \tag{3.2.173}$$

$$\overline{y}\, F_1'(\overline{y}) - \frac{1}{\chi} = 0 \tag{3.2.174}$$

which give the following solutions:

$$f_1(y_+) = \frac{1}{\chi}\ln(y_+) + d_1 \tag{3.2.175}$$

$$F_1(\overline{y}) = \frac{1}{\chi}\ln(\overline{y}) + D_1 \tag{3.2.176}$$

Combining the two solutions yields:

$$u_1\left(\frac{1}{\chi}\ln(y_+) + d_1\right) = U_0 + U_1\left(\frac{1}{\chi}\ln(\overline{y}) + D_1\right) \tag{3.2.177}$$

giving:

$$d_1 - D_1 = E_1 \tag{3.2.178}$$

Second case: $\gamma_1 > 0$ *or* $\gamma_1 < 0$

We can derive 3.2.159 and 3.2.168 with respect to y_+:

$$y_+ f_1''(y_+) - \gamma_1 f_1'(y_-) = 0 \tag{3.2.179}$$

$$\overline{y} F_1''(\overline{y}) - \gamma_1 F_1'(\overline{y}) = 0 \tag{3.2.180}$$

So that the solution to 3.2.159 and 3.2.168 are:

$$f_1(y_+) = c_1 (y_+)^{\gamma_1} - \frac{1}{\gamma_1 \chi_i} \tag{3.2.181}$$

$$F_1(\overline{y}) = C_1 (\overline{y})^{\gamma_1} - \frac{1}{\gamma_1 \chi_o} \tag{3.2.182}$$

Combining the two solutions yields here:

$$c_1 u_1 y_+^{\gamma_1} - \frac{u_1}{\gamma_1 \chi_i} = U_0 + C_1 U_1 (\overline{y})^{\gamma_1} - \frac{U_1}{\gamma_1 \chi_o} \tag{3.2.183}$$

$$c_1 \frac{u_1}{U_1} y_+^{\gamma_1} - C_1 (\overline{y})^{\gamma_1} = \frac{U_0}{U_1} + \frac{1}{\gamma_1 \chi_i} \left(\frac{u_1}{U_1} - \frac{\chi_i}{\chi_o} \right) \tag{3.2.184}$$

$$A_2 + \left(-\frac{1}{\chi_i \gamma_1} \right) A_1 \epsilon^{\gamma_1} + (C_1 - c_1 A_1)(\overline{y})^{\gamma_1} = 0 \tag{3.2.185}$$

There are two independent parameters in this equation, therefore:

$$A_2 = 0 \tag{3.2.186}$$

$$\frac{A_1}{\chi_i} = 0 \tag{3.2.187}$$

$$c_1 A_1 = C_1 \tag{3.2.188}$$

However, $A_1 = 0$ is a degenerate case. Therefore, we have:

$$A_2 = \frac{1}{\chi_i} = \frac{1}{\chi_0} = 0 \tag{3.2.189}$$

And, the matching conditions reduce to:

$$\frac{u_1}{U_1} = A_1 \epsilon^{\gamma_1} \tag{3.2.190}$$

$$U_0 = 0 \tag{3.2.191}$$

Then, the solutions are:

$$f_1(y_+) = c_1 (y_+)^{\gamma_1} \tag{3.2.192}$$

$$F_1(\overline{y}) = C_1 (\overline{y})^{\gamma_1} \tag{3.2.193}$$

where:

$$c_1 A_1 = C_1 \tag{3.2.194}$$

3.3 A COMMENT

It is extremely striking that the matching conditions found for the power law are analogous to the relations expressing the ratio of the KOLMOGOROFF scales to the big eddies scales:

$$\frac{v_K}{u} = \left(\frac{\eta_K}{l}\right)^{\frac{1}{3}} \tag{3.3.195}$$

where η_K and v_K are KOLMOGOROFF length and velocity scales and u, l, are representative of the big eddies. If we express the different ratios as function of the Reynolds' number representative of the big eddies,

$$\Re_l = \frac{ul}{\nu} \tag{3.3.196}$$

we have:

$$\frac{\eta_K}{l} = \Re_l^{-\frac{3}{4}} \tag{3.3.197}$$

$$\frac{v_K}{u} = \Re_l^{-\frac{1}{4}} \tag{3.3.198}$$

and the ratio of time scales is:

$$\frac{\tau}{\theta} = \Re_l^{-\frac{1}{2}} \tag{3.3.199}$$

where τ is KOLMOGOROFF time scale and θ is the time scale representative from the big eddies.

To conclude this topic, we express our velocities and length scales ratios in the same way as KOLMOGOROFF's ones:

$$\frac{\eta}{\delta} = \Re_\delta^{-\frac{1}{1+\gamma}} \tag{3.3.200}$$

$$\frac{u_\tau}{U_\infty} = \Re_\delta^{-\frac{\gamma}{1+\gamma}} \tag{3.3.201}$$

3.4 CONCLUSION

Assuming an Velocity Defect form for the velocity in the outer flow:

$$U(\epsilon, y_+) = u_1(\epsilon) f_1(y_+) + ... \tag{3.4.202}$$

and in the inner region:

$$U(\epsilon, \overline{y}) = U_0(\epsilon) + U_1(\epsilon)\ F_1(\overline{y}) + ... \tag{3.4.203}$$

where the velocity scale are:

$$u_1 = U_1 = u_\tau \tag{3.4.204}$$

$$U_0 = U_\infty \tag{3.4.205}$$

and applying the *Asymptotic Invariance Principle* yields that the leading term in the matched region is given by a *log-law*[18]:

$$\frac{U_0}{u_1} = \frac{1}{\chi} \ln\left(\frac{1}{\epsilon}\right) + E \tag{3.4.206}$$

[18] From now on, the constants notation is simplified.

$$f_1(y_+) = \frac{1}{\chi}\ln(y_+) + d + \ldots \tag{3.4.207}$$

$$F_1(\overline{y}) = \frac{1}{\chi}\ln(\overline{y}) + D \tag{3.4.208}$$

where:

$$d - D = E \tag{3.4.209}$$

On the other hand, with a Strict Similarity assumption for the outer region:

$$U(\epsilon, y_+) = u_1(\epsilon) f_1(y_+) + \ldots \tag{3.4.210}$$

and for the inner region:

$$U(\epsilon, \overline{y}) = U_1(\epsilon)\ F_1(\overline{y}) + \ldots \tag{3.4.211}$$

where the velocity scales are:

$$u_1 = u_\tau \tag{3.4.212}$$

$$U_1 = U_\infty \tag{3.4.213}$$

it is easy to apply the A.I.P. in the same way as done for the Velocity Defect and show that the leading term in the matched region is given by a *power-law*:

$$\frac{u_1}{U_1} = A\epsilon^\gamma \tag{3.4.214}$$

$$f_1(y_+) = c(y_+)^\gamma + \ldots \tag{3.4.215}$$

$$F_1(\overline{y}) = C(\overline{y})^\gamma + \ldots \tag{3.4.216}$$

where:

$$cA = C \tag{3.4.217}$$

Chapter 4 BOUNDARY LAYER PARAMETERS RATIOS, X-DEPENDENCE AND FRICTION COEFFICIENT

We derive in this chapter some relations between the boundary layer parameters δ^* and θ using a power law as being the leading term in the matched layer. Two derivations yielding the same result will be presented. The second one, following GEORGE (1989), based on an expression for the composite velocity is very efficient in this respect. A more primitive, but nevertheless mathematically presentable, derivation is done first.

We note that explicit expressions are obtained for the x dependence and friction coefficient, which is essential to the experimentalists[19].

4.1 FIRST DERIVATION

We assume that the outer edge of the inner region moves as the inner scale, and that the inner edge of the outer region moves as the outer scale. We will pick $(k\eta)$ "in" the matched layer, i.e., we assume that the leading term in the matched expansion is reached for $y_+ > (k\eta)$. Similarly, we pick $(K\delta)$ "in" the matched layer, so that the leading term in the matched region is reached for $\overline{y} < (K\delta)$. Assuming an overlap, we have to the first order:

$$u = \begin{cases} u_1 f(y_+) & 0 \le y_+ \le k \\ u_1 c y_-^{\gamma} + \ldots = U_1 C(\overline{y})^{\gamma} + \ldots & k \le y_+ \text{ and } \overline{y} \le K \\ U_1 F(\overline{y}) & K \le \overline{y} \le 1 \end{cases} \qquad (4.1.218)$$

4.1.1 Displacement thickness

The displacement thickness is given by:

$$\frac{\delta^*}{\delta} = \frac{1}{\delta}\int_0^{\infty}\left(1 - \frac{u}{U_1}\right)dy \qquad (4.1.219)$$

[19] See for instance in the next chapter, the problem of expressing the friction coefficient as a function of local variables.

breaking the integral into three pieces:

$$\frac{\delta^*}{\delta} = \epsilon \int_0^k \left(1 - \frac{u_1}{U_1}\frac{u}{u_1}\right) dy_+ + \int_{k\epsilon}^K \left(1 - \frac{u}{U_1}\right) d\overline{y} + \int_K^\infty \left(1 - \frac{u}{U_1}\right) d\overline{y} \quad (4.1.220)$$

or

$$\frac{\delta^*}{\delta} = \epsilon \int_0^k \left(1 - \frac{u_1}{U_1} f(y_+)\right) dy_+ + \int_{k\epsilon}^K \left(1 - C(\overline{y})^\gamma\right) d\overline{y} + \int_K^\infty (1 - F(\overline{y}))\, d\overline{y} \quad (4.1.221)$$

Let us note:

$$(1 - K) - I_K = \int_K^\infty (1 - F(\overline{y}))\, d\overline{y} \quad (4.1.222)$$

$$I_k = \int_0^k f(y_+)\, dy_+ \quad (4.1.223)$$

and notice that:

$$\int_{k\epsilon}^K \left(1 - C(\overline{y})^\gamma\right) d\overline{y} = (K - k\epsilon) - \frac{1}{1+\gamma}\left(CK^{\gamma+1} - C(k\epsilon)^{\gamma+1}\right) \quad (4.1.224)$$

so that 4.1.221 becomes:

$$\frac{\delta^*}{\delta} = \left[1 - \left(\frac{CK^{1-\gamma}}{1-\gamma} - I_K\right)\right] + \epsilon\left[\frac{1}{1+\gamma}\left(C(k)^{\gamma+1}(\epsilon)^\gamma\right) - \frac{u_1}{U_1} I_k\right] \quad (4.1.225)$$

or, using the matching condition:

$$\frac{\delta^*}{\delta} = \left[1 - \left(\frac{CK^{1-\gamma}}{1-\gamma} + I_K\right)\right] + \left[\frac{c(k)^{\gamma+1}}{1+\gamma} - I_k\right]\frac{u_1}{U_1}\epsilon \quad (4.1.226)$$

or equivalently:

$$\frac{\delta^*}{\epsilon} = [1 - I_O] + [I_{I1} - I_I]\, A\epsilon^{\gamma-1} \quad (4.1.227)$$

introducing:

$$1 - I_O = \int_0^\infty (1 - F(\overline{y}))\, d\overline{y} \tag{4.1.228}$$

$$I_{I1} - I_I = \int_0^\infty \left(c y_+^\gamma - f(y_+)\right) dy_+ \tag{4.1.229}$$

4.1.2 Momentum thickness

Let us do the same with the momentum thickness:

$$\frac{\theta}{\delta} = \frac{1}{\delta} \int_0^\infty \frac{u}{U_1} \left(1 - \frac{u}{U_1}\right) dy \tag{4.1.230}$$

breaking the integral in three pieces:

$$\frac{\theta}{\delta} = \epsilon \int_0^k \frac{u_1}{U_1}\frac{u}{u_1}\left(1 - \frac{u_1}{U_1}\frac{u}{u_1}\right) dy_+ + \int_{k\epsilon}^K \frac{u}{U_1}\left(1 - \frac{u}{U_1}\right) d\overline{y} + \int_K^\infty \frac{u}{U_1}\left(1 - \frac{u}{U_1}\right) d\overline{y} \tag{4.1.231}$$

We note:

$$J_k = \int_0^k f^2(y_+)\, dy_+ \tag{4.1.232}$$

$$(1 - K) - J_K = \int_K^\infty \left(1 - F^2(\overline{y})\right) d\overline{y} \tag{4.1.233}$$

and notice that:

$$\int_{k\epsilon}^K \frac{u}{U_1}\left(1 - \frac{u}{U_1}\right) d\overline{y} = \frac{1}{1+\gamma}\left(CK^{1+\gamma} - C(k\epsilon)^{\gamma+1}\right) - \frac{1}{1+2\gamma}\left(C^2K^{2\gamma+1} - C^2(k\epsilon)^{2\gamma+1}\right) \tag{4.1.234}$$

So that 4.1.231 becomes:

$$\frac{\theta}{\delta} = \epsilon\frac{u_1}{U_1}I_k - \epsilon\left(\frac{u_1}{U_1}\right)^2 J_k + I_K - J_K$$
$$+\frac{1}{1+\gamma}\left(C_1K^{1+\gamma} - C\left(k\epsilon\right)^{\gamma+1}\right) - \frac{1}{1+2\gamma}\left(C^2K^{1+2\gamma} - C^2\left(k\epsilon\right)^{2\gamma+1}\right) \tag{4.1.235}$$

or

$$\frac{\theta}{\delta} = \left[\left(I_K + \frac{CK^{1+\gamma}}{1+\gamma}\right) - \left(J_K + \frac{C^2K^{1+2\gamma}}{1+2\gamma}\right)\right]$$
$$+\left[I_k - \frac{1}{1+\gamma}c\left(k\right)^{\gamma+1}\right]\left(\frac{u_1}{U_1}\right)\epsilon - \left[J_k - \frac{1}{1+2\gamma}c^2\left(k\right)^{1-2\gamma}\right]\left(\frac{u_1}{U_1}\right)^2\epsilon \tag{4.1.236}$$

or more synthetically:

$$\frac{\theta}{\delta} = \left[I_O - J_O\right] - \left[I_{I1} - I_I\right]A\epsilon^{\gamma+1} + \left[J_{I1} - J_I\right]A^2\epsilon^{2\gamma+1} \tag{4.1.237}$$

which gives to the second order:

$$\frac{\theta}{\delta} \simeq \left[I_O - J_O\right] - \left[I_{I1} - I_I\right]A\epsilon^{\gamma+1} \tag{4.1.238}$$

where:

$$I_O - J_O = \int_0^\infty \left(F\left(\overline{y}\right) - F^2\left(\overline{y}\right)\right)d\overline{y} \tag{4.1.239}$$

$$J_{I1} - J_I = \int_0^\infty \left(\left(cy_+^\gamma\right)^2 - f^2\left(y_+\right)\right)dy_+ \tag{4.1.240}$$

4.1.3 Shape factor

From 4.1.227 and 4.1.237, we can deduce the shape factor:

$$\frac{\theta}{\delta^*} = \frac{1}{H} = -1$$
$$+\left[\left(1 - J_O\right) + \left[J_{I1} - J_I\right]A^2\epsilon^{2\gamma+1}\right] / \left[\left(1 - I_O\right) + \left[I_{I1} - I_I\right]A\epsilon^{\gamma+1}\right] \tag{4.1.241}$$

or

$$\frac{1}{H} = -1 + \frac{1 - J_O}{1 - I_O}\left[1 + \frac{J_{I1} - J_I}{1 - J_O} A^2 \epsilon^{2\gamma+1}\right] / \left[1 + \frac{I_{I1} - I_I}{1 - I_O} A\epsilon^{\gamma+1}\right] \quad (4.1.242)$$

isolating the leading term yields:

$$\frac{1}{H} = \frac{I_O - J_O}{1 - I_O} - \frac{1 - J_O}{1 - I_O}\left[\frac{I_{I1} - I_I}{1 - I_O} A\epsilon^{\gamma+1} - \frac{J_{I1} - J_I}{1 - J_O} A^2 \epsilon^{2\gamma+1} + ...\right] \quad (4.1.243)$$

which gives to the second order:

$$\frac{1}{H} \simeq \frac{I_O - J_O}{1 - I_O} - \frac{(1 - J_O)(I_{I1} - I_I)}{(1 - I_O)^2} A\epsilon^{\gamma+1} \quad (4.1.244)$$

4.2 SECOND DERIVATION

Following GEORGE et al. (1989), we express the solution valid in the matched layer as a composite velocity, i.e., the sum of the outer and the inner solutions minus the common part, here the power law, which we express for convenience in inner variables:

$$u = U_1 F(\overline{y}) + u_1 \left(f(y_+) - c y_+^{\gamma}\right) + ... \quad (4.2.245)$$

The displacement thickness is given by:

$$\frac{\delta^*}{\delta} = \int_0^{\infty} (1 - F(\overline{y}))\, d\overline{y} - \epsilon \frac{u_1}{U_1} \int_0^{\infty} \left(f(y_+) - c y_+^{\gamma}\right) dy_+ \quad (4.2.246)$$

giving as a result:

$$\frac{\delta^*}{\delta} = [1 - I_O] + [I_{I1} - I_I] A\epsilon^{\gamma+1} \quad (4.2.247)$$

The momentum thickness is on the other hand given by:

$$\frac{\theta}{\delta} = \int_0^{\infty} \left(F(\overline{y}) + \frac{u_1}{U_1}\left(f(\epsilon\overline{y}) - c(\epsilon\overline{y})^{\gamma}\right)\right) \left(1 - F(\overline{y}) - \frac{u_1}{U_1}\left(f(\epsilon\overline{y}) - c(\epsilon\overline{y})^{\gamma}\right)\right) d\overline{y} \quad (4.2.248)$$

or

$$\frac{\theta}{\delta} = \int_0^\infty F(\overline{y})\,(1 - F(\overline{y}))\,d\overline{y} + \epsilon\frac{u_1}{U_1}\int_0^\infty \left(f(y_+) - c(y_+)^\gamma\right) dy_-$$

$$-2\epsilon\frac{u_1}{U_1}\int_0^\infty F\left(\frac{y_+}{\epsilon}\right)\left(f(y_+) - c(y_+)^\gamma\right) dy_+ \qquad (4.2.249)$$

$$-\epsilon\left(\frac{u_1}{U_1}\right)^2\int_0^\infty \left(f(y_+) - c(y_+)^\gamma\right)^2 dy_+$$

For the third integral, we can say that in the region where the inner function, f, is different from the asymptotic power law, i.e., in the very inner region, the outer function , F, reaches its asymptotic state, i.e., a power law:

$$-2\epsilon\frac{u_1}{U_1}\int_0^\infty F\left(\frac{y_+}{\epsilon}\right)\left(f(y_+) - c(y_+)^\gamma\right) dy_+$$

$$\simeq -2\epsilon\left(\frac{u_1}{U_1}\right)^2\int_0^\infty c(y_+)^\gamma\left(f(y_+) - c(y_+)^\gamma\right) dy_- \qquad (4.2.250)$$

From which it follows that we find the same result, 4.1.237, as previously:

$$\frac{\theta}{\delta} = [I_O - J_O] - [I_{I1} - I_I]\,A\epsilon^{\gamma+1} + [J_{I1} - J_I]\,A^2\epsilon^{2\gamma+1} \qquad (4.2.251)$$

4.3 X-DEPENDENCE, FRICTION COEFFICIENT

In a zero pressure gradient flow, the momentum integral is:

$$\frac{d\theta}{dx} = \frac{1}{2}c_f \qquad (4.3.252)$$

or:

$$\frac{d\Re_\theta}{d\Re_x} = A\Re_\delta^{-\frac{2\gamma}{1+\gamma}} \qquad (4.3.253)$$

With our expression of the momentum thickness, 4.2.251, 4.3.253 becomes:

$$\left([I_O - J_O] + \frac{\gamma}{1+\gamma}[J_I - J_{I1}](\Re_\delta)^{-\frac{\gamma}{1+\gamma}-1}\right)\frac{d\Re_\delta}{d\Re_x} = A^2\Re_\delta^{-\frac{2\gamma}{1+\gamma}} \quad (4.3.254)$$

$$\left([I_O - J_O](\Re_\delta)^{\frac{2\gamma}{1-\gamma}} + \frac{\gamma}{1+\gamma}[J_I - J_{I1}](\Re_\delta)^{-\frac{1}{1-\gamma}}\right)d\Re_\delta = A^2 d\Re_x \quad (4.3.255)$$

$$\frac{1+\gamma}{1+3\gamma}[I_O - J_O](\Re_\delta)^{\frac{1+3\gamma}{1+\gamma}} + [J_I - J_{I1}](\Re_\delta)^{\frac{\gamma}{1+\gamma}} = A^2(\Re_x - \Re_{x_0}) \quad (4.3.256)$$

$$\frac{1+\gamma}{1+3\gamma}[I_O - J_O]\Re_\delta + [J_I - J_{I1}](\Re_\delta)^{-\frac{\gamma}{1-\gamma}} = \frac{c_f}{2}(\Re_x - \Re_{x_0}) \quad (4.3.257)$$

4.4 SUMMARY-REMARKS

Let us rewrite our equations as follows:

$$\Re_{\delta^*} = [1 - I_O]\Re_\delta + [I_{I1} - I_I] \quad (4.4.258)$$

$$\Re_\theta = [I_O - J_O]\Re_\delta - [I_{I1} - I_I] + [J_{I1} - J_I]\Re_\delta^{-\frac{\gamma}{1+\gamma}} \quad (4.4.259)$$

$$\frac{1+\gamma}{1+3\gamma}[I_O - J_O]\frac{1}{A^2}(\Re_\delta)^{\frac{1+3\gamma}{1-\gamma}} - [J_{I1} - J_I]\frac{1}{A^2}(\Re_\delta)^{\frac{\gamma}{1+\gamma}} = \Re_x - \Re_{x_0} \quad (4.4.260)$$

or equivalently:

$$\frac{1+\gamma}{1+3\gamma}[I_O - J_O]\frac{1}{A^2}\left(\frac{1}{A^2}\frac{c_f}{2}\right)^{-\frac{1+3\gamma}{2\gamma}} - [J_{I1} - J_I]\frac{1}{A^2}\left(\frac{1}{A^2}\frac{c_f}{2}\right)^{-\frac{1}{2}} = \Re_x - \Re_{x_0} \quad (4.4.261)$$

where:

$$[1 - I_O] = \int_0^\infty (1 - F(\overline{y}))\,d\overline{y} \quad (4.4.262)$$

$$[I_O - J_O] = \int_0^\infty F(\overline{y})\,(1 - F(\overline{y}))\,d\overline{y} \quad (4.4.263)$$

$$[I_{I1} - I_I] = \int_0^\infty \left(c y_+^\gamma - f(y_+)\right) dy_+ \tag{4.4.264}$$

$$[J_{I1} - J_I] = \int_0^\infty \left(\left(c y_+^\gamma\right)^2 - f^2(y_+)\right) dy_+ \tag{4.4.265}$$

The shape factor is given by:

$$\frac{1}{H} = \frac{[I_O - J_O]}{[1 - I_O]} - \frac{[1 - J_O]}{[1 - I_O]} \Re_\delta^{-1} \left[\frac{[I_{I1} - I_I]}{[1 - I_O]} - \frac{[J_{I1} - J_I]}{[1 - J_O]} \Re_\delta^{-\frac{\gamma}{1+\gamma}} + \ldots \right] \tag{4.4.266}$$

which gives a simpler expression to the second order:

$$\frac{1}{H} \simeq \frac{[I_O - J_O]}{[1 - I_O]} - \frac{[1 - J_O][I_{I1} - I_I]}{[1 - I_O]^2} \Re_\delta^{-1} \tag{4.4.267}$$

Note that all the expressions in brackets are positive, since for the whole boundary layer:

$$F(\overline{y}) > C(\overline{y})^\gamma \tag{4.4.268}$$

$$f(y_+) < c(y_+)^\gamma \tag{4.4.269}$$

As mentioned by GEORGE (1989), COLES results forecast that the shape factor goes asymptotically to 1. Also, the ratios of the conventional boundary layer thickness to the displacement and momentum thickness is asymptotically undefined.

On the other hand, we see that in our equations, the first order terms, $[1 - I_O]$ and $[I_O - J_O]$, are only given by the outer behavior, the higher order terms, $[I_{I1} - I_I]$ and $[J_{I1} - J_I]$, are given by the difference of the leading term in the matched region, the power law, and the inner behavior. The present theory does not forecast the values of the different constants.

Chapter 5 EXPERIMENTAL DATA

5.1 EXPERIMENTS DESCRIPTION

In this section we will present a brief description of the experimental data that have been used.

5.1.1 SCHULTZ and GRUNOW(1941)

SCHULTZ and GRUNOW (1941) determined the friction coefficient in two ways: momentum loss computations from velocity profiles and a floating element device measurements, i.e., the friction resistance was also measured directly on a rectangular test plate mounted movably in a sector of the principle plate. SCHULTZ & GRUNOW noticed the latter method proved to be more accurate. Note that the same floating element method was used by KEMPF (1929). The edge of the principal plate was greatly curved to insure that the transitional region was situated on the leading edge. Furthermore, to insure the formation of a new friction layer on it, a slot was provided below this edge through which the friction layer of the blower chamber wall exhausted. Three surface were explored: a built-up plywood plate, a puttied, polished, and lacquered surface of high power metal airplane and a thick metal panel. SCHULTZ and GRUNOW deduced the following value of Van KARMAN's constant and y-intercept of the log law:

$$\frac{1}{\chi} = 5.93, \quad d = 4.07 \tag{5.1.270}$$

Let us note that these profiles are defined by a relatively small number of points, none of which lay in the viscous layer. As a consequence, computed values for the integral parameters are strongly affected by the choice of the extrapolation scheme for the different integration computations. More practically, no tabulated data are available in SCHULTZ and GRUNOW (1941), requiring the data to be determined from the graphs.

5.1.2 WIEGHARDT and TILLMANN (1944)

WIEGHARDT and TILLMANN (1944, see also, for tabulated data, COLES et al., 1968) measured velocity profiles over a flat plate. The boundary layer was tripped, a blunt nose at the leading edge fitted with a small trip wire constituted the tripping device. The model was a waxed-plywood plate with a slightly undulating surface. Data were obtained using a rake instead of a single probe. This technique fixes the relative positions of the data points, and also avoids some effects of drift in tunnel conditions by speeding up the data-taking process. However, the data might have been subject to more wall interference than usual. The tunnel turbulence level was about 0.25%.

Finally, note that no friction coefficient was given by the authors, however, COLES (1968) did provide[20] values for the friction coefficient using log law results. Also, in this experiments, no points from the viscous region were obtained so that, here too, the integrals parameters depend on the model chosen for the viscous sublayer.

5.1.3 KLEBANOFF and DIEHL (1951)

KLEBANOFF and DIEHL (1951) investigated how to trip and artificially thicken turbulent boundary layers. Various devices were used such as rods, screens, and distributed roughness to force transition of the laminar boundary layer. Distributed roughness in the form of sandpaper was found to be the most useful to trip and thicken the turbulent boundary layer. KLEBANOFF and DIEHL compared velocity profiles at various streamwise stations and found that the profiles approached an asymptotic state as the distance from the tripping device was increased. The development was verified by measurements of intensity and spectra. In this experiment, no points in the viscous layer were obtained, nor were tabulated data for the velocity provided.

5.1.4 SMITH and WALKER (1958)

The velocity profiles through the boundary layer and the friction coefficent on a smooth flat plate having zero pressure gradient were measured. The boundary layer was tripped by air ejection. The test plate was a mild steel polished to a fine finish. Although there were a few scratches, it is thought that they had little or

[20] To this respect, it is interesting to note that PURTELL et al. used as a comparison of their own friction coefficients the values computed by COLES that they attribute to WEIGHARDT and TILLMANN.

no effect on the flow. The test plate used was mounted between a pair of vertical plates to which was attached an auxiliary plate to insure a zero pressure gradient. The AMES 12–foot pressure tunnel of the variable-density type was used. The turbulence level is said to be very low.

The mean velocity was determined using a wide rectangular total-pressure tube and a static-pressure orifice in the plate located at the same longitudinal location. Note that no correction was made to account for the apparent displacement of the tube resulting from the total-pressure gradient through the boundary layer. Also, no correction was made to the velocity profiles to account for turbulence effects.

SMITH and WALKER (1958) measured the *local* surface shear stress by two techniques: the first was a floating-element device, whereas the second was a PRESTON tube (i.e., a calibrated total-pressure tube, mounted on the surface of the wall). The floating element device calibration showed good repeatability. Note that the measured data were corrected to account for change of temperature of the unit. In addition, the momentum loss was computed to give the *average* skin-friction coefficient.

The data is said to agree with those of KEMF and SCHULTZ and GRUNOW up to a Reynolds' number of $\Re_z = 45.\ 10^6$. The skin friction coefficient determined by the PRESTON tube produced lower values than the ones given by the floating element device, which led SMITH and WALKER to state that the PRESTON tube needed to be recalibrated[21]. They concluded, however, that the PRESTON tube appears to be an inexpensive and accurate measurement device for wall stress measurements. Furthermore, the average skin friction coefficient, computed from the momentum loss, was 4% lower than the local friction coefficient, given by wall-shear stress measuring devices. We point out that the four stations where the skin friction was measured were 2.5 in. behind the velocity profile measurements station. SMITH and WALKER also investigated the log law, their constants are:

$$\frac{1}{\chi} = 5.0. \quad d = 7.15 \tag{5.1.271}$$

which differ substantially from values that have been given in earlier work.

We believe that the disagreement can only come from inaccuracies in the measurement of the shear stress and/or failure to take into account total pressure

[21] PATEL (1965) obtained the same conclusion and proposed a recalibration.

tube displacement corrections. LANDWEBER (1960) has re-analyzed SMITH and WALKER's velocity measurements using MCMILLAN's displacement and turbulence corrections and has seemingly shown that the true values of the constants must be different than the one quoted by the authors.

5.1.5 PURTELL, KLEBANOFF and BUCKLEY (1981)

PURTELL et al. (1981) investigated the behavior of a turbulent boundary layer at low Reynolds' numbers. The time averaged velocity and turbulence variables were measured with a constant temperature hot wire anemometer. The boundary layer was tripped, and at the higher speeds, thickened by a region of distributed roughness at the leading edge consisting of No. 4 floor-sandpaper. The two dimensionality was checked by examining the variation of the local mean velocity U in the spanwise direction.

The friction coefficient was obtained from the momentum loss, computed graphically from measurement of θ at various x locations, and from the wall slope of the velocity profile computed graphically at $x = 2.69\,m$ for $\Re_\theta > 1340$. According to PURTELL et al., the maximum difference, inferred by the two methods was about 5%, and no trend was seen[22]. For the lower Reynolds' numbers, $\Re_\theta < 1340$, the friction coefficient values seem to be less reliable but, again according to PURTELL et al., they agreed well with values computed from the logarithmic law. For $\Re_\theta > 1340$, the relative difference of the wall stress with the friction velocity given by the logarithmic results is said to be less than 5%. Low Reynolds' number effects were also checked, however the behavior of the Van KARMAN's constant as presented in SIMPSON's formula implied, according to PURTELL et al., values for the wall stress which did not agree with the measured ones. Therefore it was concluded that the log law, as given by COLES (i.e., a truly constant value of the Van KARMAN's constant and the y-intereept of the log law) is valid at low Reynolds' numbers.

5.2 VELOCITY PROFILES

See A.2

We first plotted the friction coefficient, boundary layer thicknesses and velocity profiles from SCHULTZ & GRUNOW, and KLEBANOFF & DIEHL. Rapidly,

[22] It is not known however which method was finally taken.

it appeared to us that the procedure used was inadequate. Indeed for the velocity, the points were recorded graphically in inner and outer variables, which not only introduced an extra noise, but it also made, since there is no clear substructure to the data, the exploitation of the data tedious and empirical, i.e. it was hard to know or estimate the profile parameters, friction coefficients and boundary layer thicknesses, for a given profile. In fact, no tabulated form of the data is given in those two papers.

As a consequence, we needed a set of velocity profile data available in *tabulated* form and that covers a *large range* of *high* Reynolds' numbers (we are indeed looking for an asymptotic behavior). A thorough *investigation of the skin friction behavior* seemed also to be necessary, since it represents, so to speak, the closure to our problem. In addition, we hoped to obtain velocity measurements near the wall ($y_+ < 10$).

It appeared that no experiment at moderate or large Reynolds' numbers exhibited the viscous sublayer behavior. However, at low Reynolds' numbers, PURTELL et al. provided measurements down to $y_+ = 3$. Tabulated data of 11 profiles were given by PURTELL (private communication to W.K. GEORGE). In addition, we used SMITH and WALKER's data which not only provides a wide range of moderate and high Reynolds' numbers velocity profiles (80) but also a complete investigation (about 350 points) of the friction coefficient behavior in the same Reynolds number range ($1.4310^6 < \Re_z < 43.10^6$). Because the friction coefficient is not given by WEIGHARDT and TILLMANN for their experiment, we did not use that set of velocity profiles or COLES' friction coefficient. However, we did use the computed values of the boundary layer parameters since these were based directly on the velocity measurements. WIEGHARDT and TILLMANN's set of data overlap on the higher part of PURTELL's set and the lower part of SMITH and WALKER's set.

5.2.1 PURTELL (1981)

We plotted the velocity profiles in inner variables, as well as in a Strict Similarity form and in a Reynolds' Similarity form. For reasons discussed further, in outer variables, we only plotted the velocity profiles corresponding to a Reynolds number of: $\Re_\theta = 1340, 1840, 3480, 5100$. As far as the inner variables representations of the velocity are concerned, we plotted individually the different profiles in semi-logarithmic and logarithmic coordinates. The log law, as given

by COLES, is shown on the same plots. Moreover, we also compared the profiles with the power law, where the power has been obtained by a method which is to be described later. We remind the reader that all the parameters were tabulated for each profile, and that the friction coefficient cited was not obtained with a measuring device but was deduced from the near wall velocity measurements and/or log law results.

Inner variables: *See A.2, Fig. 2.1.2.-, Fig. 2.2.2–*

Let us first look at the behavior of the velocity profiles as given by COLES' expression. Striking is the fact that all the profiles in inner variables fall, so to speak, perfectly onto the same curve, i.e., COLES' log law line.

On the other hand, in a logarithmic coordinate axis, the matched layer seem to exhibit a power law behavior. The power has been determined using the velocity derivative function, g, defined in the previous chapter:

$$g(y_+) = y_+ \frac{du_+}{dy_+} \qquad (5.2.272)$$

Moreover, since an asymptotic state should be reached in the inner region, as the Reynolds' number increases, we chose to fix the same origin for the different profiles, i.e., $y_+ = 45$, $u_+ = 14.55$. It appears that the velocity profiles are in pretty good agreement with that log law line. We conclude that such an approximation gives a good modelization of the profile for this range of Reynolds' number.

Note that three profile, $\Re_\theta = 1340, 1840, 3480$, exhibit a characteristic behavior, an horizontal slope, very near the wall, for $y_+ \approx 2$. We interpret that phenomena as showing the limits of the measurement device, since for this set of data, we went the closest to the wall. In addition, since they have the most points, these three set of data, with the last one, $\Re_\theta = 5100$, are thought to be the most precise and are therefore plotted.

More interesting, it is seen that in logarithmic axis, although the viscous layer behavior is respected, indeed the points, for the most defined profile, follow a straight line of slope 1, these points however are not aligned with the origin point. We plotted the theoretical first order viscous behavior near the wall. For the whole set of profiles, the data near the wall are always below this theoretical line. Moreover, no general trend is seen with increasing Reynolds' numbers. This, with the fact that the velocity profiles fall extraordinaryly well onto the log law line, indicates clearly that PURTELL et al. only used COLES results to obtain

the wall shear stress. If one believes that the measurements points are correct, one has then to conclude that the friction velocity is overestimated.

See A.1, Fig. 1.4.-

To know if the measurements down to the wall are incorrect, or if the friction coefficient are to be corrected, we reprocessed PURTELL's velocity profiles with the friction velocity estimated from the wall slope, taking an average value of the slope in the region were the points were aligned on a straight line in a logarithmic coordinate system (i.e., approximately $3 < y_+ < 9$). We plotted the whole set of profiles in the inner variables computed with the friction velocity given by the wall slope, also, we compared the friction coefficient with SMITH and WALKER's set of measured data.

For the velocity profiles, it appears, as in KLINE et al., that: (i) there is a log region having approximately the same slope, although the y-intercept have higher values, (ii) the profiles do not appear in an orderly way with increasing Reynolds number, which leads to the conclusion that the computed values of the friction coefficient are not consistent among themselves. To this respect, the plot of the friction coefficient as a function of the Reynolds' number exhibits clearly that inconsistency. However, the four profile that are supposed to be the most precise, may appear to be consistent. On that plot, the y-intercept is shown to increase slowly. If we consider the velocity derivative function , g, we see that the local minimum is reached lower and lower, which implies that the Van KARMAN's constant is increasing. It is also thought that this behavior should make the y-intercept constant, d, decrease, which contradicts the behavior observed. We conclude that, when going down to the wall, a wall-measuring device interference takes place that biases the measurements strongly, preventing from computing the wall slope. This seriously questions the validity of such a procedure without wall-hot wire interaction corrections.

Outer variables: *See A.2, Fig. 2.3.2.-, Fig. 2.4.2.-*

We plotted the velocity profiles in both a Strict Similarity form and a Reynolds' number Similarity form, as proposed by Van KARMAN. Because of the range of the Reynolds' numbers, one clearly sees what is commonly interpreted as COLES' wake function, where the form parameter, II, increases with the Reynolds' number. On the other hand, in logarithmic axis, if one accept the idea of the power law, it is seen that the same behavior emerges. Indeed, the

maximum deviation decreases with the increasing Reynolds' numbers. However, because the power region is nearer to the outer flow than the log region, the maximum deviation from the power line is seen to be smaller than the maximum deviation from the logarithmic line.

5.2.2 SMITH and WALKER (1958)

A wide range of Reynolds' numbers has been recorded ($3005 < \Re_\theta < 48290$). As far as the boundary layer parameters are concerned, we used all 80 profiles parameter. We plotted the friction coefficient, given for each profile (as a function of all the flow parameters). However, these points do not lie for the different x-locations on the same curve. This is explained by the fact that the stations where the velocity was taken are further upstream than the stations where the friction coefficient was measured. SMITH and WALKER had to use some interpolation scheme to express the friction coefficient in local variables, which seemingly produced slightly different results for the different stations. We believe therefore that it was necessary to record the "root" set of measured friction coefficient, given as a function of the Reynolds' number $\Re_x$. Although all the measurements were recorded, we only show the sets that exhibited the less noise (made up of 167 and 53 points). The same procedure for the velocity was used as with PURTELL's set of data.

We choose here only to plot four characteristic profiles, $\Re_\theta = 5680, 18340, 37190, 44750$. The lowest and the highest profiles in SMITH & WALKER's set have not been taken, since they do not exhibit a smooth behavior for the velocity derivative. Moreover, the last profile boundary layer parameters are clearly underestimated when compared to the whole set. The lowest Reynolds' number that was taken corresponds to the highest Reynolds' number for PURTELL's set of data.

Inner variables: *See A.2, Fig. 2.1.1.-, Fig. 2.2.1.-*

The profiles were plotted individually in a logarithmic coordinate system, as well as in a semi-logarithmic coordinate system. The profiles were compared in a semi-logarithmic coordinate system with the log law as given by COLES (1956). We point out that the first profiles, taken from the lowest station, $x = 15.75\,in.$, show a good agreement with the data. However, the other profiles do not follow the same behavior. In fact, the measured points are above COLES's log law line, which, as mentioned previously, led SMITH and WALKER to conclude that

COLES' constants are not valid. We already discussed that matter in the previous section, arguing that the velocity measurements given by SMITH and WAKLKER have measurements errors due to total pressure gradient and turbulence effects.

In a logarithmic coordinates system, the velocity profiles were compared with the power law where the power was given by the same method as the one used for PURTELL's data. We point out that we did use the same origin point as for PURTELL's data. It appears that the data points are higher than the power line. Two reasons can be put forward: (i) displacement and turbulence phenomena that alter the velocity values or, from another point of view, (ii) the origin point for the power law may be varying with the Reynolds' number. In fact, the power law region is reached for higher values of the distance from the wall, as the Reynolds' number increases. We believe that both factors have to be considered. Nevertheless, this series of plot does not contradict our method of computing the exponent of the power law, based on the velocity derivative, since the slope of the profile is seen to be the same as the one given by the log law line.

Outer variables: *See A.2, Fig. 2.3.1.-, Fig. 2.4.1.-*

Note in Strict Similarity variables the increase of the exponent for the power law as the Reynolds' number increases. Interesting is the fact that, in a semi-logarithmic coordinate system, the wake function seems to vary with the increasing Reynolds' number, which is contradictory to COLES's analysis, where the form parameter does not change for $\Re_\theta > 5500$. Here again, we can not be affirmative until the previously discussed corrections are applied if such corrections are possible.

5.2.3 SCHULTZ & GRUNOW (1941), KLEBANOFF & DIEHL (1951)

Inner variables: *See A.2, Fig. 2.1.4.-, Fig. 2.1.5.-, Fig. 2.2.4.-, Fig. 2.2.5.-*

Four velocity profiles from SCHULTZ and GRUNOW and four velocity profiles from KLEBANOFF and DIEHL have been plotted. In a semi-logarithmic coordinate axis, it appears that, for both set of data, the points lie generally close to the log law line. On the other hand, the points in a logarithmic axis are also more or less aligned. However, as mentioned in the introduction, the noise is too important to deduce any further information.

Outer variables: *See A.2, Fig. 2.3.4.-, Fig. 2.4.4.-, Fig. 2.4.5.-*

Two remarks can be made. First, we clearly see the noise due either to the measurements or to the fact that points were taken graphically. Second, the Reynolds' number range is very narrow, which explains the fact that, in a Strict Similarity form, the power is practically not varying. Moreover, in a Velocity Defect form, the profile is only changing slightly.

5.3 VELOCITY DERIVATIVES REPRESENTATION

See A.3

PURTELL's set of velocity profiles taught us that it is difficult to estimate the friction velocity without any *a priori* knowledge of the result. SPALART, however, showed that for direct numerical simulations, it is easy to plot a velocity derivative function:

$$y_+ \frac{du_+}{dy_+} = g(y_+) \qquad (5.3.273)$$

and deduce afterward Van KARMAN's constant.

Note that the g axis is only affected by the dimension of u_+, and thus the determination of the friction velocity. On the other hand, the x-axis has the dimension of y_+, and thus is affected by the determination of the friction velocity and the viscosity. However, if one plots g as a function of the velocity, both axis have the same dimensions (of the velocity scale). The g function can also be expressed in outer variables as a function of the non-dimensionalized outer velocity. Moreover, this plot enables not only to see the logarithmic region, which correponds to a straight horizontal line, but also the power law region, which is a straight line going through the origin point.

The velocity derivatives were computed with a 3 points expression for the derivative, using a regular Taylor expansion for the velocity. 2 and 5 points expressions were studied but it appeared that the 3 points expression had the best compromise for noise reduction and accuracy.

5.3.1 PURTELL (1981)

See A.3, Fig. 3.1.2.-, Fig. 3.2.2.-

The inner region, the log and power region, and the wake region are clearly seen. It is also pointed out that the wake region shows a similarity behavior. Note that there is quite some noise but nevertheless the essential features of the

different regions are present. Clearly, it is seen that there is a power law region which is located after the local minimum region, or the log law region.

See A.3, Fig. 3.1.2.-; A.1, Fig. 1.3

The exponent of the power law was obtained by fitting a curve through the points that seem to belong to the power law region. In fact, as mentioned earlier, the values of the power obtained by this method are in good agreement with the velocity plots. Although the results may be refined, the exponent versus the local Reynolds' number, $\Re_\delta$, shows a satisfactory consistency for the 11 profiles from PURTELL et al. and the 14 profiles from SMITH & WALKER.

Note that the profiles corresponding to the Reynolds' numbers $\Re_\theta = 1840, 3480$, and to a certain extent the one corresponding to $\Re_\theta = 5100$, show a good behavior, due to a low noise level and a larger amount of points. The profile corresponding to $\Re_\theta = 1340$ unfortunately contains two noisy points of opposite signs in the matched layer, which generates an important scatter in the derivative.

The velocity derivative in inner varibles was also plotted. For different Reynolds' numbers, the inner region exhibit a similarity behavior. The viscous region was compared with SPALART data. The first line represents points going from $y_+ = 0$ to $y_+ = 10$, the four points are given for $y_+ = 10, 20, 30, 40$. It is seen that, between $10 < y_+ < 40$, the velocity derivatives deduced from PURTELL's data are slightly overestimated, reaching a peak at $y_+ = 8$ and dropping abruptly afterward. This behavior is explained by the wall-measuring device interaction.

PURTELL's set of data seem to show stronger support for a power law than a log law. In fact, the local minimum is included in a very narrow region, especially for $\Re_\theta = 3480$. We remind the reader that we are plotting the velocity derivative as a function of velocity; if plotted against y, we would see larger domains for the log and the power law region.

5.3.2 SMITH and WALKER (1958)

See A.3, Fig. 3.1.1.-, Fig. 3.2.1.-

The same computations as before were conducted for SMITH and WALKER's set of data. We see, however, a different behavior than for PURTELL's set of data. In outer variables, this set seems rather to support the log law than the power law. Indeed, the region of local minimum, although very narrow, is broader than

the region tangent to a line going through the origin point. Note that the wake region behaves more smoothly than for PURTELL's set of data. Moreover, we see that the most important noise occurs in the log region. The wake region, on the other hand, is varying very slowly and shows also a similarity behavior.

In inner variables, it is seen that the viscous layer is not present which is not obvious when considering only the velocity profile. Even more, when comparing these measurements in inner variables with some data taken from SPALART, the first points of SMITH & WALKER simulate, so to speak, a viscous behavior. This fact reinforces our conviction that SMITH & WALKER's data are unreliable near the wall and that the total head probe is unable to measure points in the viscous layer or the lower part of the matched layer.

5.4 DETERMINATION OF THE INTEGRALS

From the boundary layer parameter ratios and the friction coefficient equations seven unknowns appear:

$$X_1 = [1 - I_O] = \int_0^\infty (1 - F(\overline{y}))\, d\overline{y} \tag{5.4.274}$$

$$X_3 = [I_O - J_O] = \int_0^\infty (F(\overline{y})(1 - F(\overline{y})))\, d\overline{y} \tag{5.4.275}$$

$$X_2 = [I_{I1} - I_{I1}] = \int_0^\infty \left(c(y_+)^\gamma - f(y_+)\right) dy_+ \tag{5.4.276}$$

$$X_4 = [J_{I1} - J_I] = \int_0^\infty \left(\left(cy_+^\gamma\right)^2 - f^2(y_+)\right) dy_+ \tag{5.4.277}$$

$$X_5 = \frac{1}{A^2} \tag{5.4.278}$$

$$X_7 = \Re_{z0} \tag{5.4.279}$$

We choose to define the last unknown as the following function of γ:

$$X_6 = \frac{1 + 3\gamma}{2\gamma} \tag{5.4.280}$$

These unknowns appear in the following equations:

$$\Re_{\delta^*} = X_1 \Re_\delta + X_2 \tag{5.4.281}$$

$$\Re_\theta = X_3 \Re_\delta - X_2 + X_4 \Re_\delta^{-\frac{1}{2(X_6-1)}} \tag{5.4.282}$$

$$\Re_x = \frac{X_6 - 1}{X_6} X_3 X_5 (\Re_{\delta^*})^{\frac{X_6}{(X_6-1)}} - X_4 X_5 (\Re_\delta)^{\frac{1}{2(X_6-1)}} + X_7 \tag{5.4.283}$$

$$\Re_x = \frac{X_6 - 1}{X_6} X_3 X_5 \left(X_5 \frac{c_f}{2}\right)^{-X_6} - X_4 X_5 \left(X_5 \frac{c_f}{2}\right)^{-\frac{1}{2}} + X_7 \tag{5.4.284}$$

5.4.1 From velocity integrals

The leading term in the displacement and momentum thicknesses expressions, X_1 and X_3, due only to the outer forms, were determined. We took for this purpose two profiles from SMITH and WALKER at high Reynolds' numbers, that exhibited a good behavior for the velocity derivative function, and extended the power region down to the wall. We remind the reader that the Reynolds' numbers taken for the computations may not be characteristic of a true asymptotic behavior. The following results were obtained:

$$X_1 = 0.128 \tag{5.4.285}$$

$$X_3 = 0.103 \tag{5.4.286}$$

One may think that the same procedure can be applied to X_2 and X_4, respectively the difference between the inner form of the velocity, i.e., the Law of the Wall, and the leading term in the matched region, i.e., the power law, and the difference between the same terms squared. An attempt was made in this sense, and will be described in the next section. But we can already state that these two constants are highly dependent on the value of the asymptotic power and the location (y,U) where the power law is reached.

5.4.2 From the boundary layer parameter and the friction coefficient

We chose to use a Gaussian Least Square Differential Correction algorithm (GLSDC) to determine these equations. We first briefly explain the algorithm.

Let us note X, the vector of unknowns to be determined, and $\overline{Y}$ the vector of the measurements, the overline indicates that the vector of measurements is considered to be noisy. We note Y, the noise-free measurements vector. Y is a function of X:

$$Y = F(X) \tag{5.4.287}$$

We note A the Jacobian of F:

$$A = \frac{\partial F}{\partial X} \tag{5.4.288}$$

At the k^{th} iteration, we compute:

$$\Delta X_{k+1} = \left(A^T W A\right)^{-1} A^T W \left(\Delta Y_k\right) \tag{5.4.289}$$

where W is a weight matrix and ΔY_k is given by:

$$\Delta Y_k = \overline{Y} - Y_k \tag{5.4.290}$$

with Y_k being the measurements vector computed from X_k . This enables us to determine a new value for X:

$$X_{k+1} = X_k + \Delta X_{k+1} \tag{5.4.291}$$

We chose to define the measurement vector as such, for $1 < i < p$:

$$Y_i = \Re_{\delta^*}(i) = \Re_{\delta^*}\left(\Re_{\delta,i}\right) \tag{5.4.292}$$

(being given by 5.4.281),

$$Y_{i-p} = \Re_\theta(i) = \Re_\theta\left(\Re_{\delta,i}\right) \tag{5.4.293}$$

(being given by 5.4.282),

$$Y_{i-2p} = \Re_x(i) = \Re_x\left(\Re_{\delta,i}\right) \tag{5.4.294}$$

(given by 5.4.283). and for $1 < j < m$:

$$Y_{j+3p} = \Re_z(j) = \Re_z\left(c_{f,j}\right) \tag{5.4.295}$$

(as given by 5.4.284). We note p, m, being respectively the number of velocity profiles and the number of friction measurements taken into account. We give here the non-zero components of the Jacobian. For $1 < i < p$:

$$A(i,1) = \Re_{\delta,i} \tag{5.4.296}$$

$$A(i,2) = \Re_{\delta,i} \tag{5.4.297}$$

$$A(i+p,2) = -1 \tag{5.4.298}$$

$$A(i+p,3) = \Re_{\delta,i} \tag{5.4.299}$$

$$A(i+p,4) = -\left(\Re_{\delta,i}\right)^{-\frac{1}{2(X_6-1)}} \tag{5.4.300}$$

$$A(i+p,6) = -\frac{1}{2(X_6-1)^2} \ln\left(\Re_{\delta,i}\right) X_4 \left(\Re_{\delta},i\right)^{-\frac{1}{2(X_6-1)}} \tag{5.4.301}$$

$$A(i+2p,3) = \frac{X_6-1}{X_6} X_5 \left(\Re_{\delta,i}\right)^{\frac{X_6}{X_6-1}} \tag{5.4.302}$$

$$A(i+2p,4) = X_5 \left(\Re_{\delta,i}\right)^{\frac{1}{2(X_6-1)}} \tag{5.4.303}$$

$$A(i+2p,5) = \frac{X_6-1}{X_6} X_3 \left(\Re_{\delta,i}\right)^{\frac{X_6}{X_6-1}} + X_4 \left(\Re_{\delta,i}\right)^{\frac{1}{2(X_6-1)}} \tag{5.4.304}$$

$$\begin{aligned} A(i+2p,6) &= \frac{1}{X_6^2} X_3 X_5 \left(\Re_{\delta,i}\right)^{\frac{X_6}{X_6-1}} \\ &-\frac{1}{(X_6-1)^2} \frac{X_6-1}{X_6} X_3 X_5 \ln\left(\Re_{\delta,i}\right) \left(\Re_{\delta,i}\right)^{\frac{X_6}{X_6-1}} \\ &-\frac{1}{2(X_6-1)^2} X_4 X_5 \ln\left(\Re_{\delta,i}\right) \left(\Re_{\delta,i}\right)^{\frac{1}{2(X_6-1)}} \end{aligned} \tag{5.4.305}$$

$$A(i+2p,7)=1 \tag{5.4.306}$$

and for $1 < j < m$:

$$A(j+3p,3)=\frac{X_6-1}{X_6}X_5\ (X_5 c_{f,j})^{-X_6} \tag{5.4.307}$$

$$A(j+3p,4)=X_5\ (X_5\ c_{f,j})^{-\frac{1}{2}} \tag{5.4.308}$$

$$A(j+3p,5)=(1-X_6)\frac{X_6-1}{X_6}X_3\ (X_5\ c_{f,j})^{-X_6}-\frac{1}{2}X_4\ (X_5\ c_{f,j})^{-\frac{1}{2}} \tag{5.4.309}$$

$$A(j+3p,6)=\frac{1}{X_6^2}X_3X_5\ (X_5\ c_{f,j})^{-X_6}$$
$$-\frac{X_6-1}{X_6}X_3X_5\ \ln(X_5\ c_{f,j})\ (X_5\ c_{f,j})^{-X_6} \tag{5.4.310}$$

$$A(j+3p,7)=1 \tag{5.4.311}$$

GLSDC applied to the full expressions of the boundary layer parameters, x-dependence and friction coefficient

We used the GLSDC algorithm applied to the full expressions of equations 5.4.281, 5.4.282, 5.4.283, 5.4.284. 79 profiles parameters (the highest Reynolds' number has been excluded) were taken for the first three equations and 167 friction coefficient points were taken for the last one. The weight matrix is chosen such that the friction coefficient equation has the same overall weight as the other three equations. It is assumed that initial condition effects and tripping bias can be neglected especially in the x-depence equation.

The following results were obtained:

$$X_1=0.14075 \tag{5.4.312}$$

$$X_3=0.10277 \tag{5.4.313}$$

$$X_2 = -936.02 \tag{5.4.314}$$

$$X_4 = -2834.3 \tag{5.4.315}$$

$$X_5 = 152.05 \tag{5.4.316}$$

$$X_7 = -419235. \tag{5.4.317}$$

and

$$\gamma = 13.18 \tag{5.4.318}$$

Notice that the sign of both X_2 and X_4 are not correct. In addition, the value of X_1 is too high. A simple least square applied to the displacement and the momentum thicknesses gives:

$$\Re_{\delta^*} = 0.1257\,\Re_\delta + 2414. \tag{5.4.319}$$

$$\Re_{\delta^*} = 0.0999\,\Re_\delta + 1462. \tag{5.4.320}$$

which indicates clearly that the constant in the momentum thickness has the same sign as in the displacement thickness. The representation of the displacement thickness clearly shows that because we constrain both constants to have opposite signs, the slope of the displacement thickness is found to increase.

Enabling the X_2 constant to have different values in the two equations 5.4.281 and 5.4.282 yields the folowing results:

$$X_1 = 0.12742 \tag{5.4.321}$$

$$X_3 = 0.10277 \tag{5.4.322}$$

$$X_4 = -2837.7 \tag{5.4.323}$$

$$X_5 = 152.05 \tag{5.4.324}$$

$$X_7 = -420323. \tag{5.4.325}$$

and

$$\gamma = 13.18 \tag{5.4.326}$$

The constant in the displacement thickness equation comes out to be:

$$X_2 = 1966.3 \tag{5.4.327}$$

whereas the constant in the momentum thickness equation is:

$$X_2 = -2033.7 \tag{5.4.328}$$

which gives an overall positive sign for the constant in the momentum thickness equation. Moreover, X_1 has a value closer to the value obtained by integration of the velocity profile.

GLSDC applied to the expressions of the boundary layer parameters, x-dependence and friction coefficient only keeping the linear terms

Since X_2 and X_4 have unacceptable values, we considered only the linear terms in both the displacement and momentum equations and therefore the x-dependence and friction coefficient equations. Furthermore, we allowed the two constants to be different, 5.4.281, 5.4.282, 5.4.283 and 5.4.284 are transformed into:

$$\Re_{\delta^*} = X_1 \Re_\delta + Z_{21} \tag{5.4.329}$$

$$\Re_\theta = X_3 \Re_\delta - Z_{22} \tag{5.4.330}$$

$$\Re_x = \frac{1+\gamma}{1+3\gamma} X_3 X_5 (\Re_\delta)^{\frac{1+3\gamma}{1+\gamma}} + X_7 \tag{5.4.331}$$

$$\Re_x = \frac{1+\gamma}{1+3\gamma} X_3 X_5 \left(X_5 \frac{c_f}{2}\right)^{-\frac{1+3\gamma}{2\gamma}} + X_7 \tag{5.4.332}$$

The following constants were obtained:

$$X_1 = 0.12742 \tag{5.4.333}$$

$$X_3 = 0.10336 \tag{5.4.334}$$

$$X_5 = 152.00 \tag{5.4.335}$$

$$X_7 = -490757. \tag{5.4.336}$$

$$\gamma = 13.18 \tag{5.4.337}$$

$$Z_{21} = 1966.3 \tag{5.4.338}$$

$$Z_{22} = -695.11 \tag{5.4.339}$$

We will see that a good agreements with the experimental data is obtained in this case.

5.5 BOUNDARY LAYER PARAMETERS REPRESENTATIONS

See A.4

See A.4, Fig. 4.1.-

Boundary layer parameters of SMITH & WALKER, PURTELL and WIEGHARDT and TILLMANN are plotted. The friction coefficient, given by SMITH and WALKER in the velocity profile parameters table, as a function of the Reynolds' number, $\Re_\delta$, was plotted. As mentioned previously, the friction coefficient in this plot shows some scatter depending on the x-location.

The plots of $\Re_{\delta^*} vs. \Re_\delta$ and $\Re_\theta vs. \Re_\varepsilon$ shows a very good agreement between the different sets of data. However, a scatter appears in the shape ratio behavior, i.e., the ratio of the displacement thickness over the momentum thickness. Moreover, the shape factor of WIEGHARDT et al. is seen to be underestimated. As every experiment used has its own tripping and thickening procedure, no information can be obtained when plotting the Reynolds' number based on x, $\Re_x$, against the Reynolds' number based on the conventional boundary layer thickness, $\Re_\delta$. The friction coefficients of PURTELL et al., SMITH & WALKER and SCHULTZ and GRUNOW, as a function of a local variable, $\Re_\delta$, shows a good agreement in the overlap of the different sets.

5.5.1 Verification of COLES's analysis

See A.4, Fig. 4.2.-

We have plotted SMITH & WALKER's data with COLES' expression for the boundary layer parameter as well as for the friction coefficient. Note that because we are only interested in the asymptotic behavior and because there is some argument as far as the low Reynolds' number behavior is concerned, only the behavior for an constant shape parameter:

$$\Pi = 0.55 \tag{5.5.340}$$

i.e., for $\Re_\theta > 5500$, was represented.

We first note that, generally, see for instance COLES et al. (1968), only the shape parameter and the friction coefficient is shown in the literature. And, in fact, both the shape factor and the friction coefficient show a relatively good agreement with the data, although we may think that the log law result for the shape factor is not decreasing enough at high Reynolds number. However, it is striking that, although the shape factor exhibits a good behavior, the momentum and displacement thickness are both strongly underestimated. One may explain that scatter by the lack of rigor in the definition of the conventional boundary layer thickness, $\Re_\delta$. However, if such an argument is made, it has also to be made for the friction coefficient plot that does not exhibit such a scatter.

5.5.2 Power law verification

We represented the power law results for the boundary layer thicknesses and the friction coefficient for:

$$0 < \Re_\delta < 500000 \tag{5.5.341}$$

Undoubtedly, the results from the asymptotic power law should be verified at high Reynolds' numbers only.

See A.4, Fig. 4.3.-

As mentioned in the previous section, if all the terms in the boundary layer parameters equation are kept, the boundary layer displacement thickness yields a too high value for $[1 - I_O]$. This is clearly seen in the boundary layer thickness plot. It follows that the shape factor is overestimated.

See A.4, Fig. 4.4.-

If only the linear term in the momentum thickness expression are kept (the same terms being used in the friction coefficient and the x-dependence equations), consistent results with the boundary layer parameters, x-dependence and friction coefficient data are obtained.

5.6 INNER AND OUTER EXPANSIONS

See A.1, Fig. 15.-

We were interested to give the inner and outer form of the velocity. It appears in the boundary layer parameters calculations that, contrary to the traditional way of representing both forms, the matched term, i.e., the power law, is naturally subtracted from the inner form, i.e., the Law of the Wall, and the outer form, i.e. the Strict Similarity form, is not altered and gives the asymptotic value of the shape factor. We therefore represented the outer form with its extension into the matched layer and the inner form where the leading term in the matched layer was subtracted.

It is thought that if one combines these two representations in a composite velocity form, a variable power law where the exponent is Reynolds' number dependent may be obtained. However, we are afraid that this procedure, if successful, may be used as being a valid argument. The present author strongly objects to these "velocity curve fit argument"[23]. A representation of the velocity derivatives exhibits more accurately the measurement technique deficiencies and consequently enables isolating more effectively the physics of the flow. Integral quantities, which minimizes the noise (if it is not biased), independent friction coefficient measurements, or two point velocity measurements are more valid variables to be used. Nevertheless, we have represented both inner and outer form to have a better grasp of the physics involved in the different regions.

We have taken the outer form two profiles from SMITH & WALKER at high Reynolds' numbers. The velocity derivative exhibited for these profiles a nice smooth similarity behavior. We cut the velocity derivative at the point of tangency with the power law, at $U/U_\infty = 0.75$, and used the asymptotic power line in the matched region. An asymptotic value of 1/12.67 was chosen for the exponent. Both velocity profiles exhibited remarkable similarity.

[23] It has been seen, in the velocity profile representations, that both a log law and a power law are potential candidate for the leading term in the matched region, if there is one. However, this may not be admitted if one only looks at the velocity profile in semi logarithmic axis.

For the inner region, since no measurement is going down to the viscous layer without wall interaction, we choose to use SPALART data, which exhibit a high degree of similarity in this region. The points were connected in a velocity derivative representation. The mean profile was then obtained by integration. From SPALART, were chosen the following points:

$$\begin{cases} y_+ = 0 & u_+ = 0 & y_+\frac{du_+}{dy_+} = 0 & \frac{d}{dy_+}\left(y_+\frac{du_+}{dy_+}\right) = 1 \\ y_+ = 10 & u_+ = 8.0 & y_+\frac{du_+}{dy_+} = 5.35 & \frac{d}{dy_+}\left(y_+\frac{du_+}{dy_+}\right) = 0 \\ y_+ = 20 & u_+ = 11.67 & y_+\frac{du_+}{dy_+} = 4.0 & \\ y_+ = 30 & u_+ = 13.10 & y_+\frac{du_+}{dy_+} = 3.12 & \\ y_+ = 40 & u_+ = 13.75 & y_+\frac{du_+}{dy_+} = 2.69 & \end{cases} \tag{5.6.342}$$

A fifth order polynomial, for $0 < y_+ < 10$, was found to verify all six first constraints:

$$P(y_+) = y_+ - \frac{489}{20000}\frac{1}{3!}y_+^3 + \frac{21}{3125}\frac{1}{4!}y_+^4 - \frac{87}{100000}\frac{1}{5!}y_+^5 \tag{5.6.343}$$

The terms in the series seem to be alternated, which makes an estimation of higher terms impossible. However, it is seen that the use of the velocity derivative enables to have an estimation of the velocity expansion at the wall.

The next points were joined either using a second or third order polynomial. The last point, where the inner form reaches the power law was chosen to be:

$$y_+ = 8000 \quad y_+\frac{du_+}{dy_+} = 2.25 \tag{5.6.344}$$

The arbitrariness in the choice of the last point, and in the choice of the connecting curve, should be minimized in the velocity profile since, in the integration scheme, $g(y_+)$ is divided by y_+. The true behavior of the inner form, however, is highly dependent on the asymptotic power and the last connecting curve, which has the major contribution in the estimation of $[I_{I1} - I_I]$ and $[J_{I1} - J_I]$.

Chapter 6 CONCLUSION

This conclusion is articulated around three points:

1. The A.I.P. applied to a Velocity Defect form for the outer flow yields a logarithmic law in the matched region, if applied to a Strict Similarity assumption, a power law for the matched region is obtained.

2. Velocity derivative representations show that both a logarithmic law region and a power law region exist. We have now to find out which one dominates the physics of the flow asymptotically.

3. The measurement errors due to the total pressure probe technique prevent us from drawing any definite conclusion.

Furthermore, suggestions and remarks are made for future work.

1.

In light of what has been done, both a logarithmic and a power law appear to be valid candidates for the leading term in the matched expansion, if such a process is legitimate.

Using the *Asymptotic Invariance Principle*, we have shown that:
— A Velocity Defect form for the outer flow yields a logarithmic law in the matched region.
— A Strict Similarity assumption yields a power law in the matched region.

The questions that remain to be answered are the following:
—From a mathematical point of view, which expression for the outer form of the velocity is more legitimate, a Velocity Defect or a Strict Similarity?
—Or, from an experimental point of view, is the power law region or the logarithmic region to dominate the physics of the flow at high Reynolds' numbers?

2.

From SPALART direct simulations, we have seen that Van KARMAN's constant is found to vary slightly at low Reynolds' numbers. On the other hand, for moderate Reynolds' numbers, the power of the velocity profile is shown to vary substantially. This can not however be an argument to ban the power law as a candidate for the leading term in the matched expansion.

If we consider the velocity profiles, both laws appear to give a reasonable description of the profile in the matched layer. The friction coefficient can also be described accurately by both laws. The most information is learned however from the velocity derivatives. Undoubtedly, we see from a velocity derivative representation that both a power law region and a logarithmic law region exist. PURTELL's most defined profiles, seem even to indicate that a power law may be more appropriate than a log law as the leading term in the matched region.

3.

Because it contained a large range of moderate and high Reynolds' numbers, SMITH & WALKER (1958) velocity measurements, taken with a total head tube, were used. The viscous layer ($0 < y_+ < 20$) of the velocity derivative profile should be independent of the Reynolds' number. It is found that the lower part of SMITH and WALKER's data does not corroborate with the viscous layer behavior as recorded by SPALART.

The total head probe technique is therefore questioned, since the viscous layer behavior is not obtained. The matched layer measurements may be altered by this

device imperfections. We notice that it is fortunate for the logarithmic law theory that most experiments used to support that theory were actually conducted with a impact tube technique, which seems to create artificially a logarithmic behavior.

LANDWEBER's work (1960) on SMITH and WALKER data has already been mentioned. COLES (1968a) has an interesting discussion about the impact tube technique and the corrections schemes used sometimes. COLES finds a significant disagreement between the log law and the experimental data in the first 10 to 15% of the profile nearest the wall. He explains this scatter by wall interference and local turbulence effects, and consequently excludes that part of the profile in his least square computation of c_f, Π and δ for a given profile. More interestingly, although he does not deny the existence of both kind of errors, he objects using the corrections schemes: "Firstly, I do not approve of an uncritical application of the YOUNG-MAAS correction for displacement effects; and secondly, I do not know how to estimate errors in impact-probe measurements of mean velocity when the local turbulence level is high". According to COLES (1968a), trying to correct these effects to obtain the viscous layer behavior is probably useless. Moreover, it is pointed out that the corrections depend on the probe geometry (round or rectangular).

We have therefore to conclude that the total pressure tube deficiencies prevent us from drawing any definite conclusion as to the nature of the matched layer.

If we assume that the integral quantities, displacement and momentum thickness, are less influenced by measurement errors, those quantities should constitute more reliable parameters to take into account. But, as it has been seen in the previous chapter, both laws, the log law as presented in COLES analysis, and the power law using a composite form for the velocity are unable to predict to a satisfactory degree the flow parameters data used in this present work. We have therefore, after having examined critically our experimental data, to reconsider the theoretical analysis and its foundations.

If the integrated quantities are to be accurate enough for our purpose, the use of the composite velocity for the power law result is strongly questioned. Since only the boundary layer thicknesses are not verified, and since the friction coefficient data and x dependence seem to agree to a satisfactory degree, we conclude that the use of the composite form of the velocity may not be suited to our problem. The traditional approach, inner and outer expansion, with a matched region may also be questioned.

Some remarks...

Note that we did not use any singular perturbation scheme as such. Indeed, only the first order in the velocity derivative is considered. No assumptions have been made concerning higher orders. Moreover, the *Asymptotic Invariance Principle*, introduced in this work, yields a result consistent with MILLIKAN's theory.

Also, we may point out again the lack of experimental verification for the mathematical results that have been given in the literature. We already mentioned that GILL's assumptions have not been studied experimentally. In addition, for second order theories, we note that the leading term in the matched region is given in a Velocity Defect form without further justifications. Moreover, no work has been done computing the boundary layer parameters using a composite form for the velocity, and comparing the results to existing experimental data, and *a fortiori* no work has been done on the x-dependence of the boundary layer parameters and friction coefficient.

... and further suggestions

The discrepancy in the displacement and momentum thicknesses may indicate that a finer structure exists in the boundary layer, so that the use of a composite form for the velocity may be too crude a tool that does not reflect the whole structure of the boundary layer. Recent advances in mathematics, one may think of a triple deck method for a singular perturbation method or other more effective techniques, such as the Intermediate Asymptotics Method, may provide a better insight into the physics of a turbulent boundary layer.

We can only regret that the advantages of the hot wire technique have not been used to provide a more accurate description of the flow near the wall. Although we have seen that there is some wall interference in PURTELL's experiments, only the very viscous layer is affected, approximately $0 < y_+ < 10$, for the range of Reynolds' numbers used. It is expected that at higher Reynolds' numbers, the viscous layer can not be described by the same accuracy as in PURTELL's set of profile. Nevertheless, compared with a total pressure tube technique, the interaction with the wall will be significantly reduced.

Finally, since Direct Simulation allows so far only to compute low Reynolds' number flow, we can only hope that an experiment similar in the Reynolds' number range to those of SMITH and WALKER, is conducted using a hot wire probe. This would constitute valuable material for future turbulence research.

Bibliography

1. AFZAL Noor, 1976, "MILLIKAN's Argument at Moderately Large Reynolds' Number", Phys. Fluids, Vol. 19, pp. 600–602
2. AFZAL Noor and YAJNIK Kirit, 1973, "Analysis of Turbulent Pipe and Channel Flow at Moderately Large Reynolds' Number", J. Fluid Mech., Vol. 61, part 1, pp. 23–31
3. BUSH William B. and FENDELL Francis E., 1972, "Asymptotic Analysis of Turbulent Channel and Boundary Layer Flow". J. Fluid Mech., Vol. 56, part 4, pp. 657–681
4. BUSH William B. and FENDELL Francis E., 1973, "Asymptotic Analysis of Turbulent Channel Flow for Mean Turbulent Energy Closures", Phys. Fluids, Vol. 16, part 4, pp. 1189–1197
5. BUSH William B. and FENDELL Francis E., 1974, "Asymptotic Analysis of Turbulent Channel Flow for Mixing Length Theory", SIAM, J. Appl. Math. Vol. 26, pp. 314–427
6. CLAUSER Francis H., 1954, "Turbulent Boundary Layer in Adverse Pressure Gradients", J. Aero. Sci., Vol 21, pp. 91–108
7. CLAUSER Francis H., 1954, "The Turbulent Boundary Layer", Advances in Applied Mechanics IV, pp.1–51
8. COLE Julian D., 1968, "Perturbation Methods in Applied Mathematics", Blaisdell Publishing Company
9. COLES Donald E., 1956, "The Law of the Wake in Turbulent Boundary Layer", J. of Fluid Mech., Vol. 1, pp.191–226
10. COLES Donald E., 1962, "The Turbulent Boundary Layer in a Compressible Fluid", Rand Report R-403–PR
11. COLES Donald E. and HIRST E. A., 1968, "Proceedings of AFOSR-IFP-Stanford Conference on Computation of Turbulent Boundary Layers", Vol. II, Stanford University, Stanford, Ca.
12. COLES Donald E., 1968a, "The Young Person's Guide to the Data", in "Proceedings of AFOSR-IFP-Stanford Conference on Computation of Turbulent Boundary Layers", Vol. II, Stanford University, Stanford, Ca.
13. Van DYKE Milton, 1964, 1975, "Perturbation Methods in Fluids Mechanics", The Parabolic Press
14. FENDELL Francis E., 1972, "Singular Perturbation and Turbulent Shear Flow Near Walls", J. Astro. Sciences, Vol. 20, pp. 129–165

15. GEORGE William K., 1988, "Another Look at the Log (Or is it a Power Law?) Profile for the Zero Pressure Gradient Boundary Layer", Bulletin of the American Physical Society, V.33, No. 10, p. 2224.
16. GEORGE William K. and BOWER Daniel, 1989, "Another Look at the Log (Or is it a Power Law?) Profile for the Zero Pressure Gradient Boundary Layer", presentation manuscript for the 3rd Joint ASME/ASCE Mech. Conf. LaJolla, Ca
17. GILL A.E. (1968), "The Reynolds' Number Similarity Argument", J. Math. Phys. 47, pp. 437–441
18. HAMA Francis R., 1954, "Boundary-Layer Characteristic for Smooth and Rough Surfaces", Trans. Soc. Naval Architecs Marine Engrs. 62, pp.333–358
19. Von KARMAN Theodore, 1930a, "Mechanische Aehnlichkeit und Turbulenz", Nachr. Ges Wiss. Goetingen, pp. 68
20. Von KARMAN Theodore, 1930b, "Mechanishe Aehnlichkeit und Turbulenz", Proc. Third Intern. Congress for Appl. Mech., Stockholm, pp.8
21. KEMPF G., 1929, " Neue Ergebnisse der Widerstandsforschung", Werf, Reederei, Hafen Vol.10
22. KLEBANOFF P. S. and DIEHL Z.W., 1951, "Some Features of Artificially Thickened Fully Developed Turbulent Boundary Layer with Zero Pressure Gradient", N.A.C.A. Tech. Note 2475
23. KLINE S. J., MORKOVIN M. V., SOVRAN G., COCKRELL D. J., 1968, "Proceedings of AFOSR-IFP-Stanford Conference on Computation of Turbulent Boundary Layers", Vol. I, Stanford University, Stanford, Ca.
24. KLINE S. J., REYNOLDS W. C., SCHRAUB F. A. and RUNDSTALER P. W., 1967, "The Structure of Turbulent Boundary Layers", J. Fluid Mech., Vol. 30, part 4, pp. 741–773
25. LANDWEBER L., 1960, "Re-analysis of Boundary Layer Data on Flat Plate", Writen Discussion of the Ninth International Towing Tank Conference, Paris, 1960. Iowa Institute of Hydraulic Research, State University of Iowa.
26. LAUFER J., 1954, NACA Rep. 1174
27. LONG Robert R. and CHEN Tien-Chay, 1981, "Experimental Evidence for the Existence of the 'Mesolayer' in Turbulent Systems", J. Fluid Mech., Vol 105, pp. 19–59
28. LUND K.O. and BUSH William B., 1980, "Asymptotic Analysis of Plane COUETTE Flow", J. Fluid Mech., Vol. 96, pp. 81–104
29. MELLOR G.L., 1971, "The Large Reynolds' Number Asymptotic Theory

of Turbulent Boundary Layers", Department of Aerospace and Mechanical Sciences, Princeton University. Rep. no. 989.
30. MILLIKAN Clark B., 1938, "A Critical Discussion of Turbulent Flows in Channels and Circular Tubes", Proc. of 5th Int. Cong. Appl. Mech., pp. 386–392
31. MONIN A.S. and YAGLOM A.M., 1971, "Statistical Fluid Mechanics", Vol. 1, Massachusetts Institute of Technology Press
32. PANTON Ronald L., 1984, "Incompressible Flow", John Wiley & Sons
33. PATEL V.C., 1965, "Calibration of the PRESTON Tube and Limitations on its use in Pressure Gradients", J. Fluid Mech., Vol. 23, part 1, pp185–208
34. PERRY A. E. and ABBEL C.J., 1975, "Scaling Laws for Pipe", J. Fluid Mech., Vol. 67, part 2, pp.257–271
35. PHILLIPS W.R.C., 1990, " COLES' Hypothesis and the Turbulent Boundary Layer at Low Reynolds Number, manuscript, communication to W. K. GEORGE
36. PRANDLT L., 1932, "Zur Turbulenten Stromung in Rohren und langs Platten", Ergeb. Aerod. Versuch. Goettingen, IV Lieferung, pp.18
37. PURTELL L. P., KLEBANOFF P. S. and BUCKLEY F. T. (1981),"Turbulent Boundary Layer at Low Reynolds' Number", Phys. Fluids, 24, pp. 802–811.
38. SCHLICHTING Hermann, 1968. "Boundary Layer Theory", 6th Edition , Mc Graw Hill
39. SCHULTZ-GRUNOW F., 1941,"New Frictional Resistance Law for Smooth Plates", N.A.C.A. Tech. Memo. 986. translated from 1940, "Neues Reibungswiderstandsgezetz fur glatte Platten", Vol.17, No. 8, pp. 239–246
40. SPALART Philippe R., (1988), "Direct Simulation of a Turbulent Layer up to $\Re_\theta = 1410$", J. Fluid Mech., Vol. 187, pp. 61–98
41. STANTON T.E. and PANNEL J.R. (1914)"Similarity of Motion in Relation of the Surface Friction of Fluids", Phil. Trans. Roy. Soc. A 214, pg.199, see also (1915) Proc. Roy. Soc. London A91, pp. 46
42. SMITH Donald W. and WALKER John H., 1958, "Skin-Friction Measurements in Incompressible Flow", N.A.C.A. Tech. Note 4231
43. SMITS A.J., MATHESON N. and JOUBERT P.N., 1983, J.Ship Res., Vol. 127, pp. 3.
44. TENNEKES H., 1968, " Outline of a Second-Order Theory of Turbulent Pipe Flow", A.I.A.A.J., Vol. 6, pp. 1735–1740
45. TENNEKES H. and LUMLEY J.L., 1972, "A First Course in Turbulence",

Massachusetts Institute of Technology Press
46. TOWNSEND A.A., 1976, "The Structure of Shear Flow", Second Edition, Cambridge University Press
47. WIEGHARDT K., 1944, "Zur turbulente Reibungsschicht bei Druckansteig", Z.W.B., Kaiser-WILHELM-Institut fur Strommungsforschung, Gottingen, U&M 6617
48. YAJNIK Kirit S., 1970, "Asymptotic Theory of Turbulent Shear Flow". J. Fluid Mech., Vol 42, part 2, pp. 411–427

A.1 GENERAL FIGURES

Fig. 1.1.1 *On the determination of the friction coefficient*: from KLINE et al. (1967).

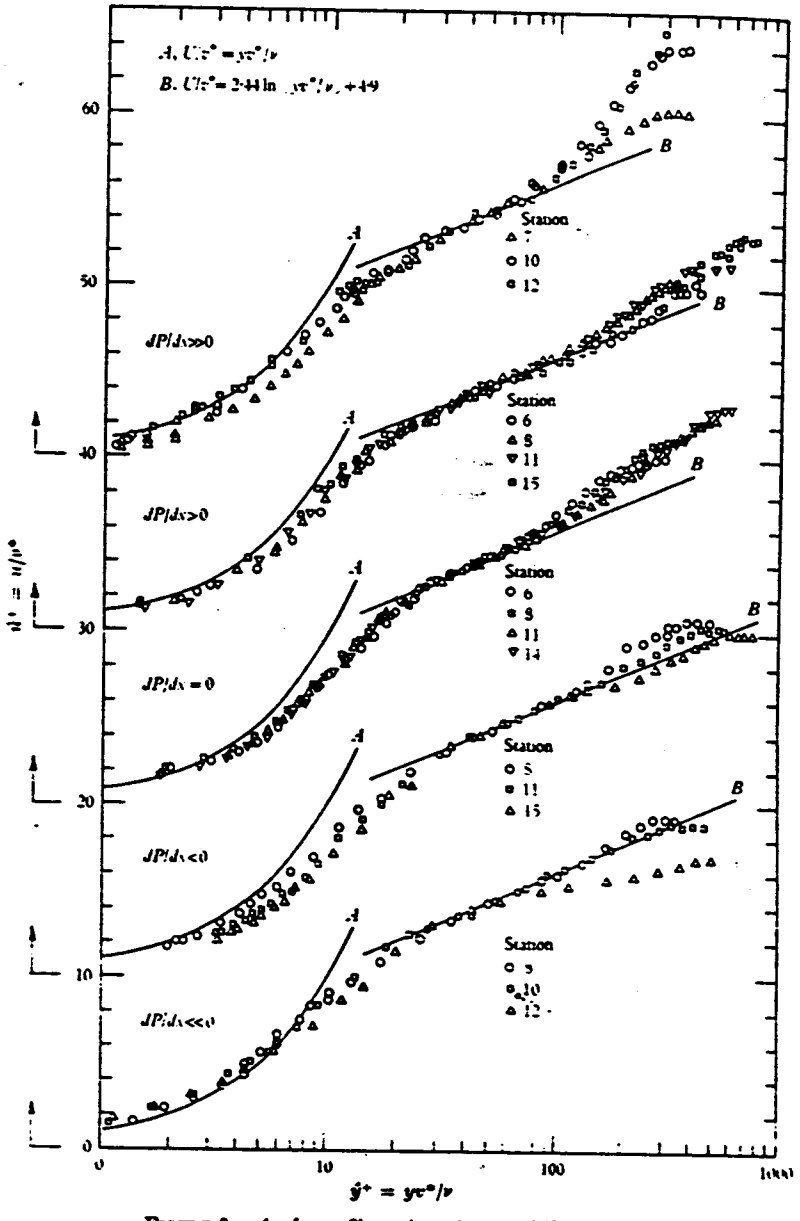

FIGURE 9a. $\hat{u}^+$–$\hat{y}^+$ profiles using v^* (note shifted origins).

Fig. 1.1.2 *On the determination of the friction coefficient*: from KLINE et al. (1967).

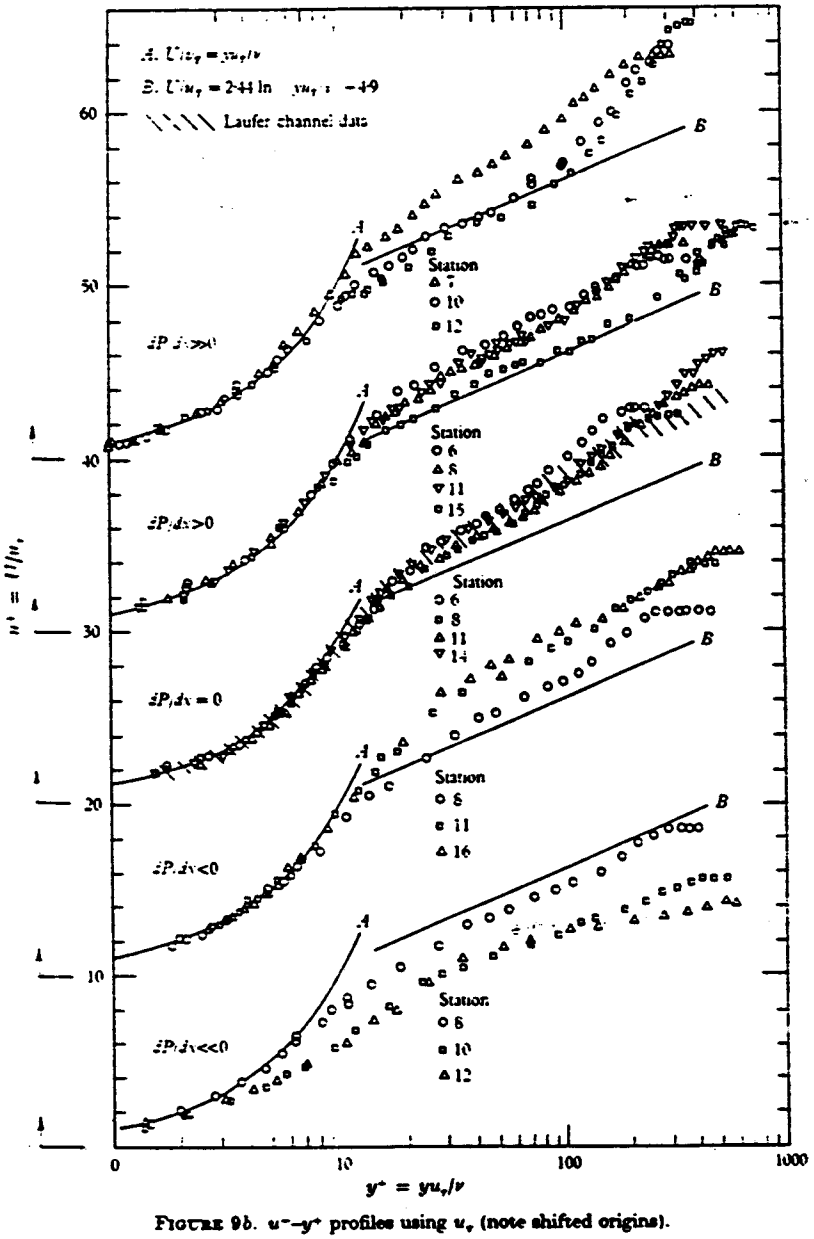

FIGURE 9b. u^+–y^+ profiles using u_τ (note shifted origins).

Fig. 1.2 *Velocity derivative from Direct Simulation:*

from SPALART (1988)

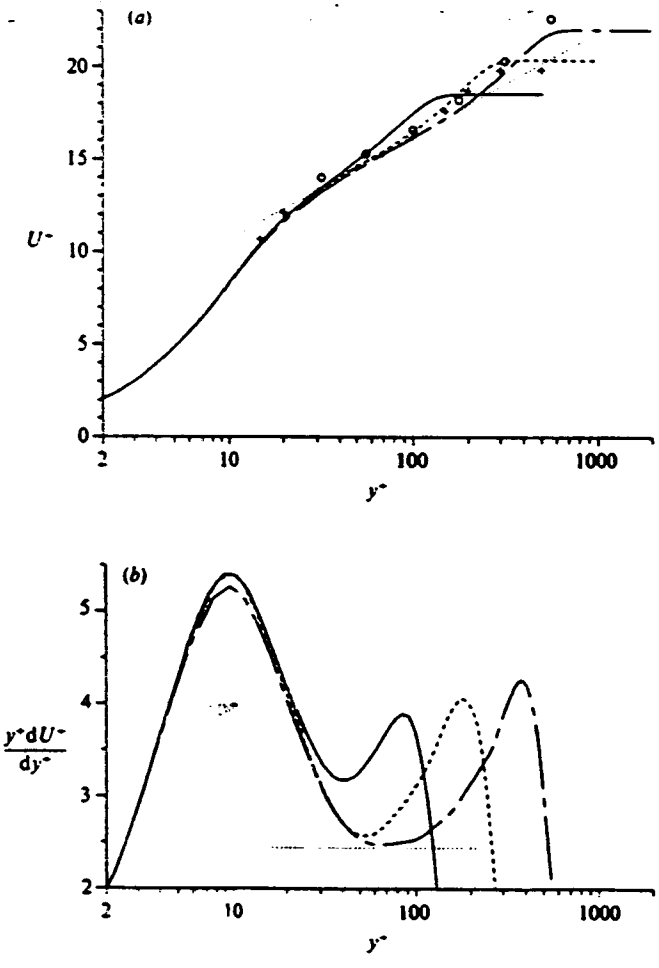

FIGURE 5. Mean-velocity profile and its derivative. ——. $R_\theta = 300$: – – –. $R_\theta = 670$: ——. $R_\theta = 1410$; ···, log law $U^+ = \log(y^+)/0.41 + 5$: +. $R_\theta = 617$ (Erm *et al.* 1985): ○. $R_\theta = 1368$ (Murlis *et al.* 1982). (*a*) U^+; (*b*) $y^+ dU^+/dy^+$.

Fig. 1.3 *Power behavior*

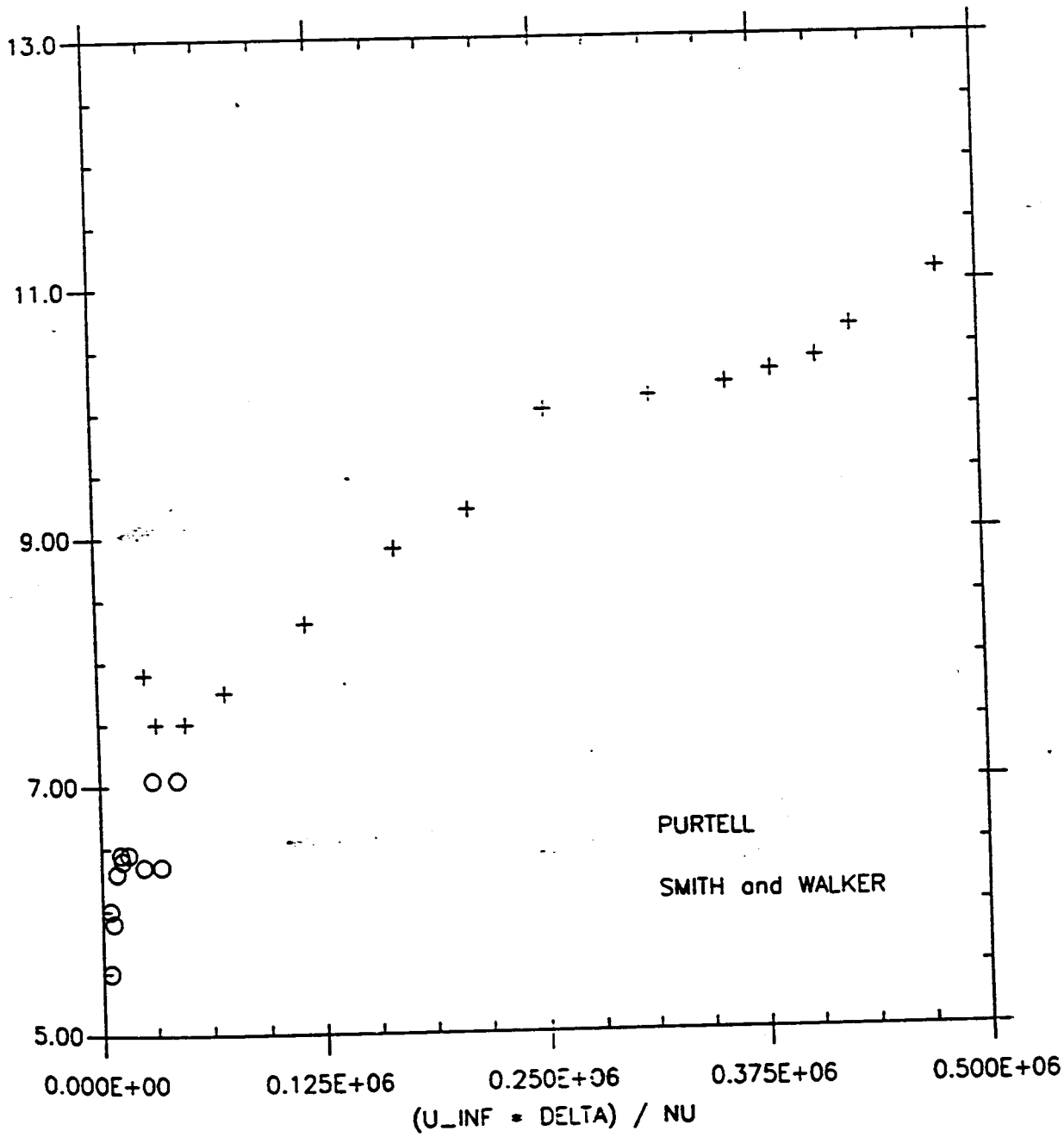

Fig. 1.4.1 *Velocity profiles obtained with a wall slope determined shear stress:*

Purtell et al.. Rth = 465, 498, 700, 1000,
1340, 1370, 1840, 2840, 3480, 4090, 5100.

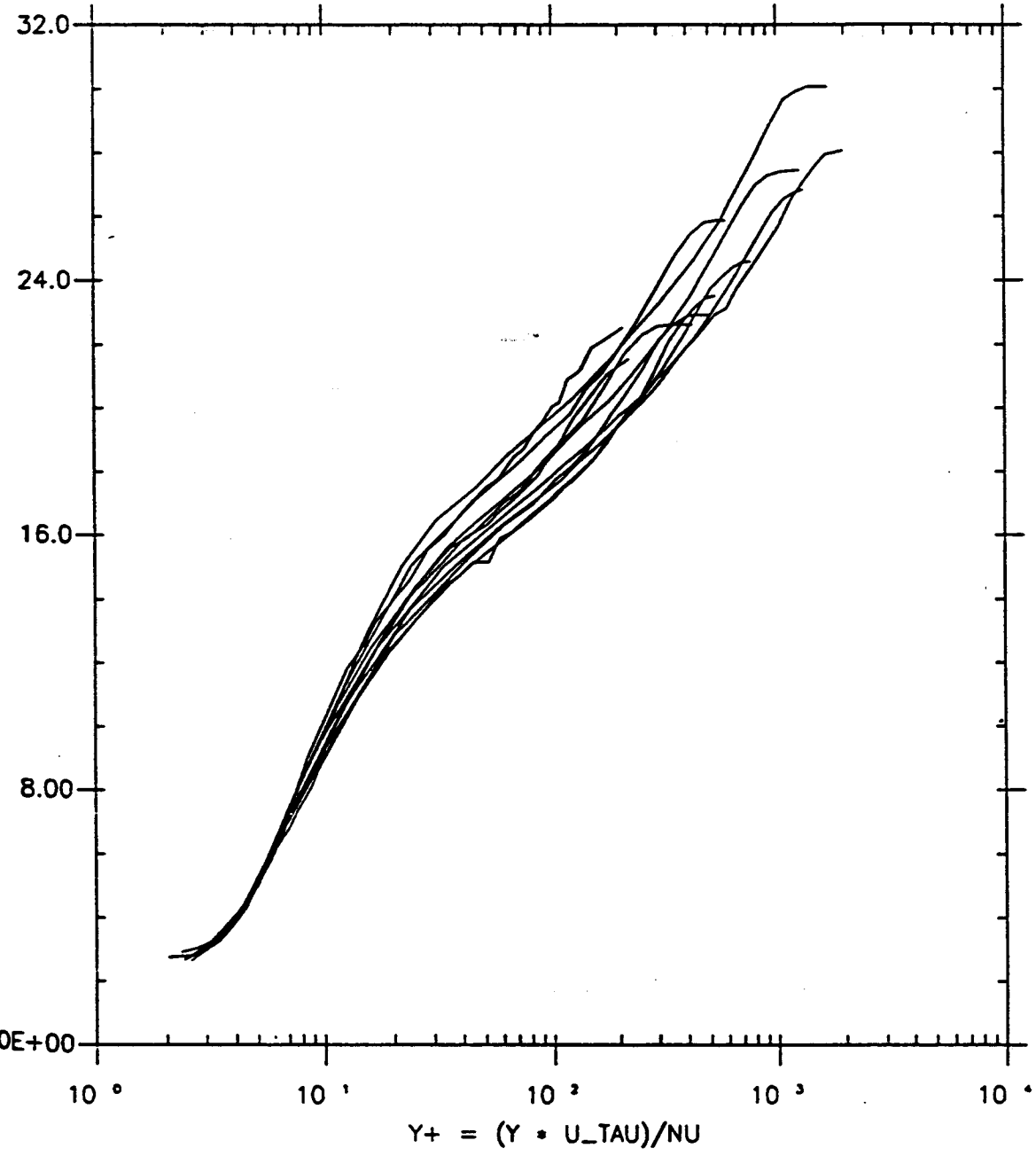

Fig. 1.4.2 *Velocity profiles obtained with a wall slope determined shear stress:* Purtell et al.. Rth = 1340, 1840, 3480, 5100.

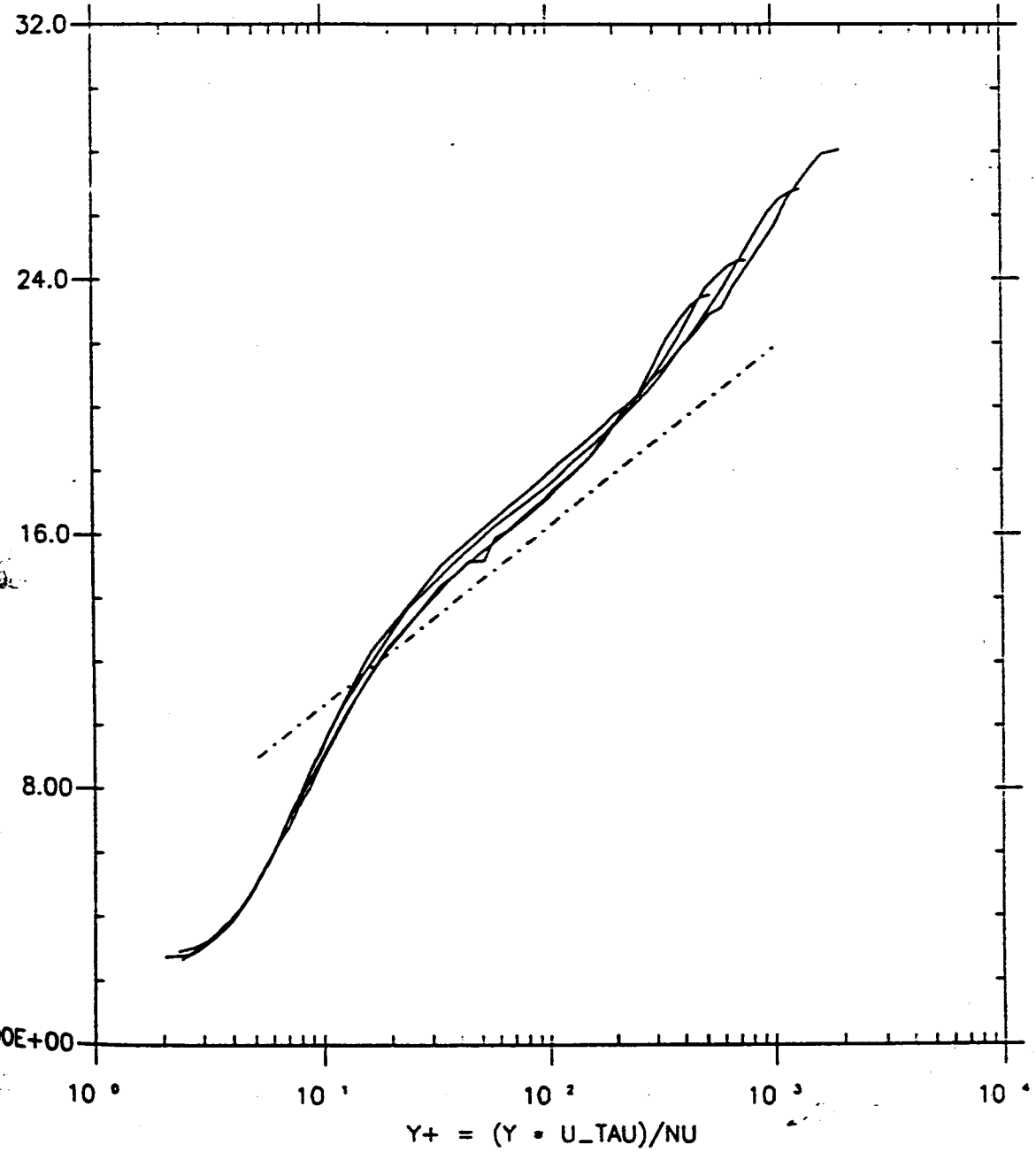

Fig. 1.4.3 *Friction coefficient obtained with a wall slope determined shear stress:*

Purtell et al., with friction coefficient as given by SMITH & WALKER.

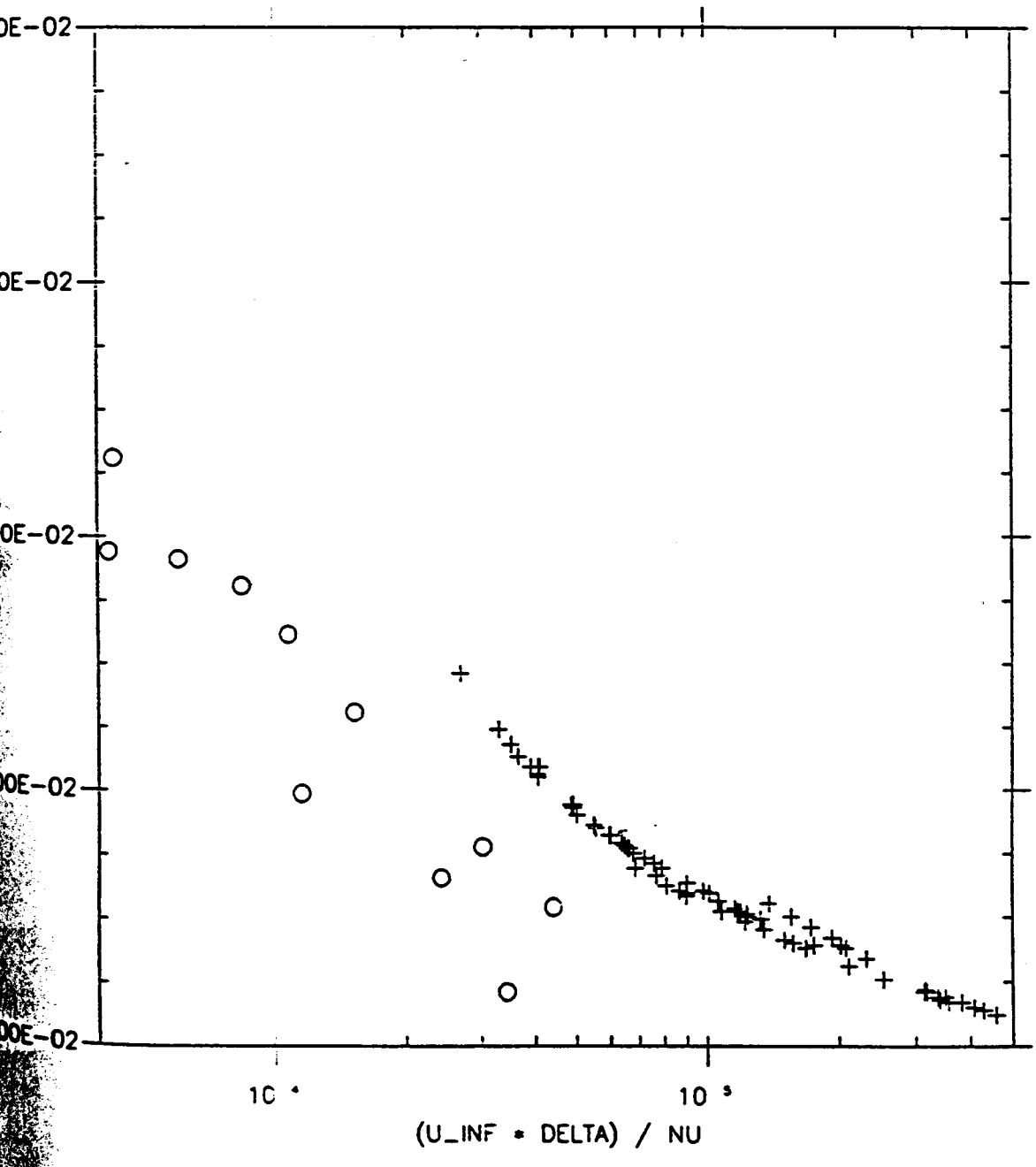

Fig. 1.5.1 *Inner expansion of the velocity derivative*

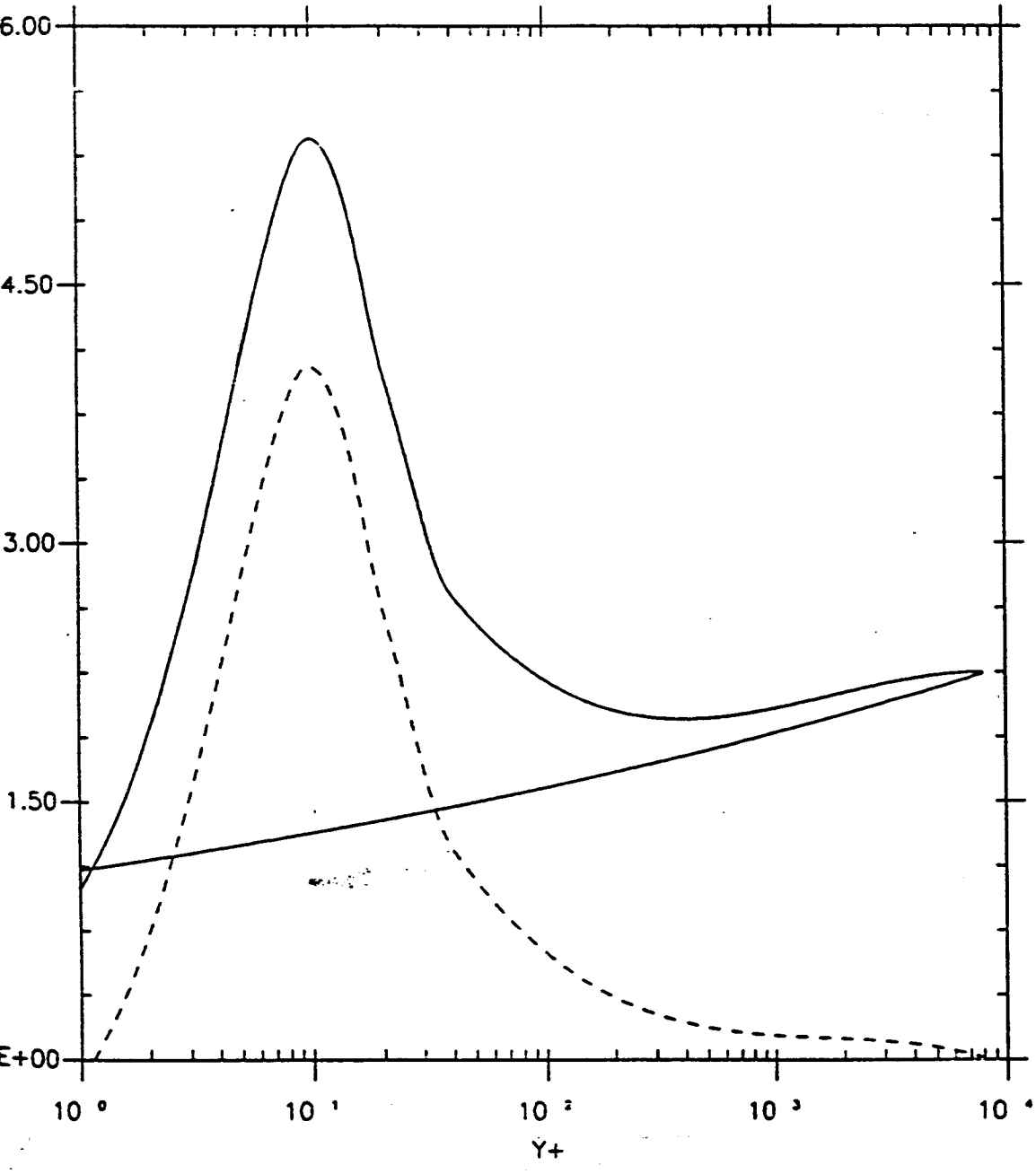

Fig. 1.5.2 *Inner expansion of the velocity*

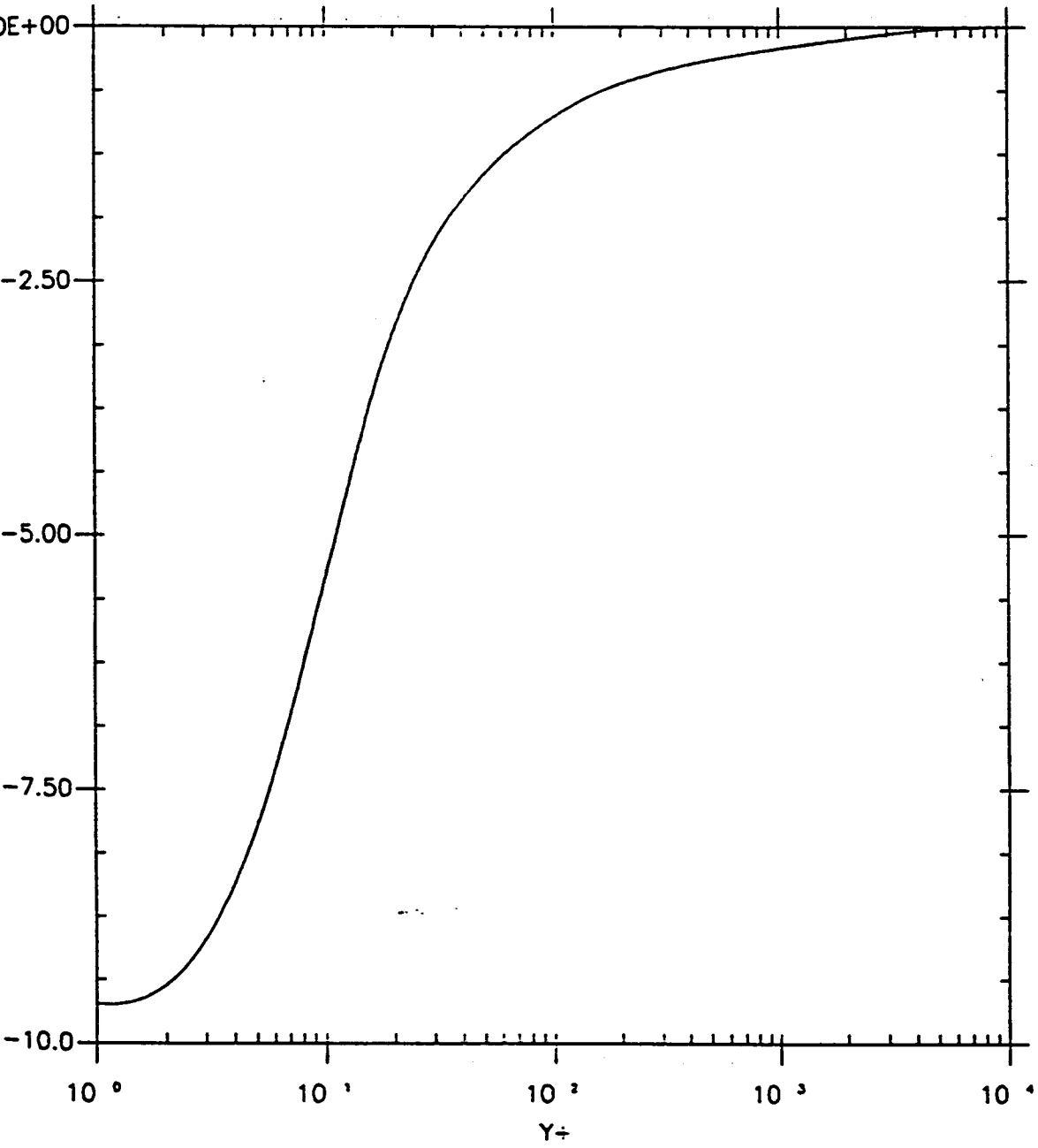

Fig. 1.5.3 *Outer expansion of the velocity derivative*

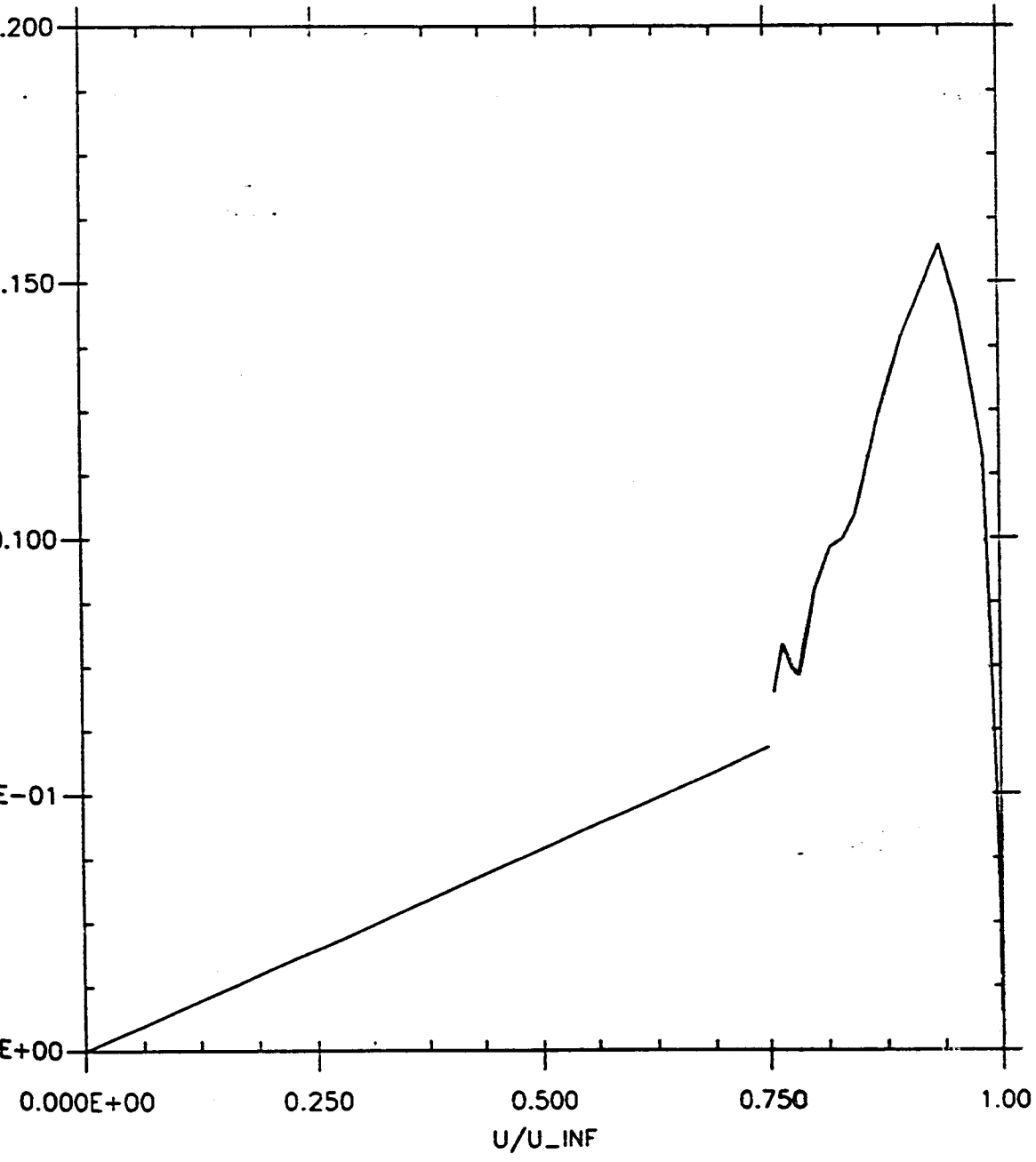

Fig. 2.1.1.1.1 *Velocity in inner variables with log law:*
Smith & Walker. Rth = 3005, 3815, 5680, 8175, 13040, 18340, 22510, 26510, 32280, 37190, 39800, 42610, 44750, 48290.

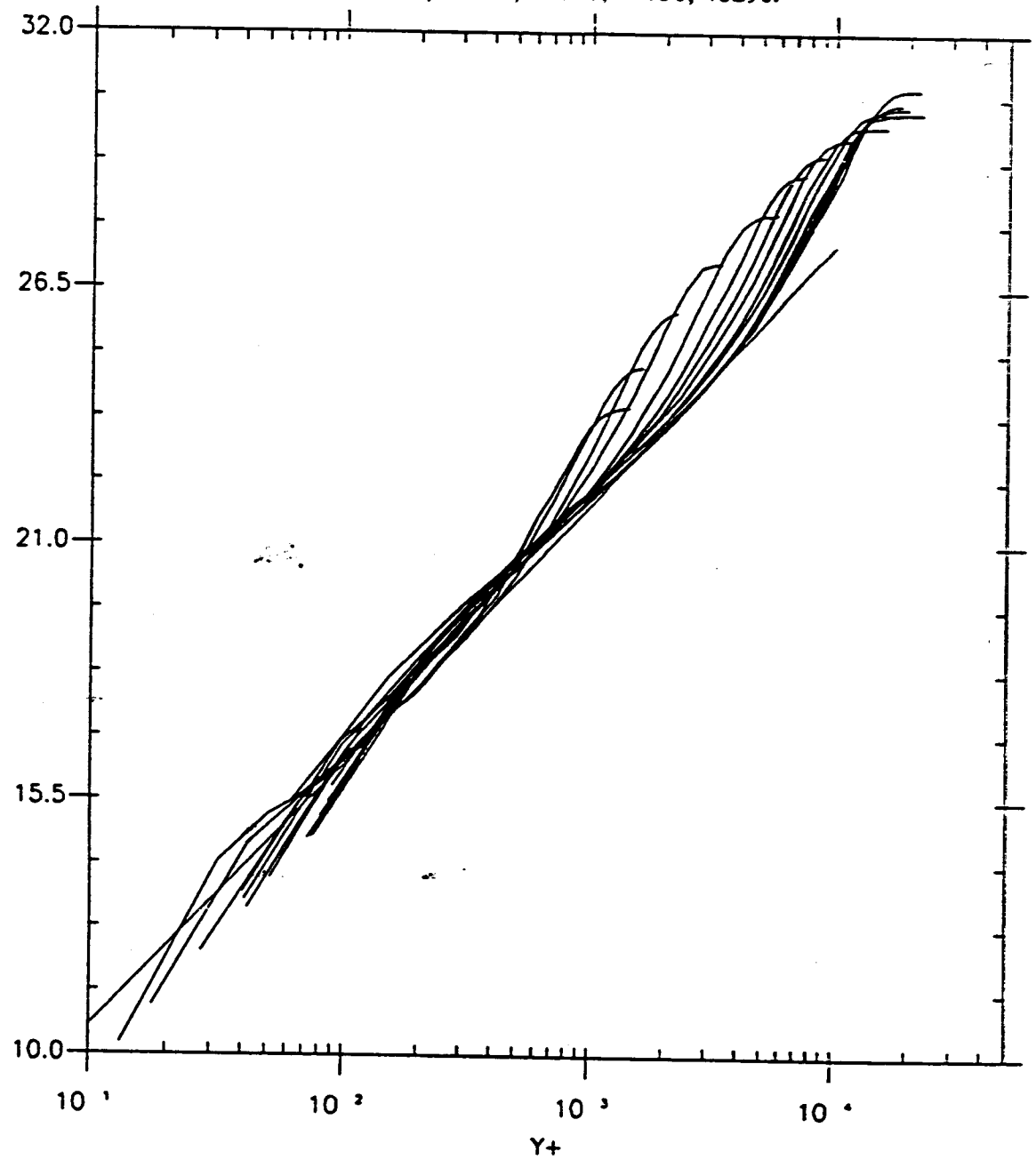

Fig. 2.1.1.1.2 *Velocity in inner variables with log law*:
Smith & Walker. Rth = 5680, 18340, 37190, 44750.

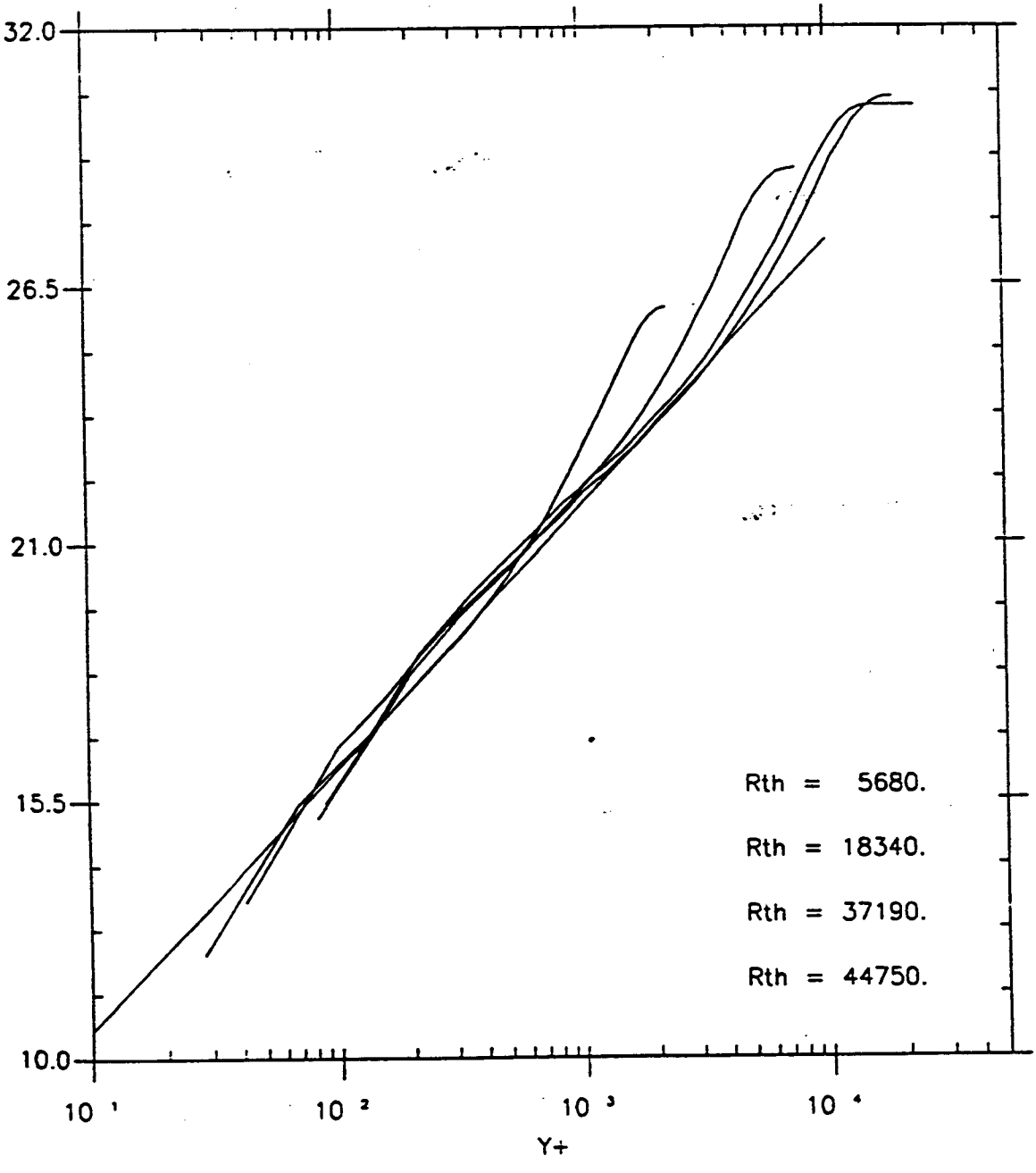

Fig. 2.1.1.2.03 *Velocity in inner variables with log law*:

Smith & Walker. Rth = 5680.

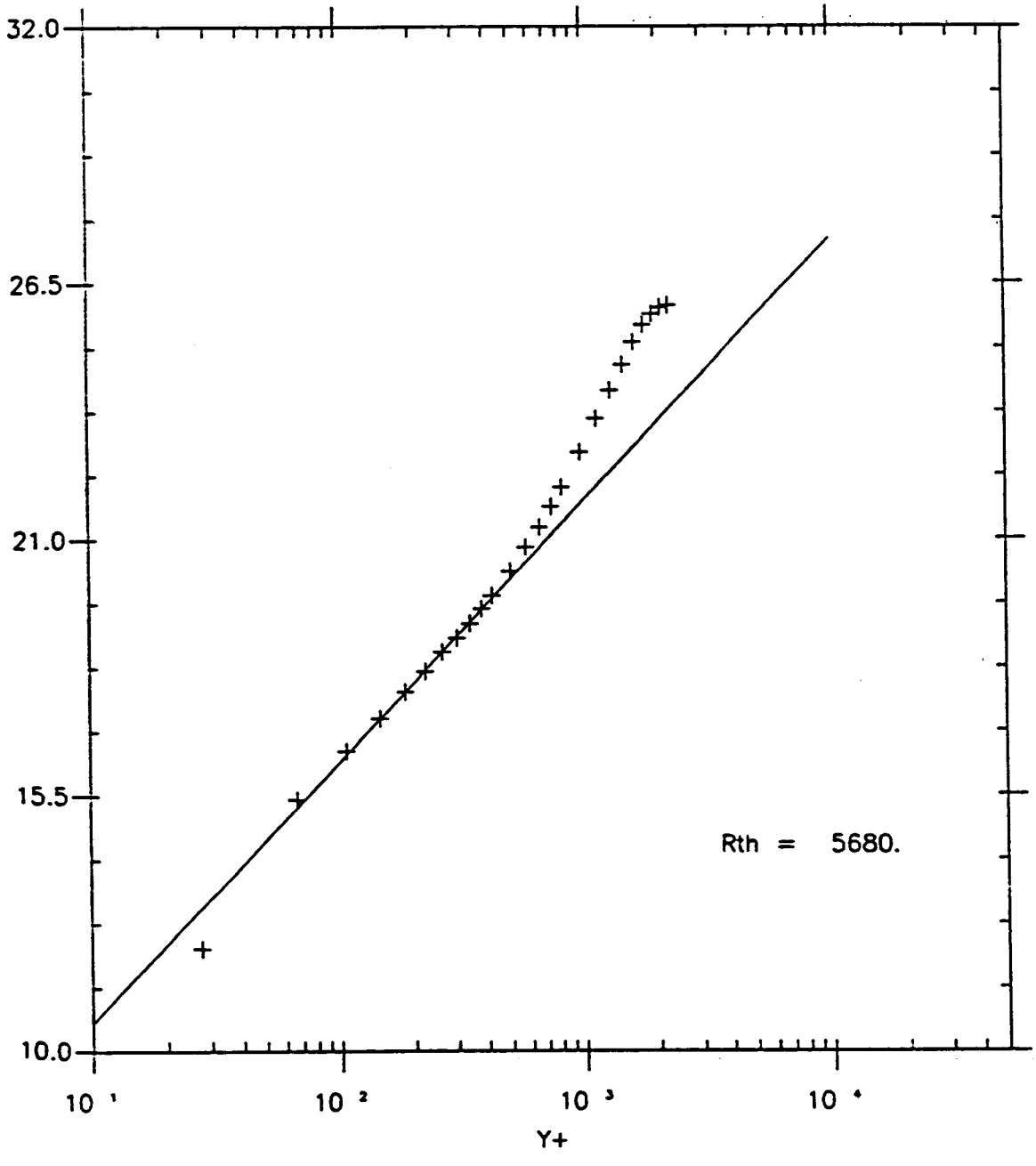

Fig. 2.1.1.2.06 *Velocity in inner variables with log law*:

Smith & Walker. Rth = 18340.

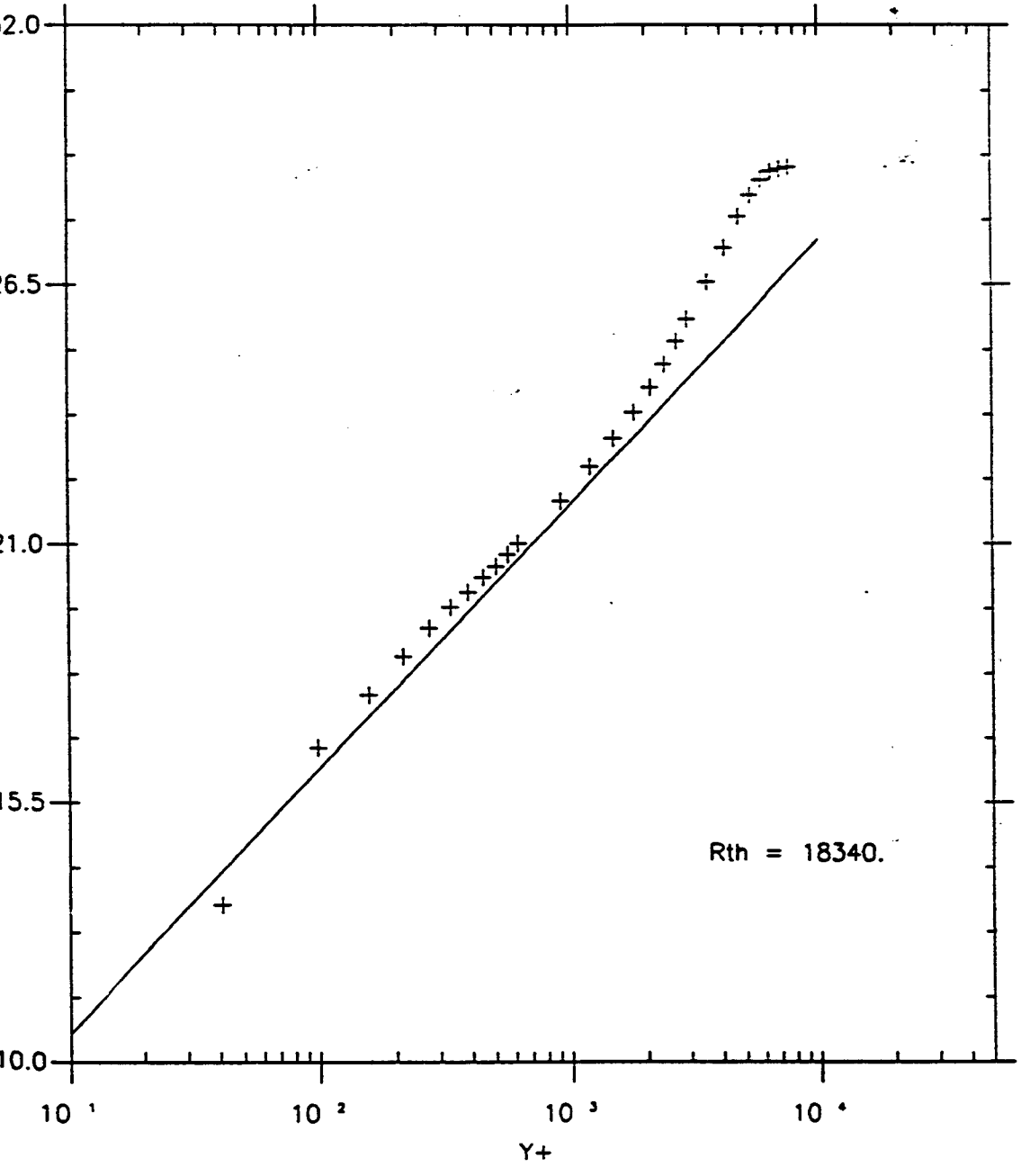

Fig. 2.1.1.2.10 *Velocity in inner variables with log law:*

Smith & Walker. Rth = 37190.

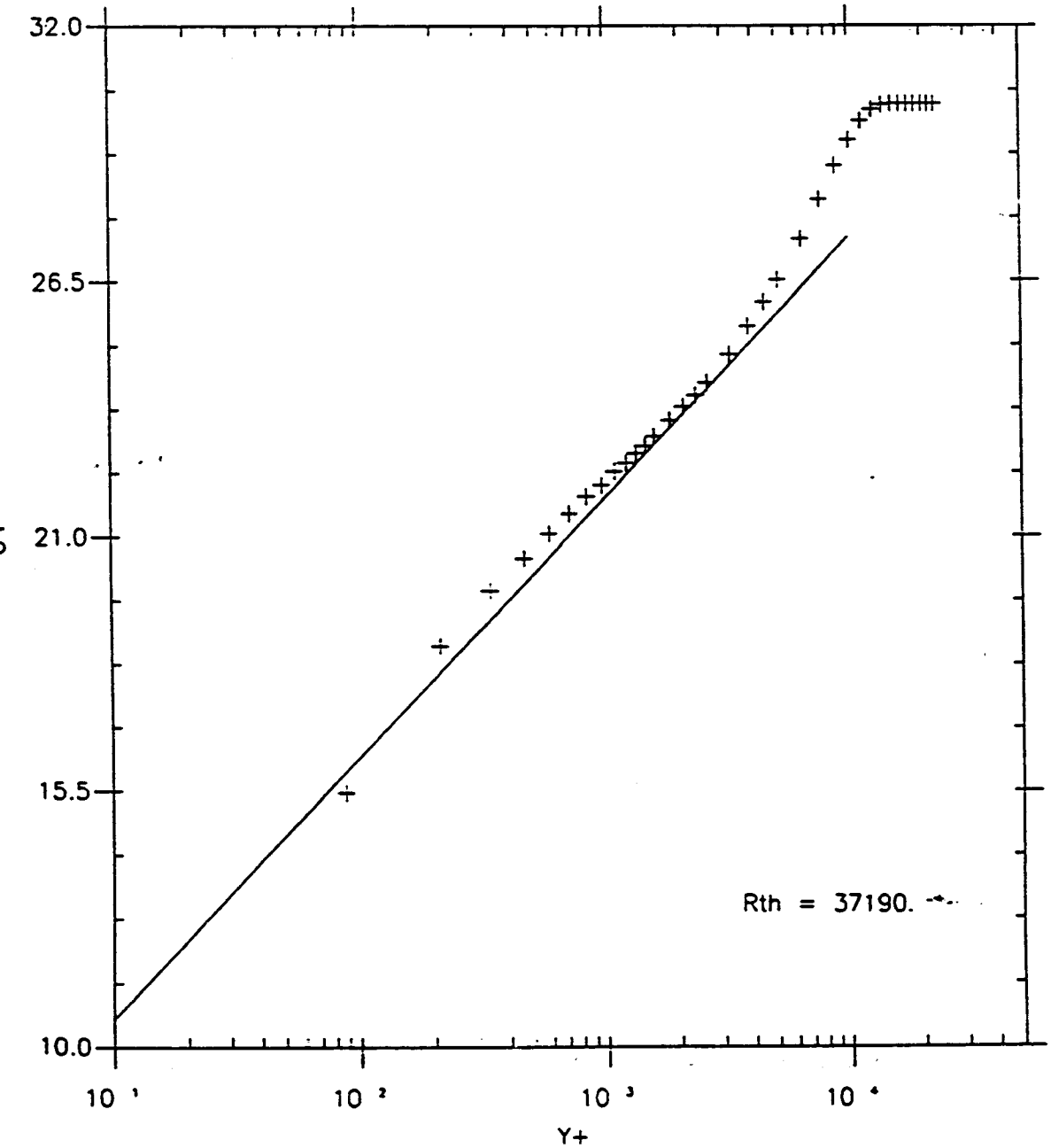

Fig. 2.1.1.2.13 *Velocity in inner variables with log law:*

Smith & Walker. Rth = 44750.

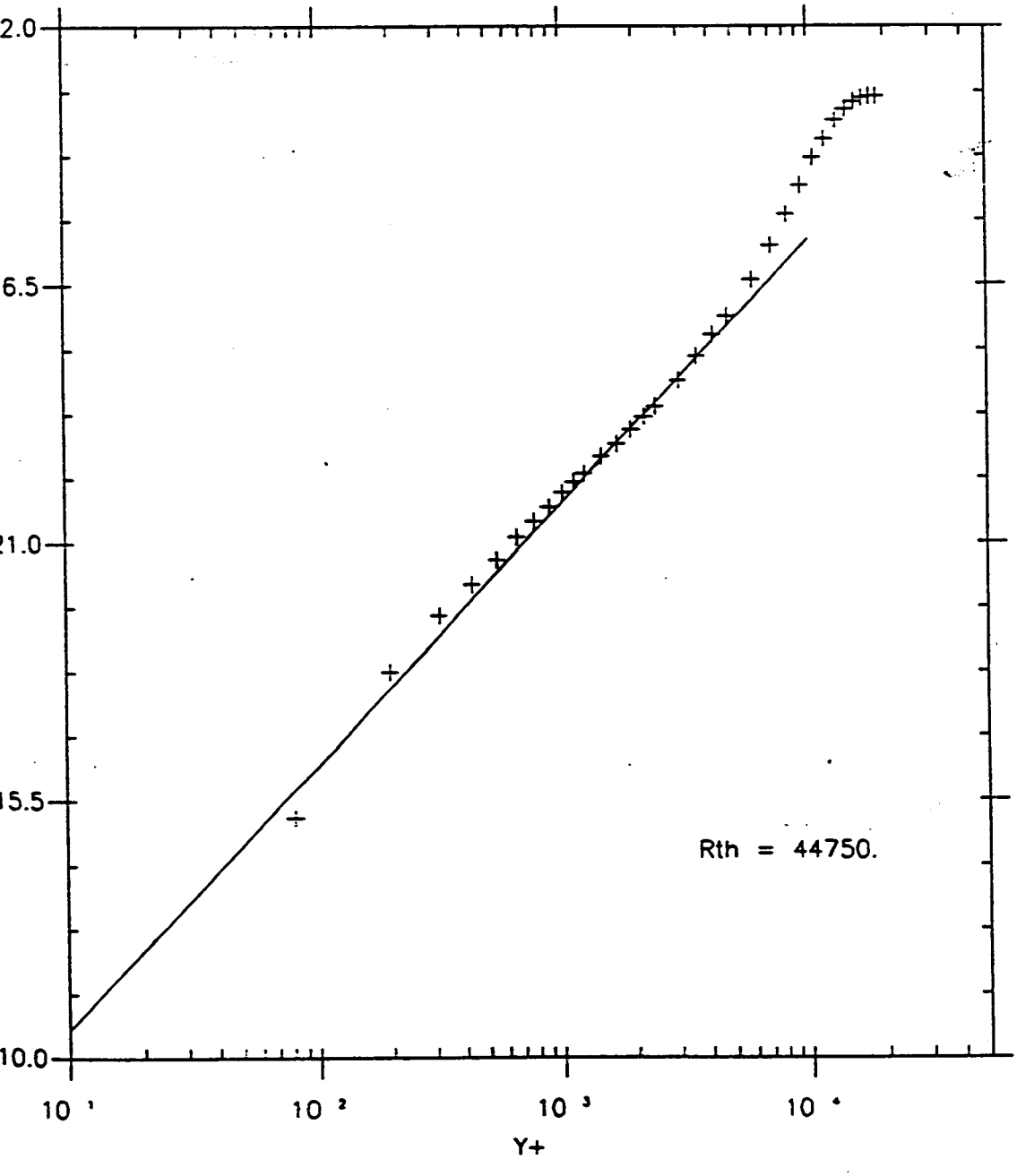

Fig. 2.1.2.1.1 *Velocity in inner variables with log law*:
Purtell et al.. Rth = 465, 498, 700, 1000, 1340, 1370, 1840, 2840, 3480, 4090, 5100.

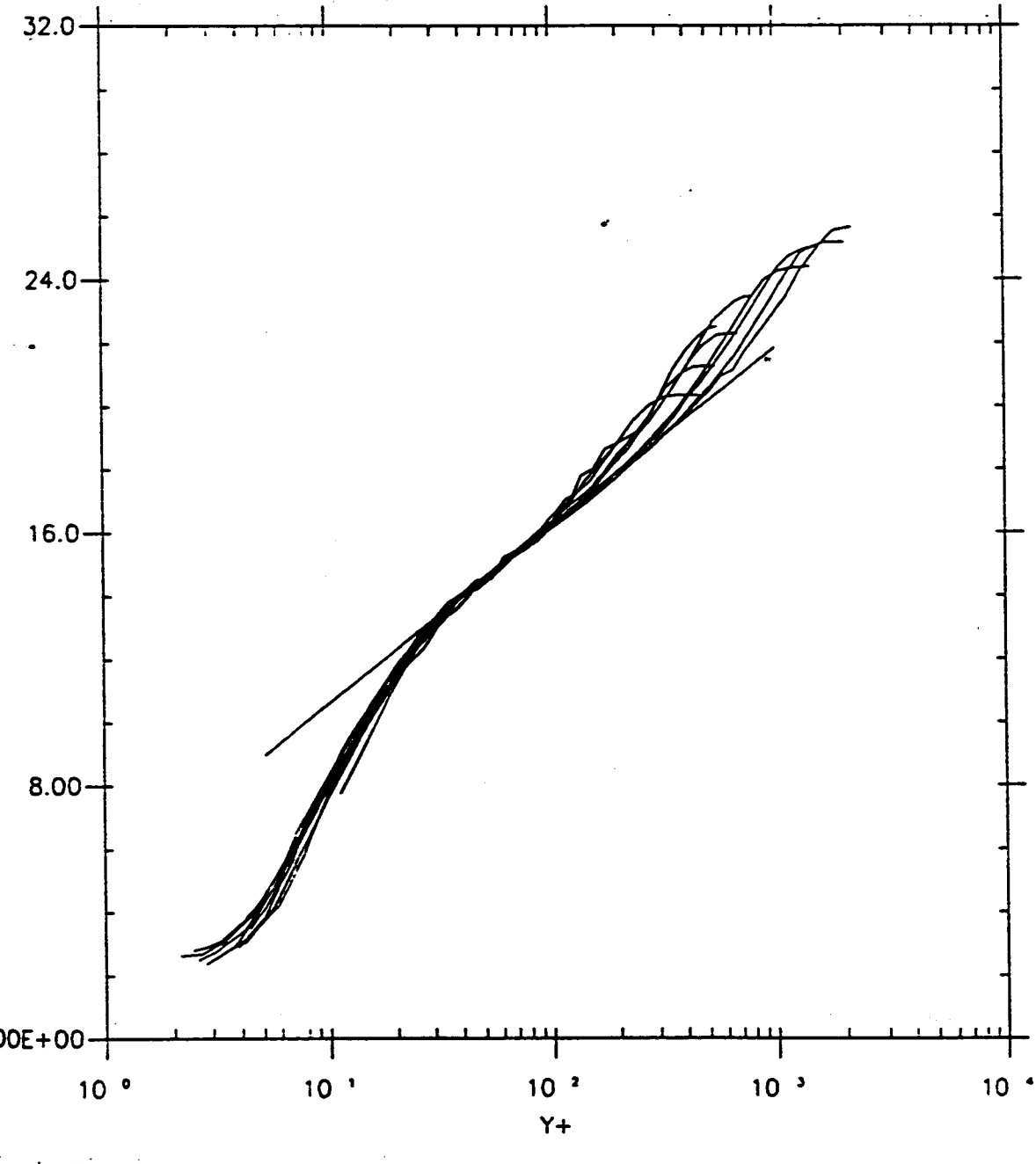

Fig. 2.1.2.1.2 *Velocity in inner variables with log law:*
Purtell et al.. Rth = 1340, 1840, 3480, 5100.

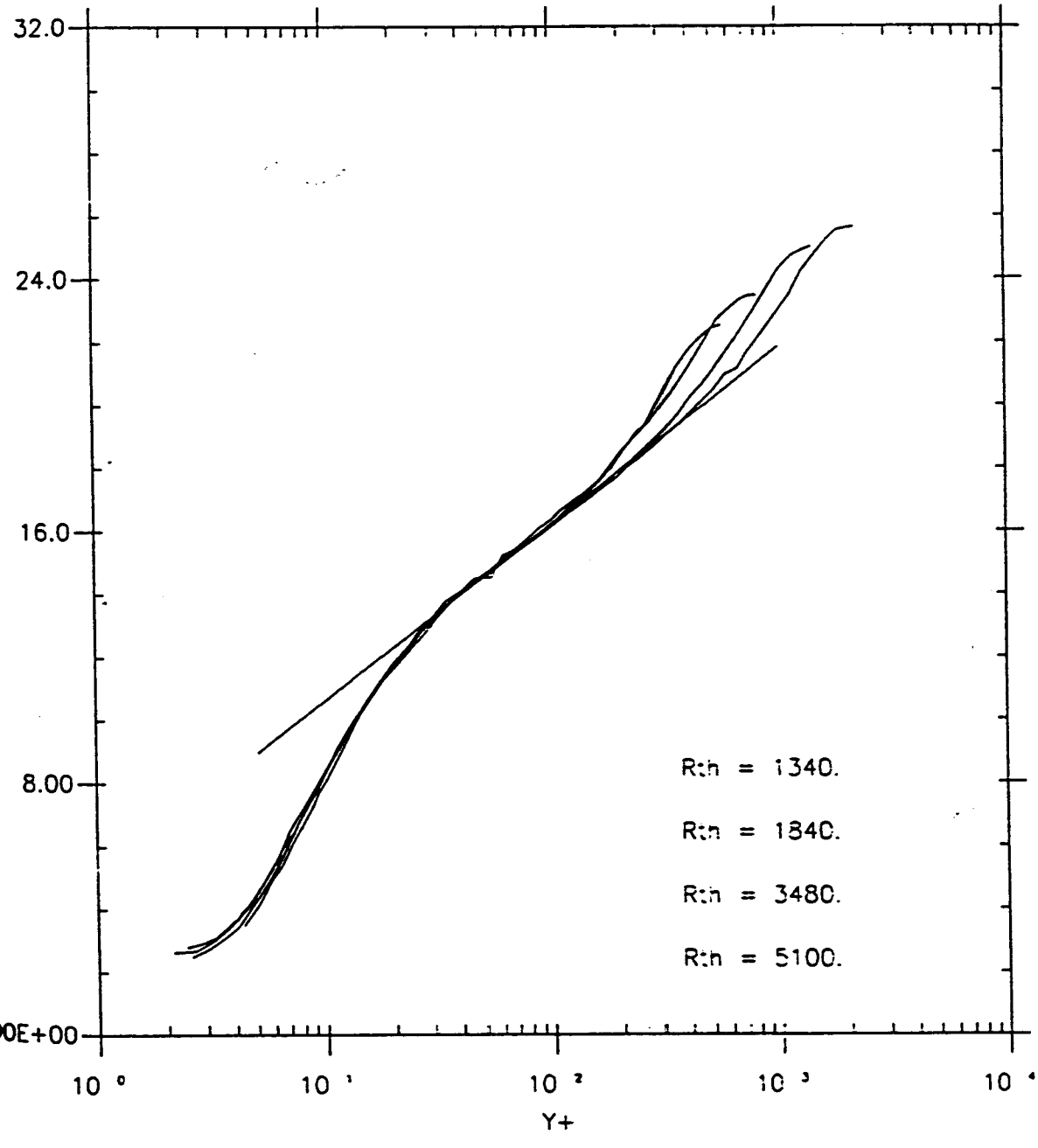

Fig. 2.1.2.2.05 *Velocity in inner variables with log law:*

Purtell et al.. Rth = 1340.

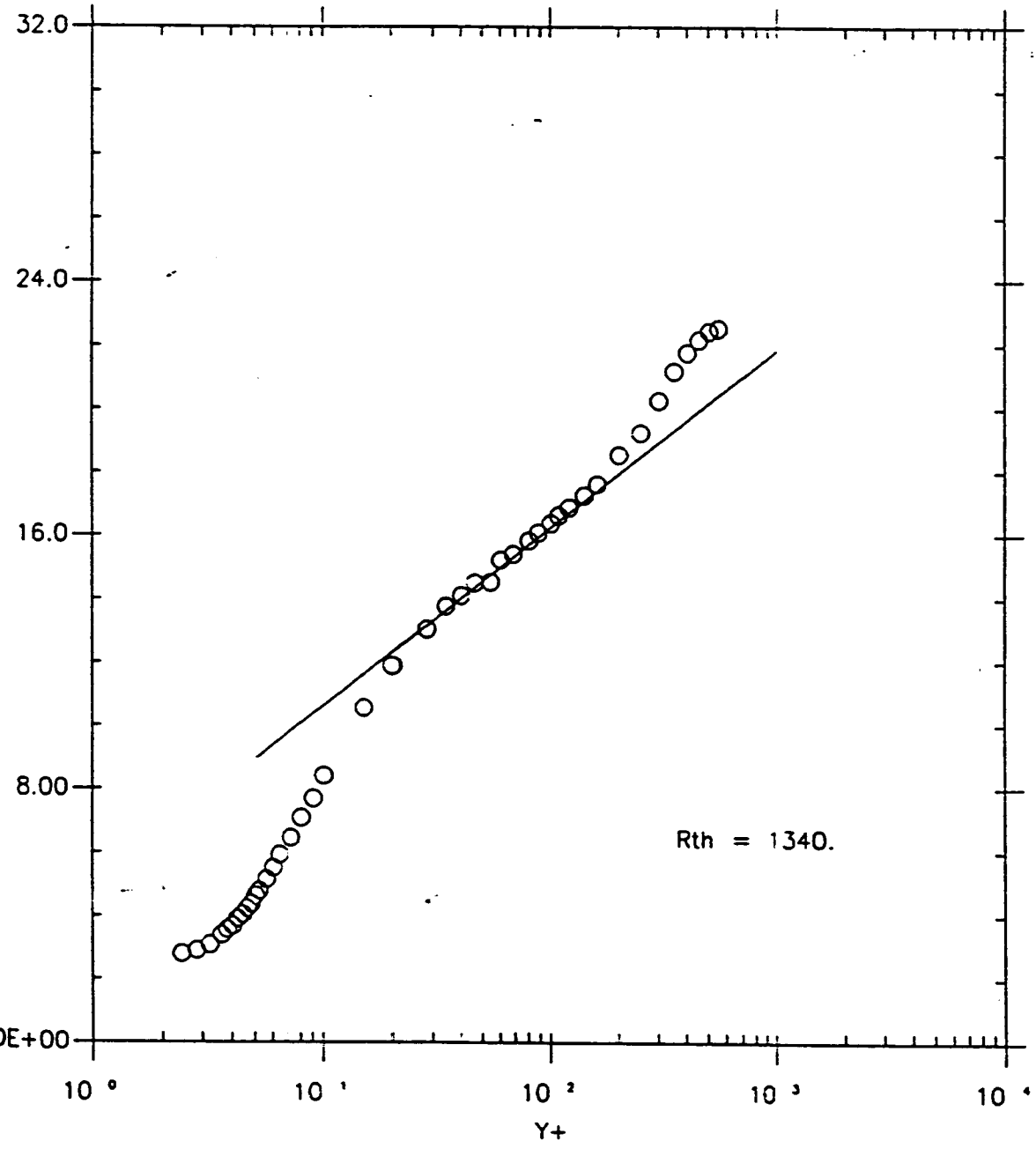

Fig. 2.1.2.2.07 *Velocity in inner variables with log law:*
Purtell et al.. Rth = 1840.

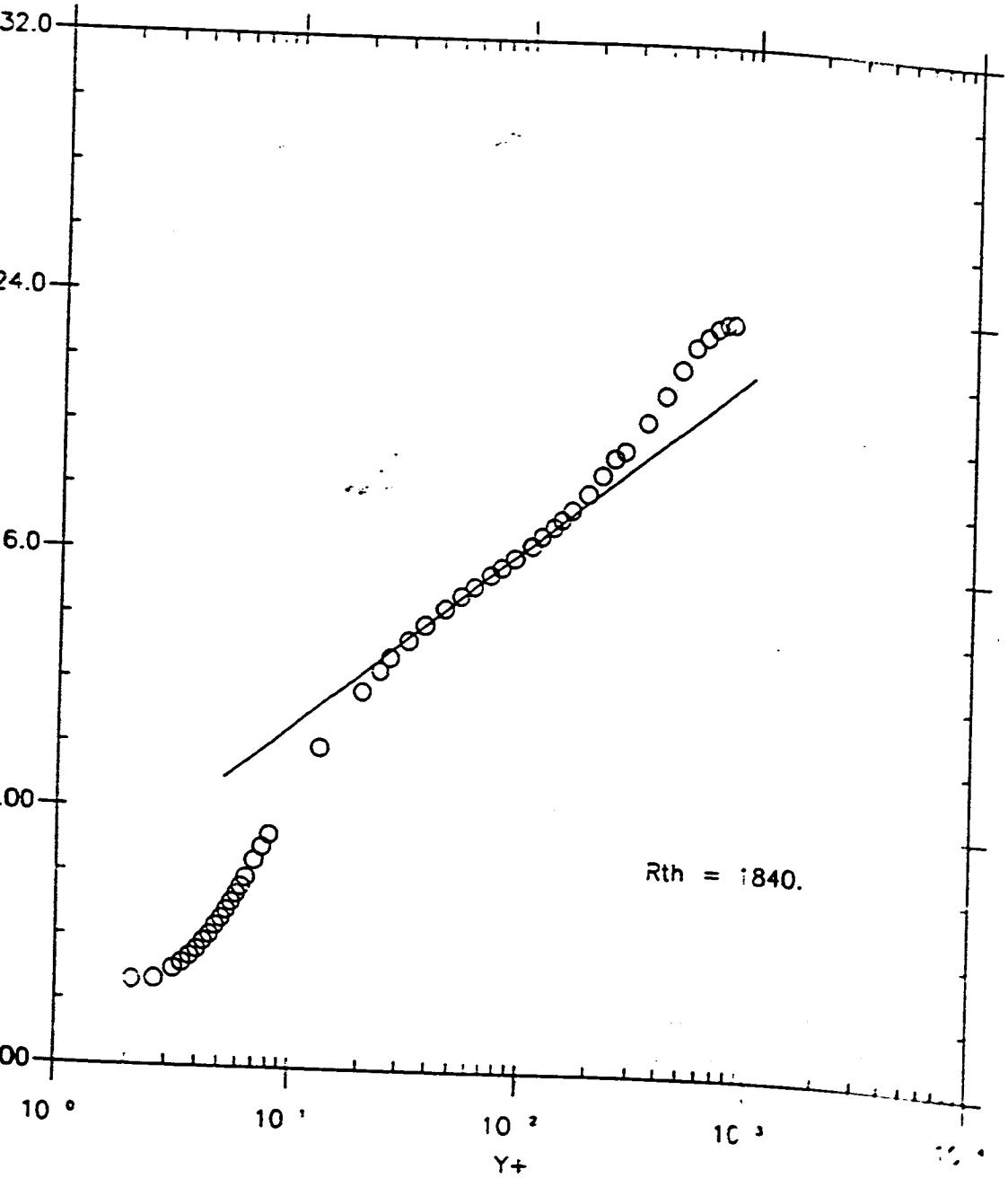

Fig. 2.1.2.2.09 *Velocity in inner variables with log law*:

Purtell et al.. Rth = 3480.

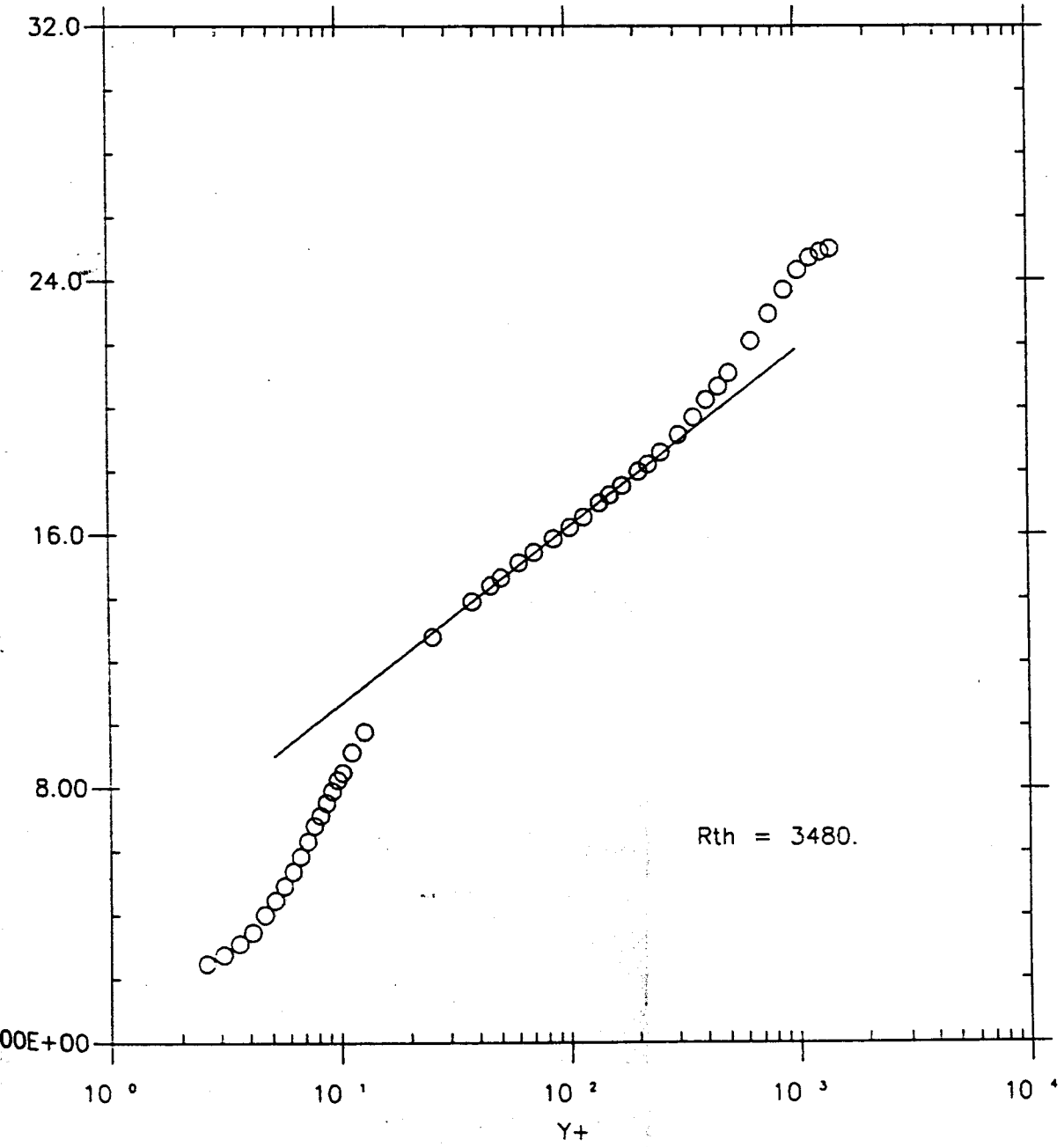

Fig. 2.1.2.2.11 *Velocity in inner variables with log law*:

Purtell et al.. Rth = 5100.

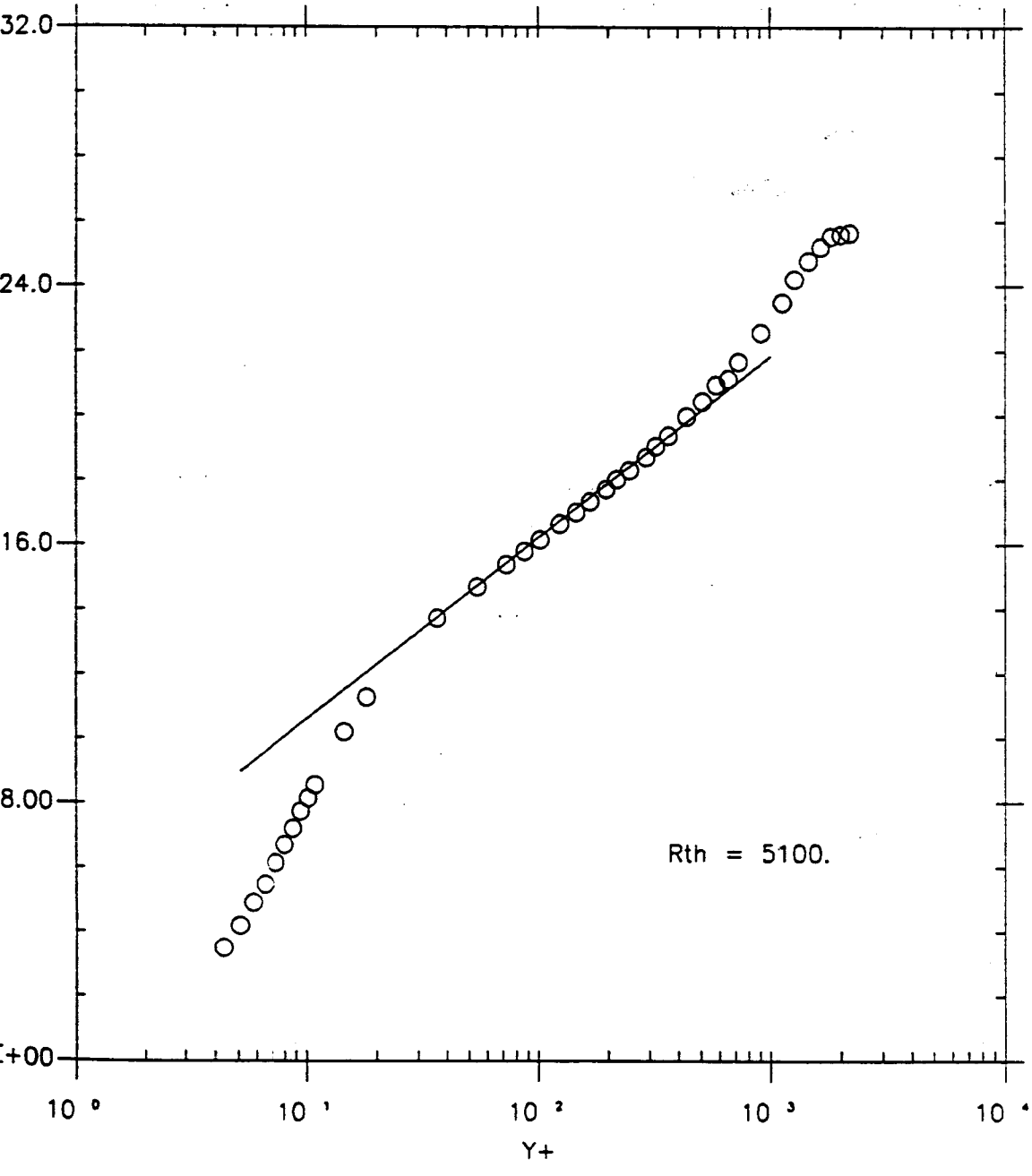

Fig. 2.1.4.1 *Velocity in inner variables with log law:*

Schultz & Grunow

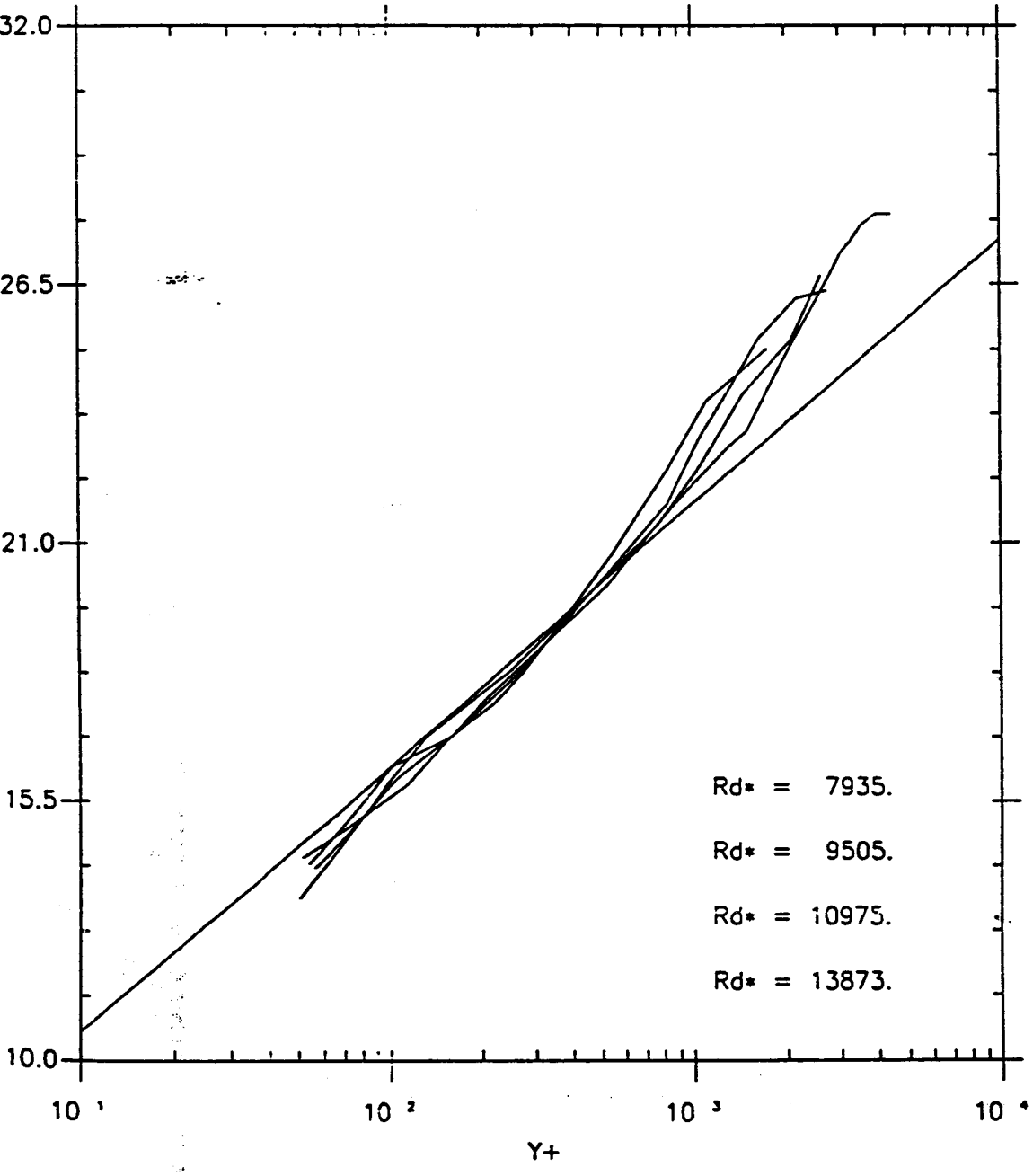

Fig. 2.1.5.1 *Velocity in inner variables with log law:*

Klebanoff & Diehl

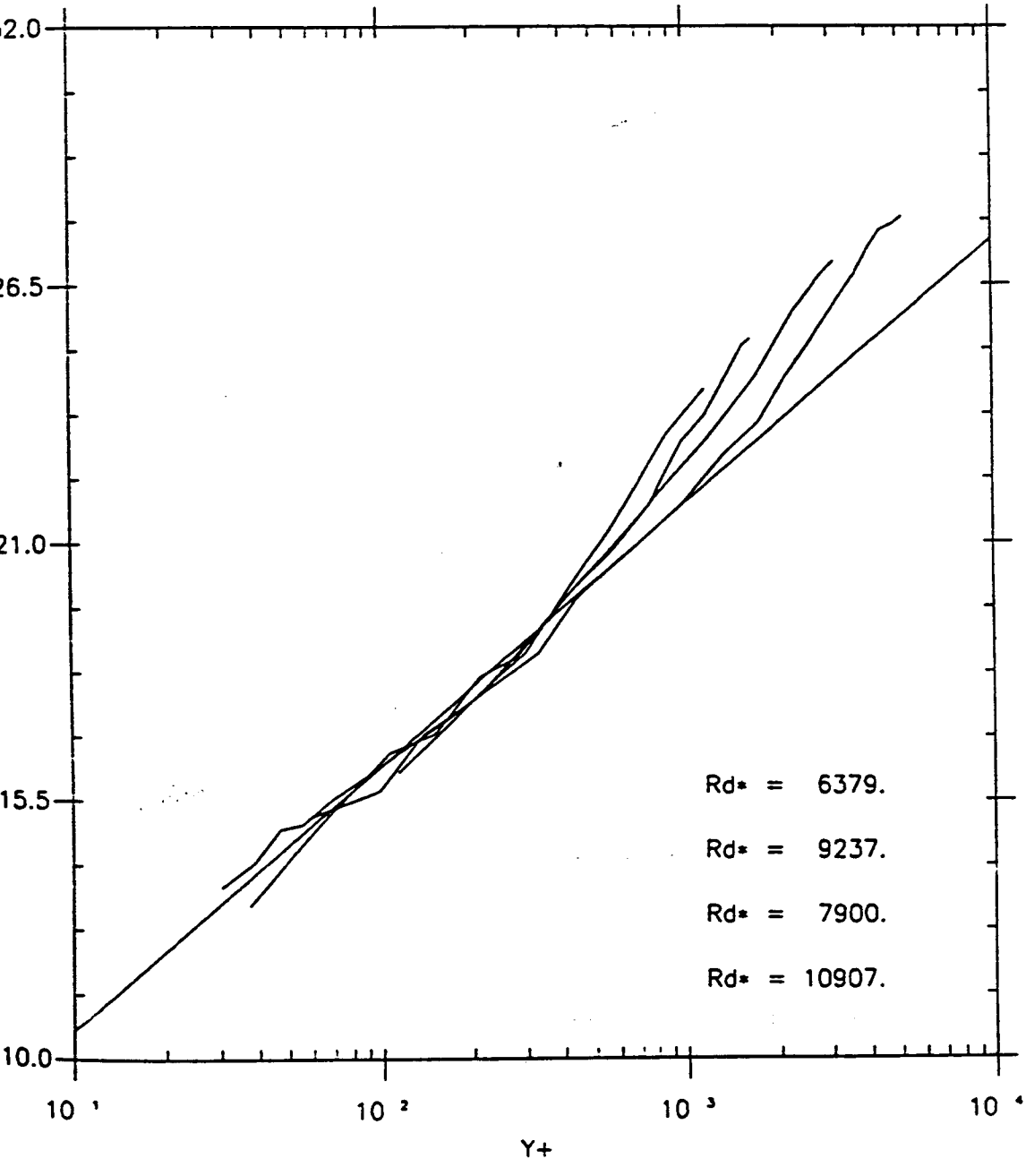

Fig. 2.2.1.1.1 *Velocity in inner variables with power law:*
Smith & Walker. Rth = 3005, 3815, 5680, 8175, 13040, 18340, 22510, 26510, 32280, 37190, 39800, 42610, 44750, 48290.

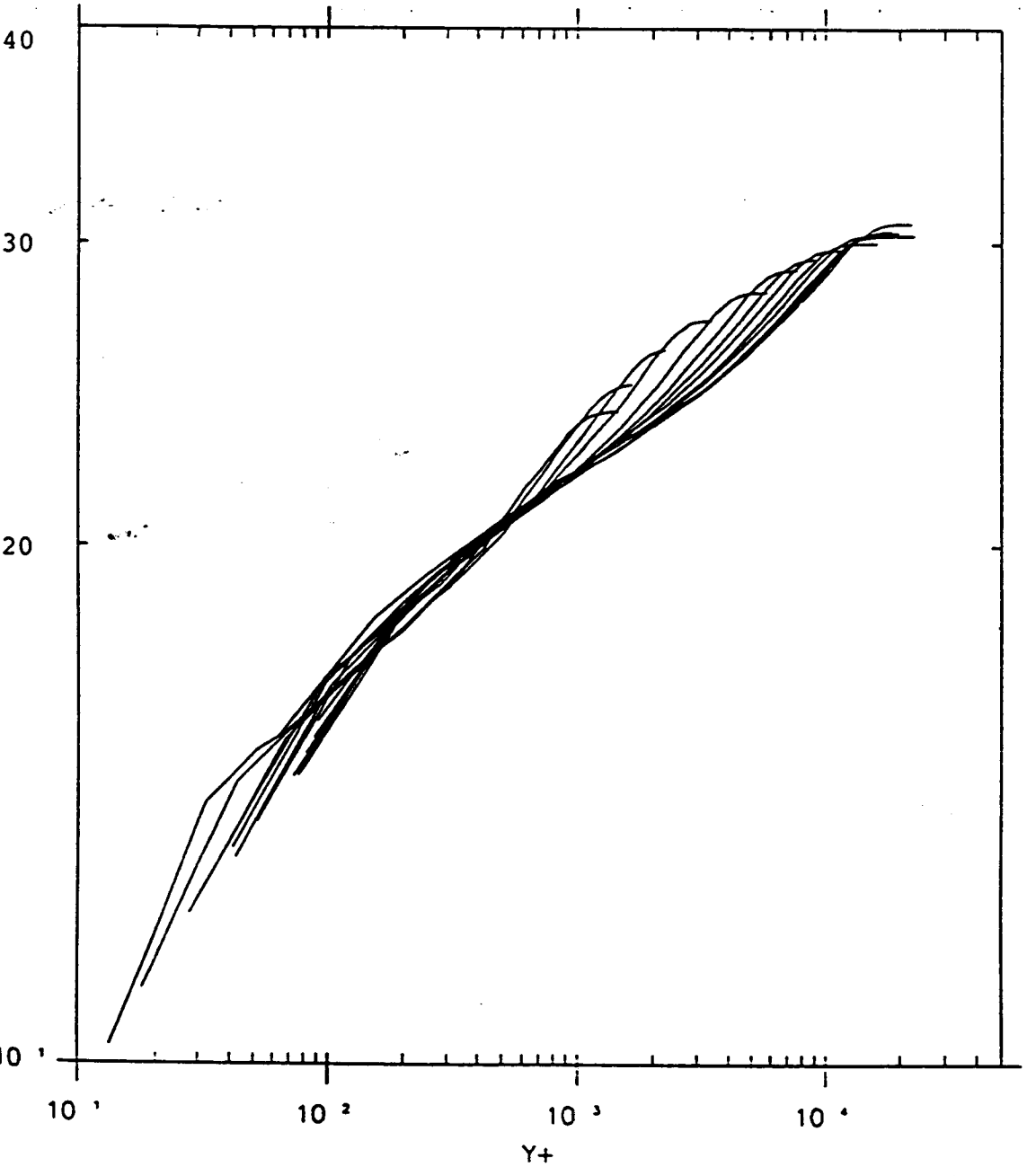

Fig. 2.2.1.1.2 *Velocity in inner variables with power law*:
Smith & Walker. Rth = 5680, 18340, 37190, 44750.

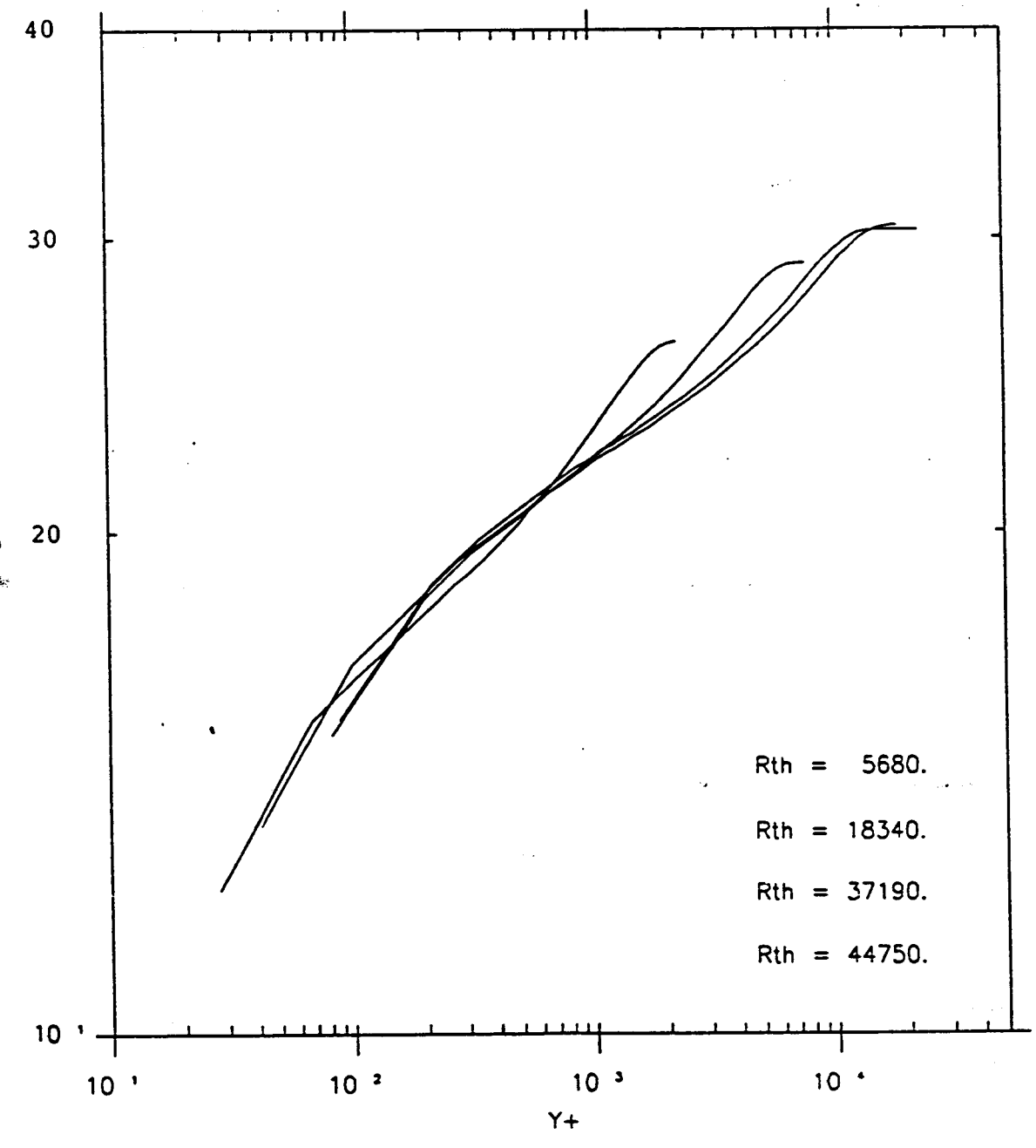

Fig. 2.2.1.2.03 *Velocity in inner variables with power law:*

Smith & Walker. Rth = 5680.

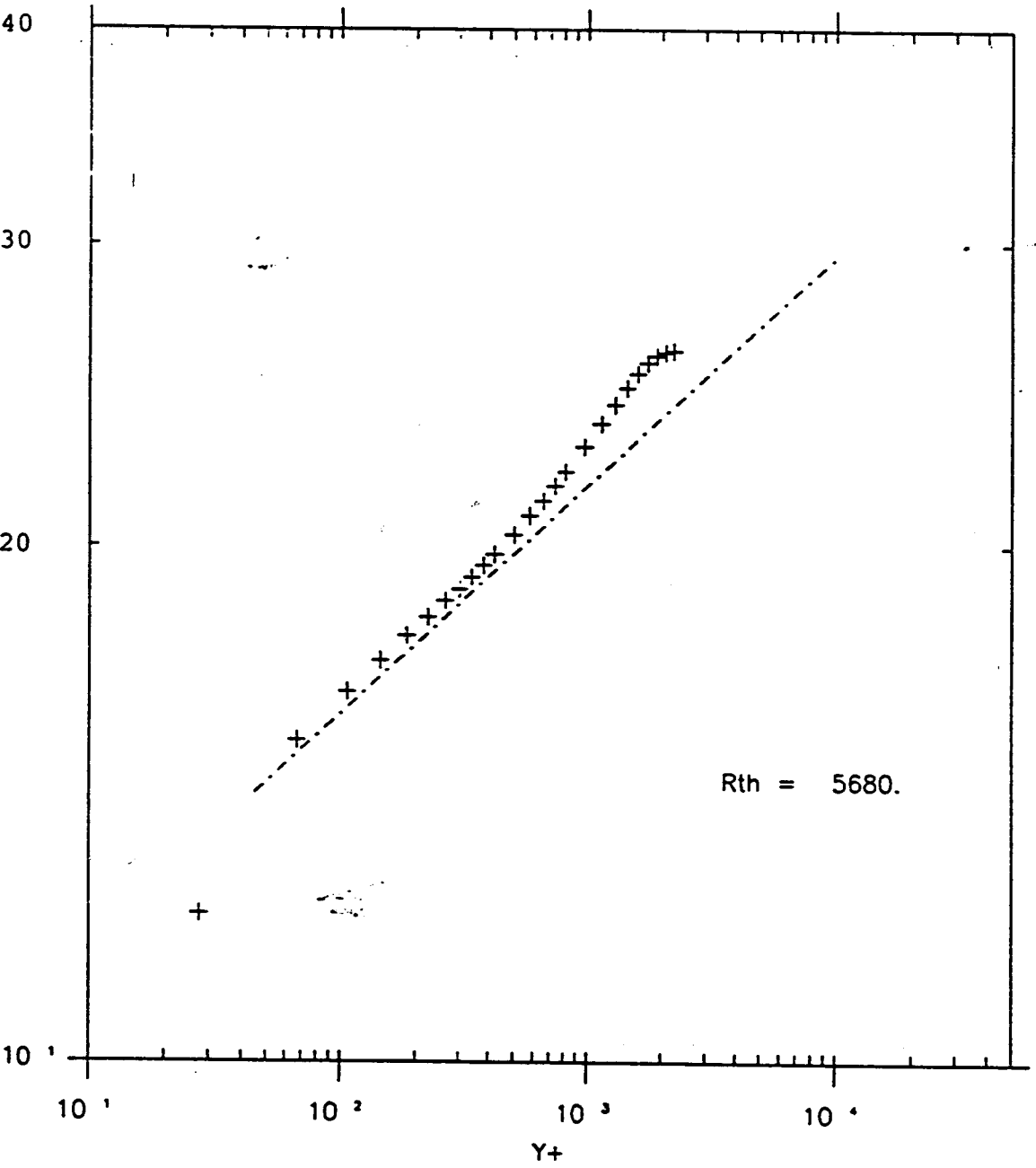

Fig. 2.2.1.2.06 *Velocity in inner variables with power law:*

Smith & Walker. Rth = 18340.

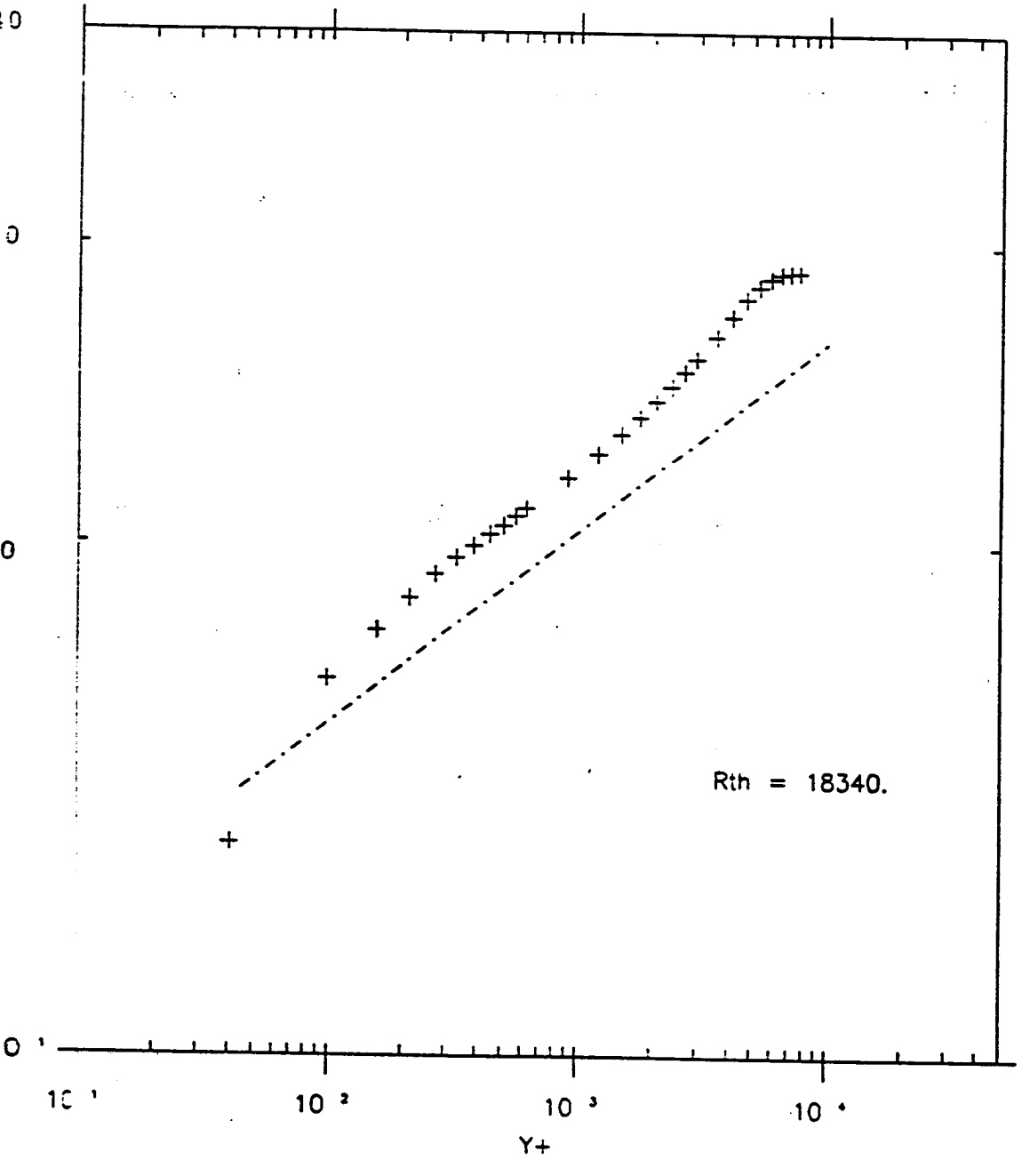

Fig. 2.2.1.2.10 *Velocity in inner variables with power law:*

Smith & Walker. Rth = 37190.

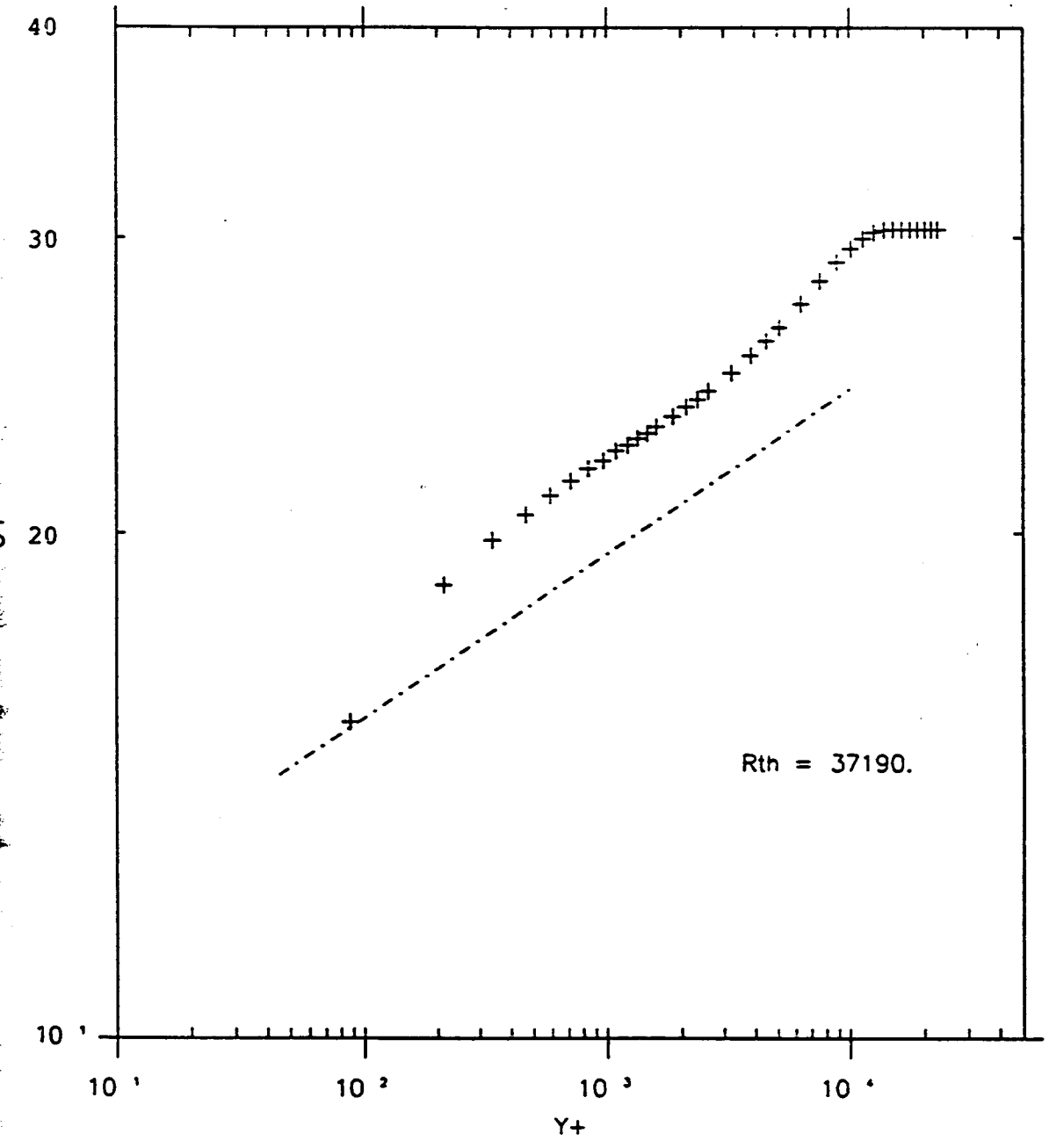

Fig. 2.2.1.2.13 *Velocity in inner variables with power law:*
Smith & Walker. Rth = 44750.

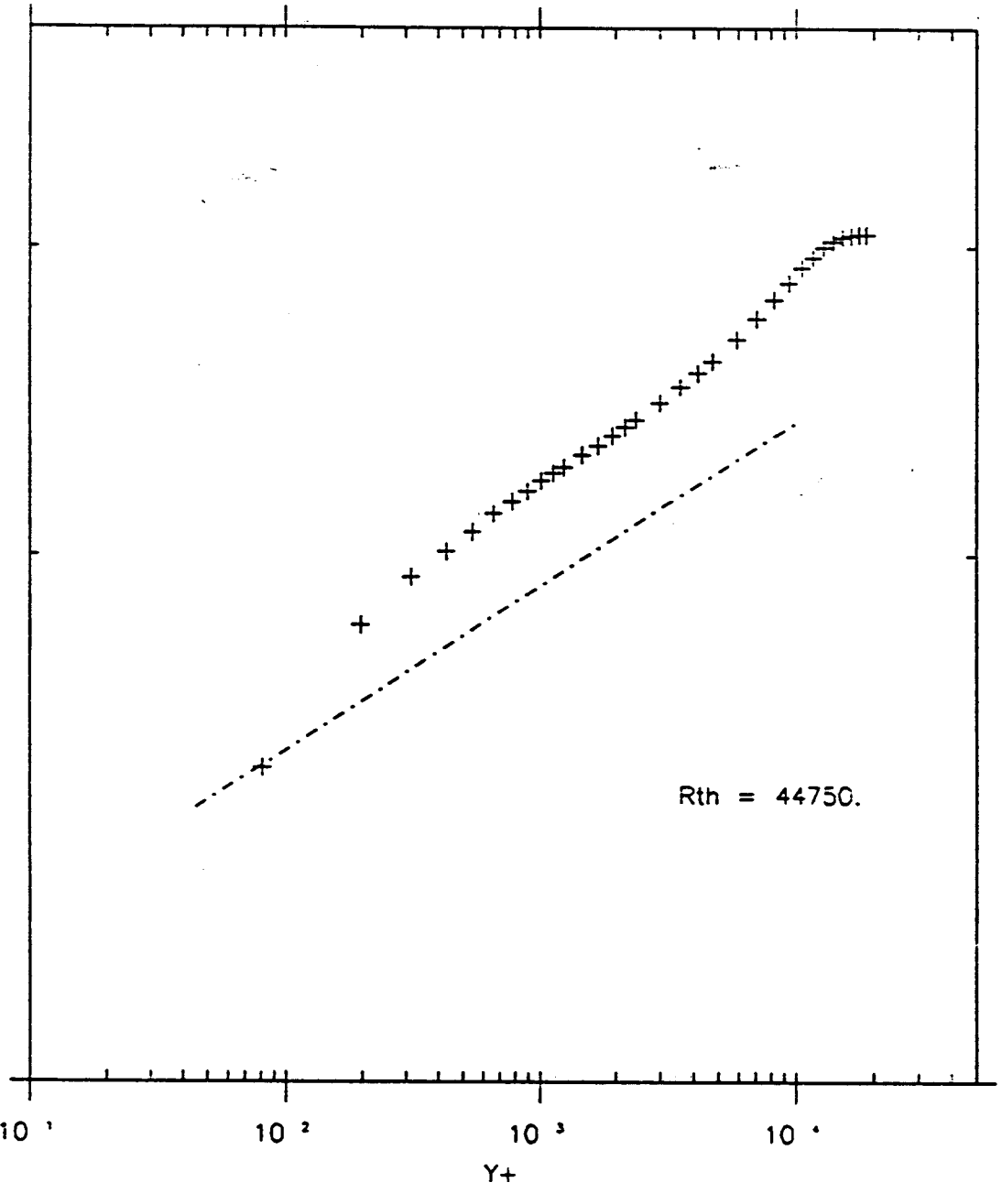

Fig. 2.2.1.2.10 *Velocity in inner variables with power law:*

Smith & Walker. Rth = 37190.

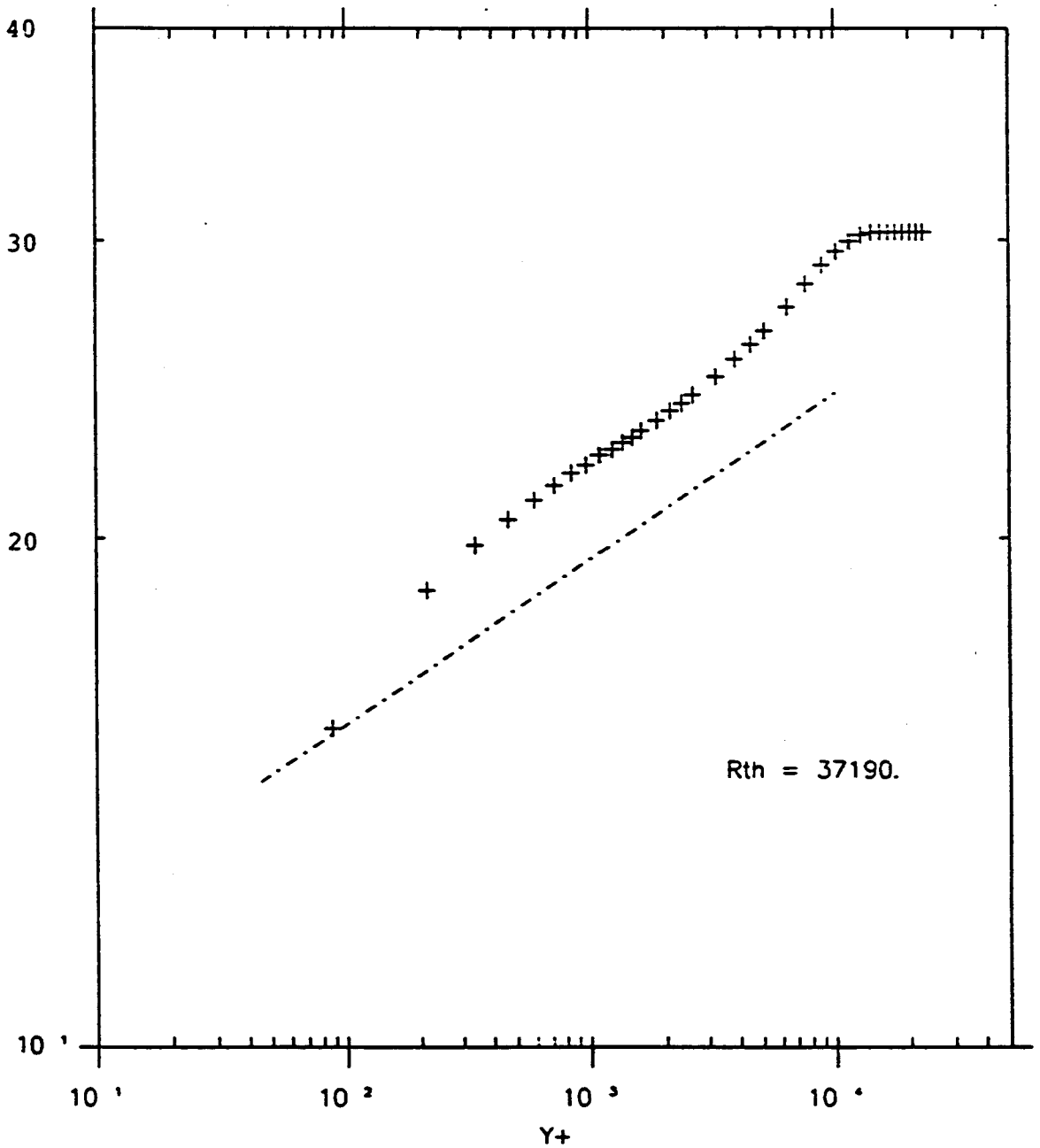

Fig. 2.2.1.2.13 *Velocity in inner variables with power law*:

Smith & Walker. Rth = 44750.

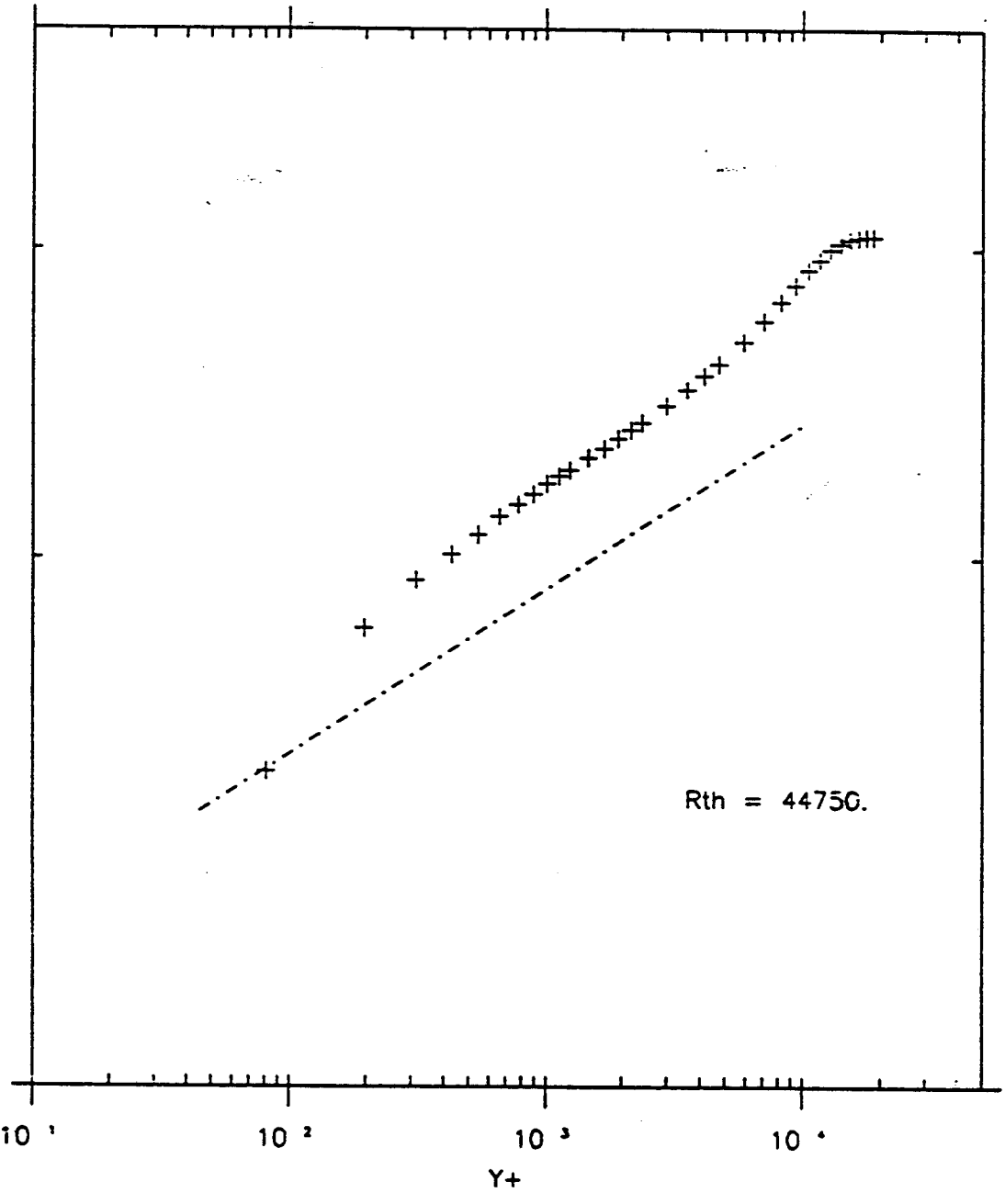

Fig. 2.2.2.1.1 *Velocity in inner variables with power law:*
Purtell et al.. Rth = 465, 498, 700, 1000, 1340, 1370, 1840, 2840, 3480, 4090, 5100.

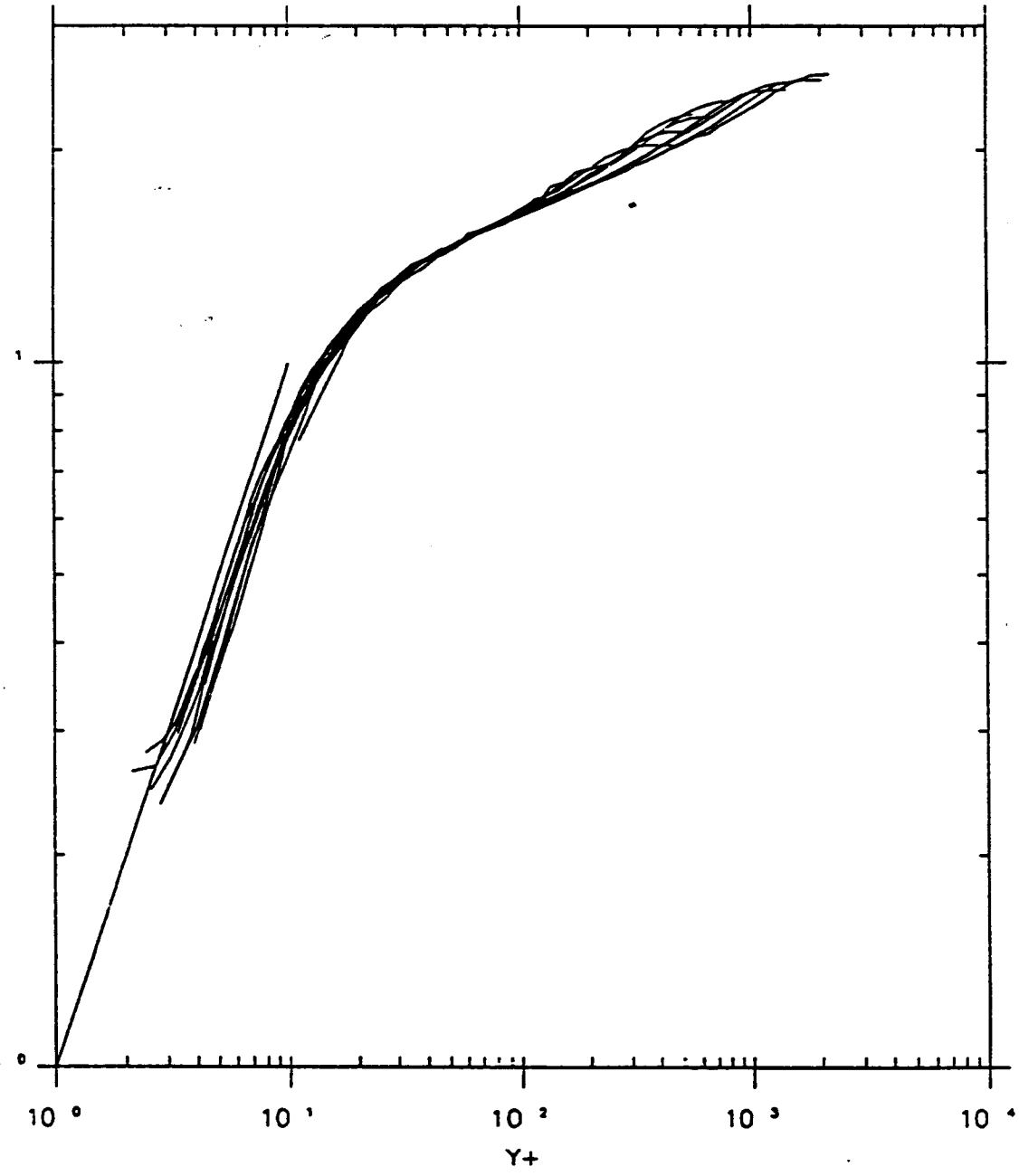

Fig. 2.2.2.1.2 *Velocity in inner variables with power law:*
Purtell et al.. Rth = 1340, 1840, 3480, 5100.

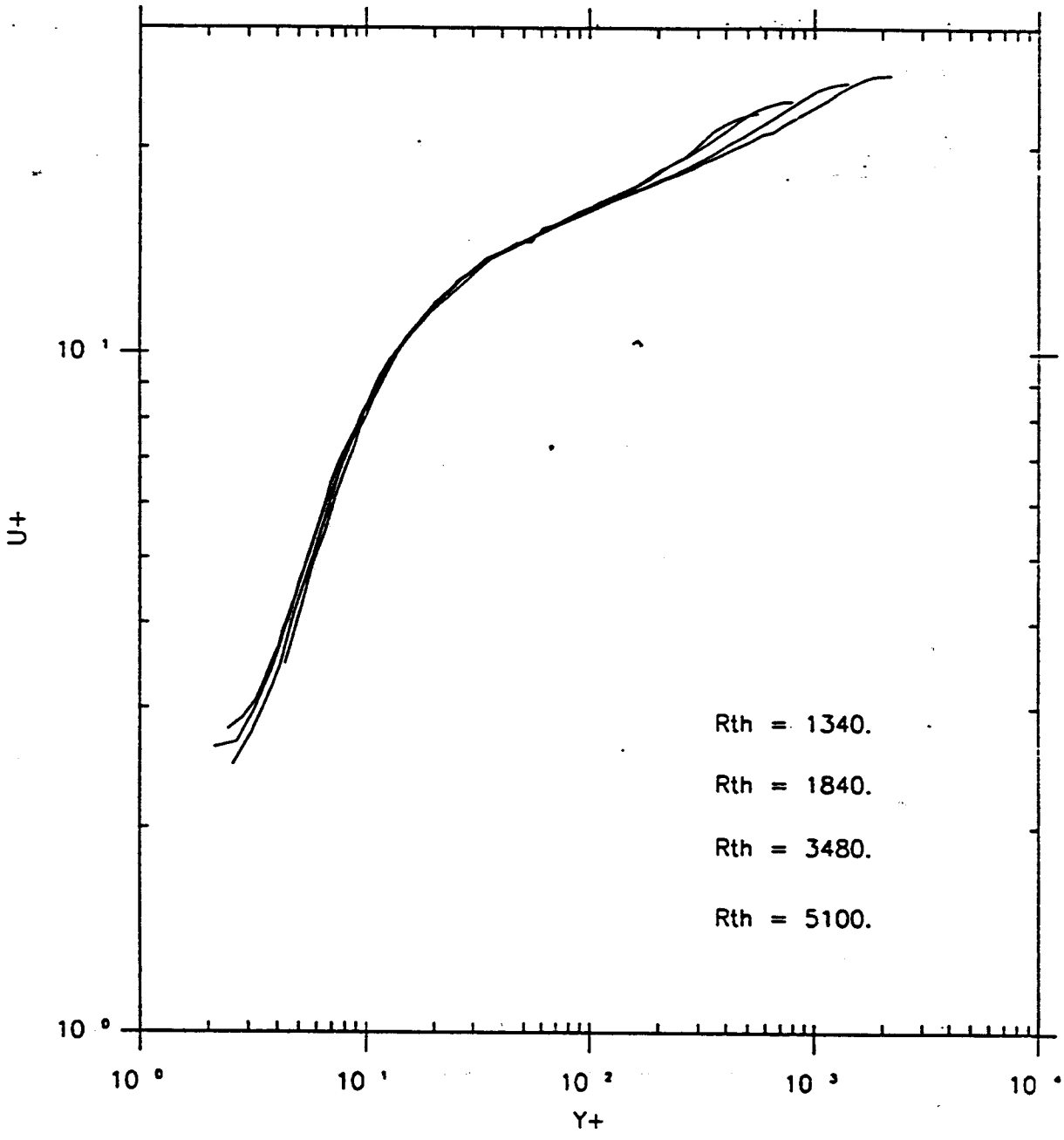

Fig. 2.2.2.2.05 *Velocity in inner variables with power law:*

Purtell et al.. Rth = 1340.

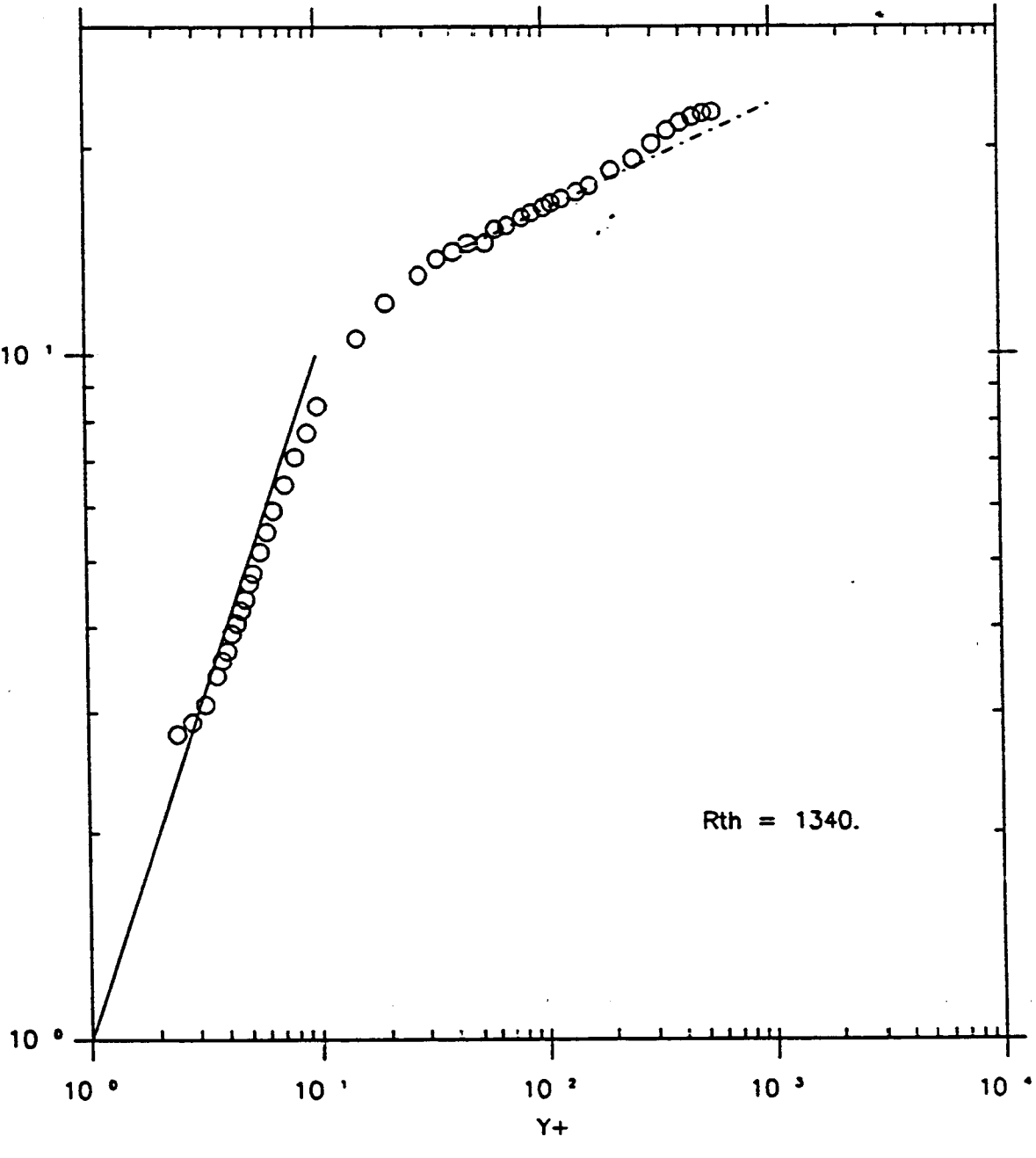

Fig. 2.2.2.2.07 *Velocity in inner variables with power law:*

Purtell et al.. Rth = 1840.

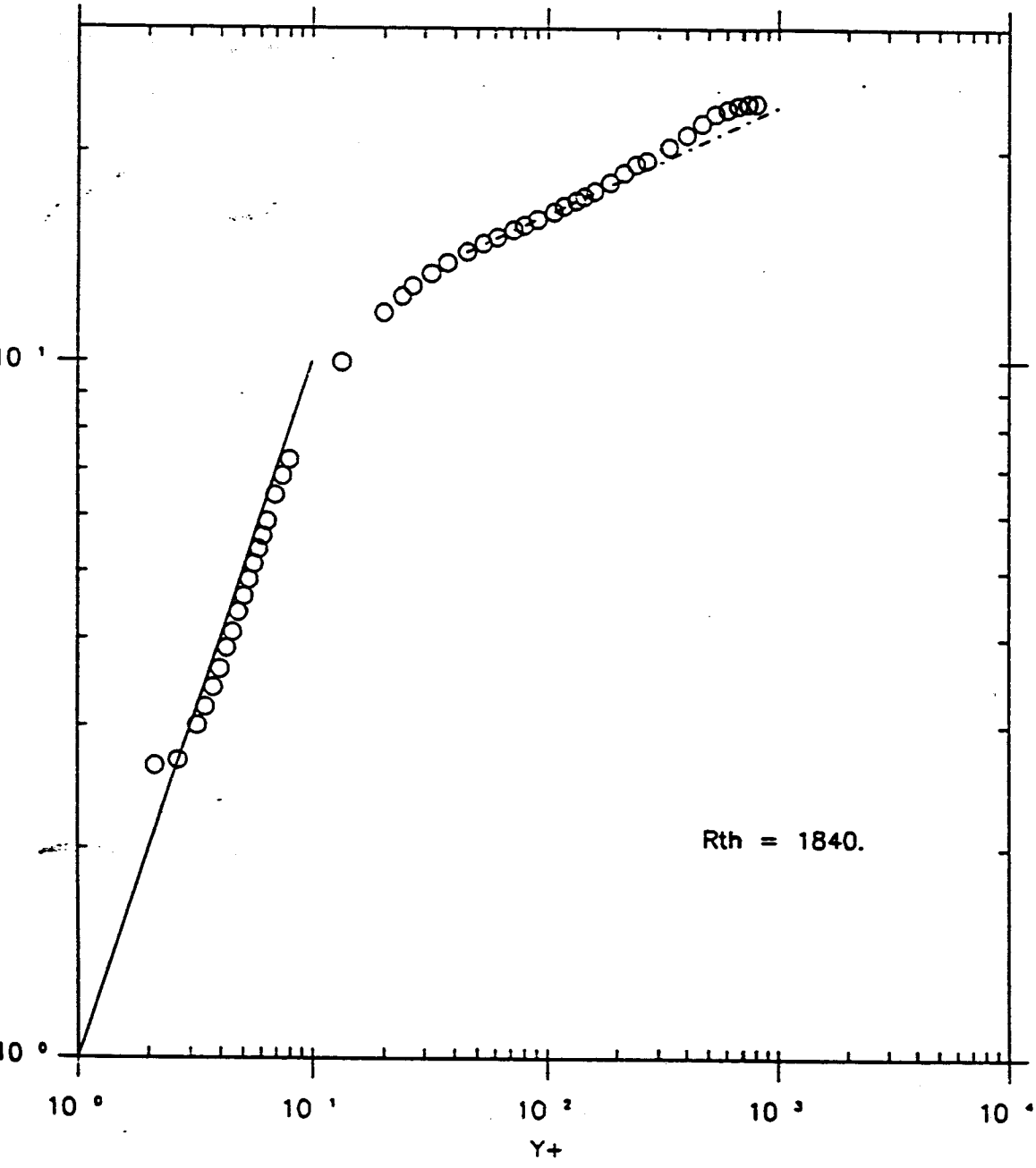

Fig. 2.2.2.2.09 *Velocity in inner variables with power law*:

Purtell et al.. Rth = 3480.

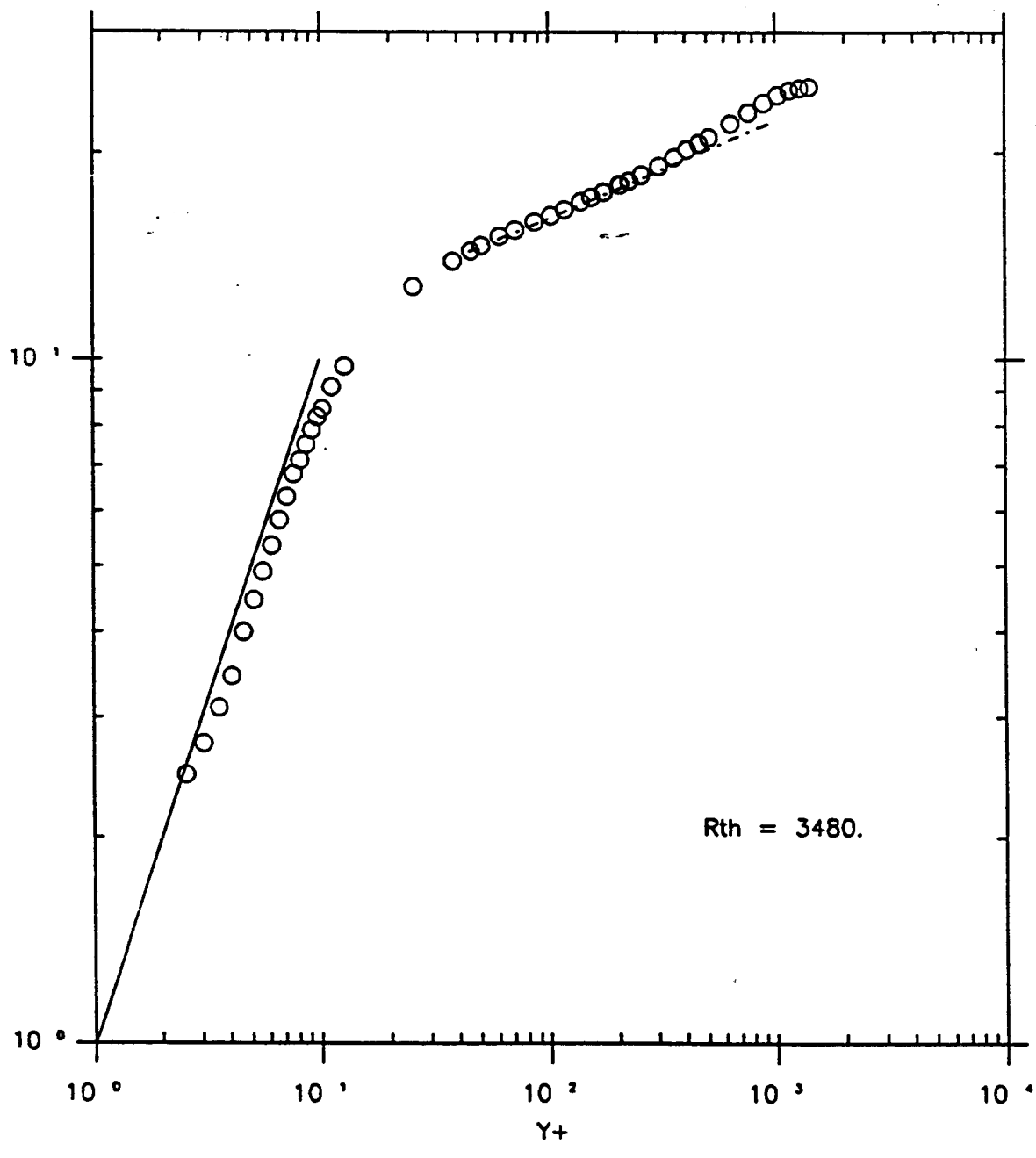

Fig. 2.2.2.2.11 *Velocity in inner variables with power law:*

Purtell et al.. Rth = 5100.

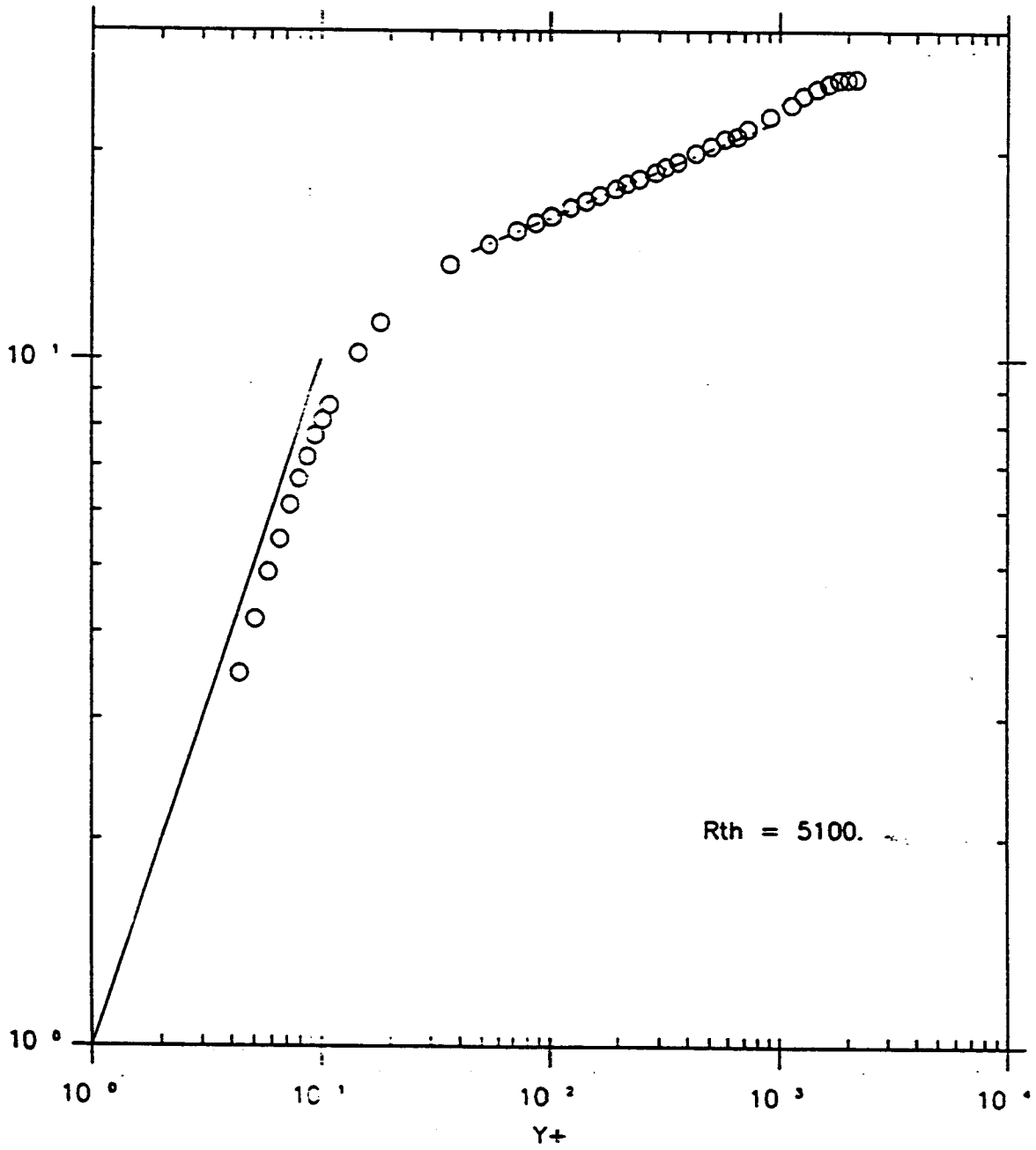

Fig. 2.2.4.1 *Velocity in inner variables with power law:*

Schultz & Grunow

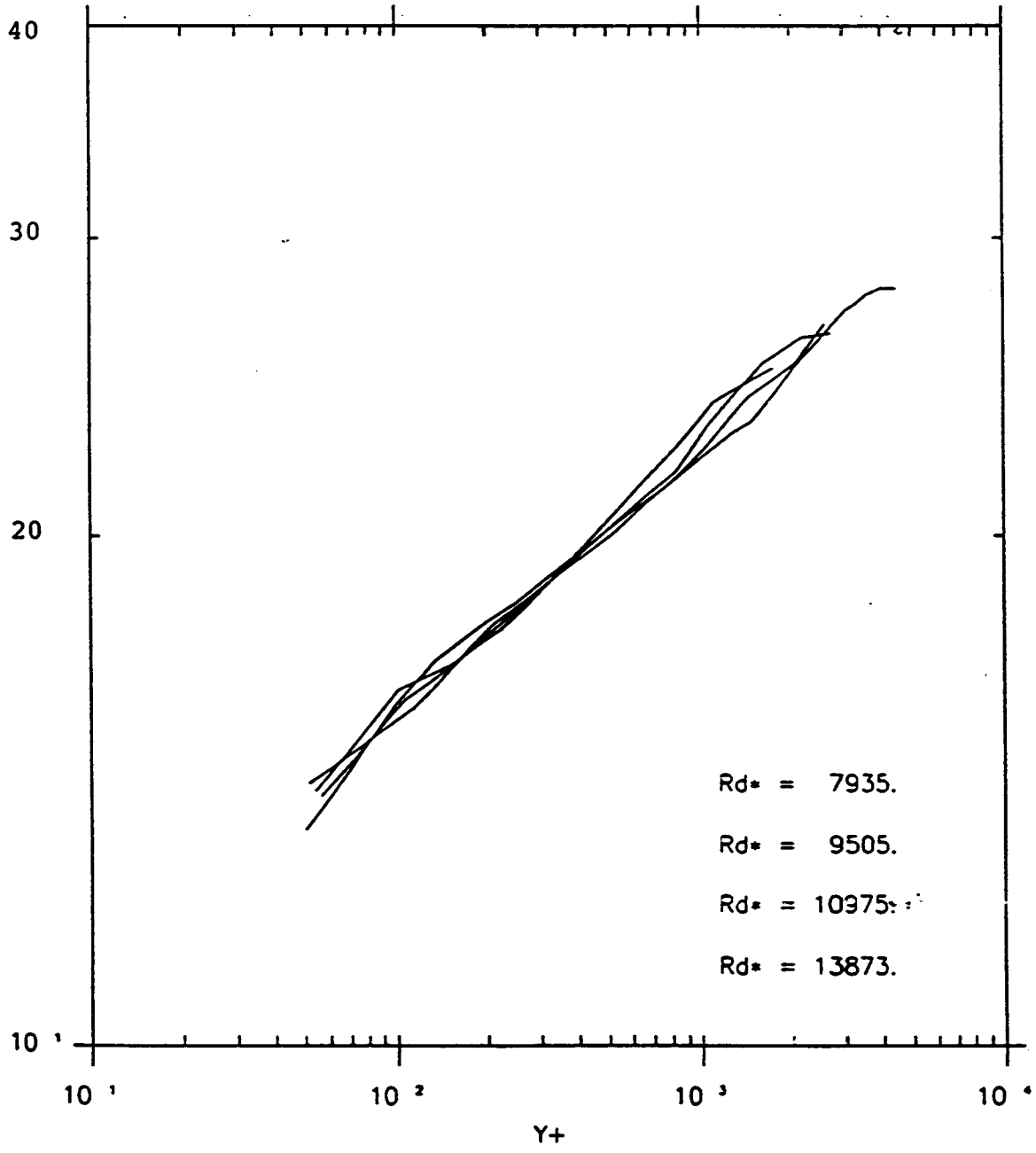

Fig. 2.2.5.1 *Velocity in inner variables with power law:*

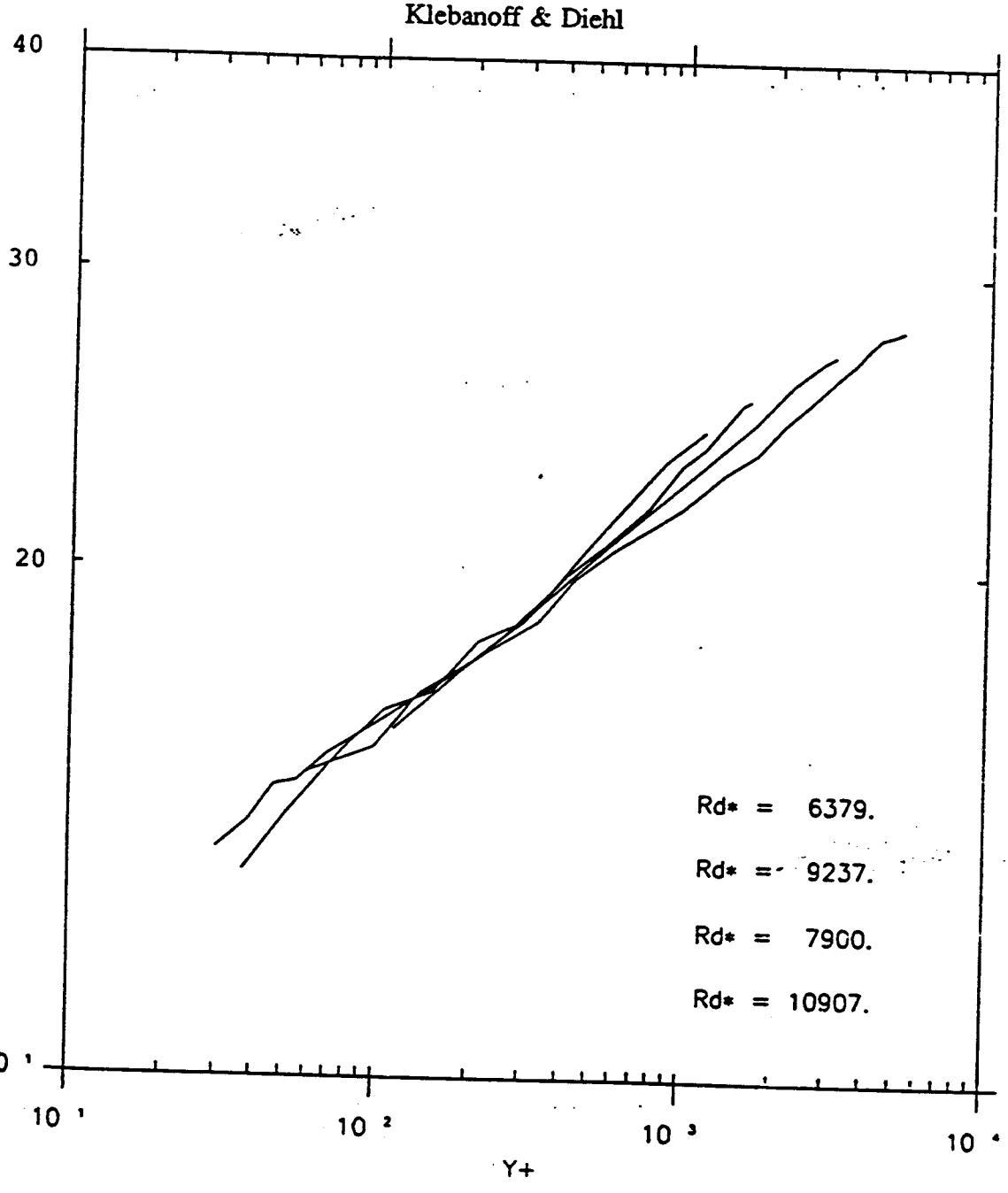

Fig. 2.3.1.1.2 *Velocity Defect:*

Smith & Walker. Rth = 5680, 18340. 37190, 44750.

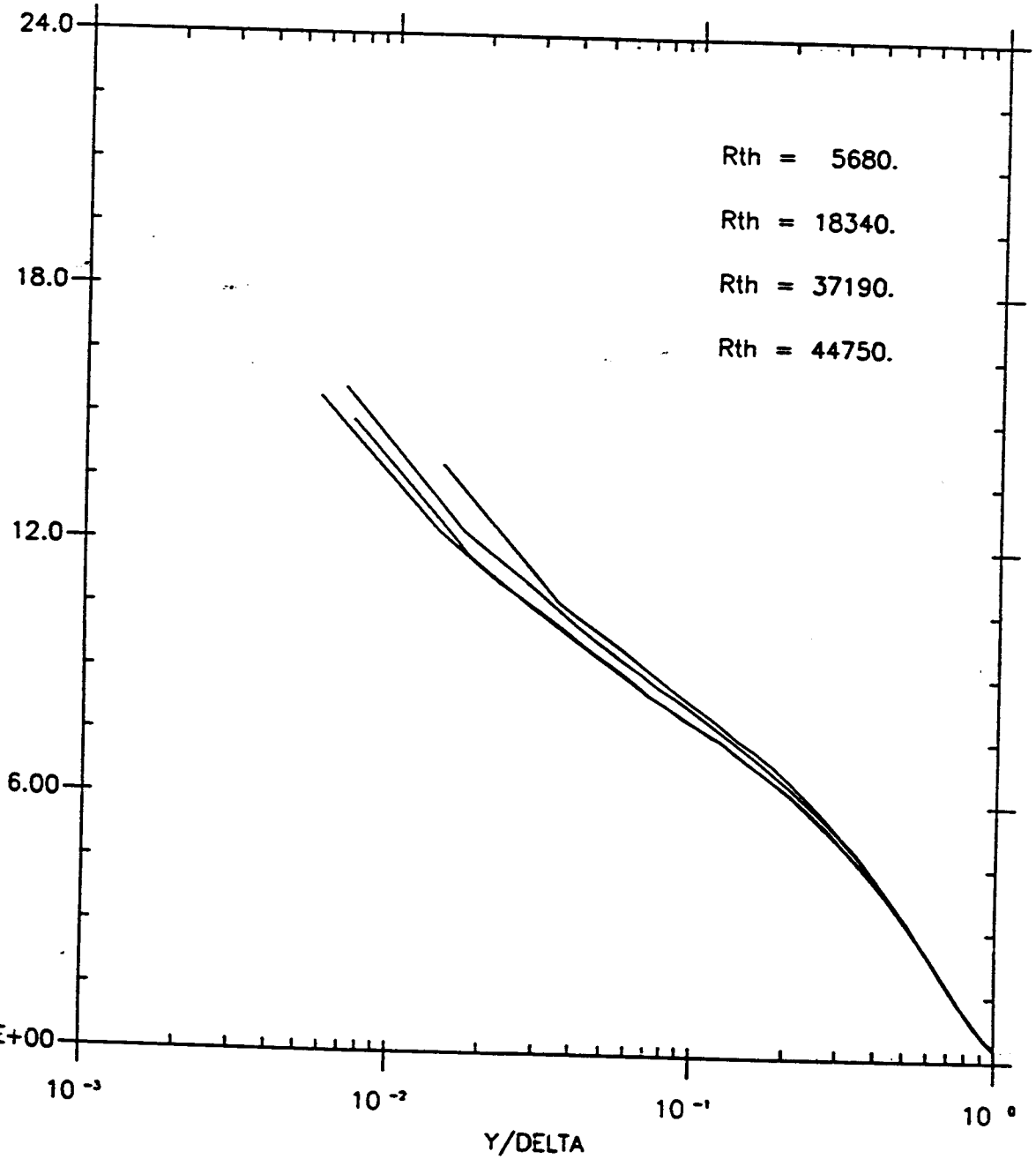

Fig. 2.3.2.1.2 *Velocity Defect*:

Purtell et al.. **Rth** = 1340, 1840, 3480, 5100.

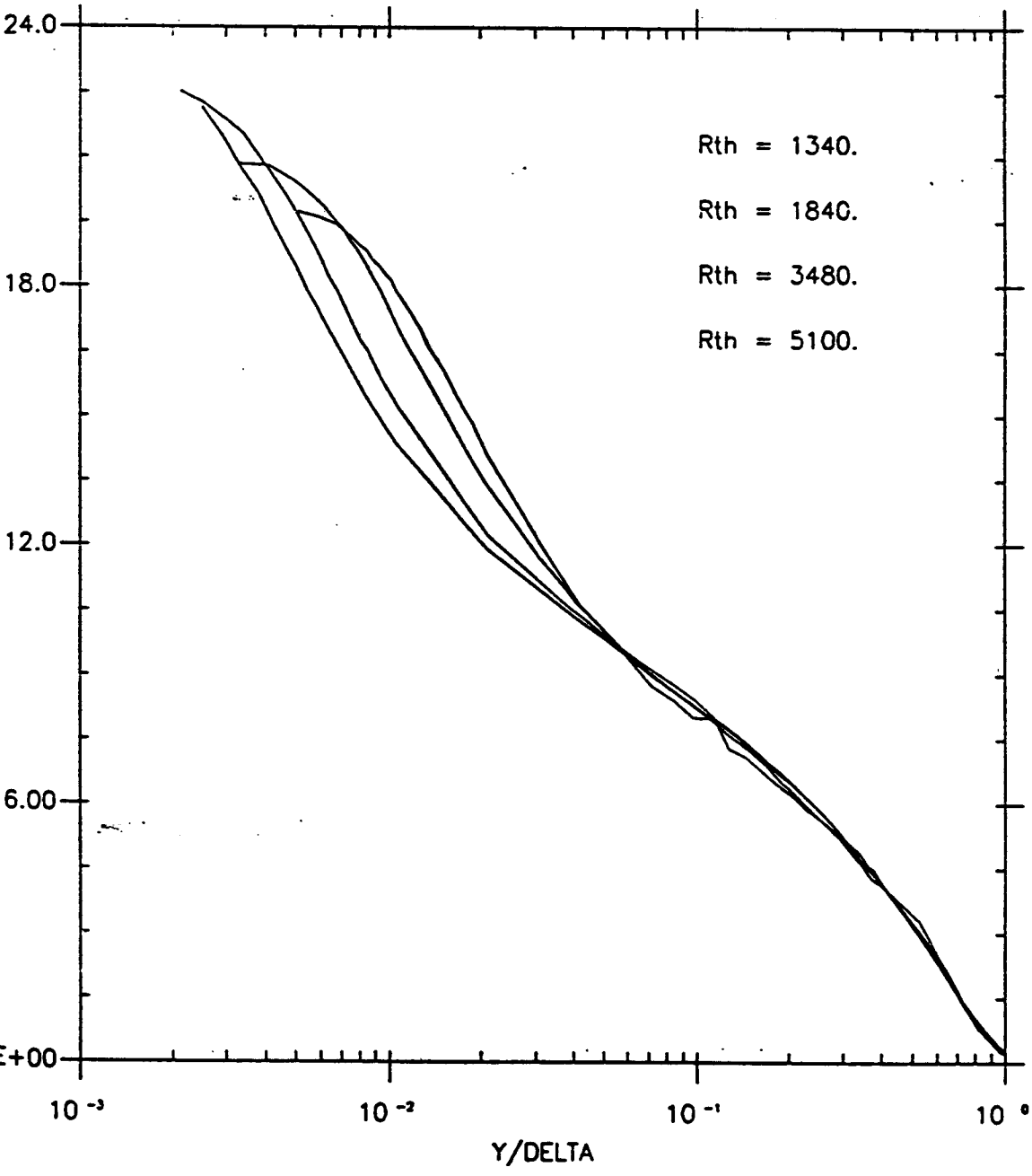

Fig. 2.3.4.1 *Velocity Defect*:

Schultz & Grunow

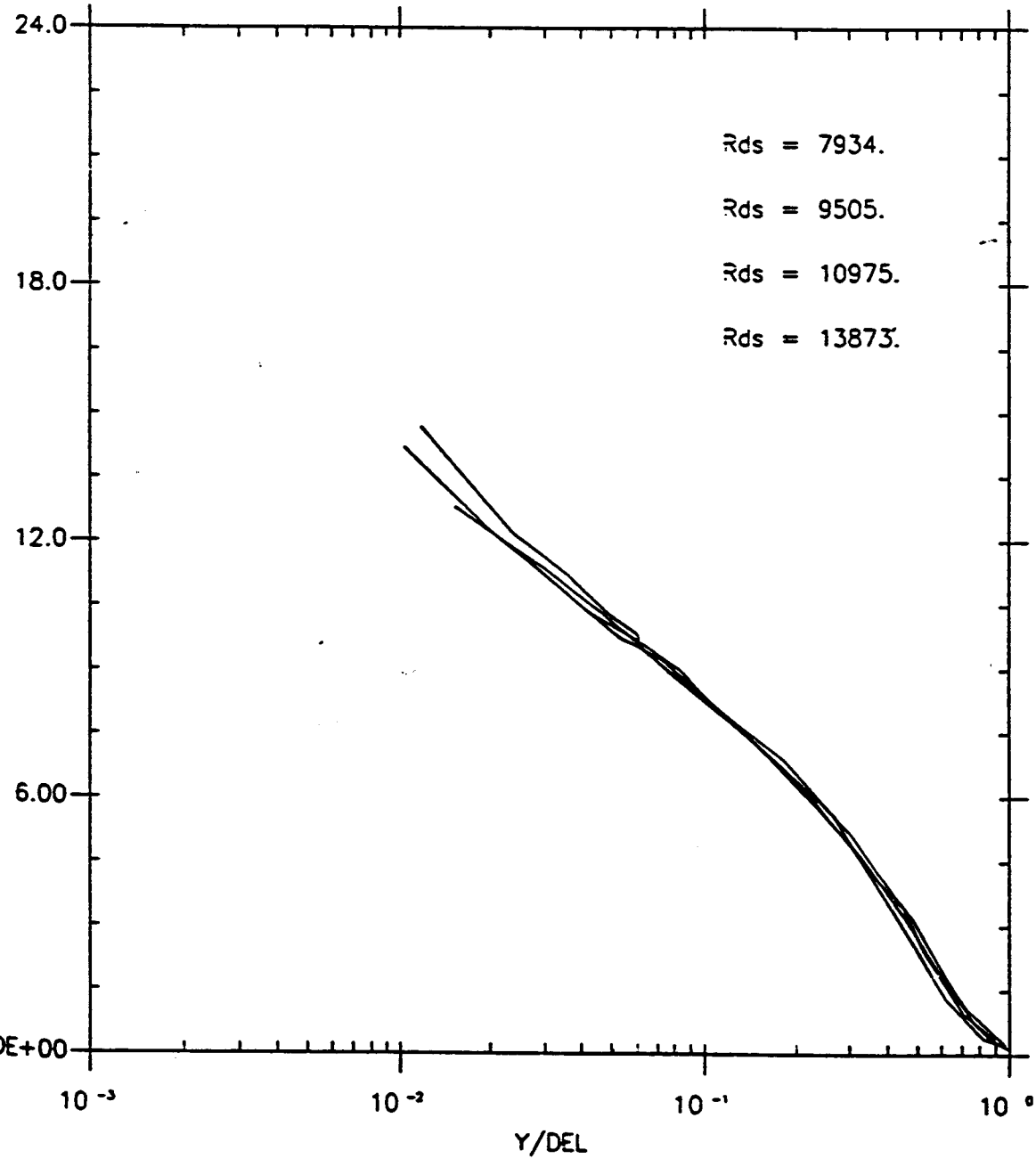

Fig. 2.4.1.1.2 *Strict Similarity*:

Smith & Walker. Rth = 5680, 18340, 37190, 44750.

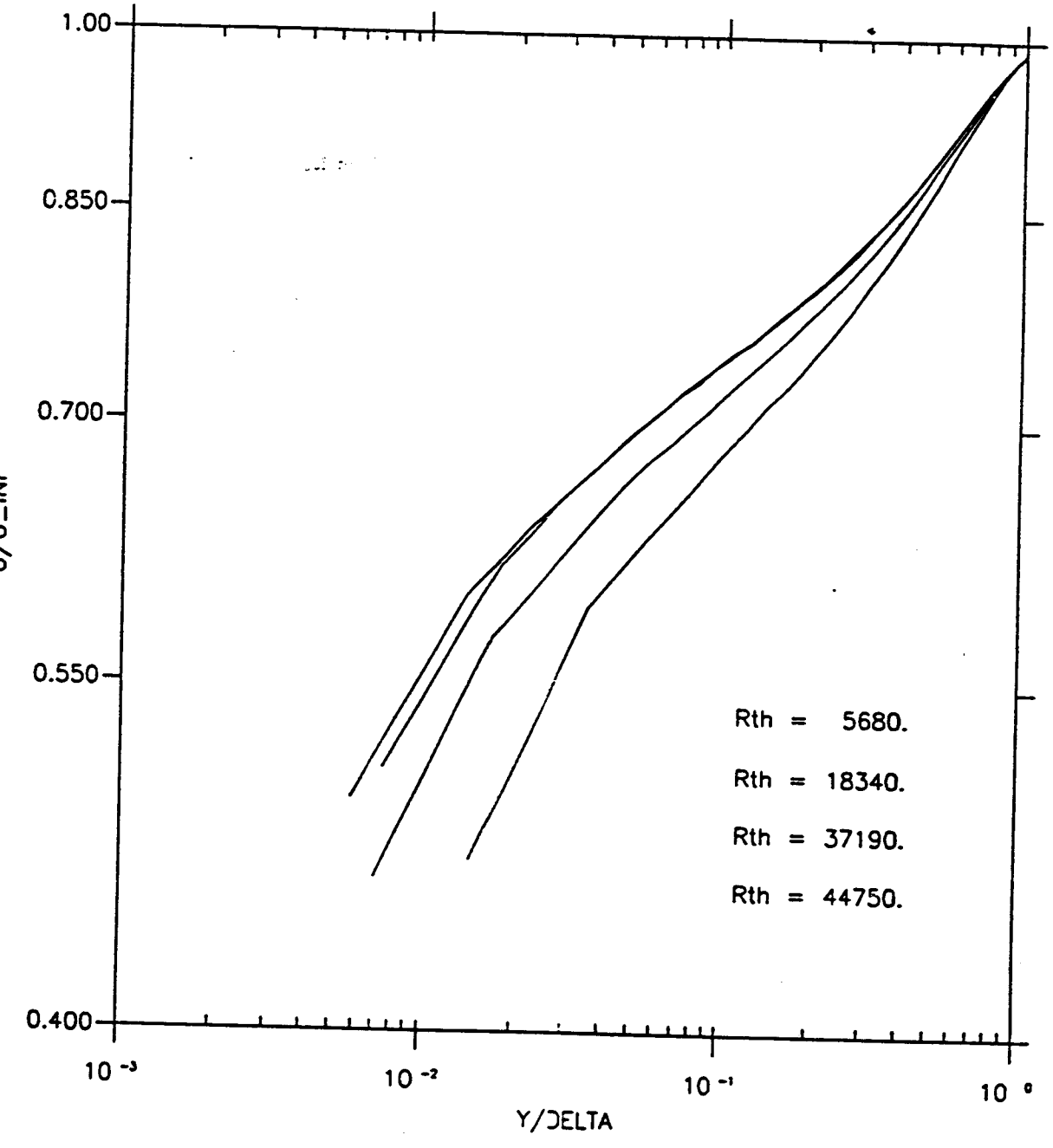

Fig. 2.4.2.1.2 *Strict Similarity*:

Purtell et al.. Rth = 1340, 1840, 3480, 5100.

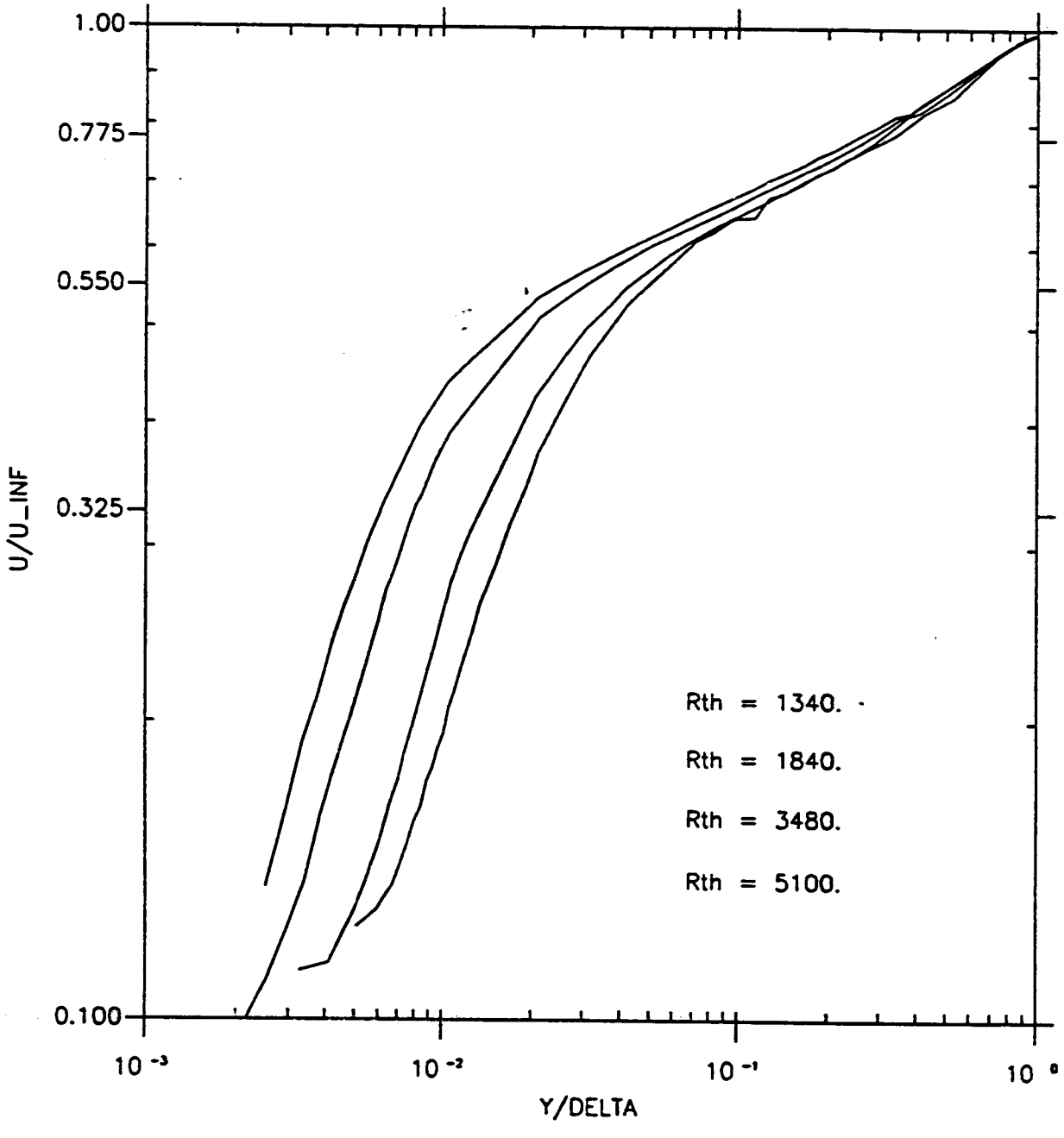

Fig. 2.4.4.1 *Strict Similarity*:

Schultz & Grunow

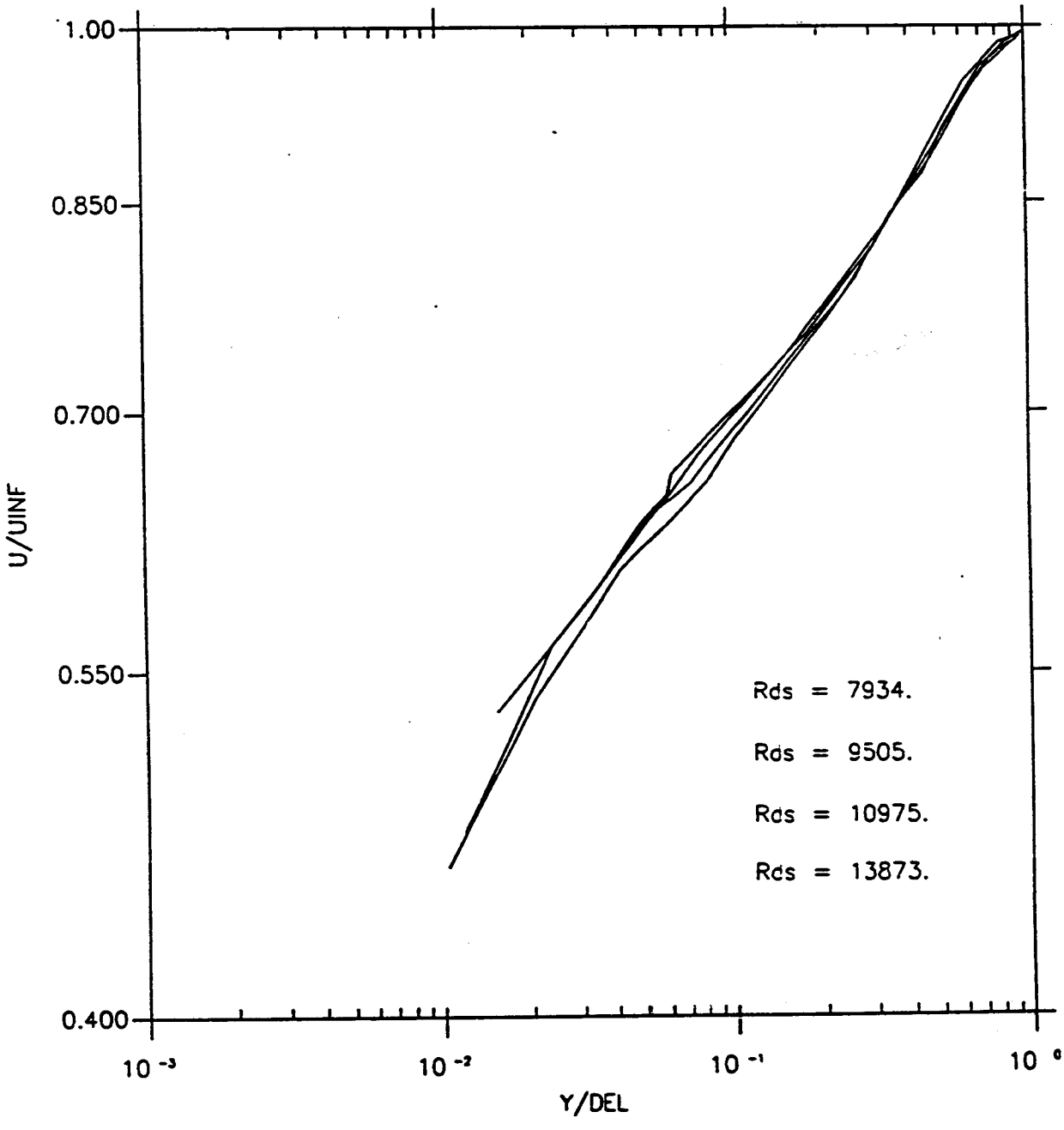

Fig. 2.4.5.1 *Strict Similarity*:

Klebanoff & Diehl

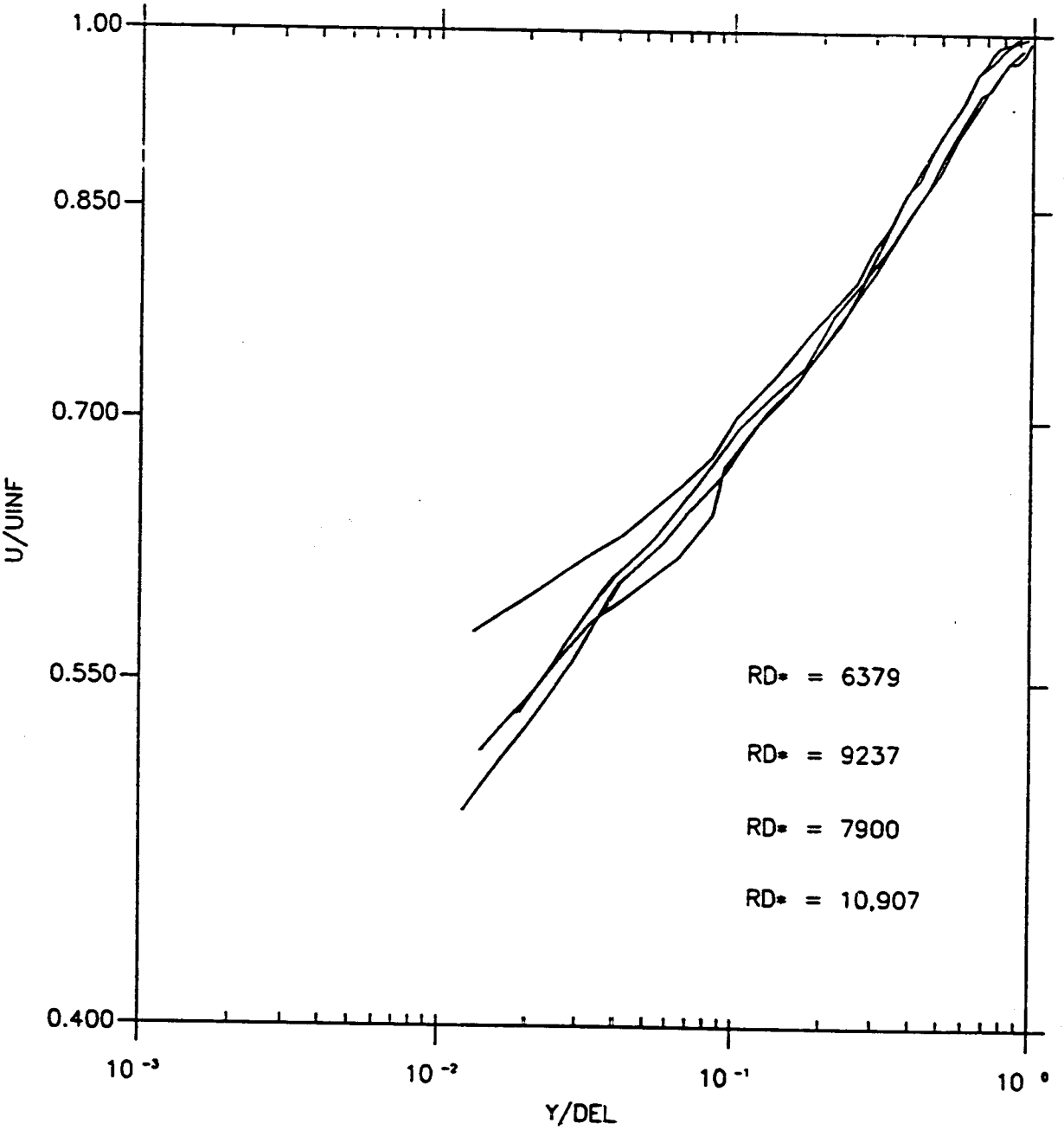

A.3 VELOCITY DERIVATIVE REPRESENTATIONS

Fig. 3.1.1.1 *Outer variables:*

Smith & Walker. Rth = 5680, 18340, 37190, 44750.

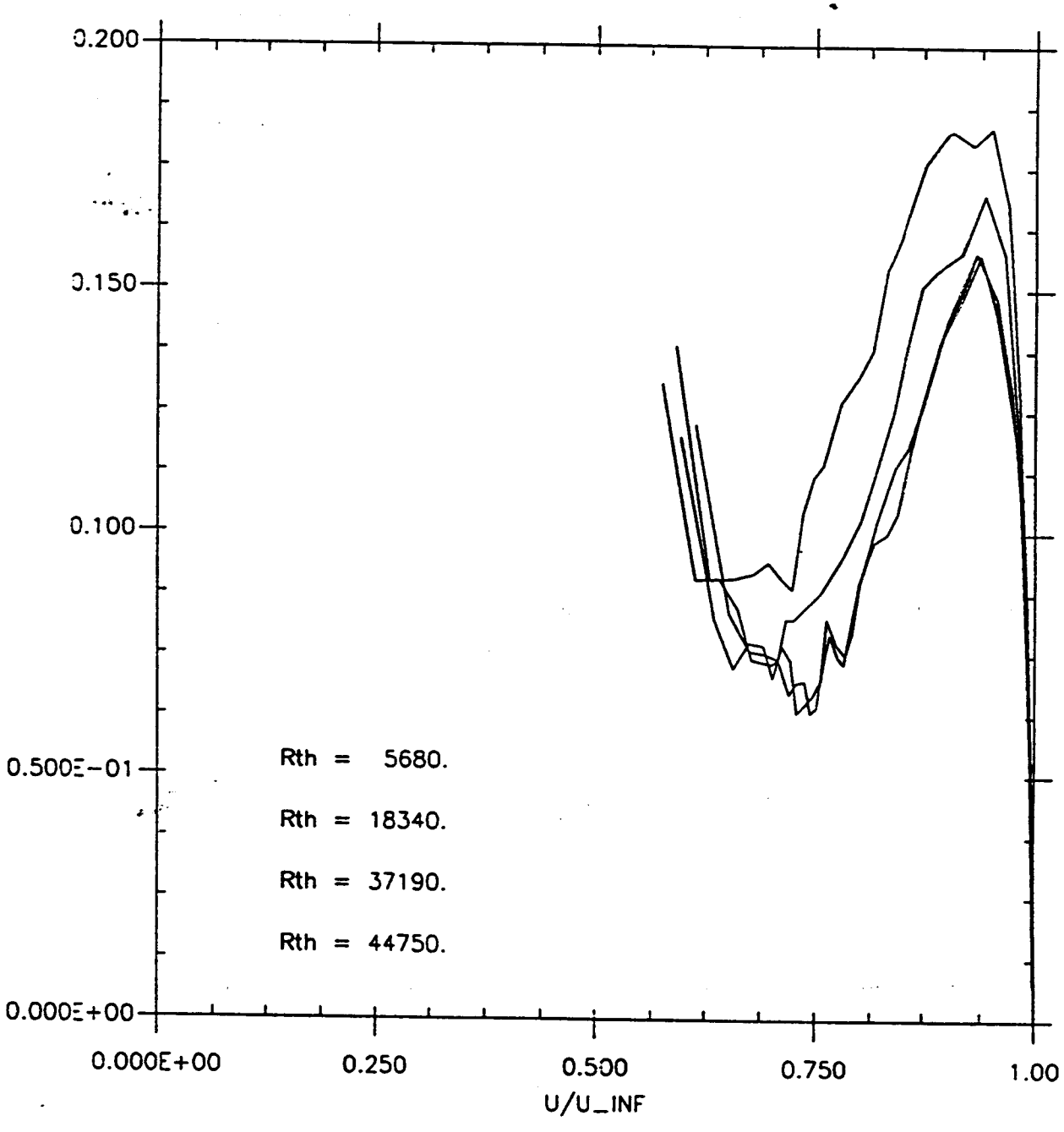

Fig. 3.1.1.2.03 *Outer variables*:

Smith & Walker. Rth = 5680.

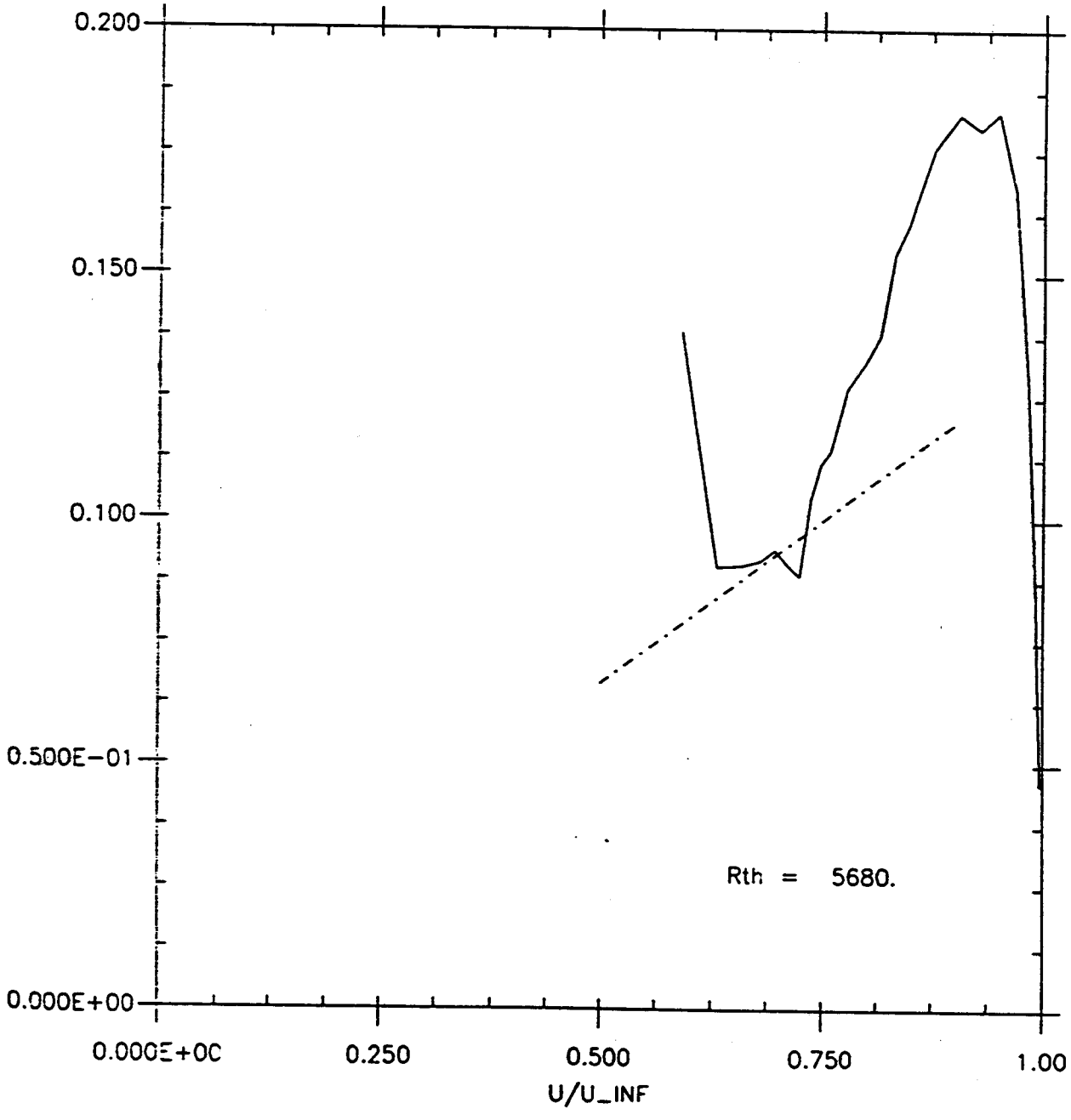

Fig. 3.1.1.2.06 *Outer variables*:

Smith & Walker. Rth = 18340.

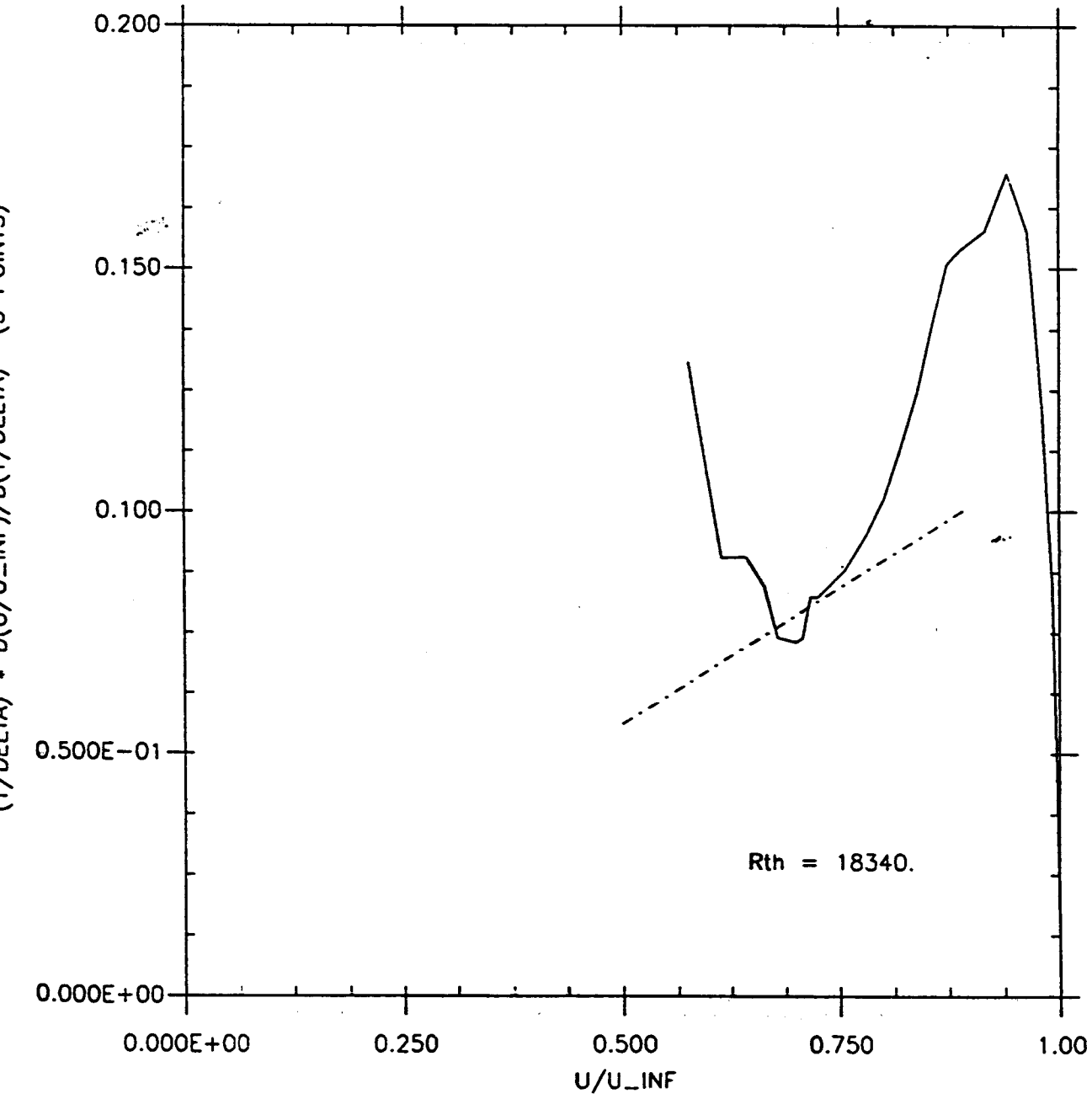

Fig. 3.1.1.2.10 *Outer variables*:

Smith & Walker. Rth = 37190.

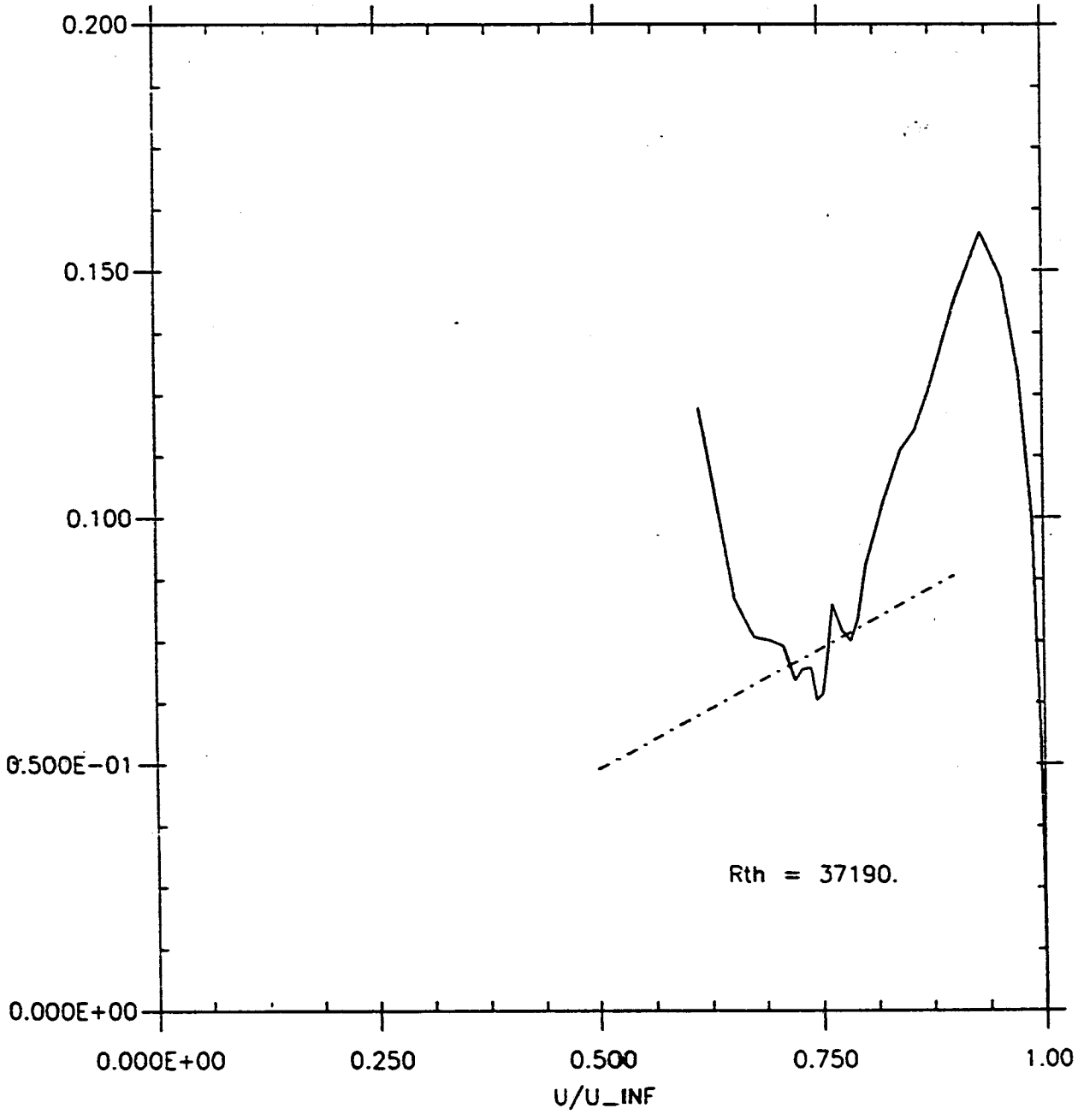

Fig. 3.1.1.2.13 *Outer variables*:

Smith & Walker. Rth = 44750.

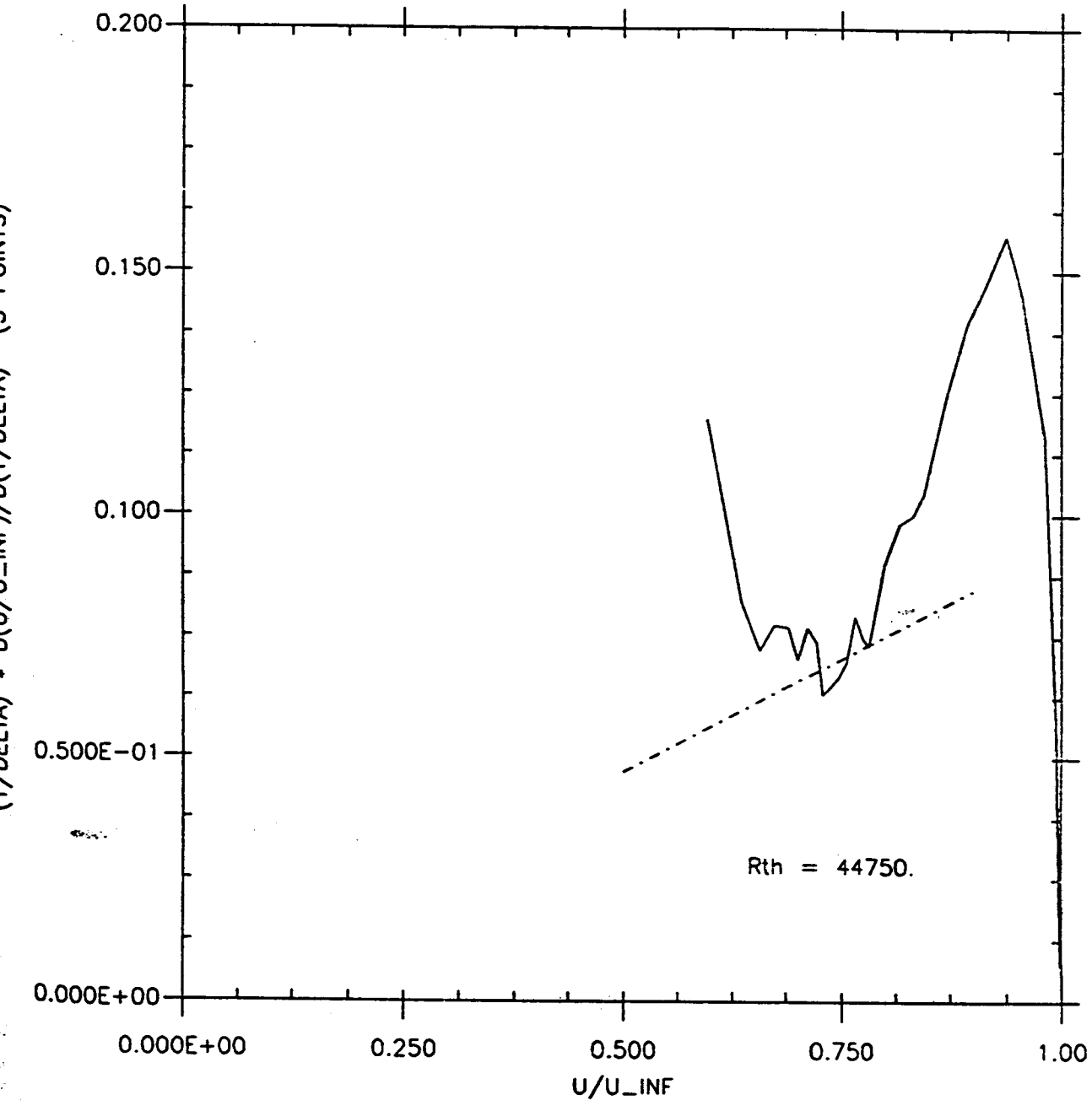

Fig.. 3.1.2.1 *Outer variables*:

Purtell et al.. Rth = 1340, 1840, 3480, 5100.

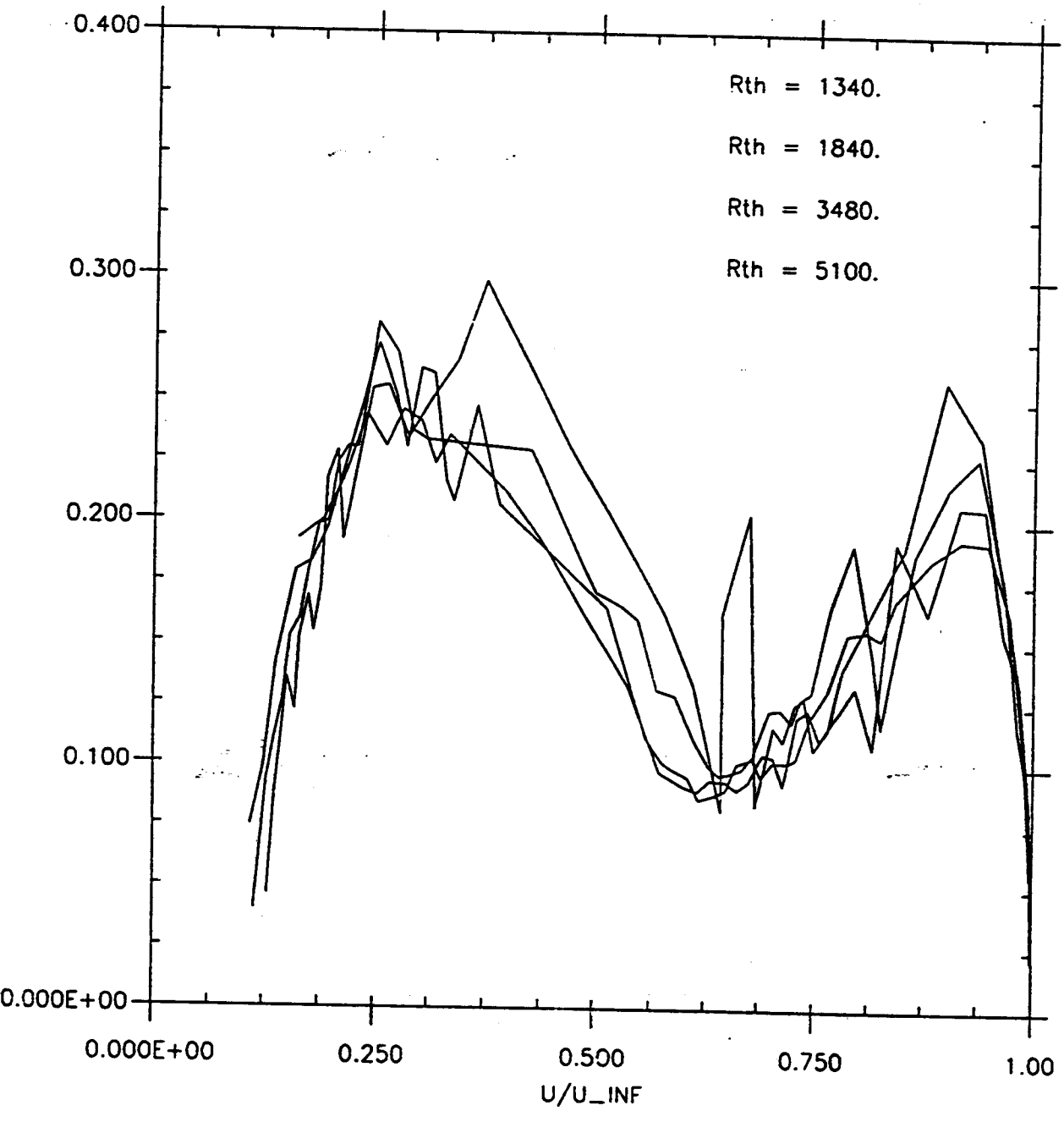

Fig. 3.1.2.2.05 *Outer variables*:

Purtell et al.. Rth = 1340.

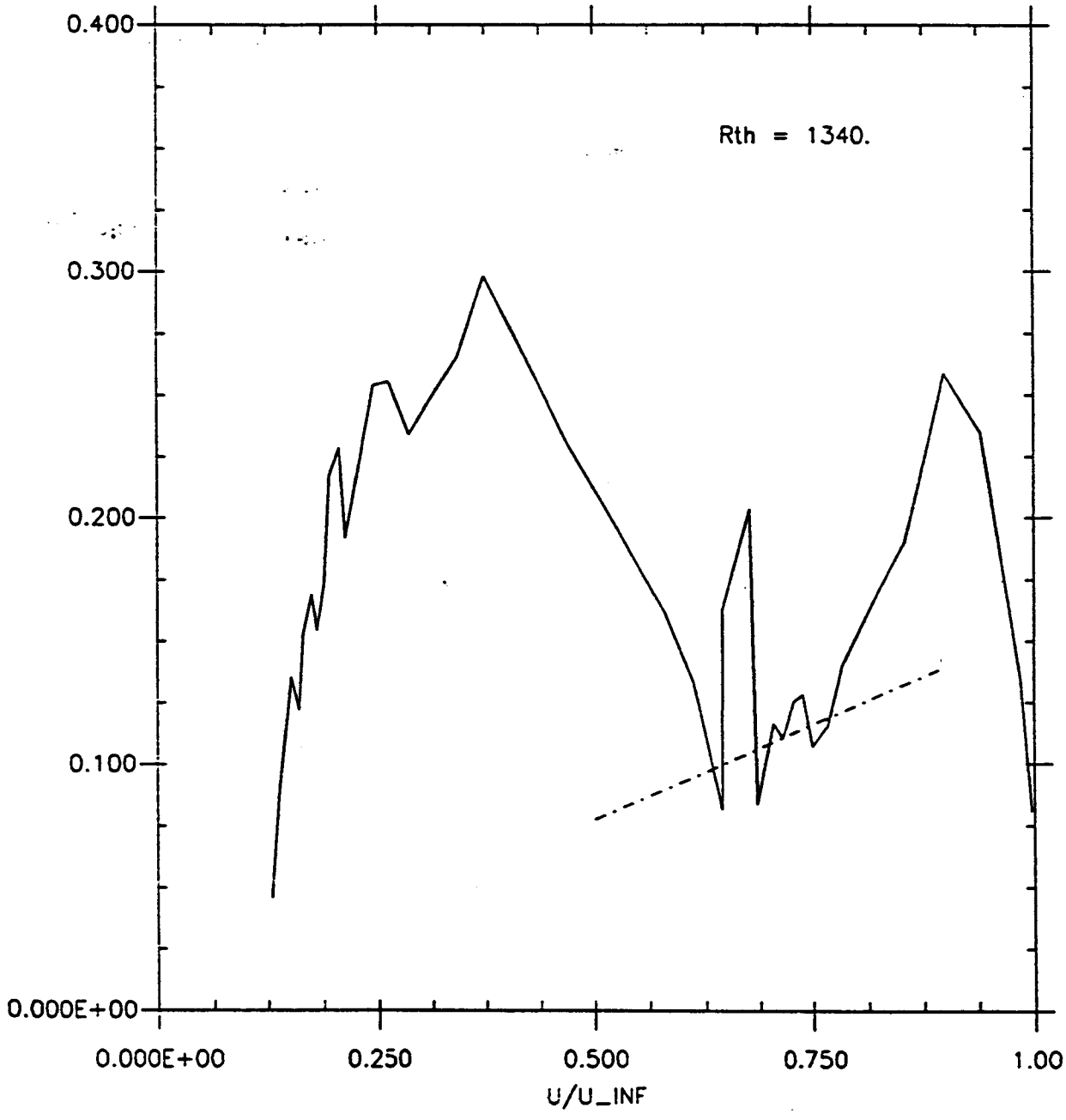

Fig. 3.1.2.2.07 *Outer variables*:

Purtell et al.. Rth = 1840.

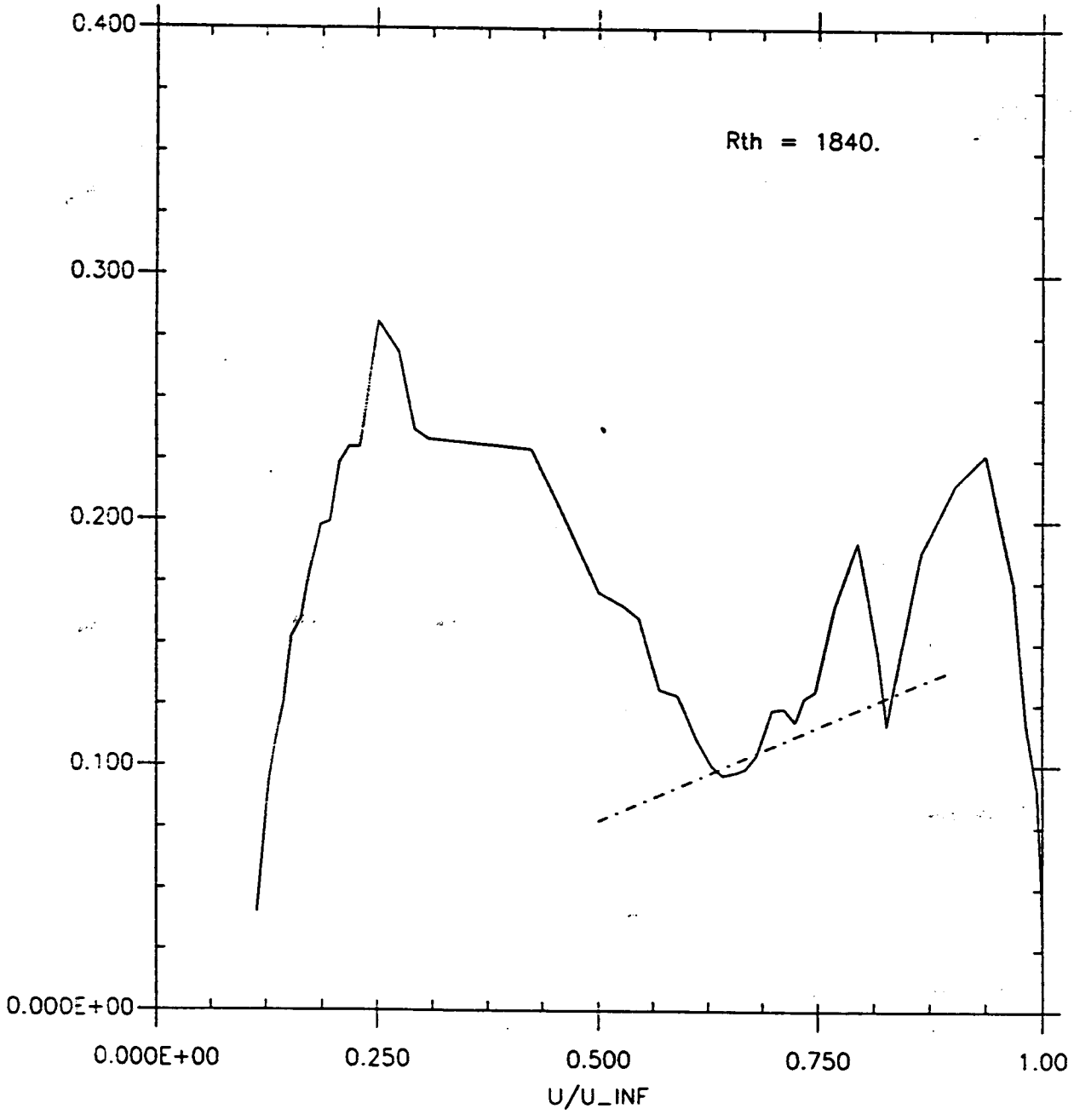

Fig. 3.1.2.2.09 *Outer variables*:

Purtell et al.. Rth = 3480.

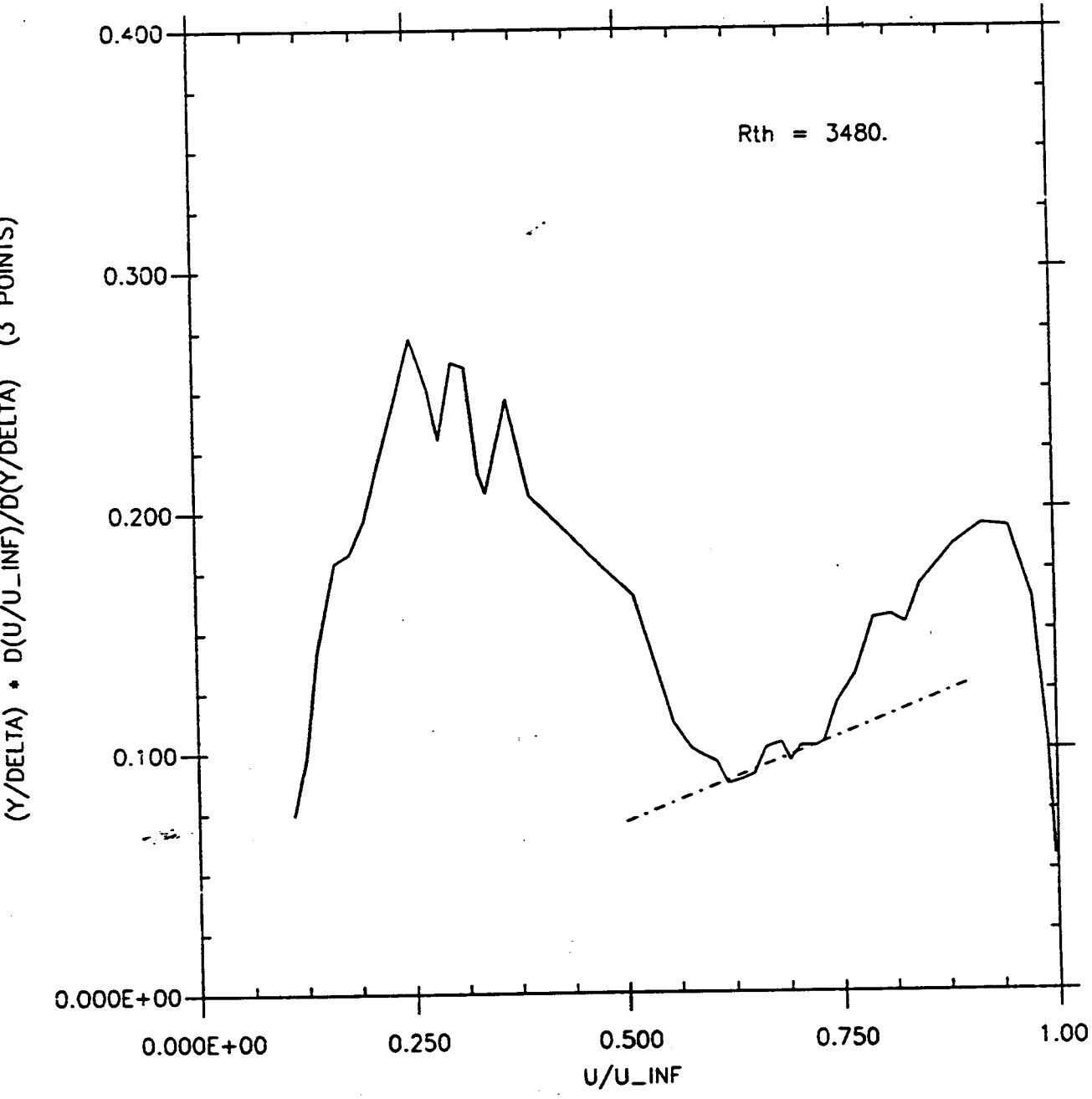

Fig. 3.1.2.2.11 *Outer variables*:

Purtell et al.. Rth = 5100.

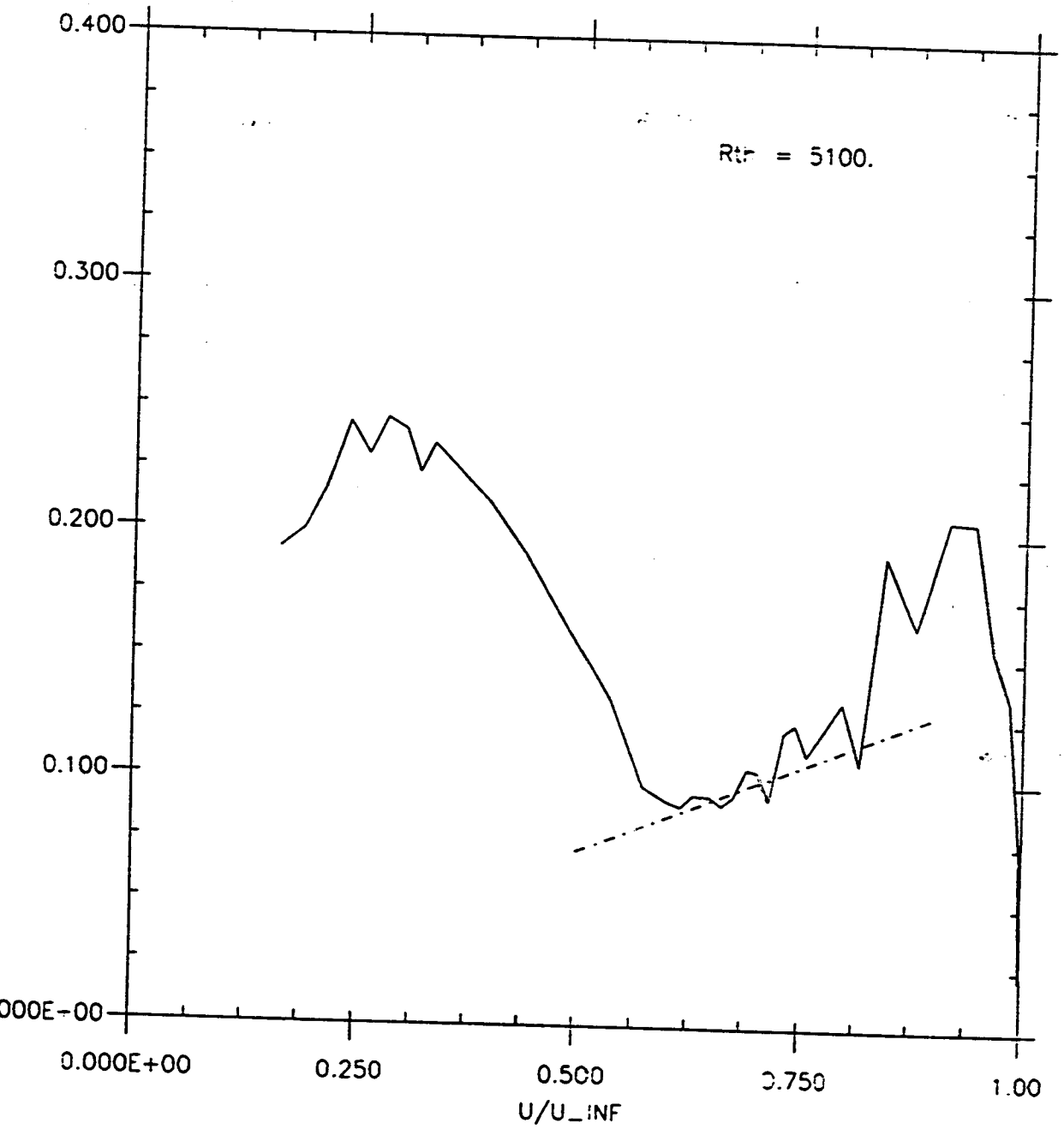

Fig. 3.2.1.1 *Inner variables*:

Smith & Walker. Rth = 5680, 18340, 37190, 44750.

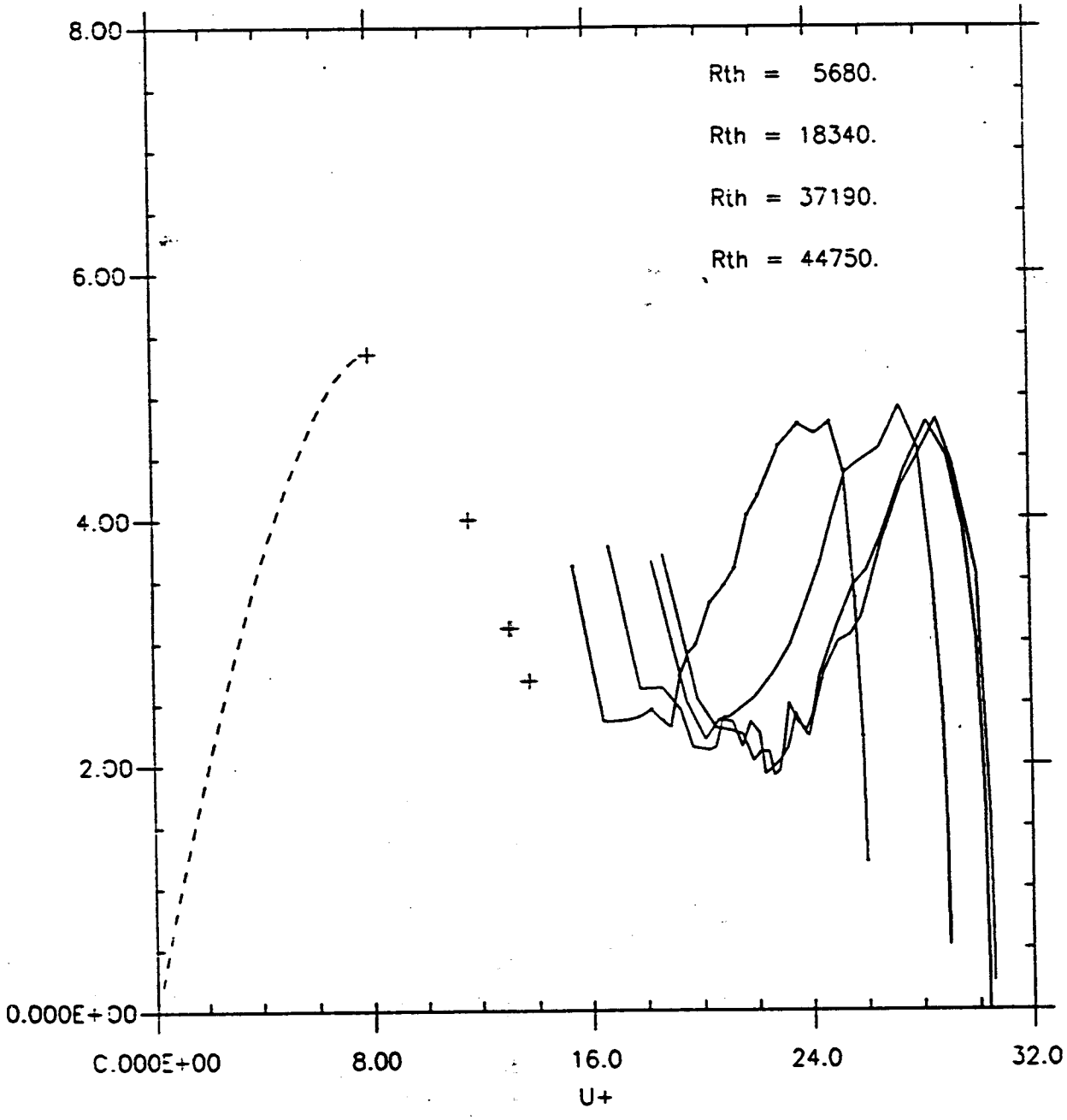

Fig. 3.2.1.2.03 *Inner variables*:

Smith & Walker. Rth = 5680.

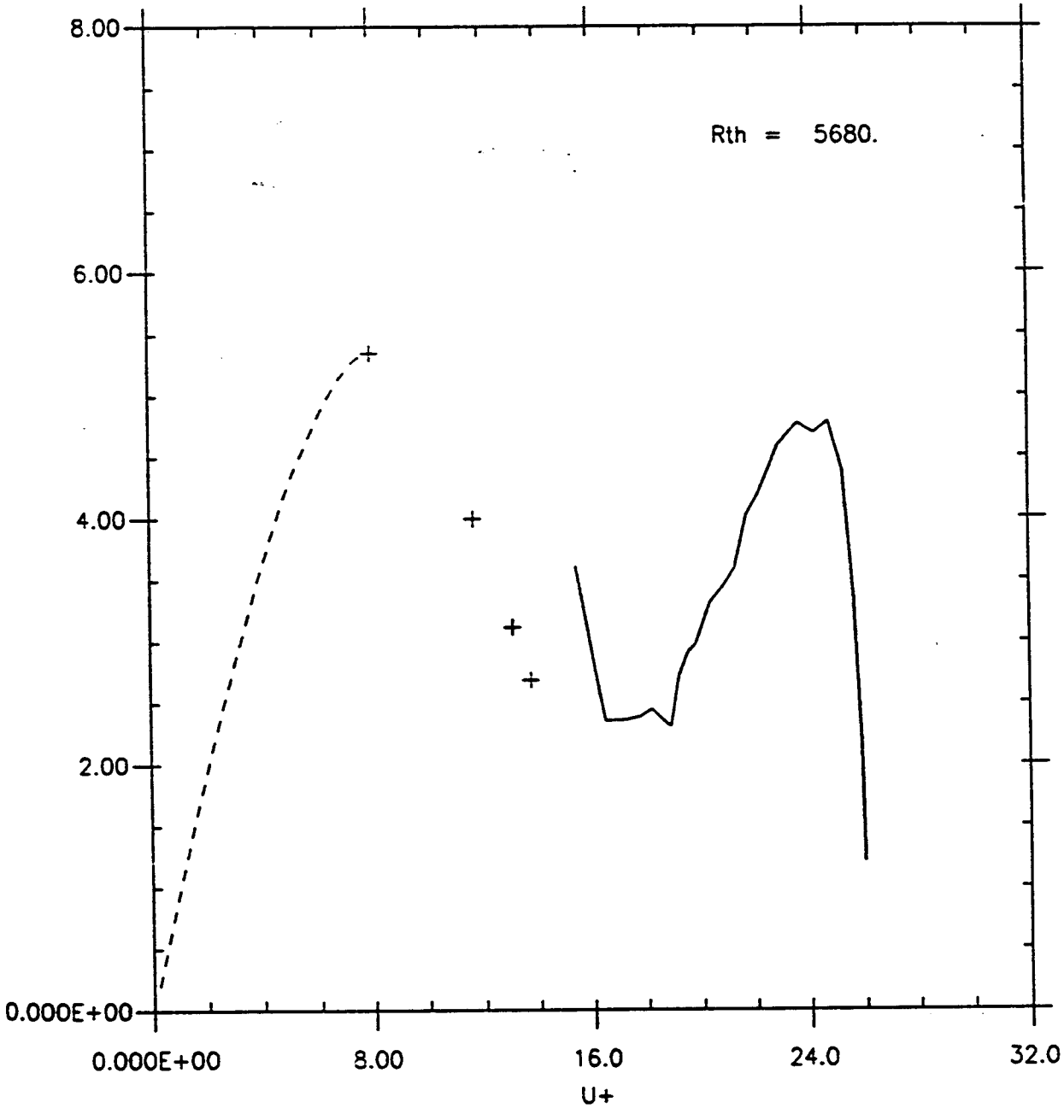

Fig. 3.2.1.2.06 *Inner variables*:

Smith & Walker. Rth = 18340.

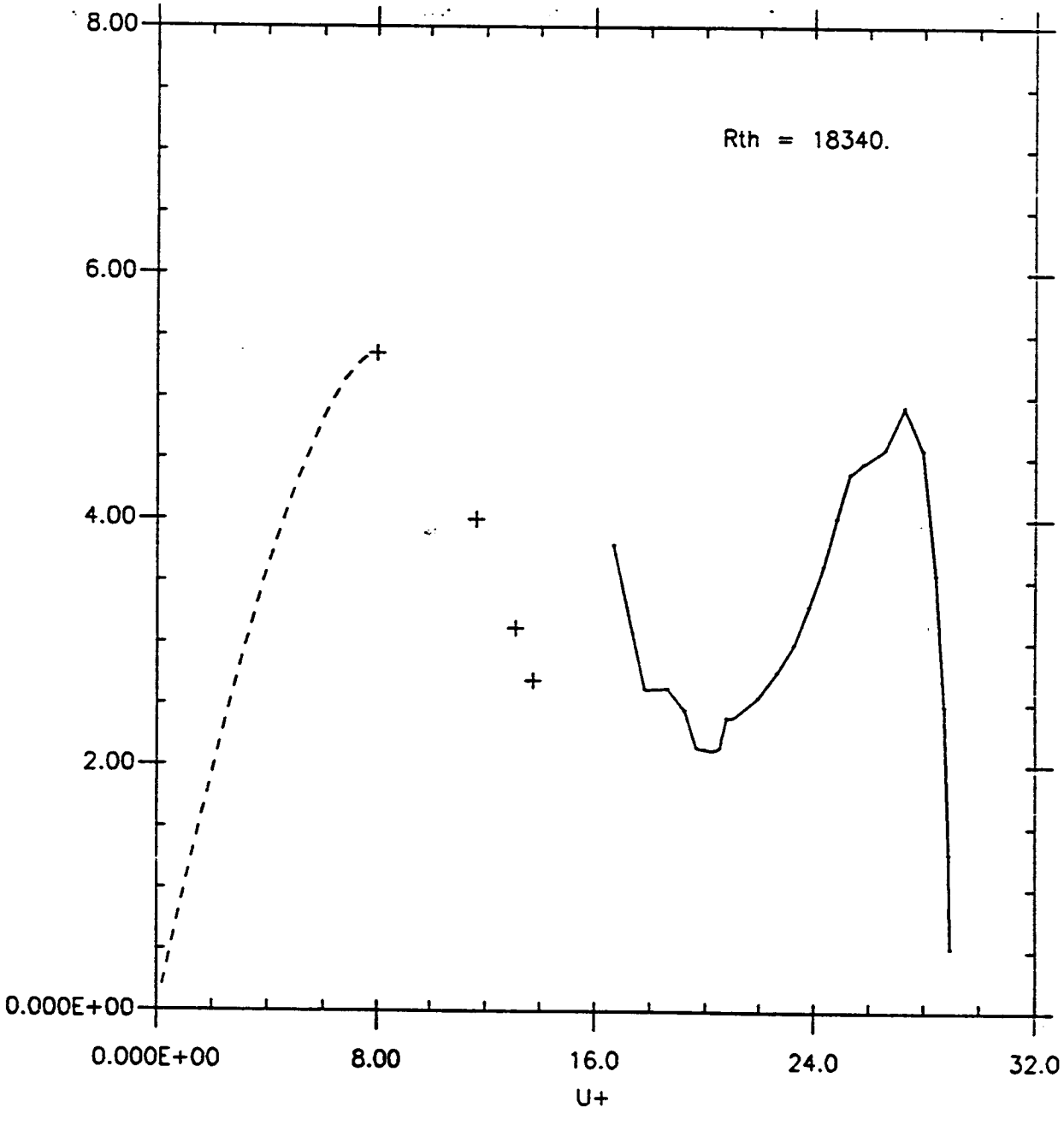

Fig. 3.2.1.2.10 *Inner variables*:
Smith & Walker. Rth = 37190.

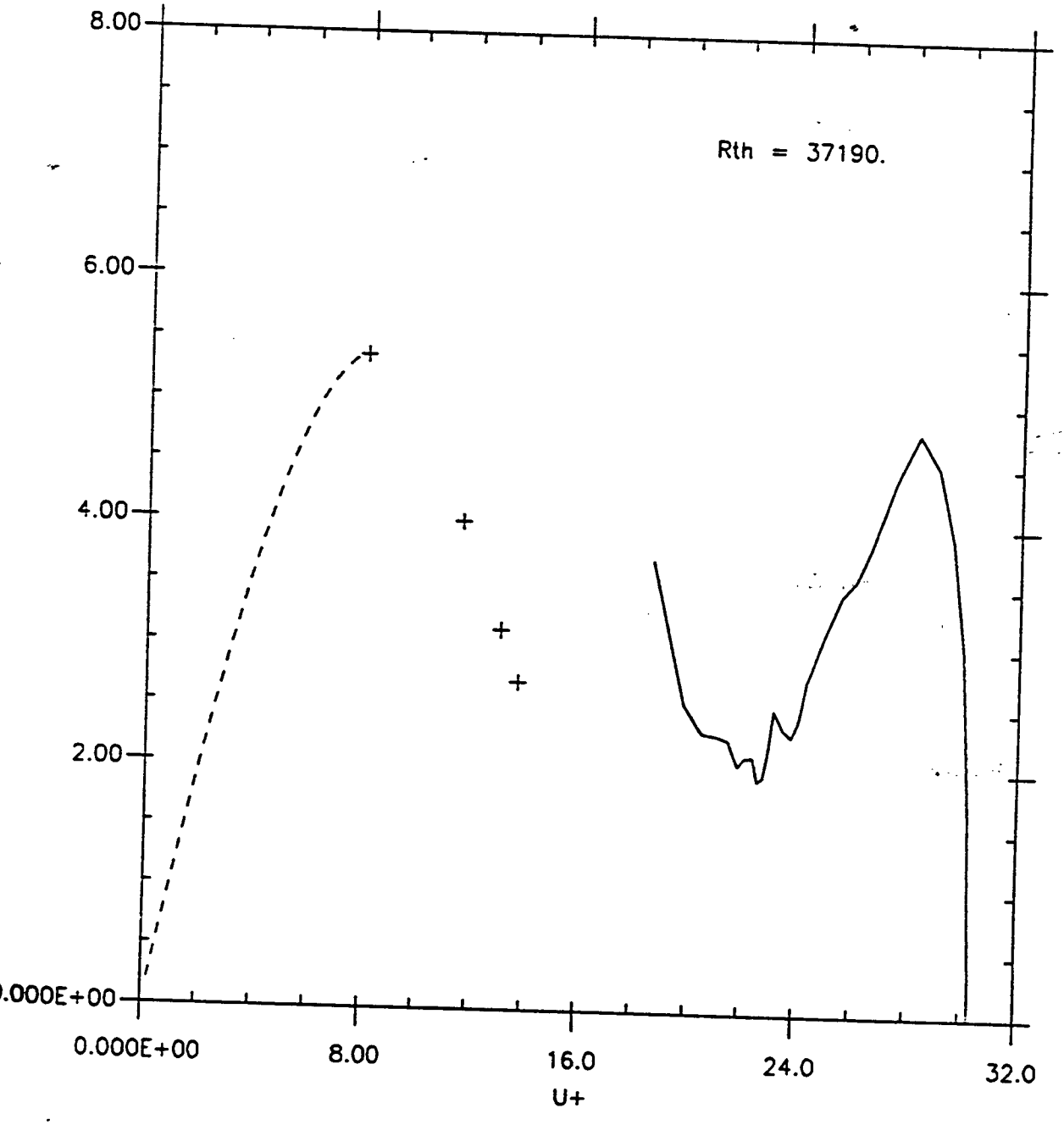

Fig. 3.2.1.2.13 *Inner variables*:

Smith & Walker. Rth = 44750.

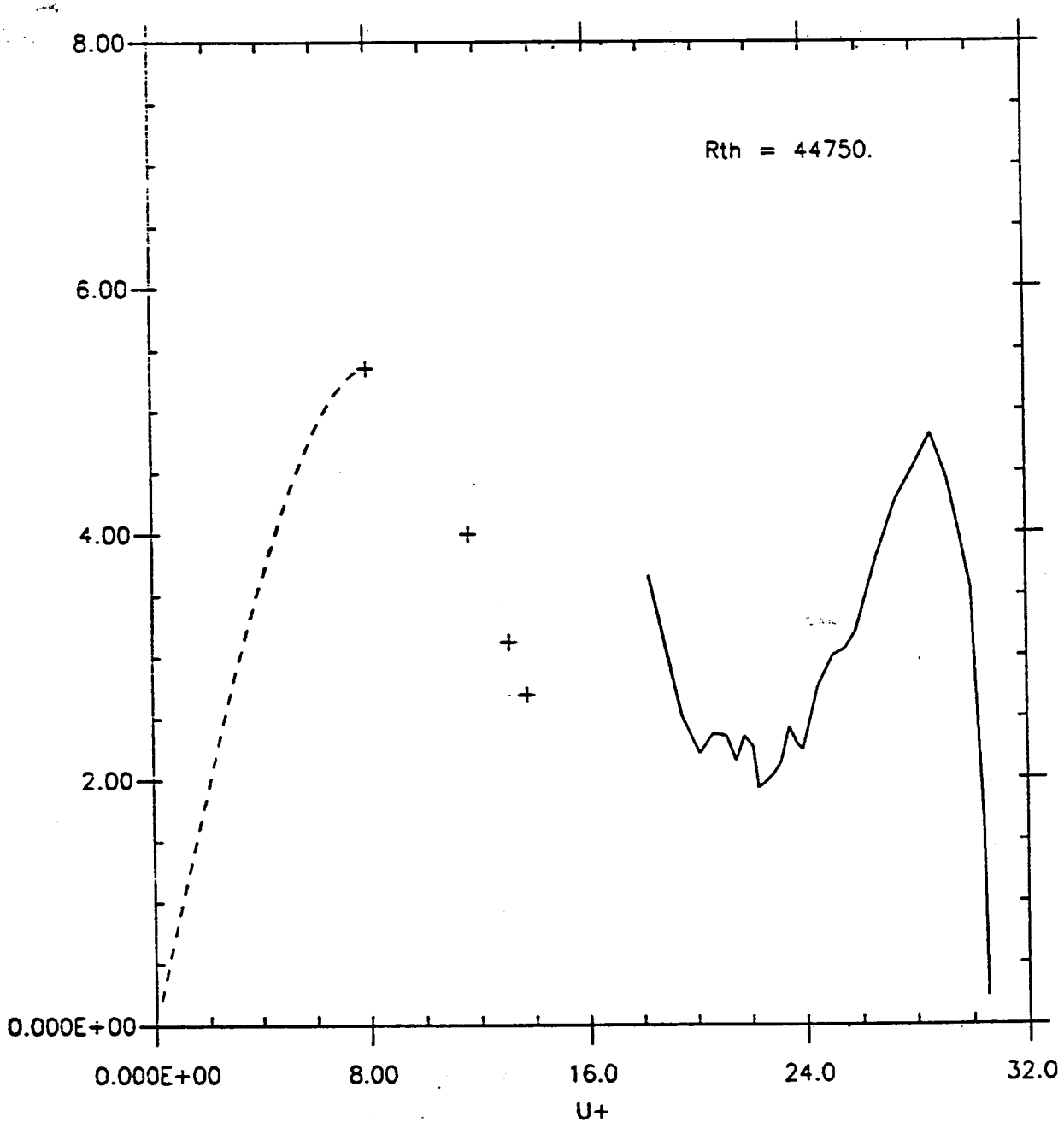

Fig. 3.2.2.1 *Inner variables*:

Purtell et al.. Rth = 1840, 3480, 5100.

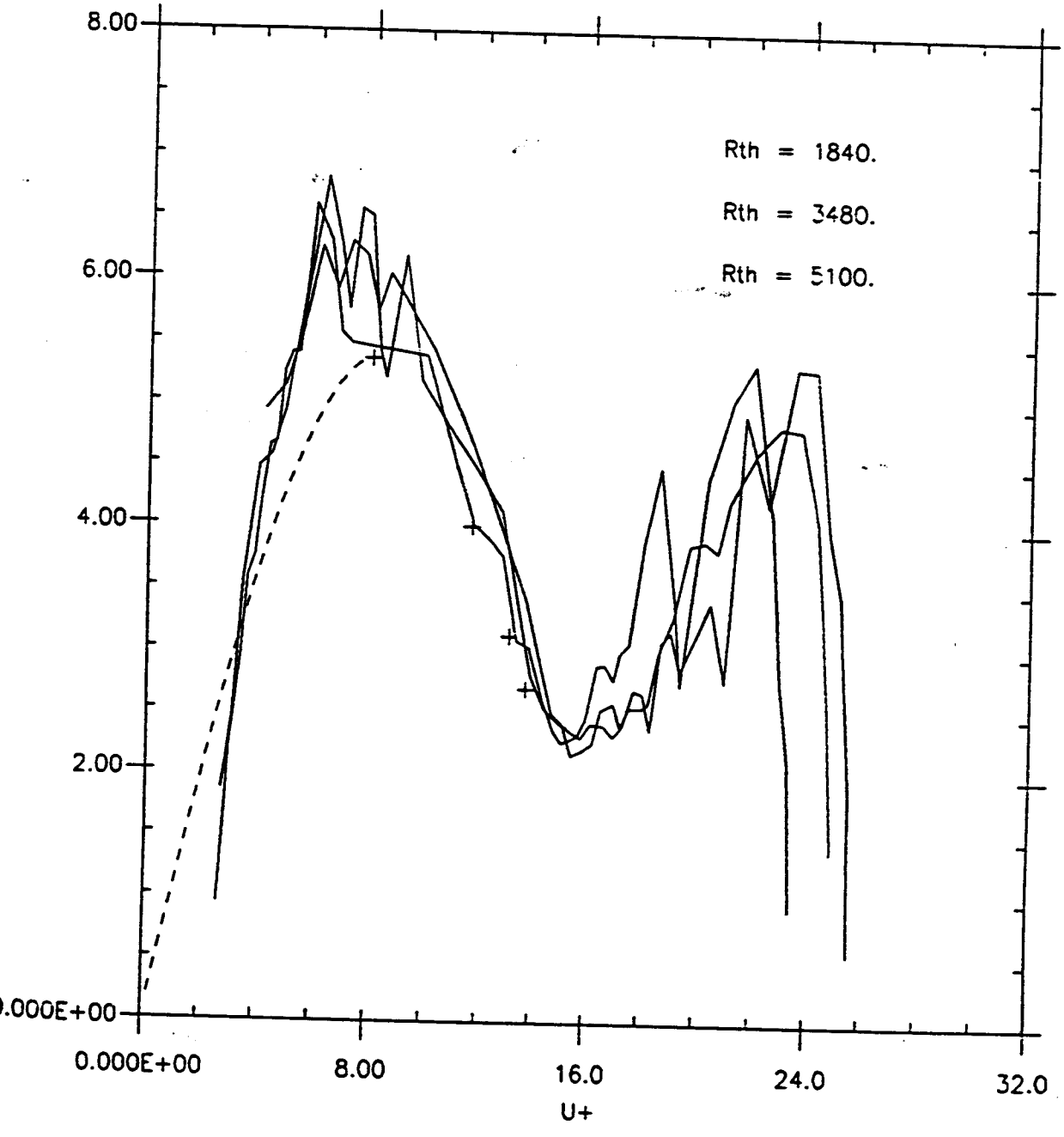

Fig. 3.2.2.2.05 *Inner variables*:

Purtell et al.. Rth = 1340.

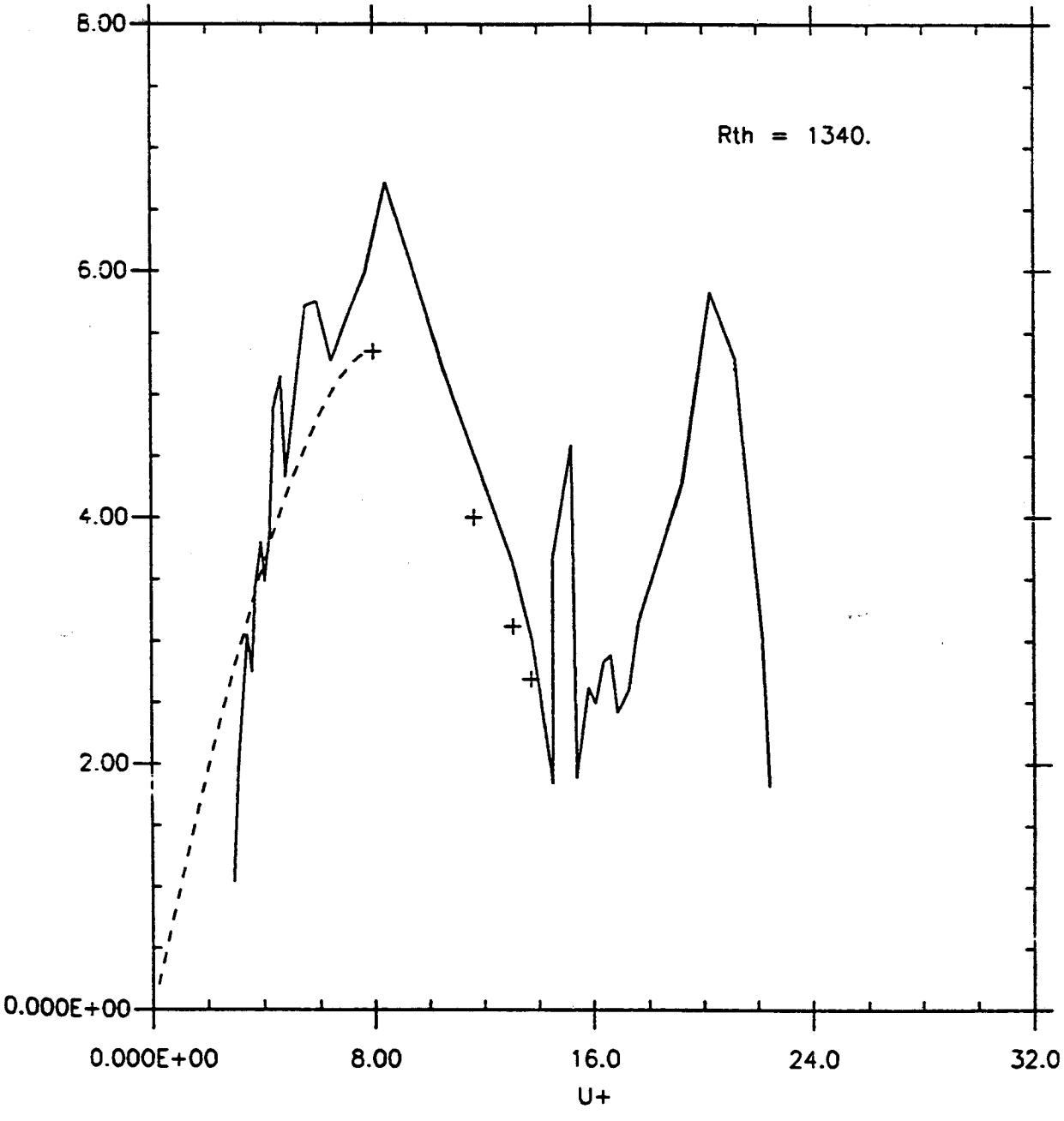

Fig. 3.2.2.2.07 *Inner variables:*

Purtell et al.. Rth = 1840.

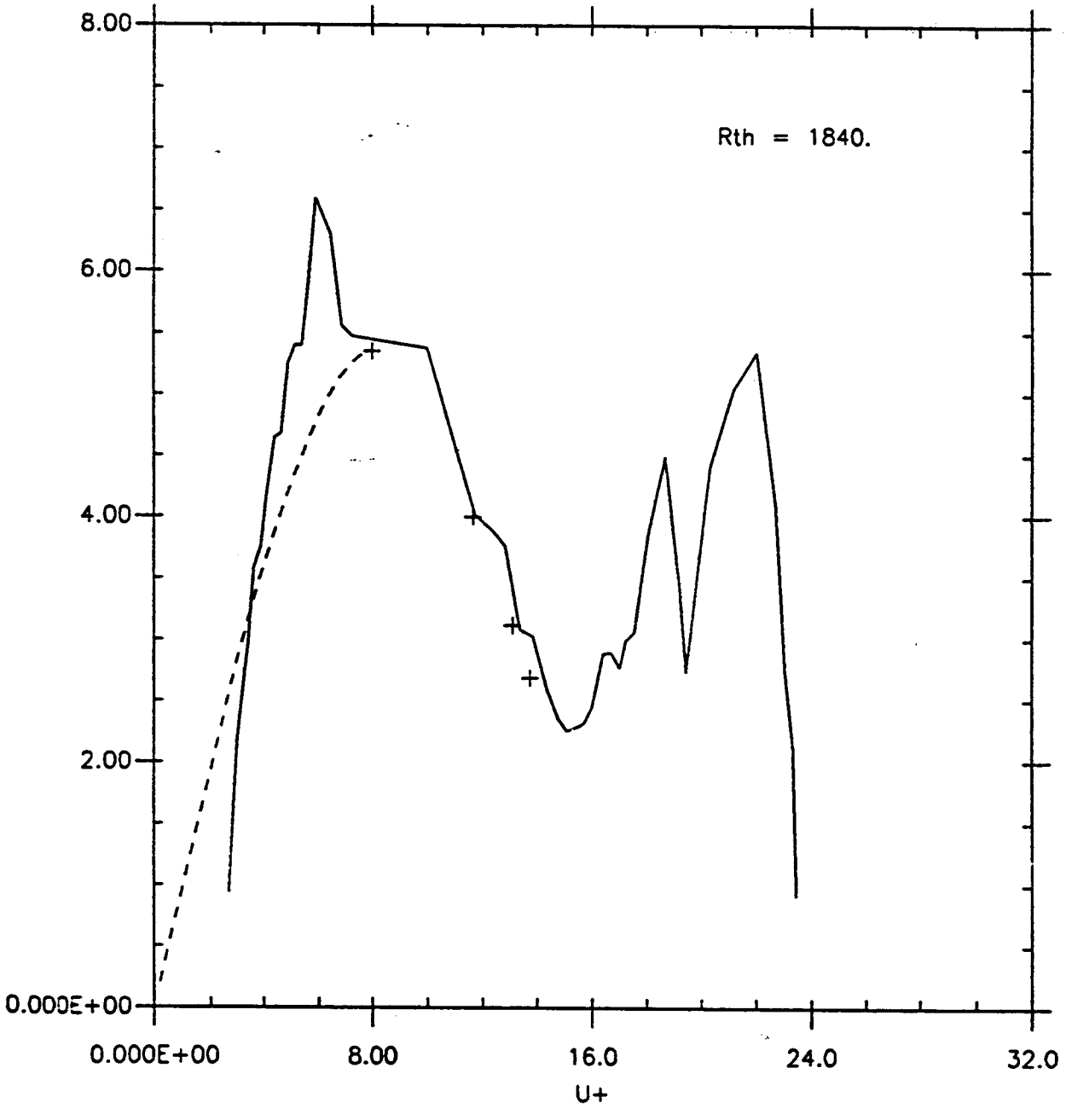

Fig. 3.2.2.2.09 *Inner variables*:

Purtell et al.. Rth = 3480.

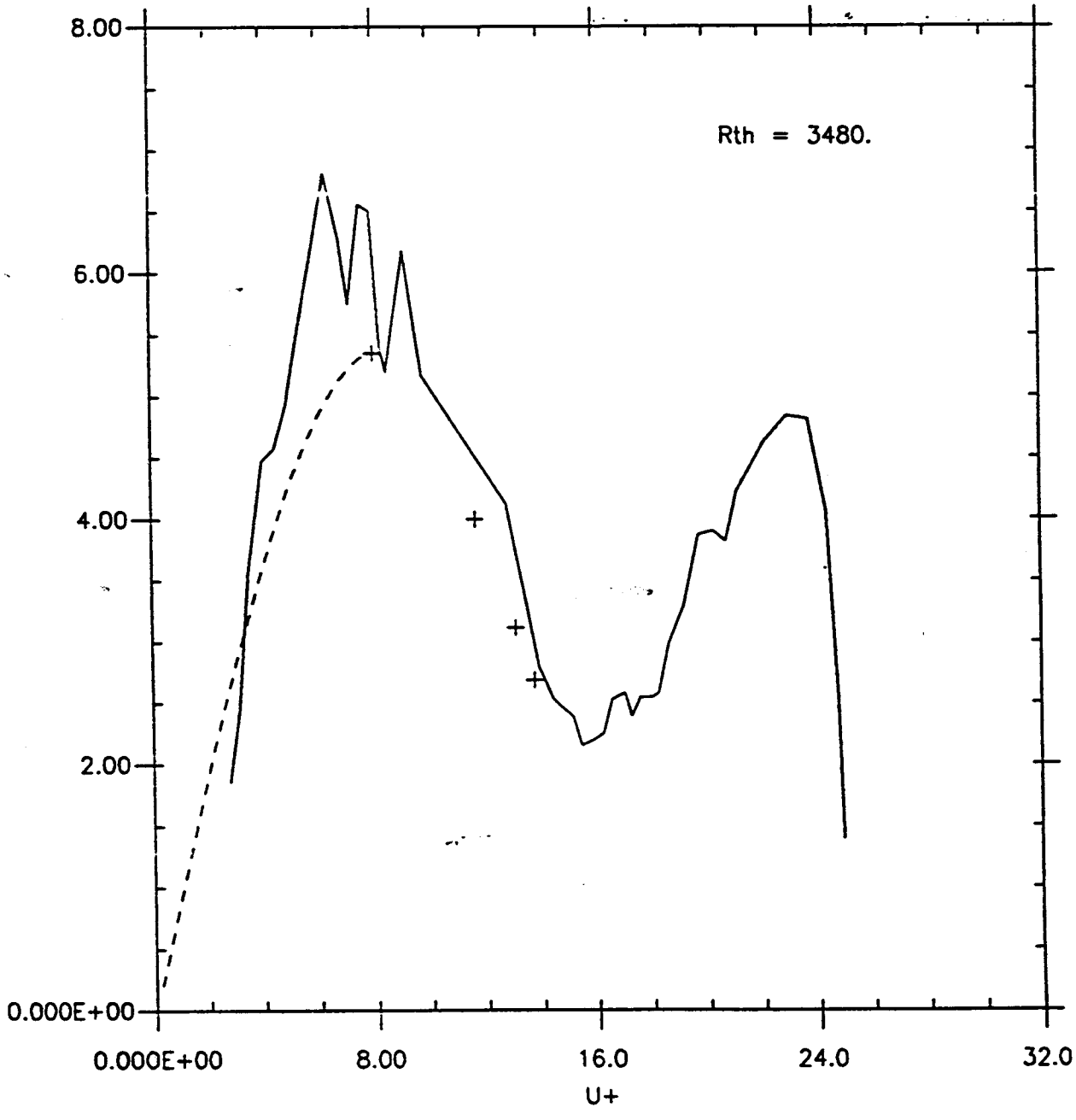

Fig. 3.2.2.2.11 *Inner variables*:

Purtell et al.. Rth = 5100.

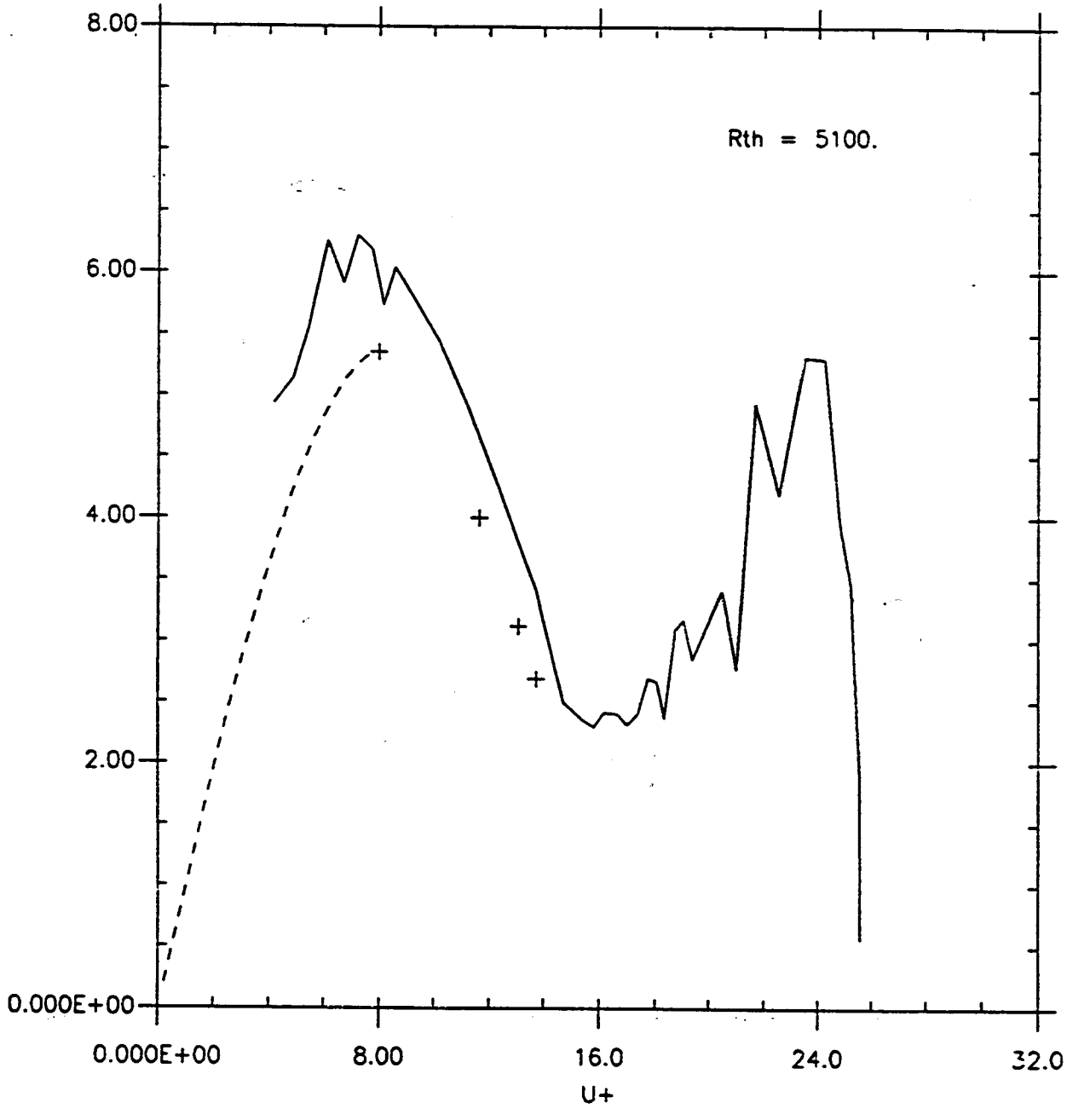

A.4 BOUNDARY LAYER PARAMETER AND FRICTION COEFFICIENT

Fig. 4.1.1.0 *Displacement thickness*:

Smith and Walker, Purtell, Wieghardt & Tillmann.

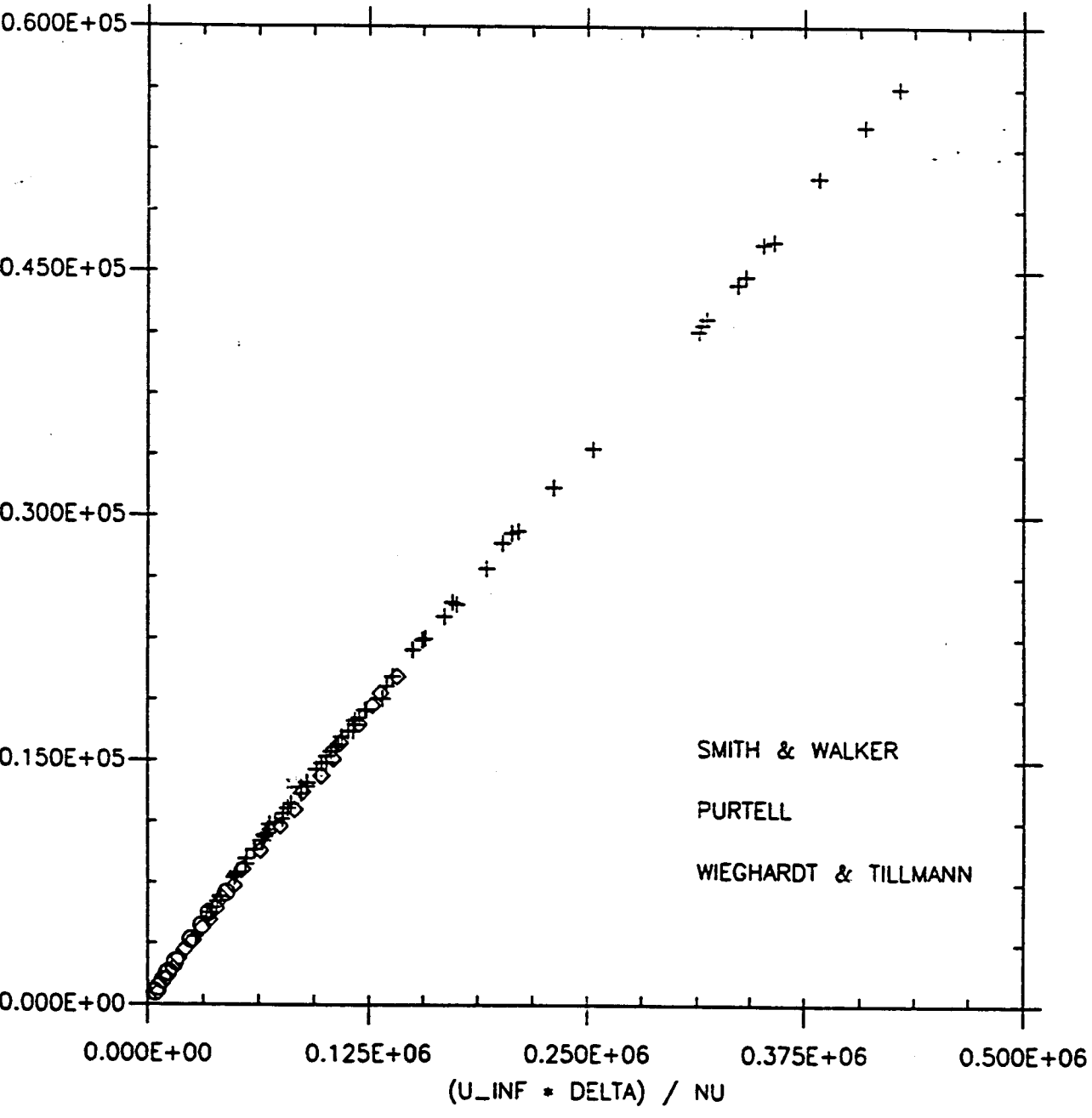

Fig. 4.1.2.0 *Momentum thickness*:

Smith and Walker, Purtell, Wieghardt & Tillmann.

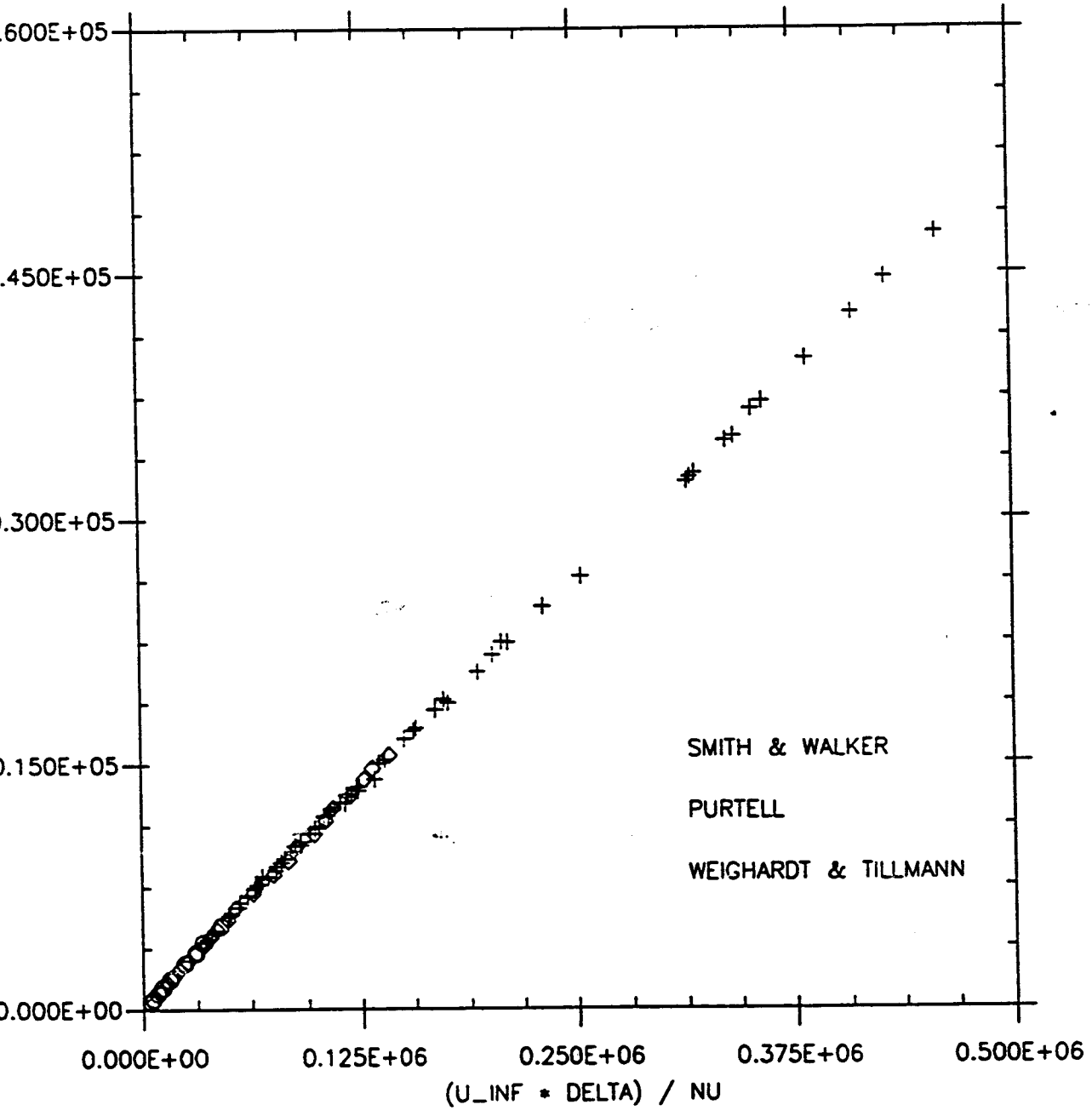

Fig. 4.1.3.0 *Shape factor*:

Smith and Walker, Purtell, Wieghardt & Tillmann.

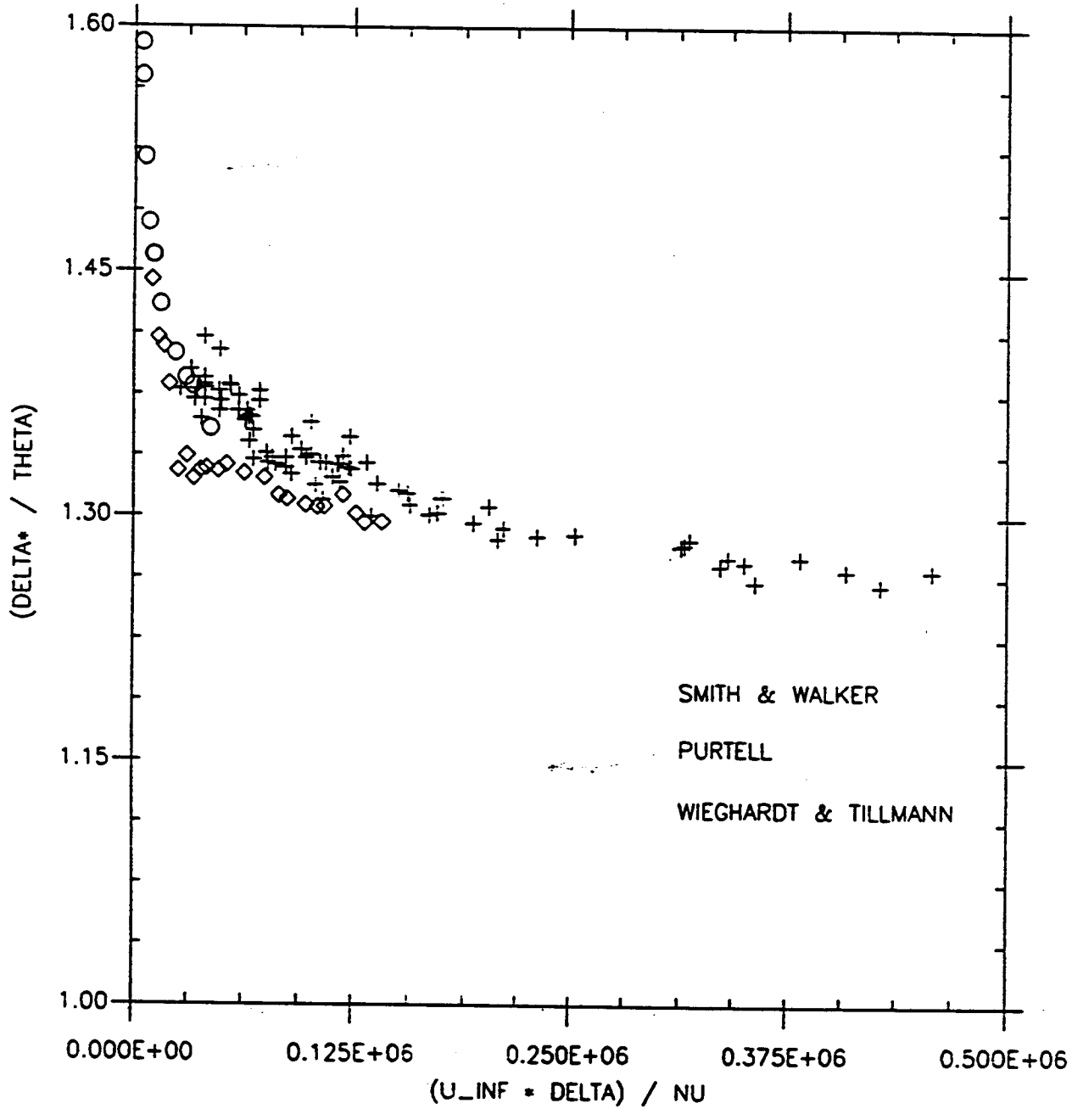

Fig. 4.1.2.0 *Momentum thickness*:

Smith and Walker, Purtell, Wieghardt & Tillmann.

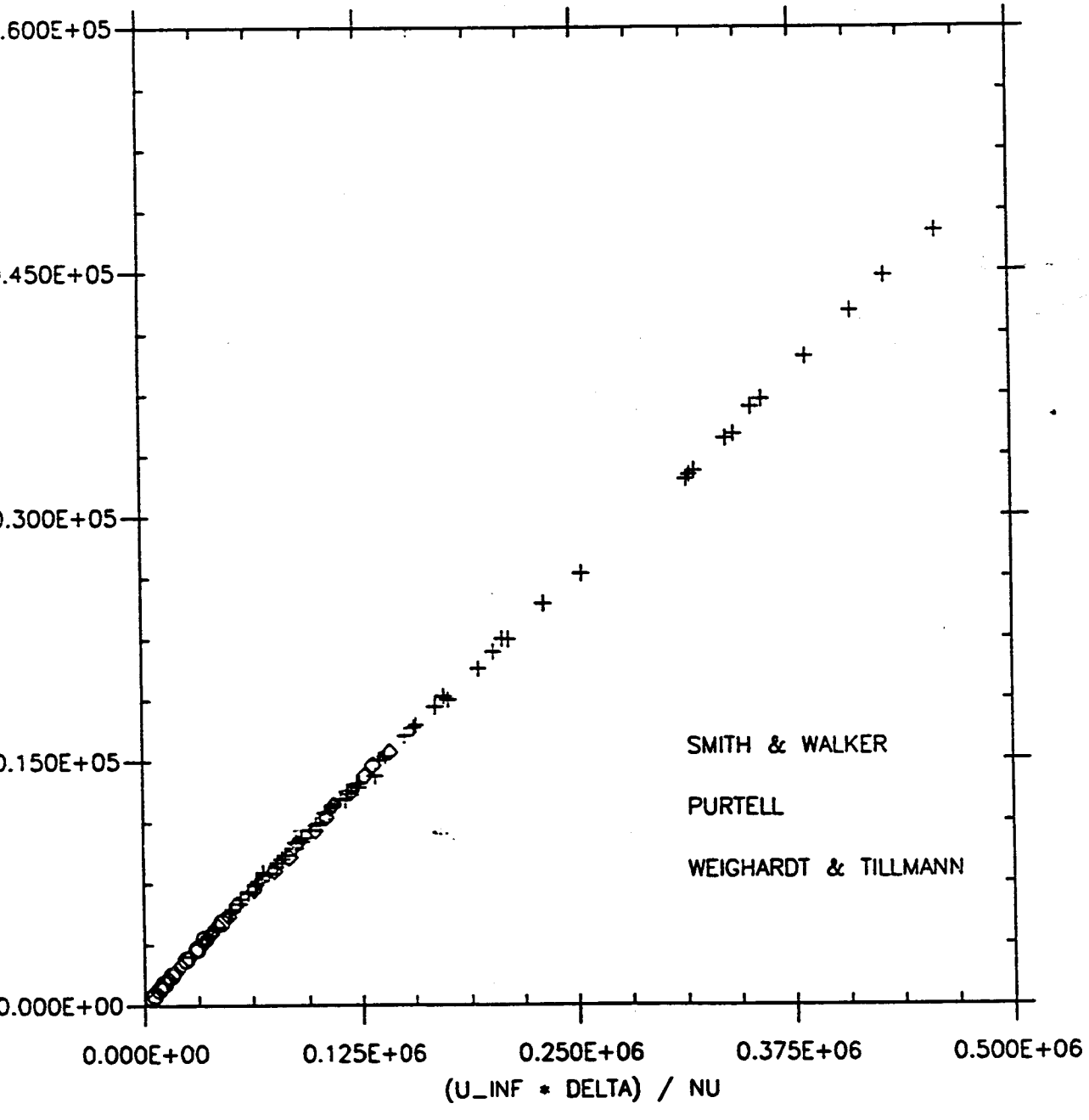

Fig. 4.1.3.0 *Shape factor:*

Smith and Walker, Purtell, Wieghardt & Tillmann.

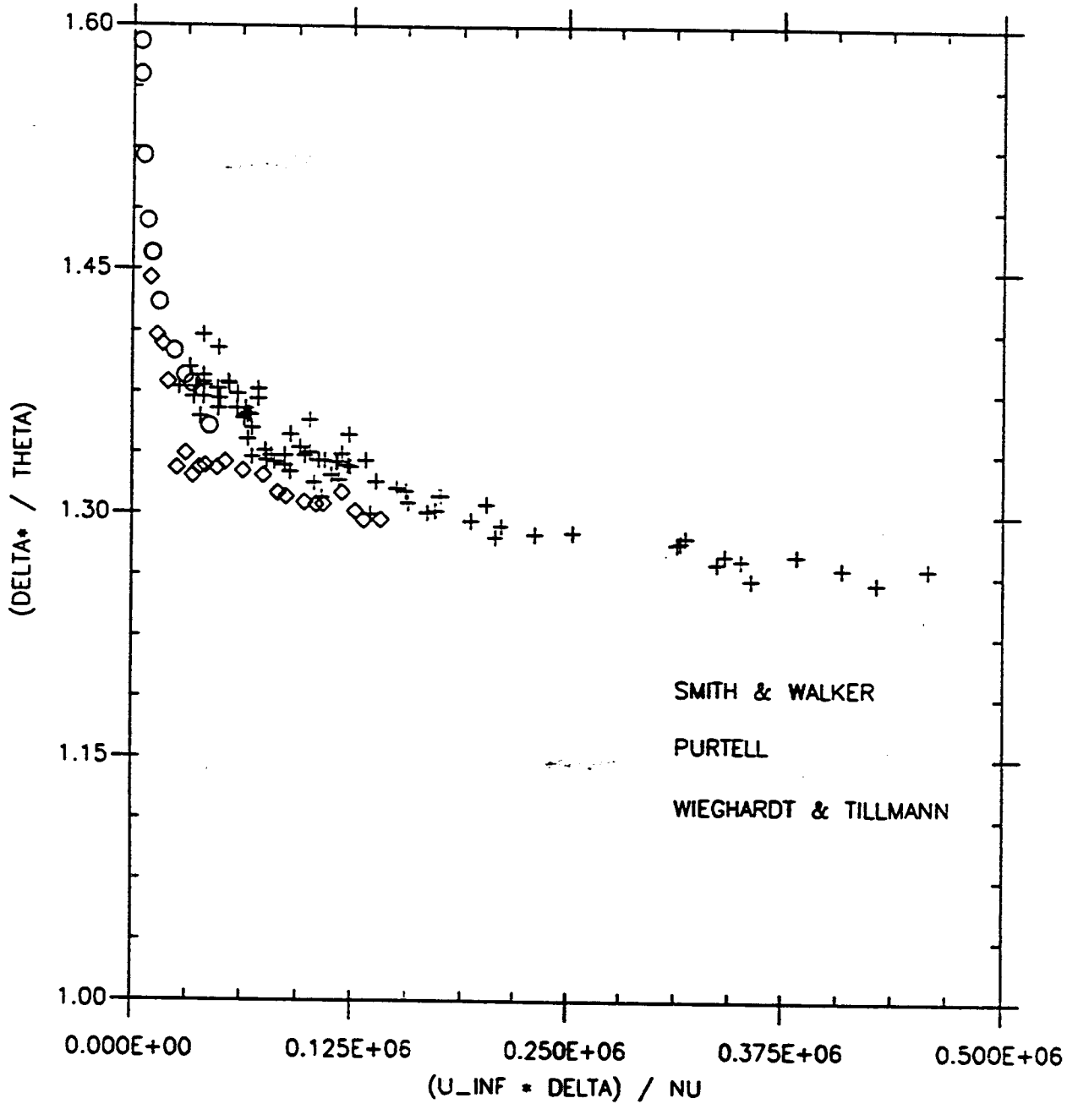

Fig. 4.1.3.0 *Friction coefficient in local variable*:
Smith and Walker, Purtell, Schultz & Grunow.

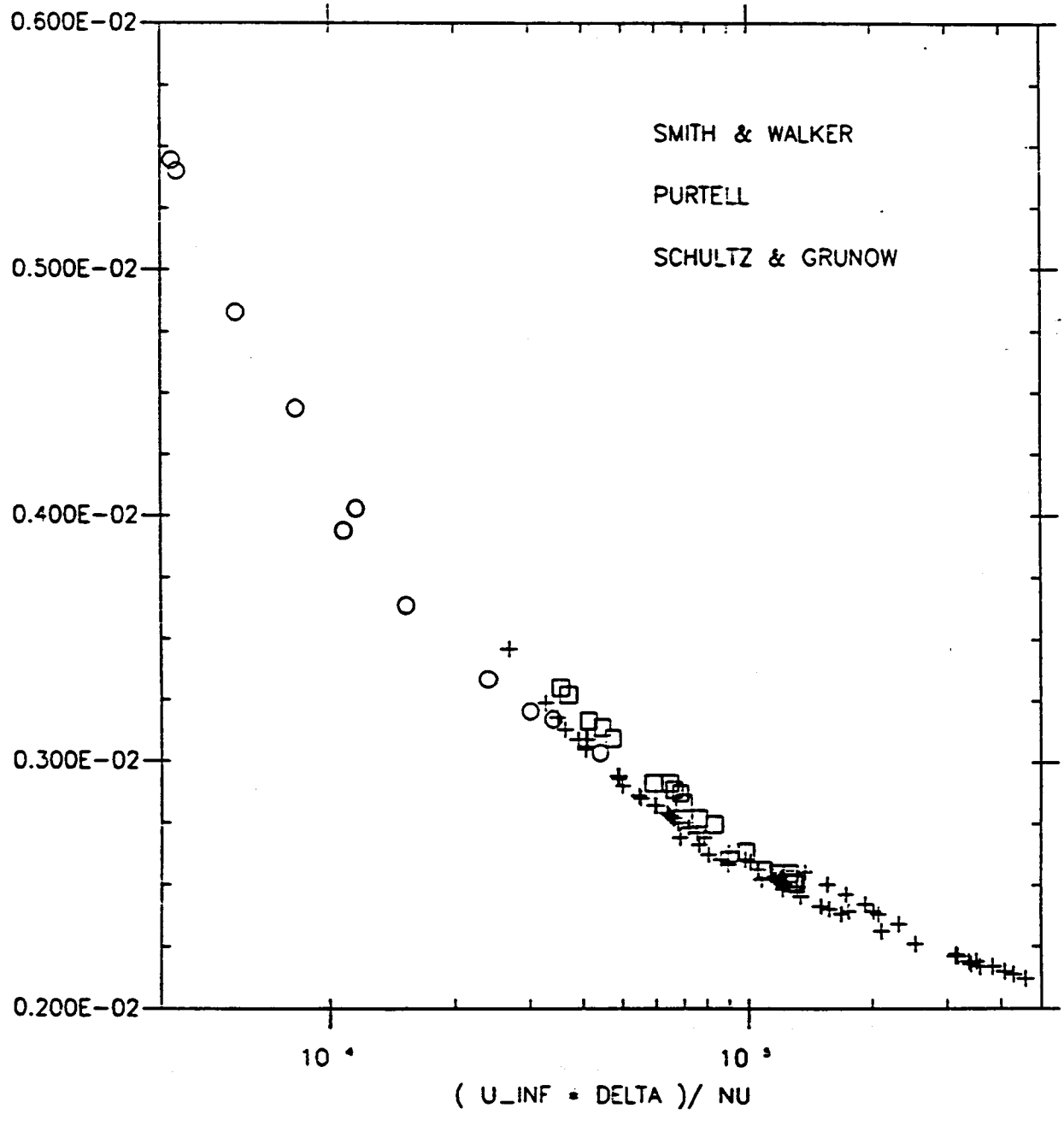

Fig. 4.1.4.0 *X dependence*:

Smith and Walker, Purtell, Wieghardt & Tillmann.

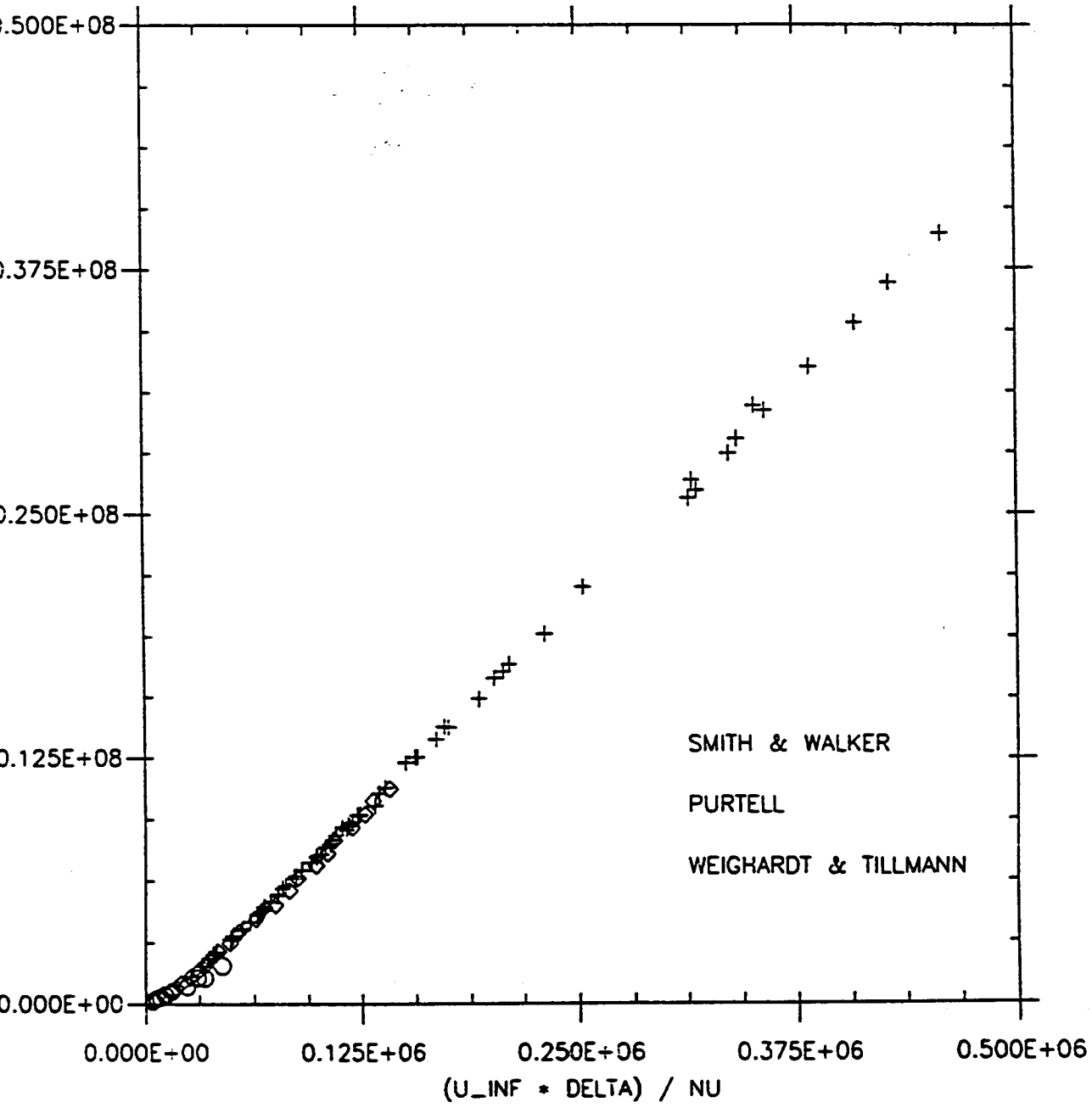

Fig. 4.1.6.0 *Friction coefficient as a function of x:*
Smith and Walker, Schultz & Grunow.

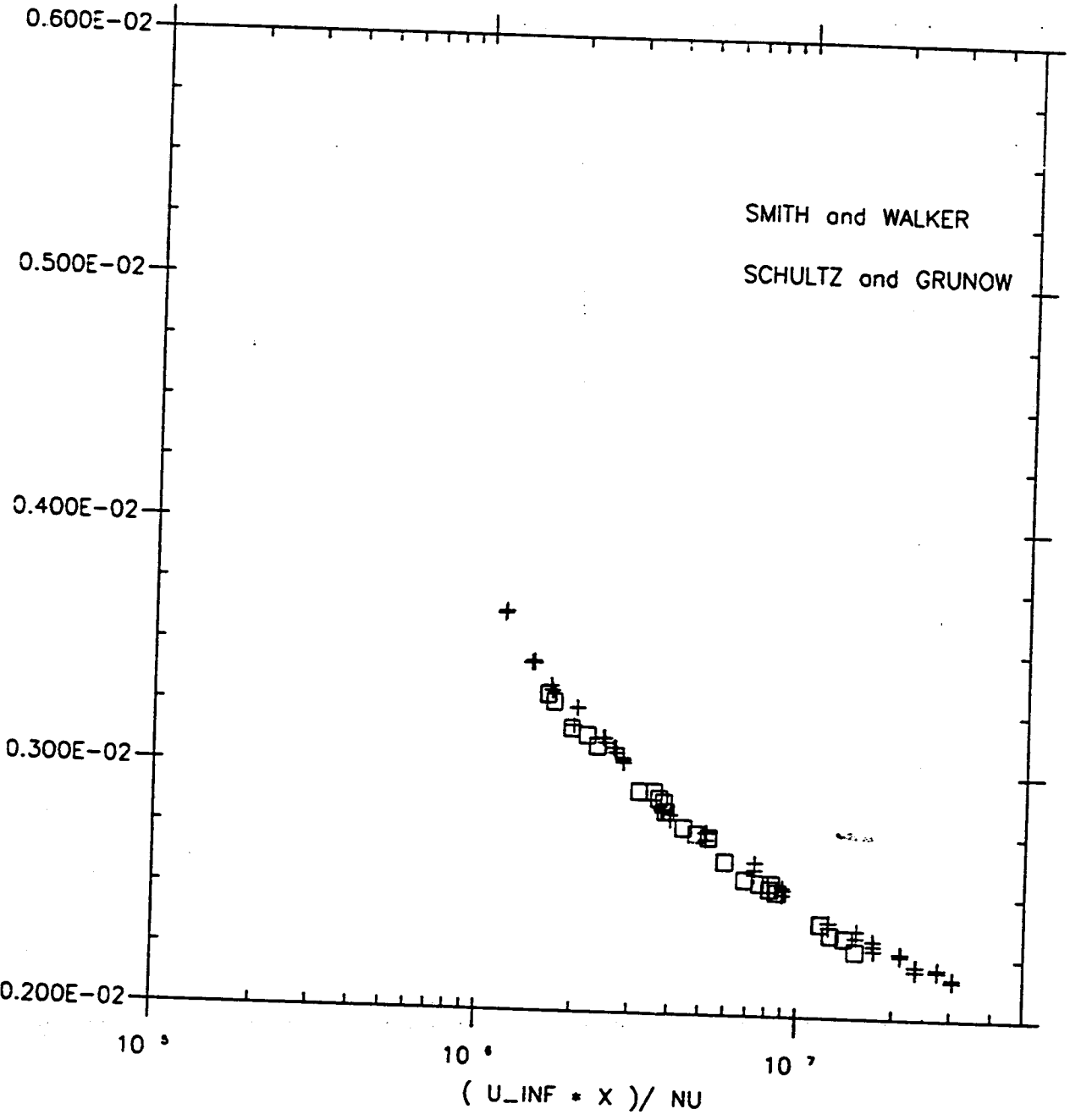

Fig. 4.1.6.1.1 *Friction coefficient as a function of x:*

Smith and Walker (53 points).

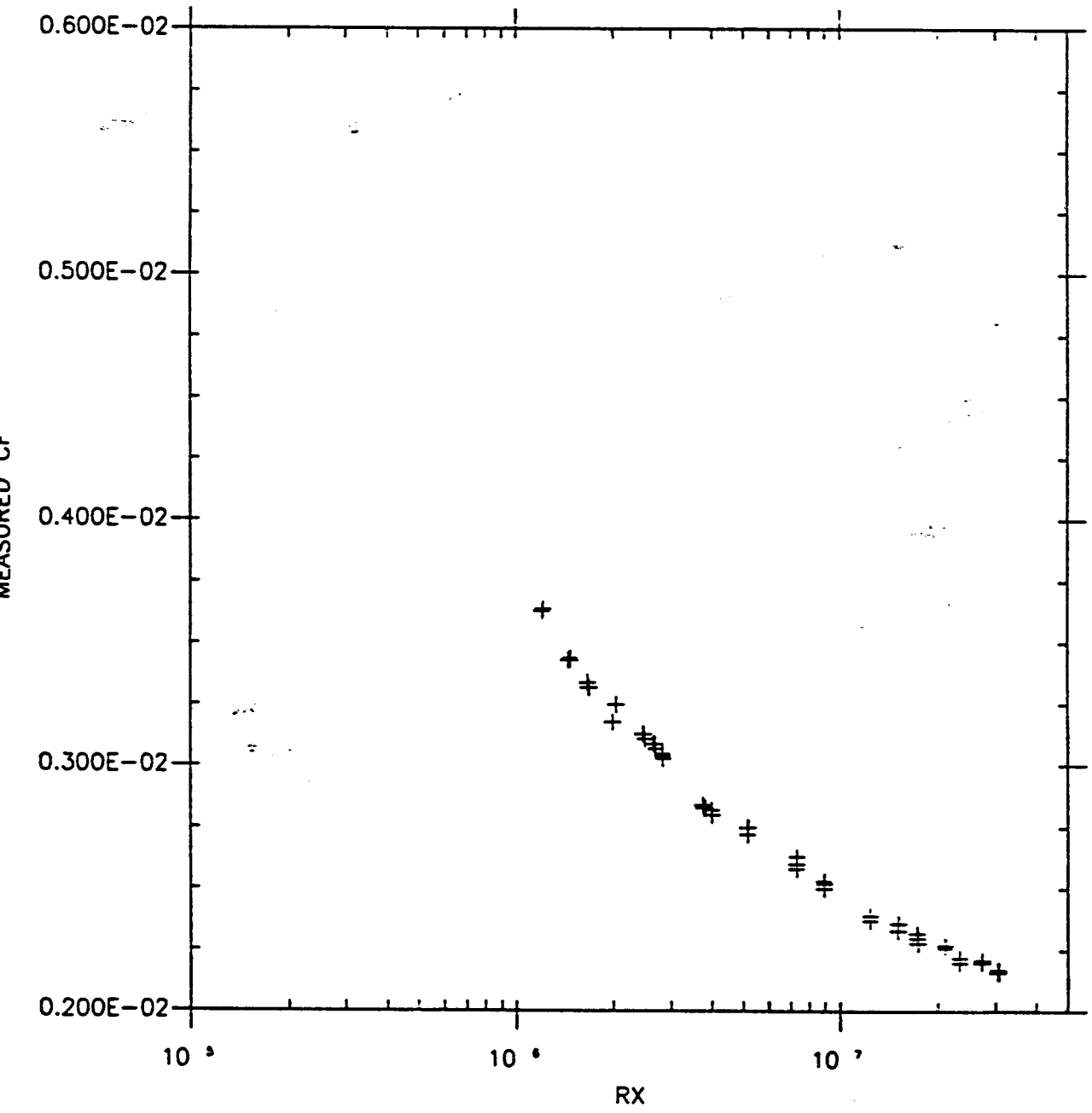

Fig. 4.1.6.1.2 *Friction coefficient as a function of x*:
Smith and Walker (167 points).

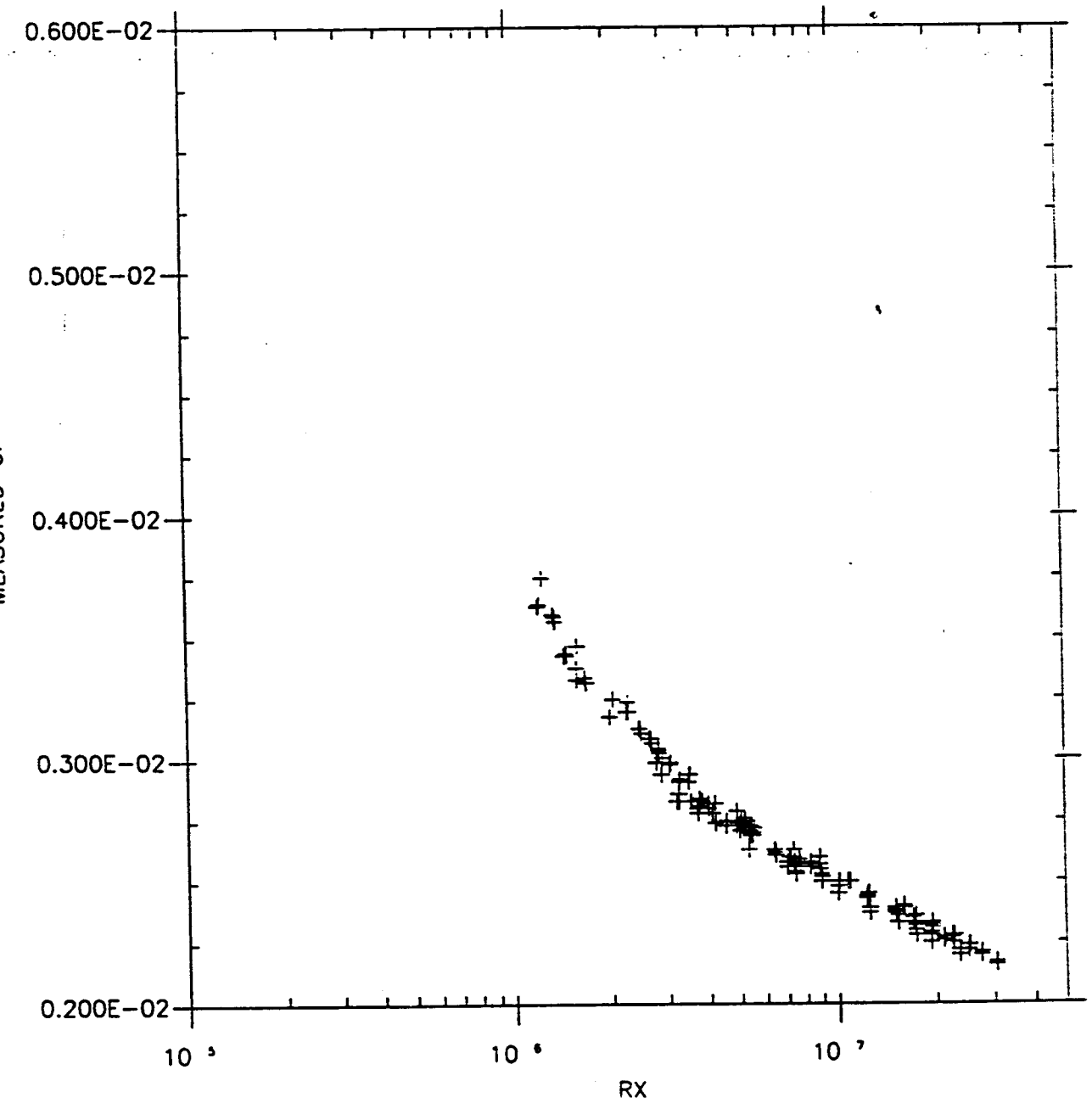

Verification of COLES' results:

Fig. 4.2.1.1.1 *Displacement thickness*:

Smith and Walker. x = 15.75 in, 27.75 in, 39.75 in, 51.75 in.

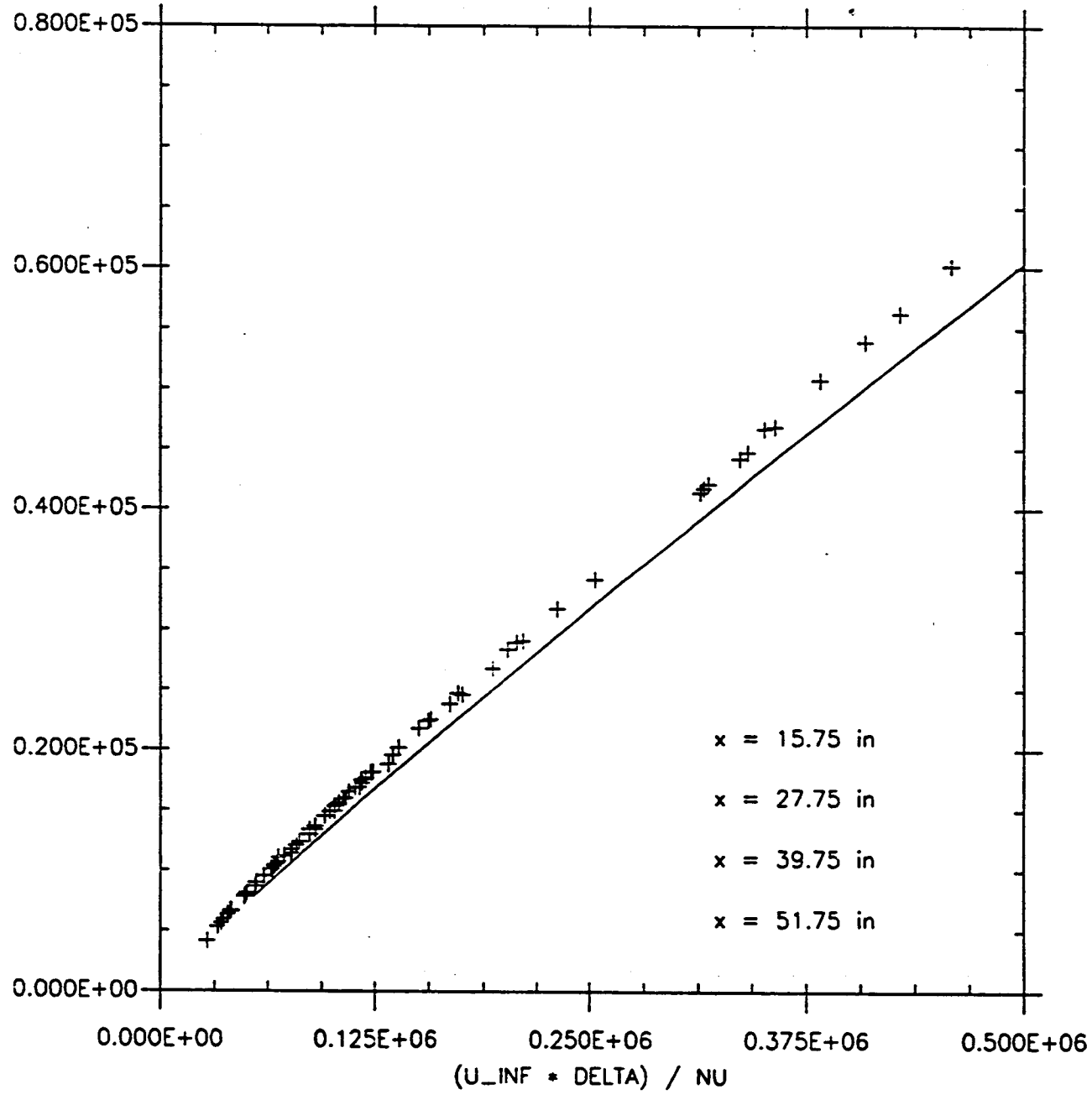

Fig. 4.2.1.2 *Displacement thickness*:

Purtell et al.

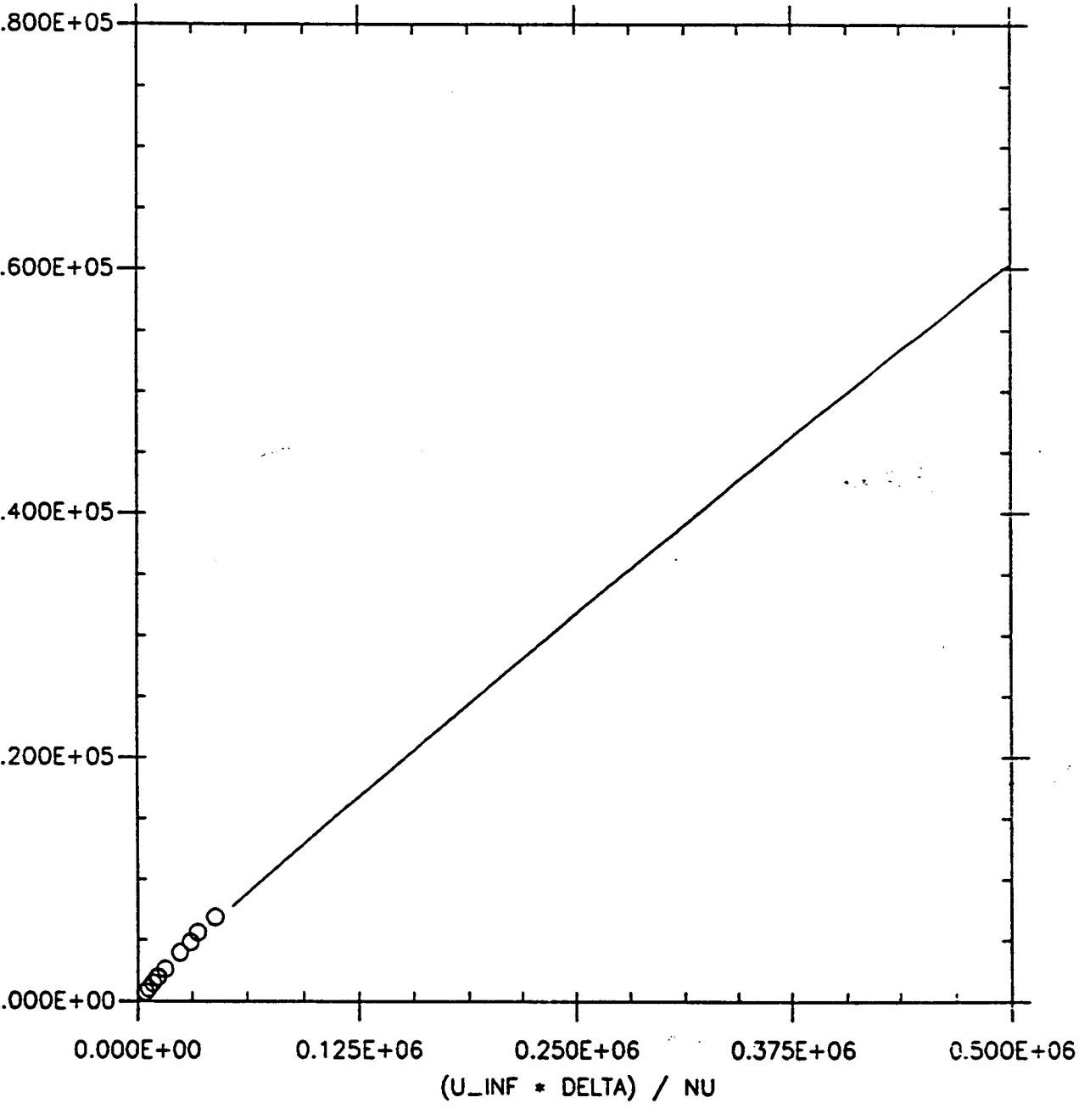

Fig. 4.2.1.3 *Displacement thickness:*

Wieghardt and Tillmann.

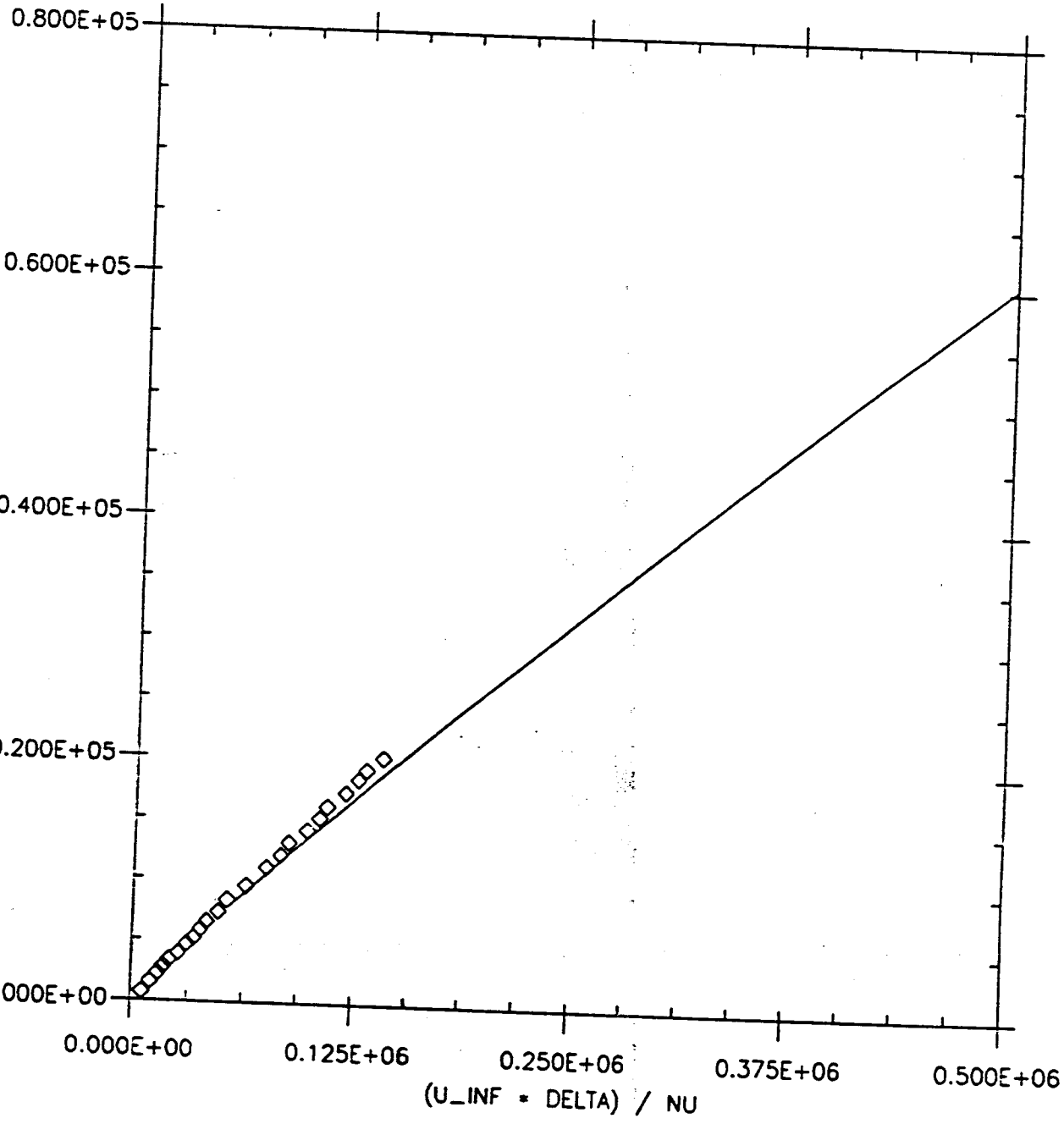

Fig. 4.2.2.1.1 *Momentum thickness*:

Smith and Walker. x = 15.75 in, 27.75 in, 39.75 in, 51.75 in.

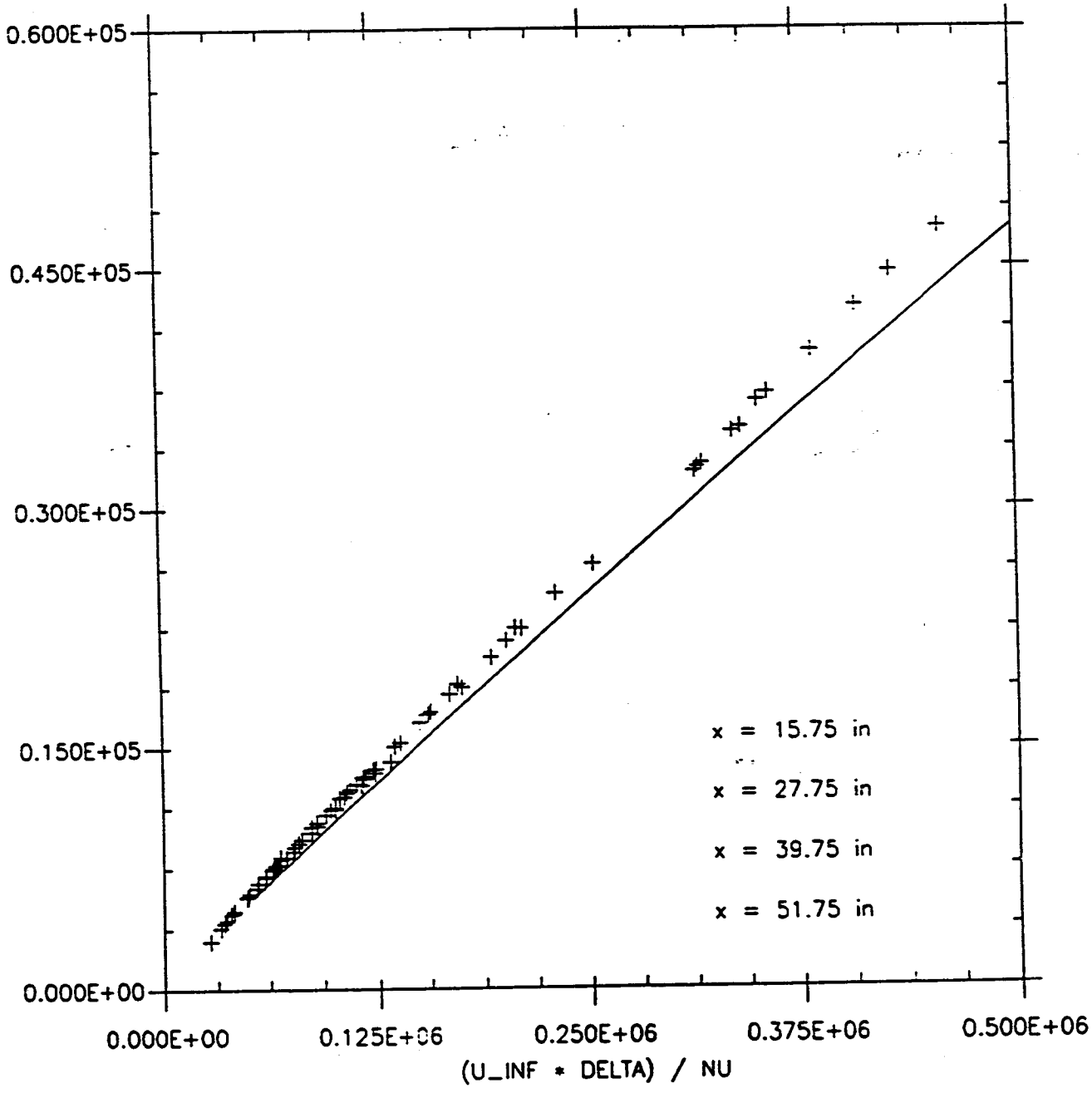

Fig. 4.2.2.2 *Momentum thickness*:

Purtell et al.

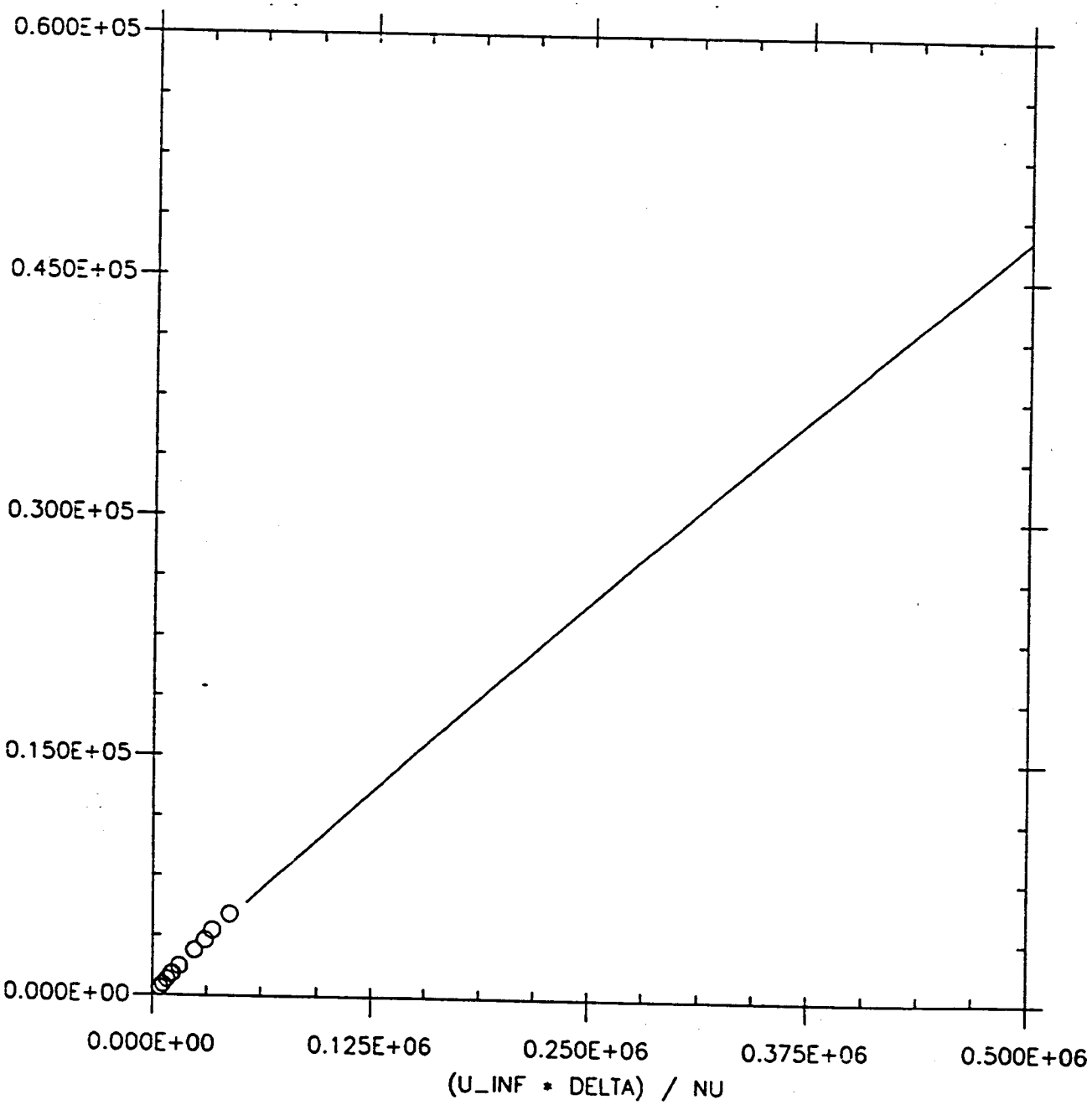

Fig. 4.2.2.3 *Momentum thickness:*

Wieghardt and Tillmann

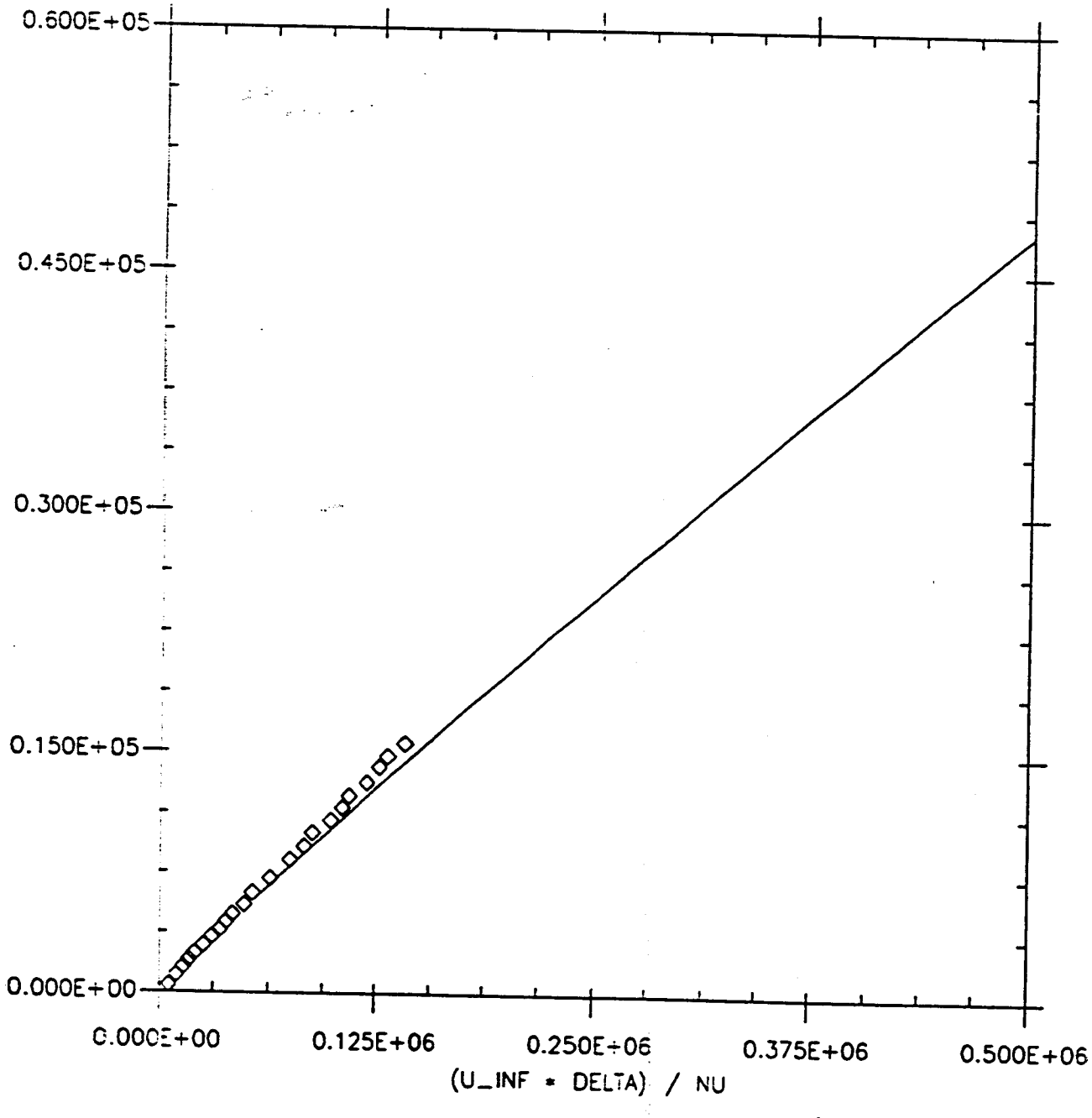

Fig. 4.2.3.1.1 *Shape factor*:

Smith and Walker. x = 15.75 in, 27.75 in, 39.75 in, 51.75 in.

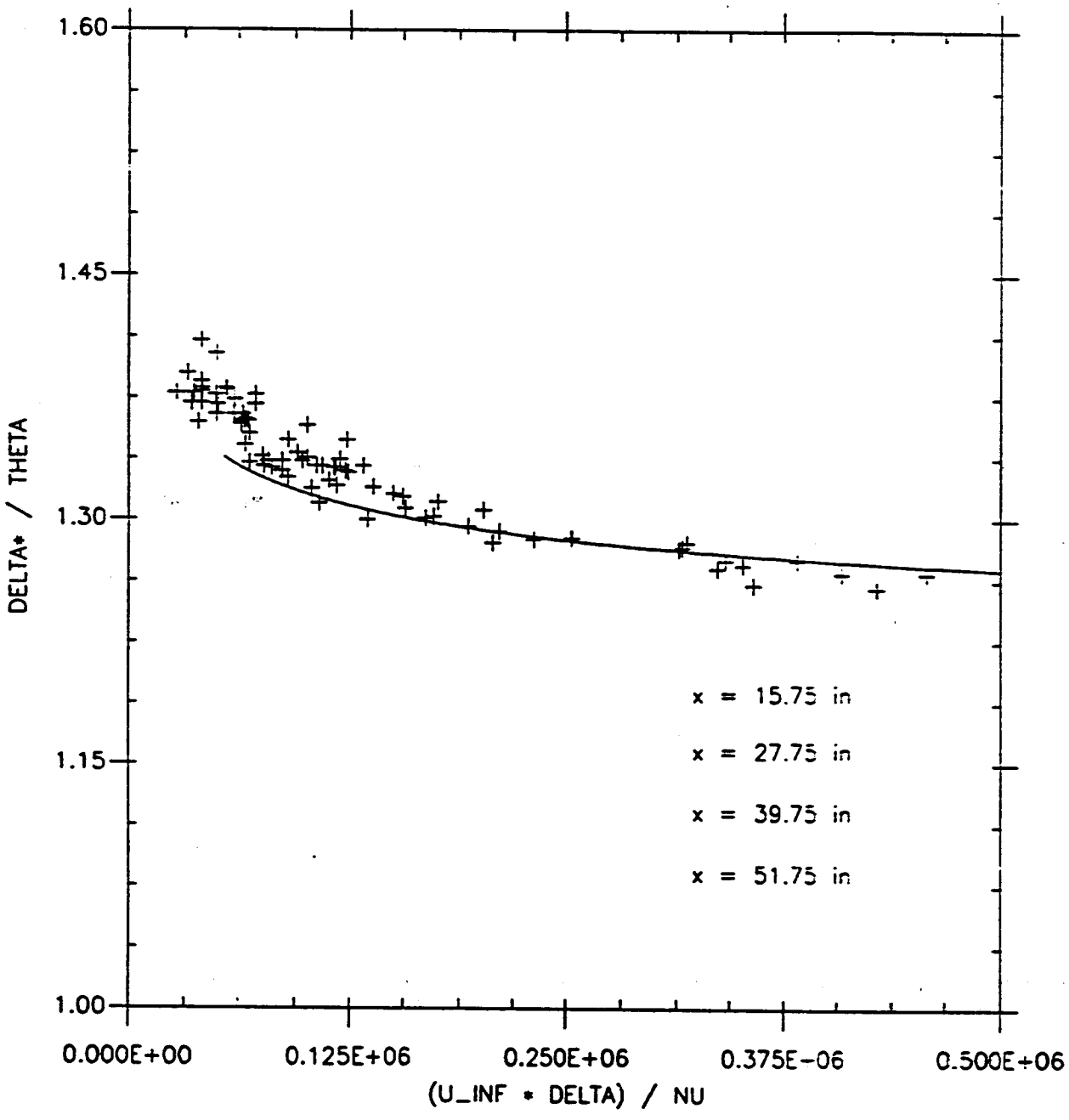

Fig. 4.2.3.2 *Shape factor*:

Purtell et al.

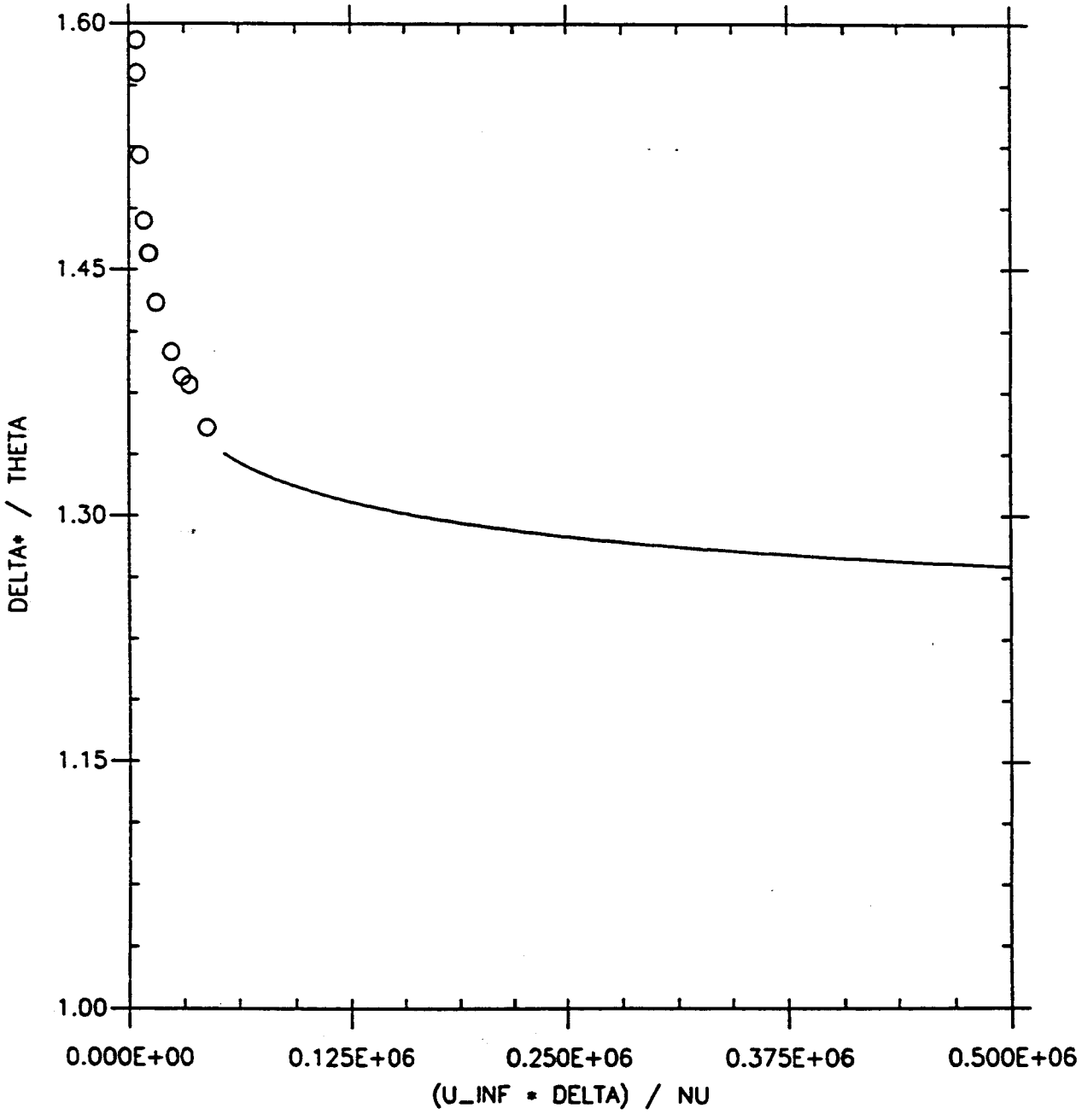

Fig. 4.2.3.3 *Shape factor*:

Wieghardt and Tillmann.

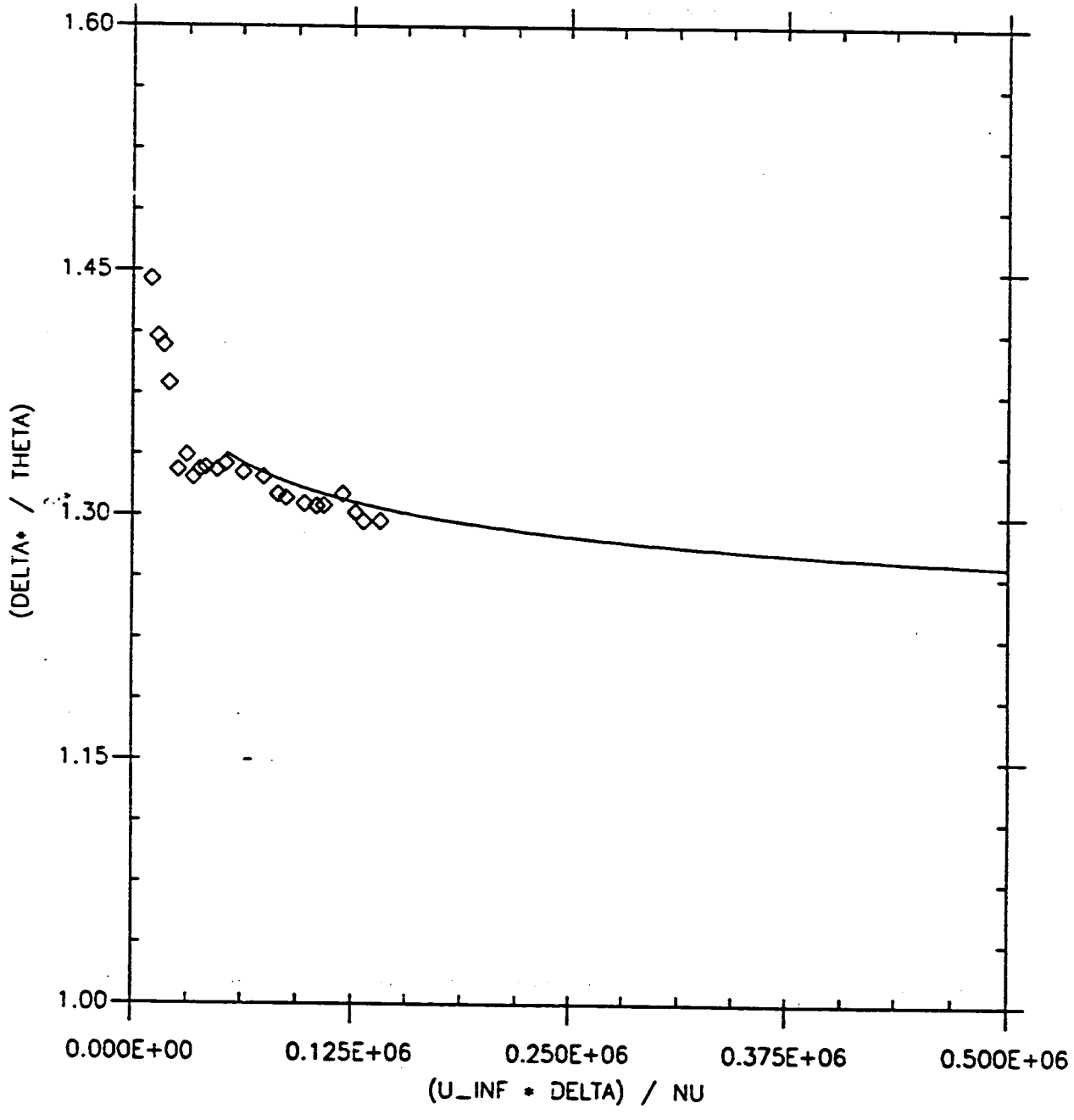

Fig. 4.2.3.2 *Shape factor:*

Purtell et al.

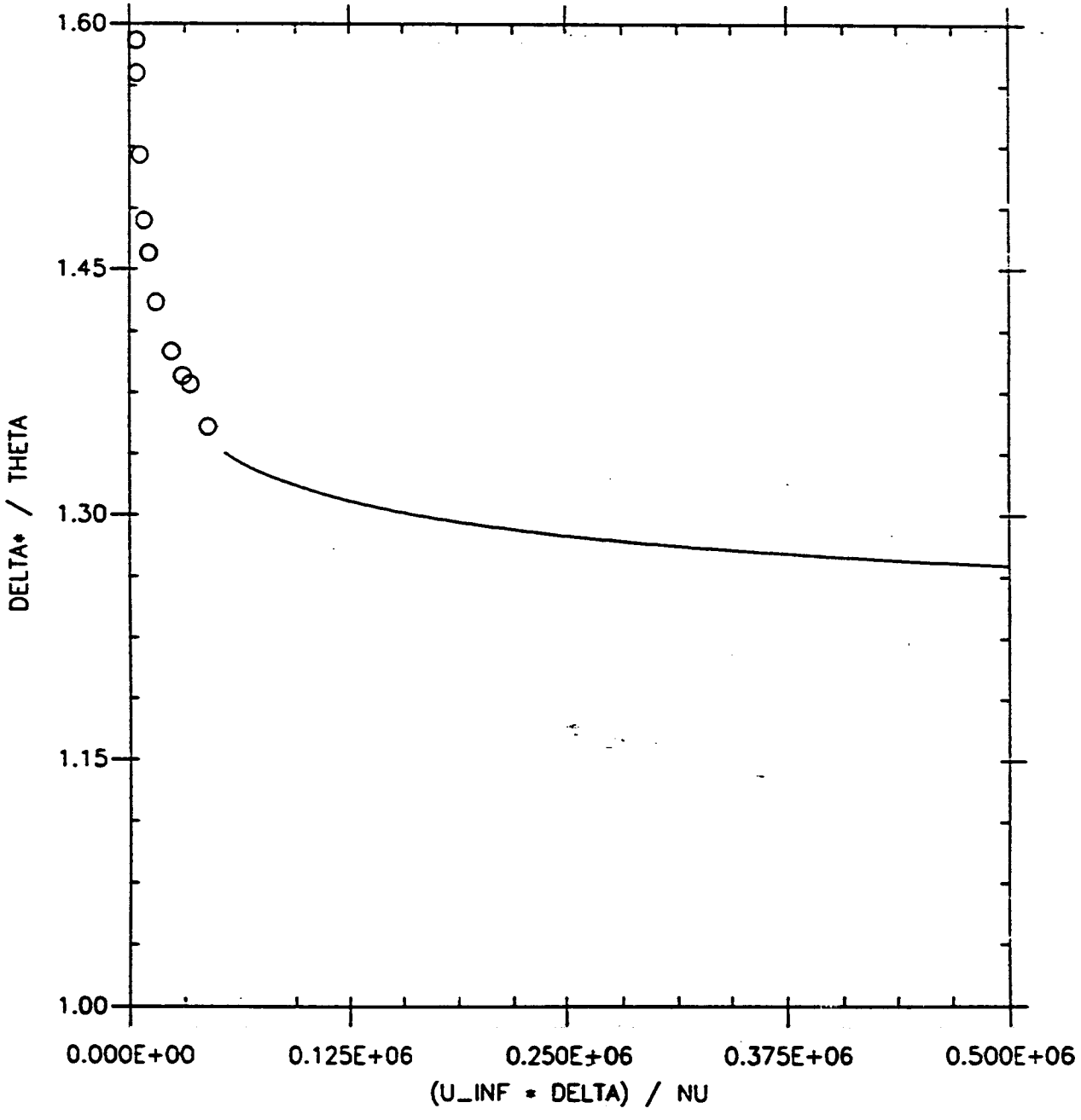

Fig. 4.2.4.2 *Friction coefficient in local variable:*

Purtell et al.

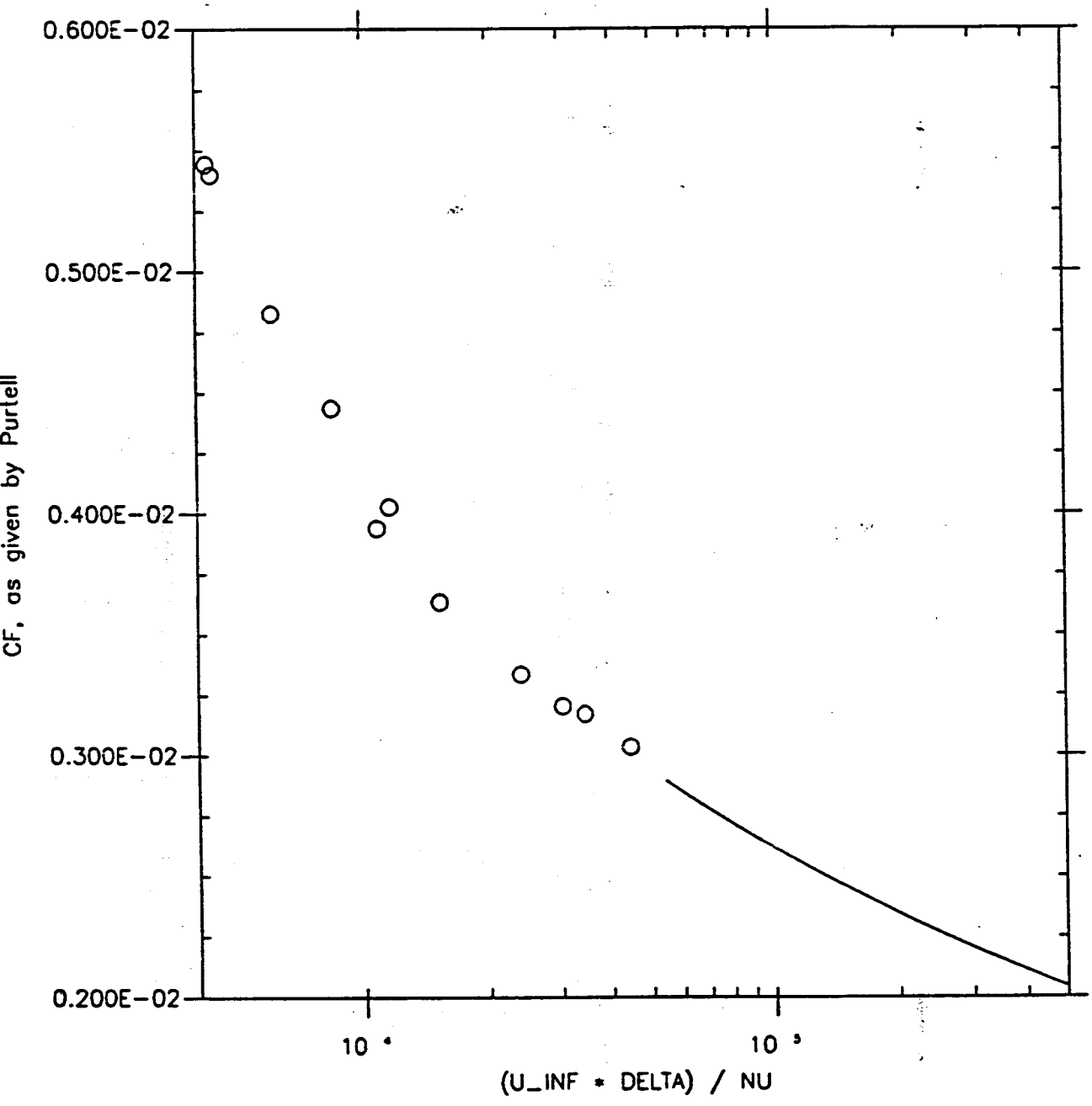

Fig. 4.2.4.4 *Friction coefficient in local variable:*

Schultz and Grunow.

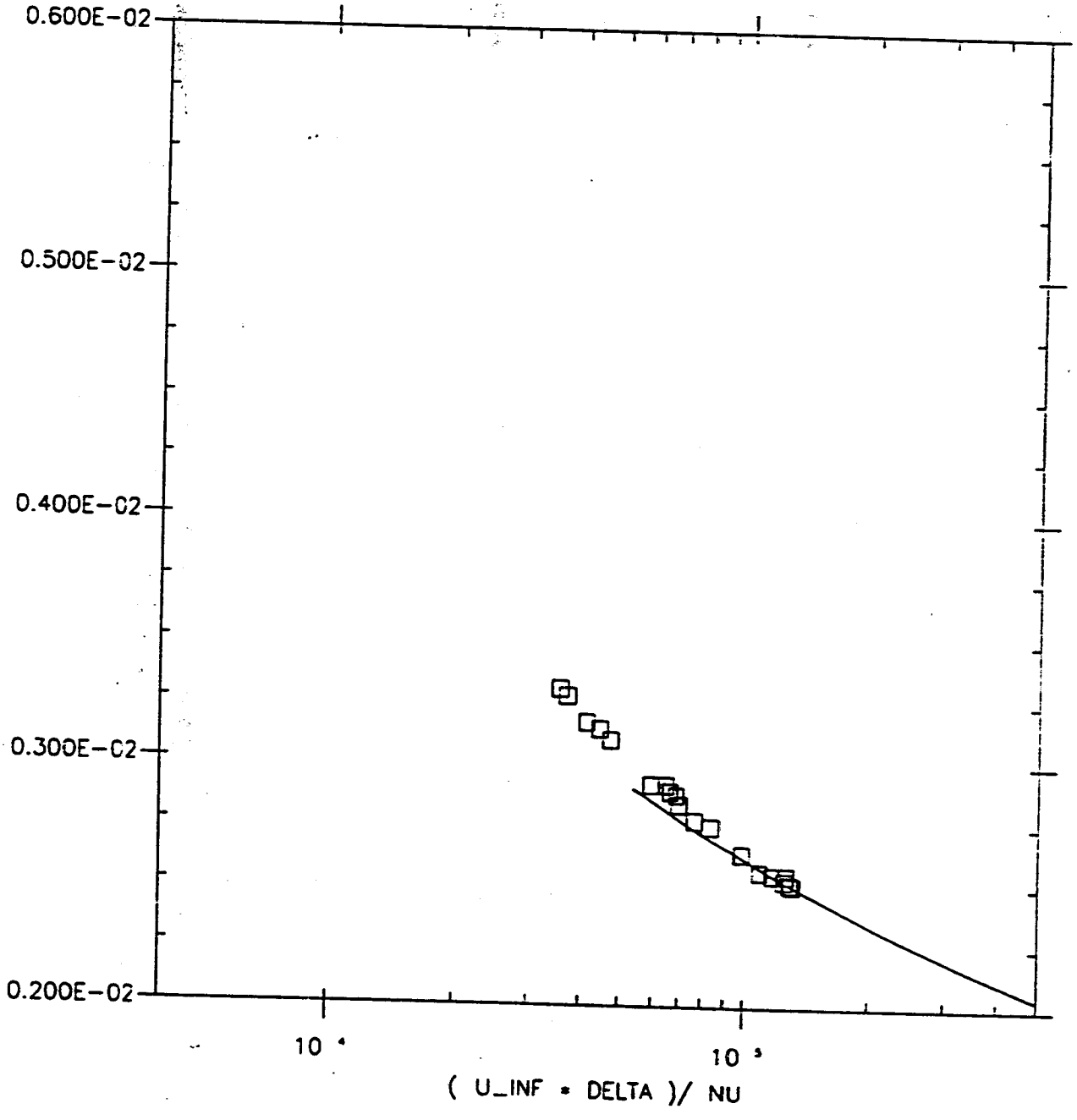

Verification of the power law results, with the full expressions derived for the boundary layer parameters, x-dependence and friction coefficient:

Fig. 4.3.1.1.1 *Displacement thickness:*

Smith and Walker. x = 15.75 in, 27.75 in, 39.75 in, 51.75 in.

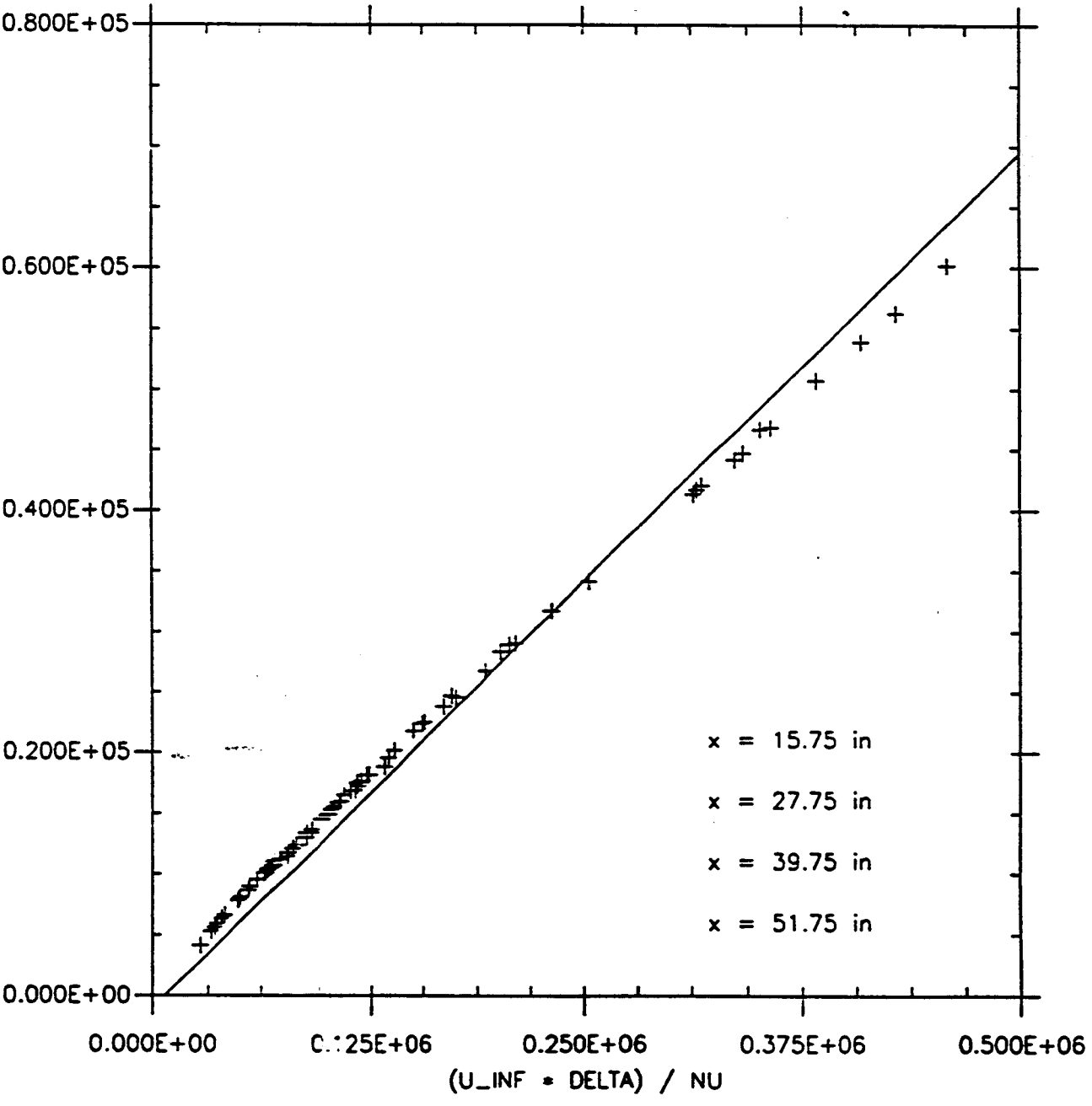

Fig. 4.3.2.1.1 *Momentum thickness:*

Smith and Walker. x = 15.75 in, 27.75 in, 39.75 in, 51.75 in.

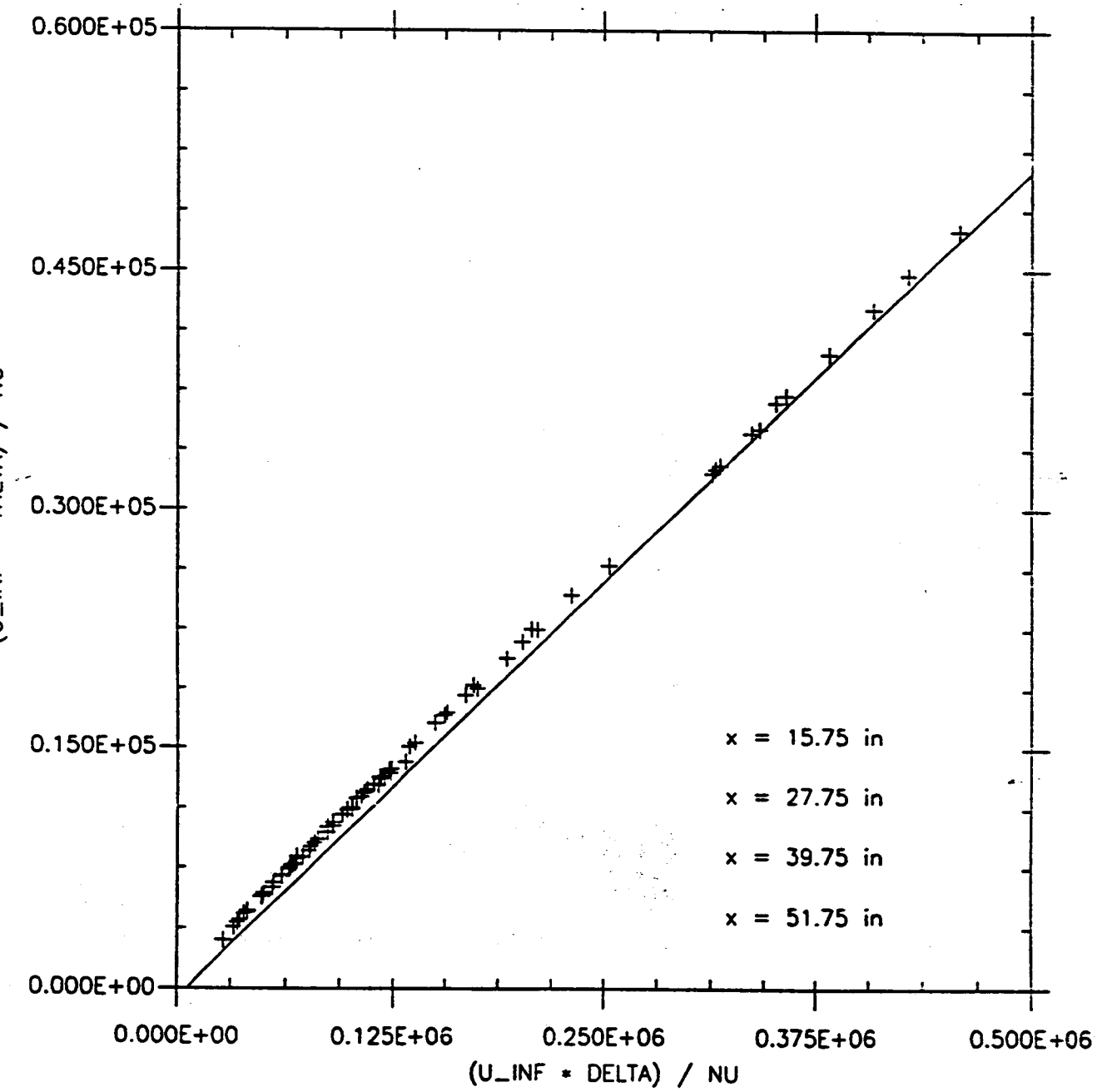

Fig. 4.3.3.1.1 *Shape factor*:

Smith and Walker. x = 15.75 in, 27.75 in, 39.75 in, 51.75 in.

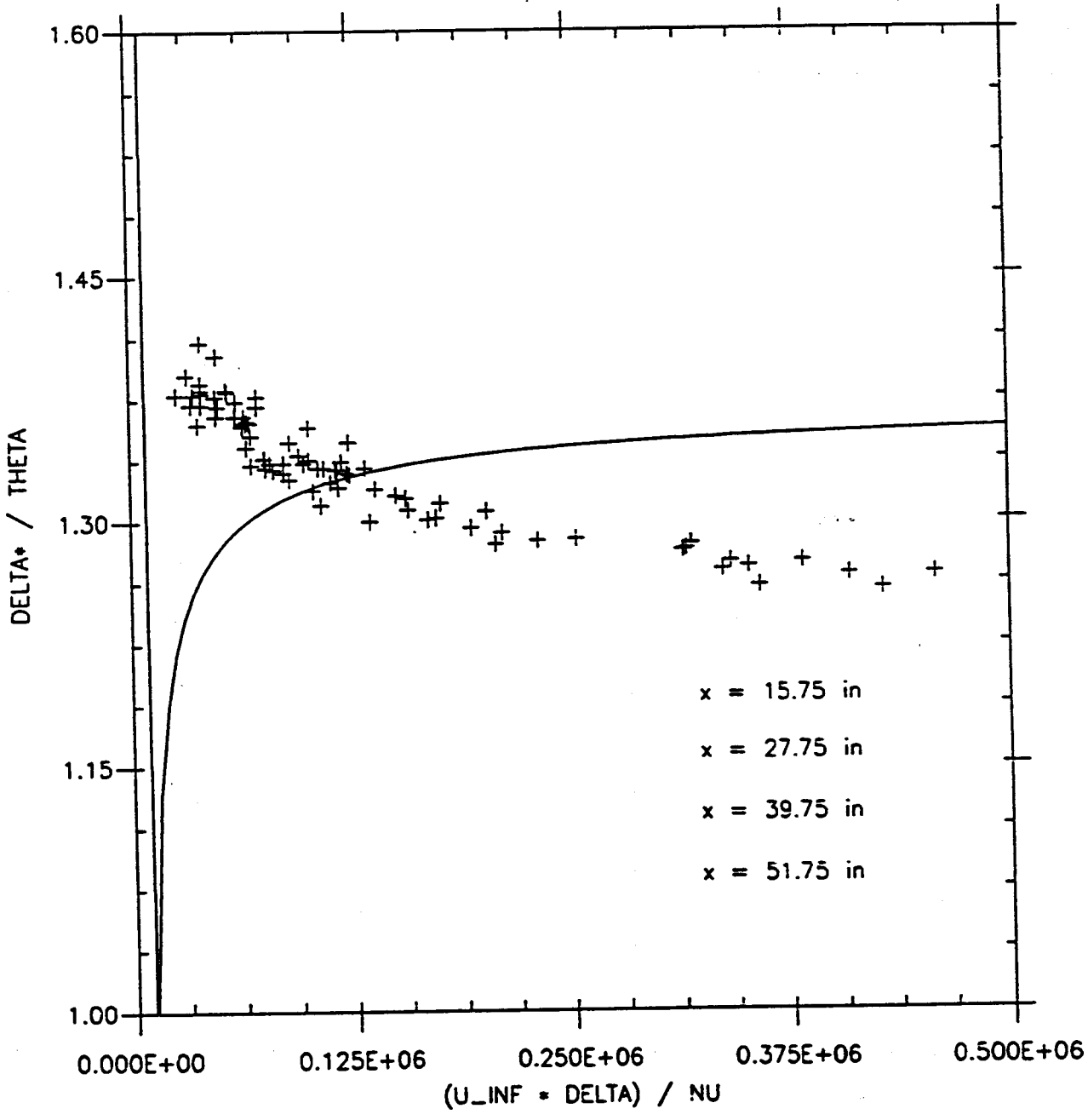

Fig. 4.3.4.1.1 *Friction coefficient in local variable*:
Smith and Walker. x = 15.75 in, 27.75 in, 39.75 in, 51.75 in.

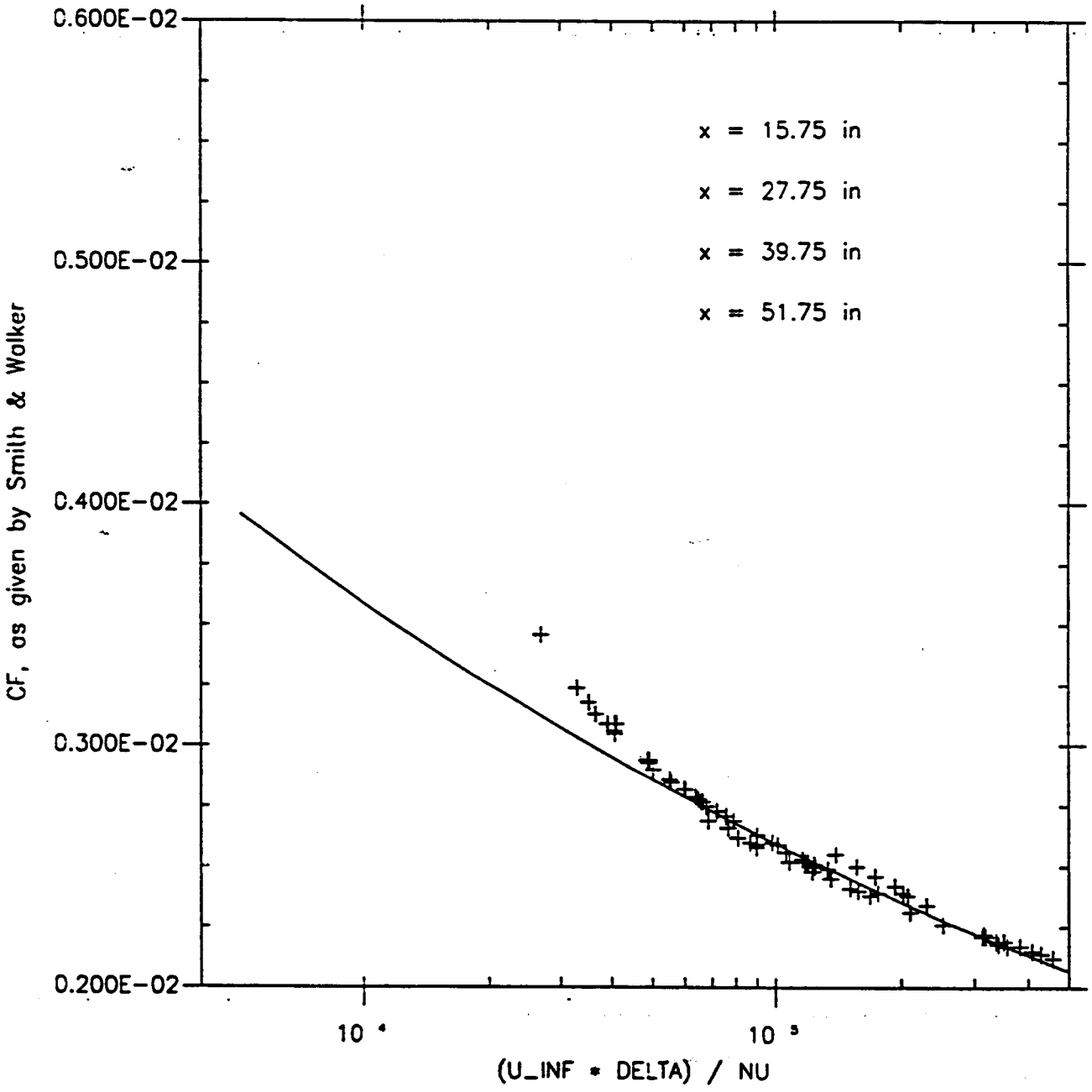

Fig. 4.3.5.1.1 *X dependence*:

Smith and Walker.

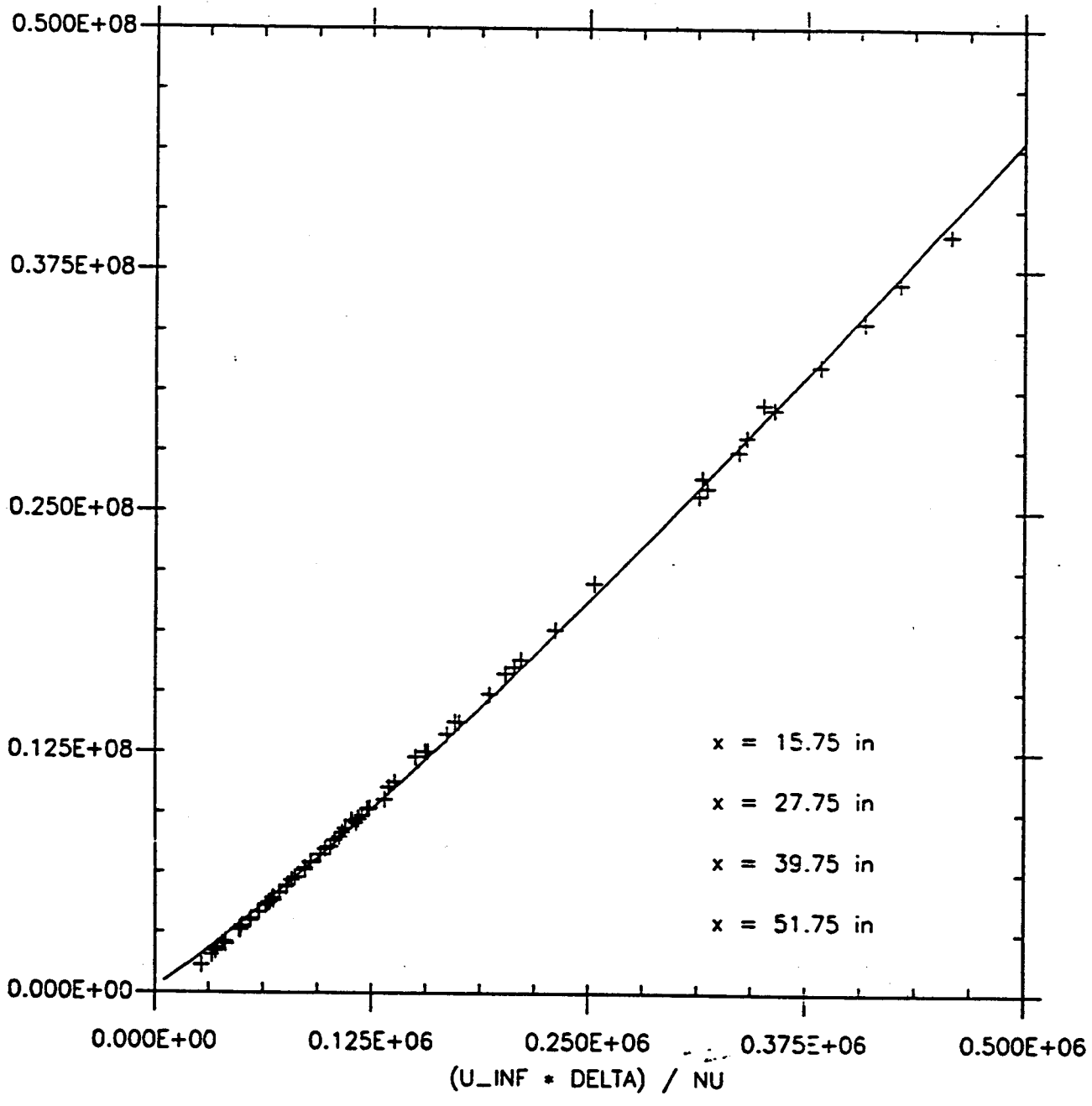

Fig. 4.3.6.1.1 *Friction coefficient as a function of x:*
Smith and Walker (53 points).

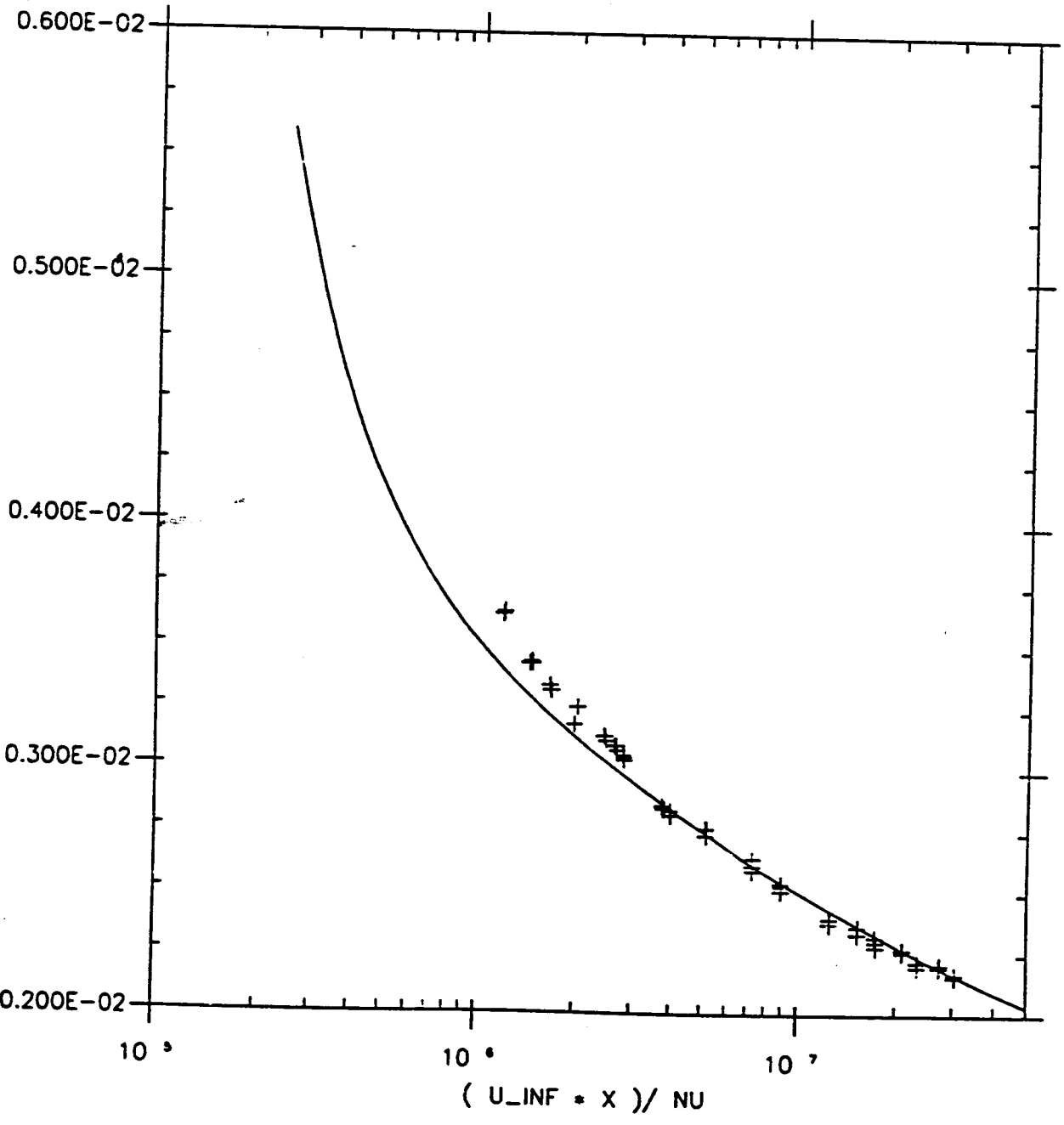

Verification of the power law, with only the linear term

Fig. 4.4.1.1.1 *Displacement thickness*:

Smith and Walker. x = 15.75 in, 27.75 in, 39.75 in. 51.75 in.

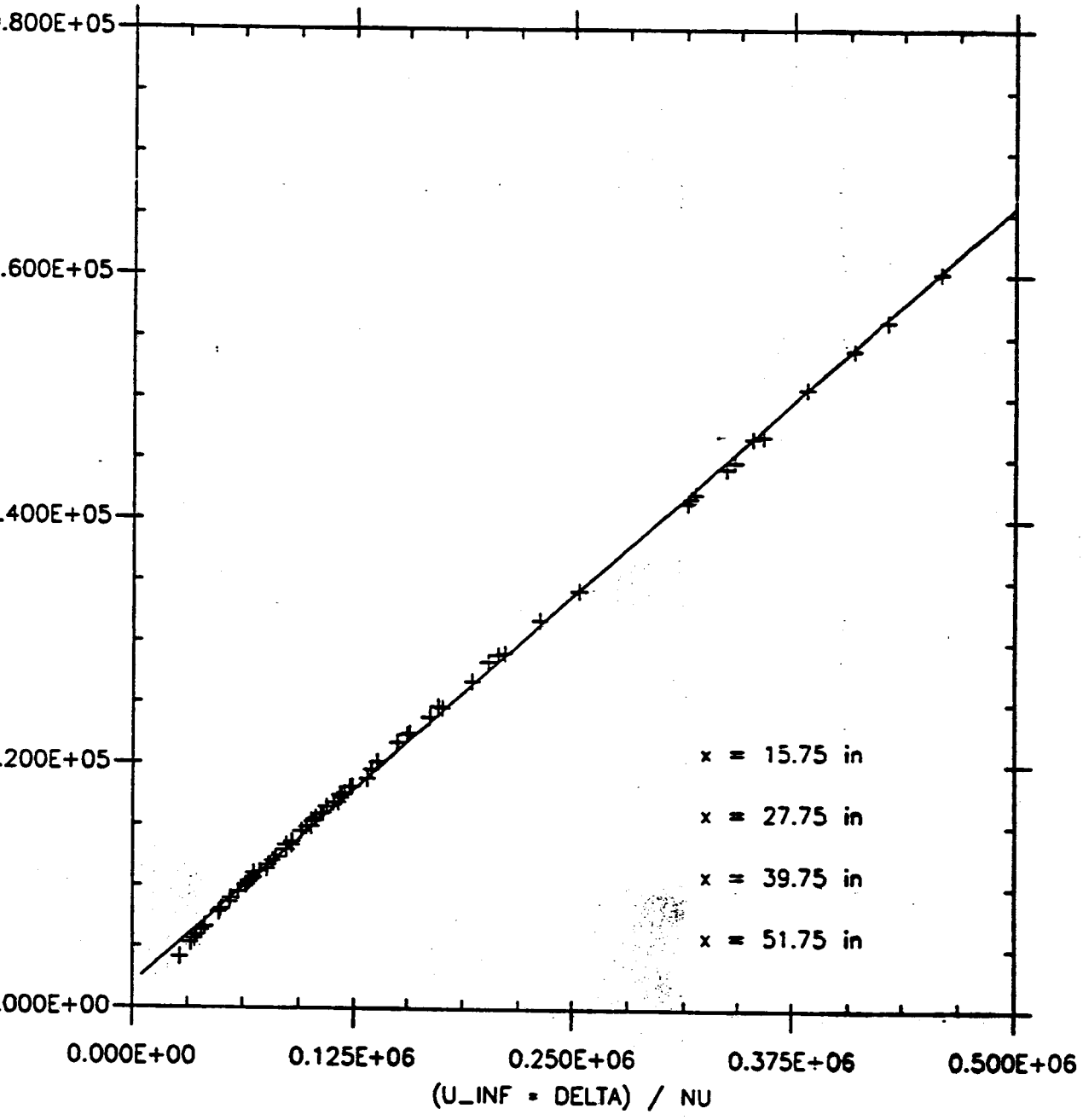

Fig. 4.4.1.2 *Displacement thickness*:

Purtell et al.

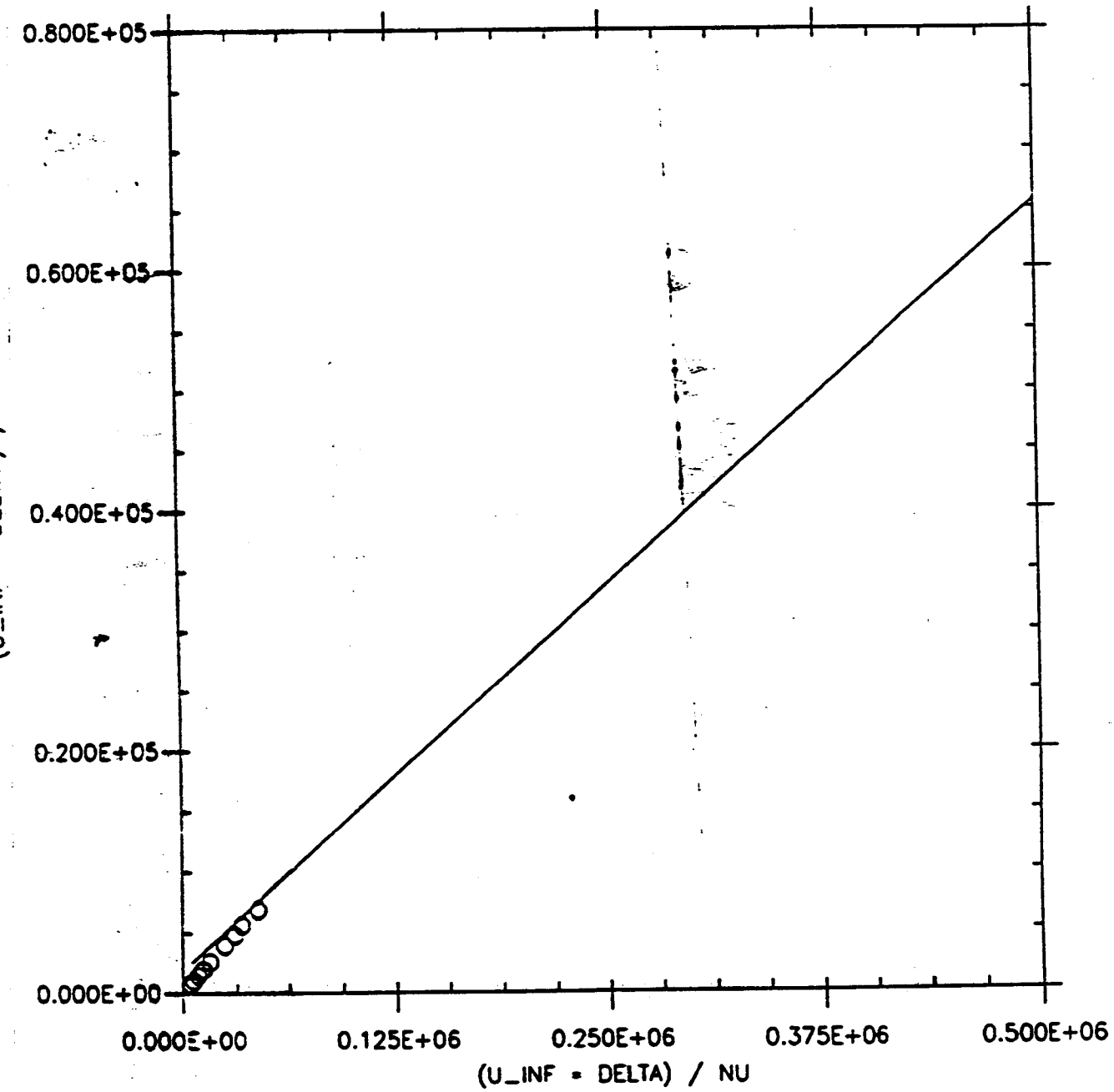

Fig. 4.4.1.3 *Displacement thickness*:

Wieghardt and Tillmann.

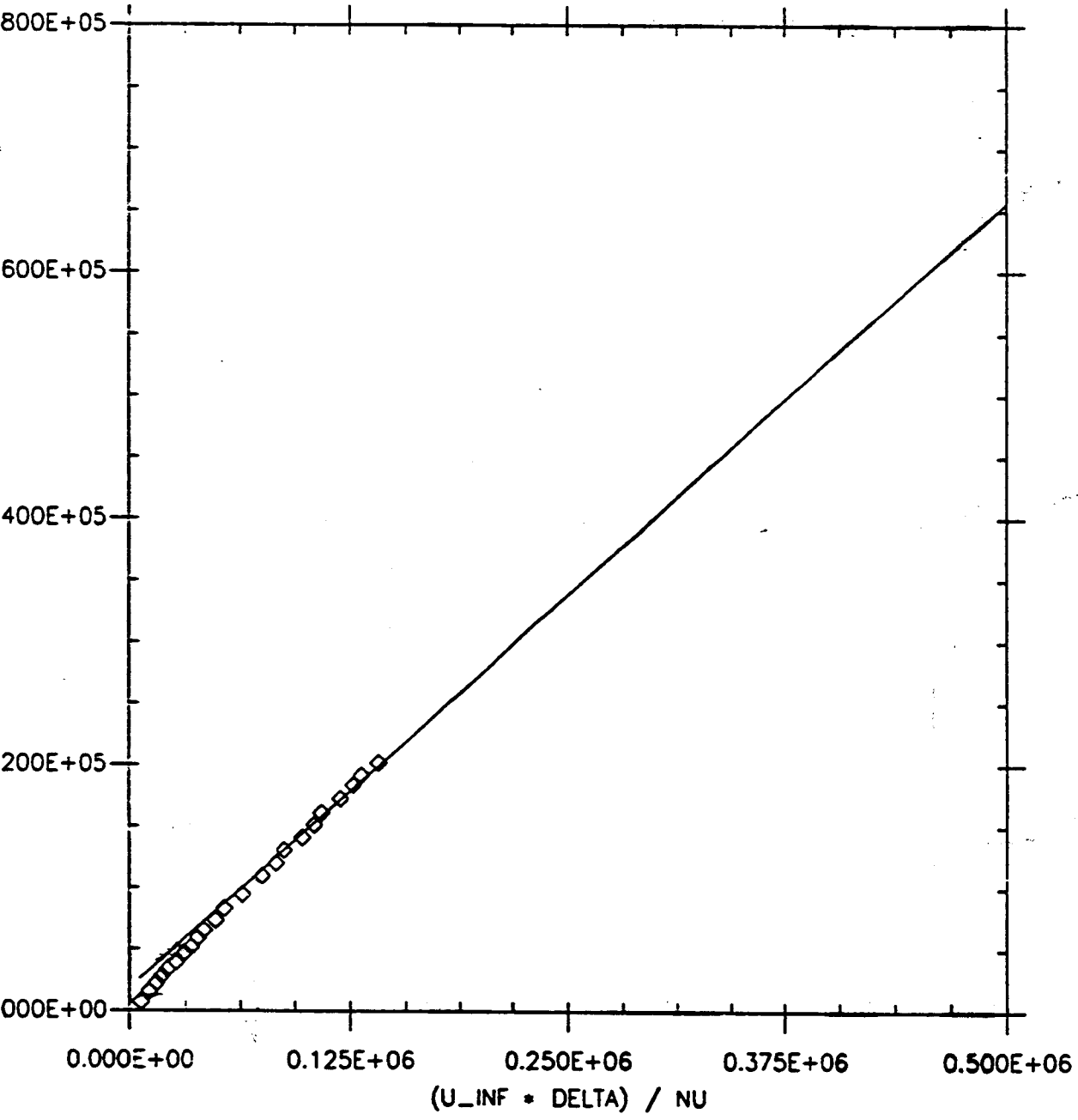

Fig. 4.4.2.1.1 *Momentum thickness*:

Smith and Walker. x = 15.75 in, 27.75 in, 39.75 in, 51.75 in.

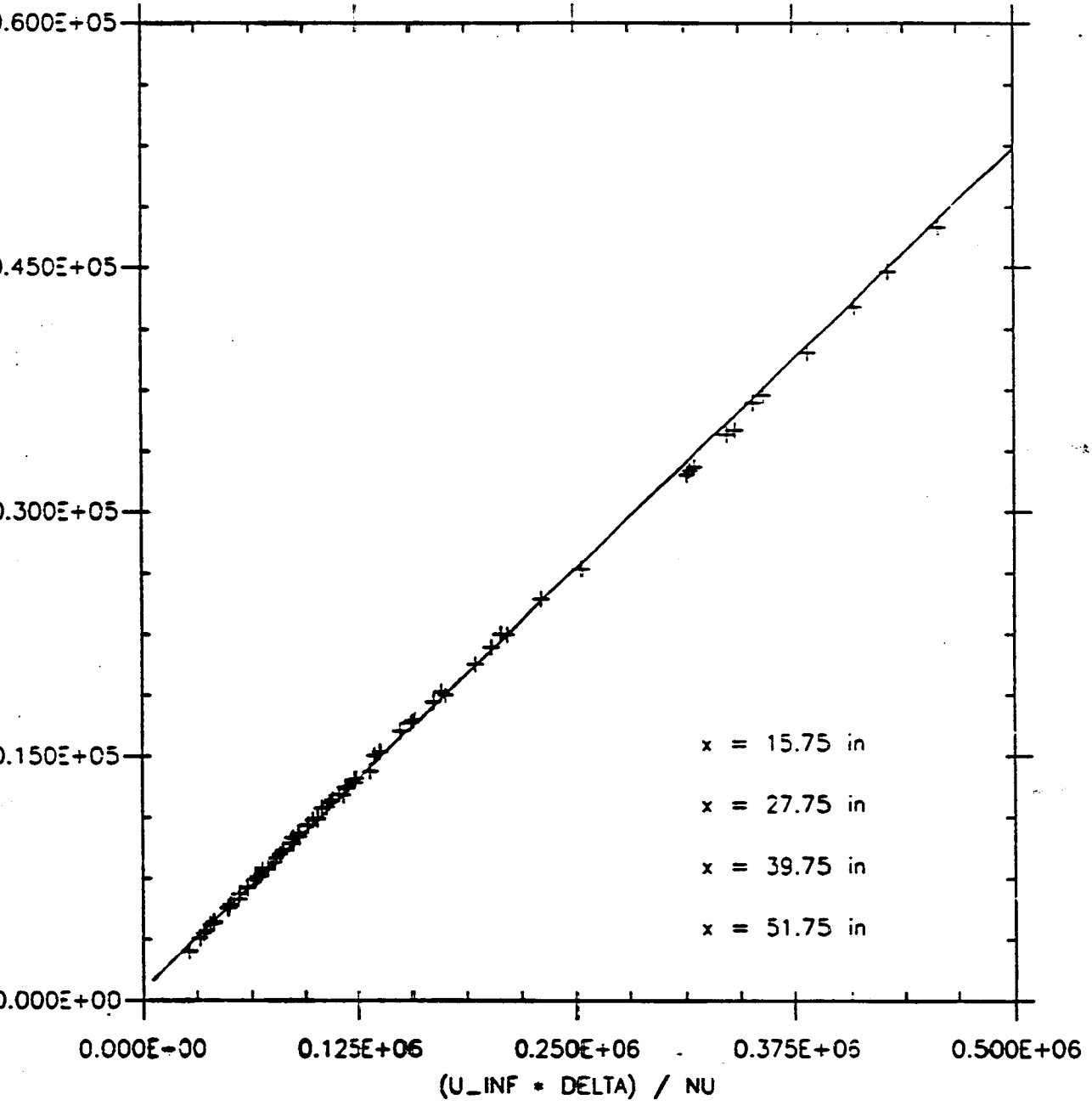

Fig. 4.4.2.2 *Momentum thickness:*

Purtell et al.

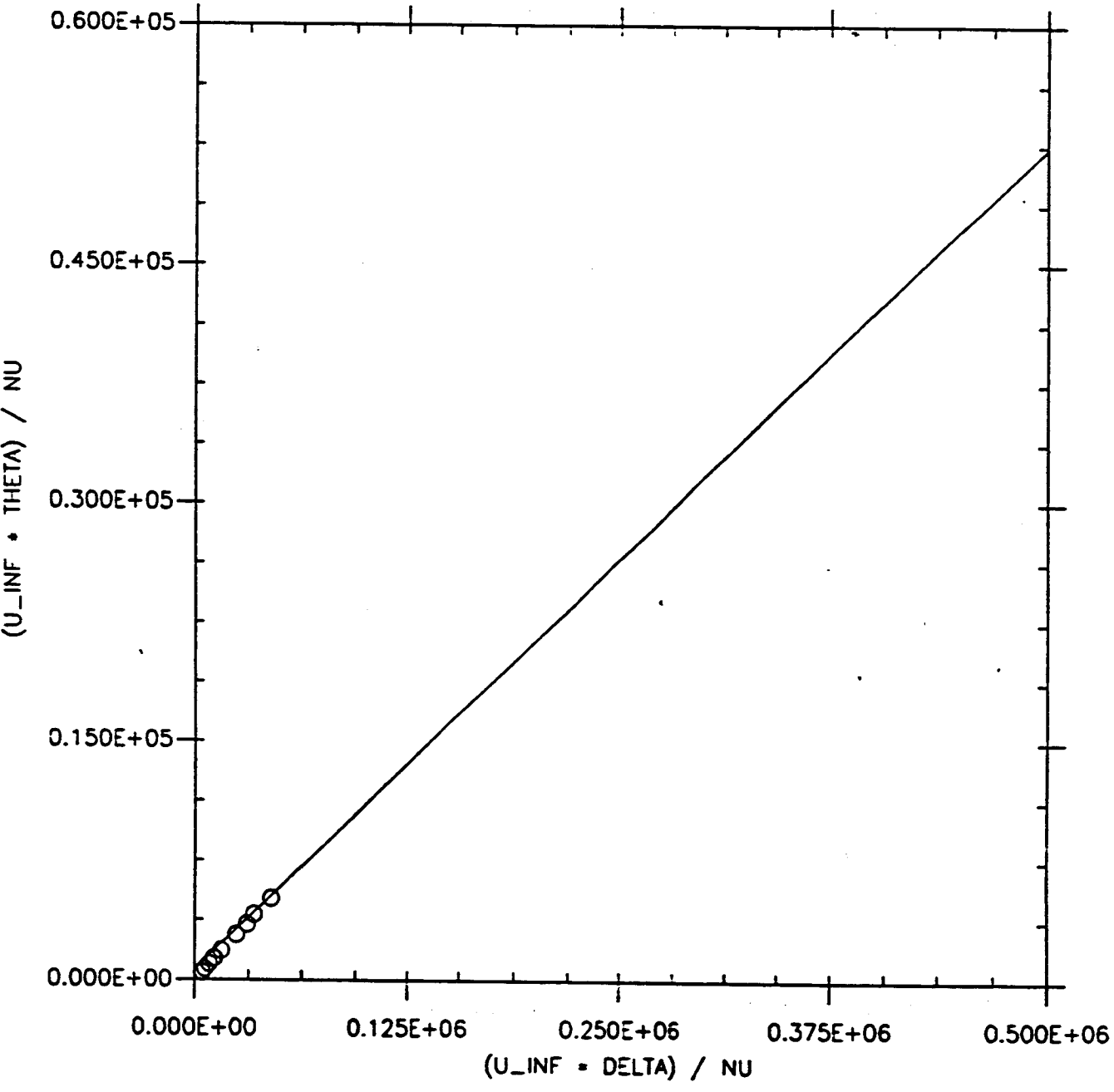

Fig. 4.4.2.3 *Momentum thickness:*

Wieghardt and Tillmann.

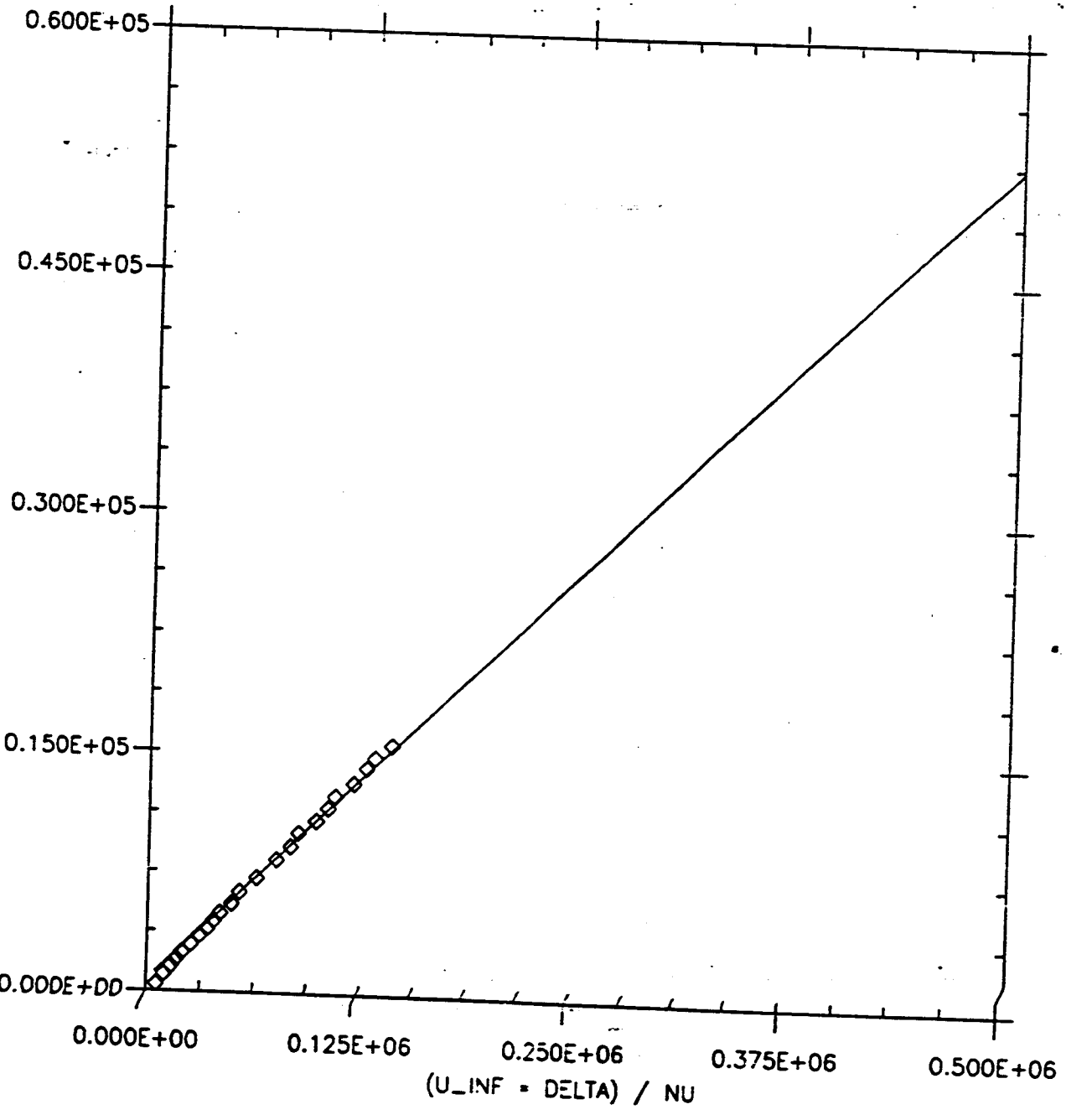

Fig. 4.4.3.1.1 *Shape factor:*

Smith and Walker. x = 15.75 in, 27.75 in, 39.75 in, 51.75 in.

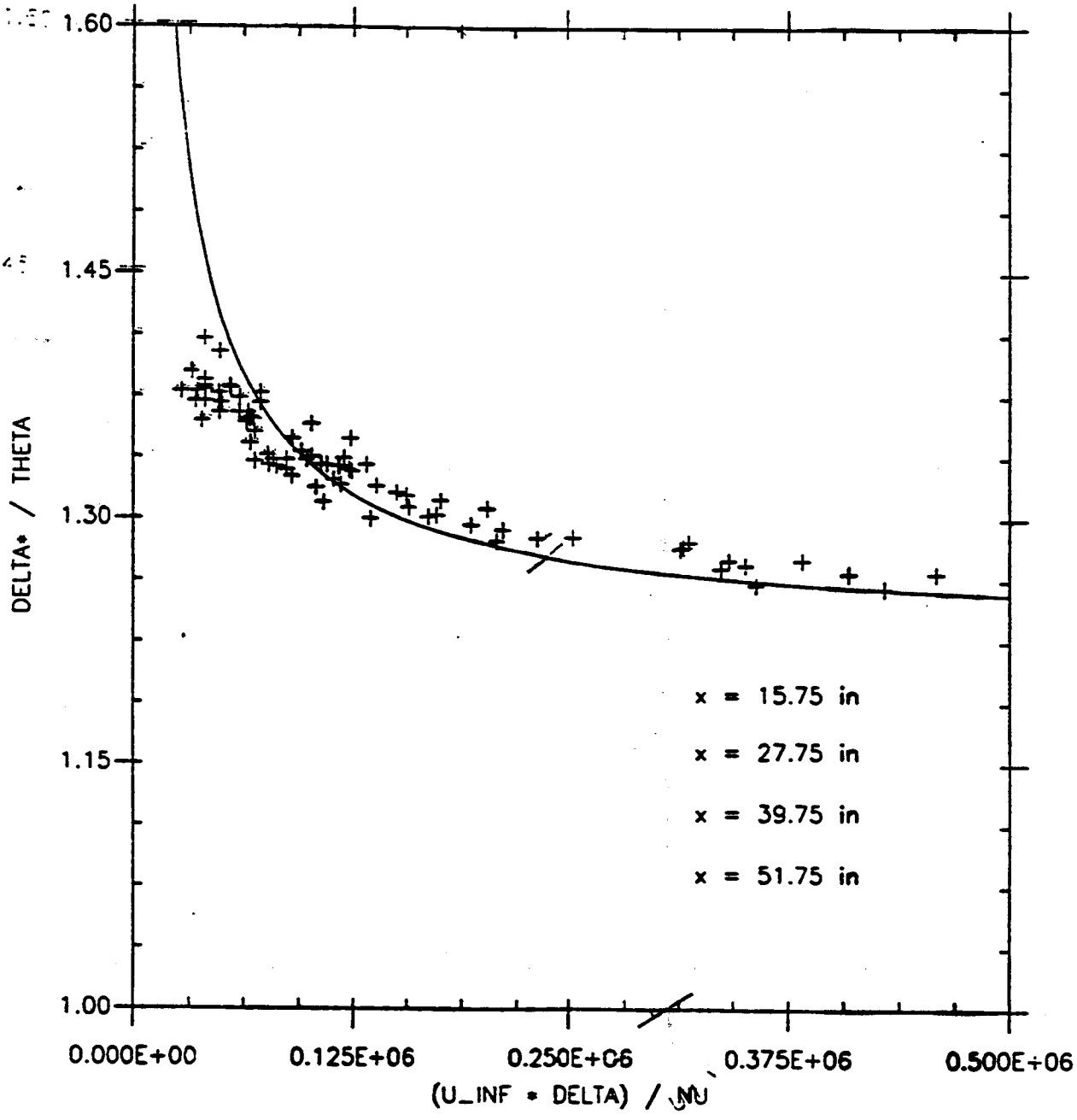

Fig. 4.4.3.2 *Shape factor*:

Purtell et al.

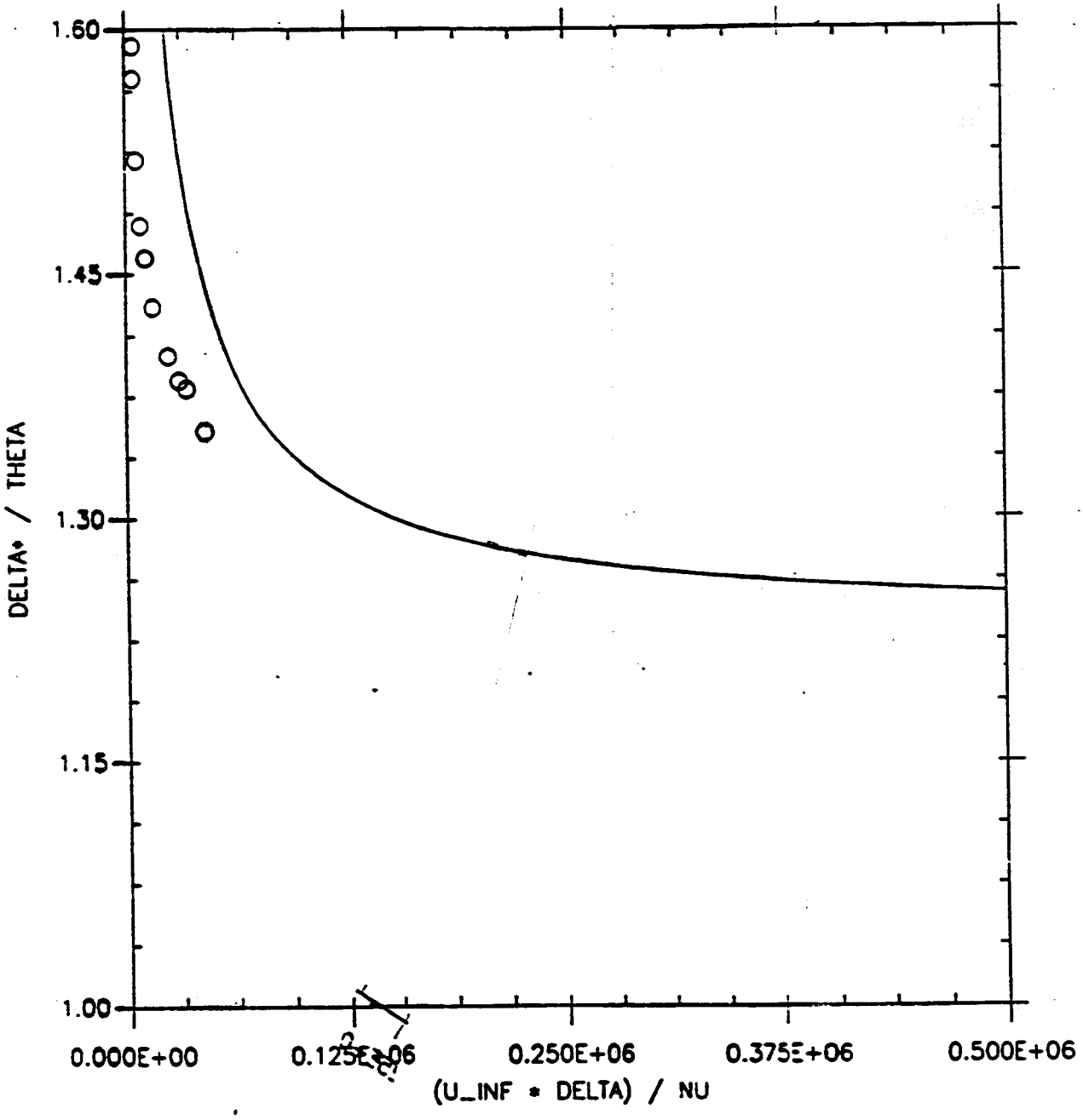

Fig. 4.4.3.3 *Shape factor*:

Wieghardt and Tillmann.

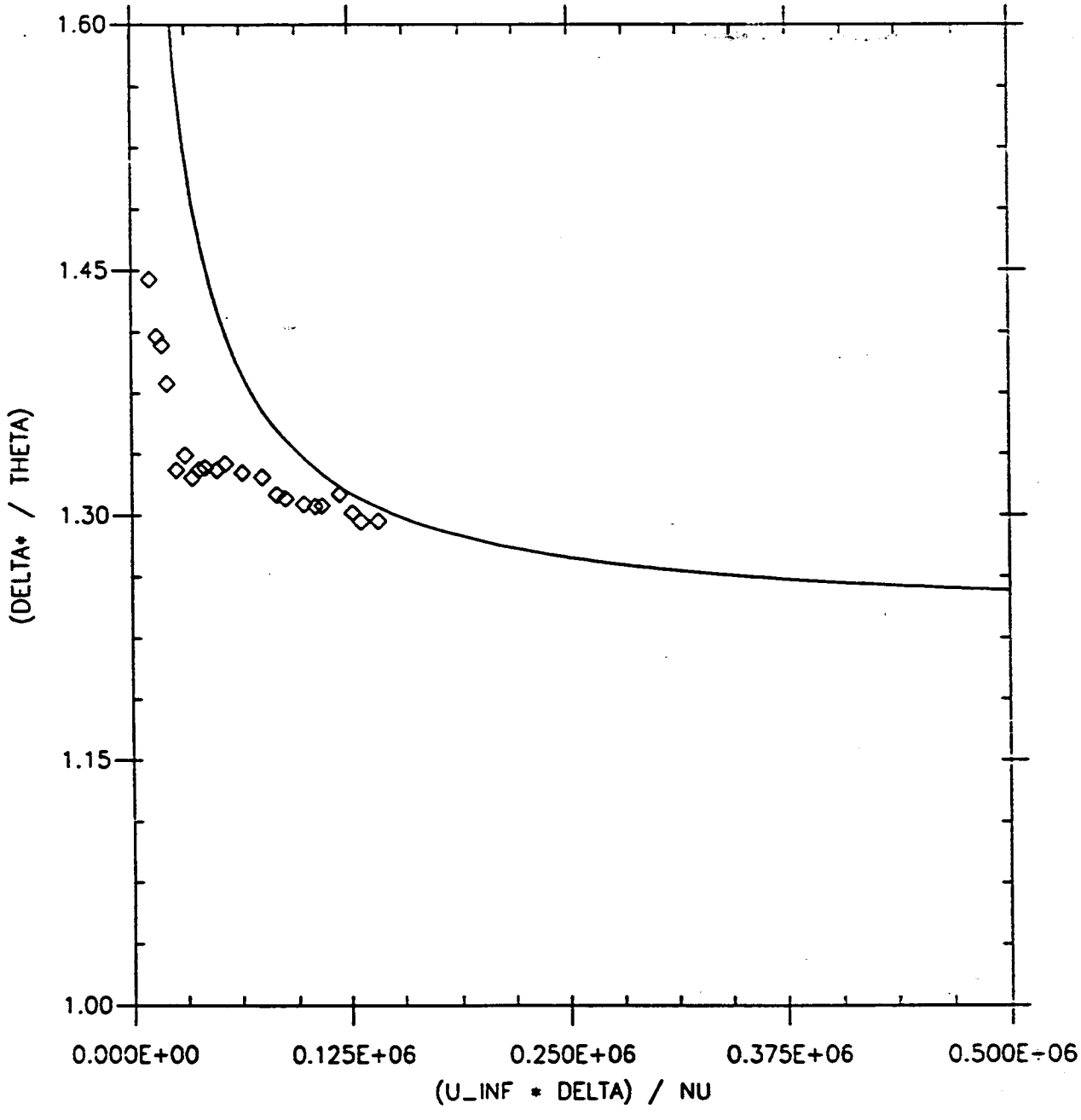

Fig. 4.4.4.1.1 *Friction coefficient in local variable*:
Smith and Walker. x = 15.75 in, 27.75 in, 39.75 in, 51.75 in.

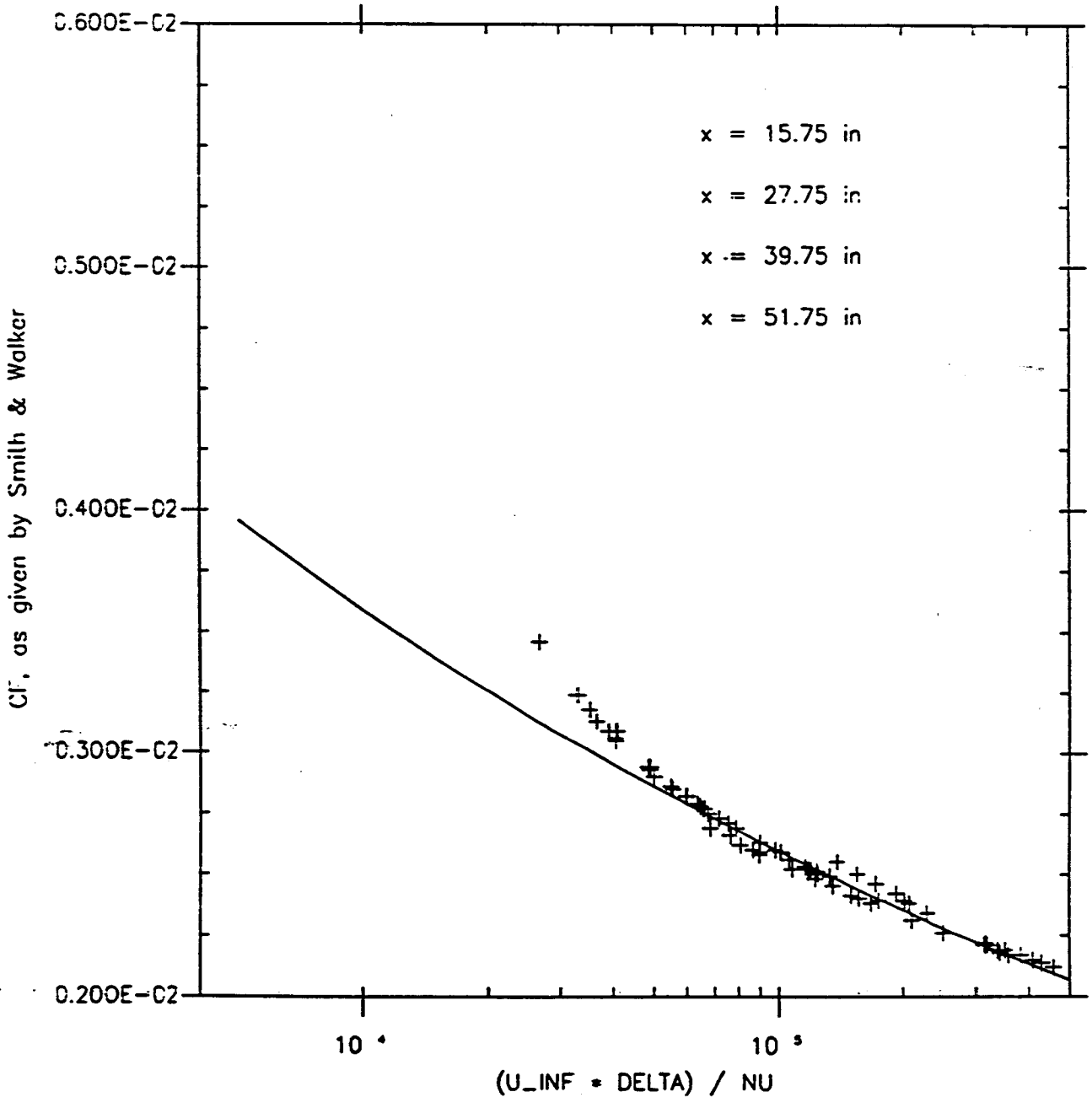

Fig. 4.4.4.2 *Friction coefficient in local variable:*

Purtell et al.

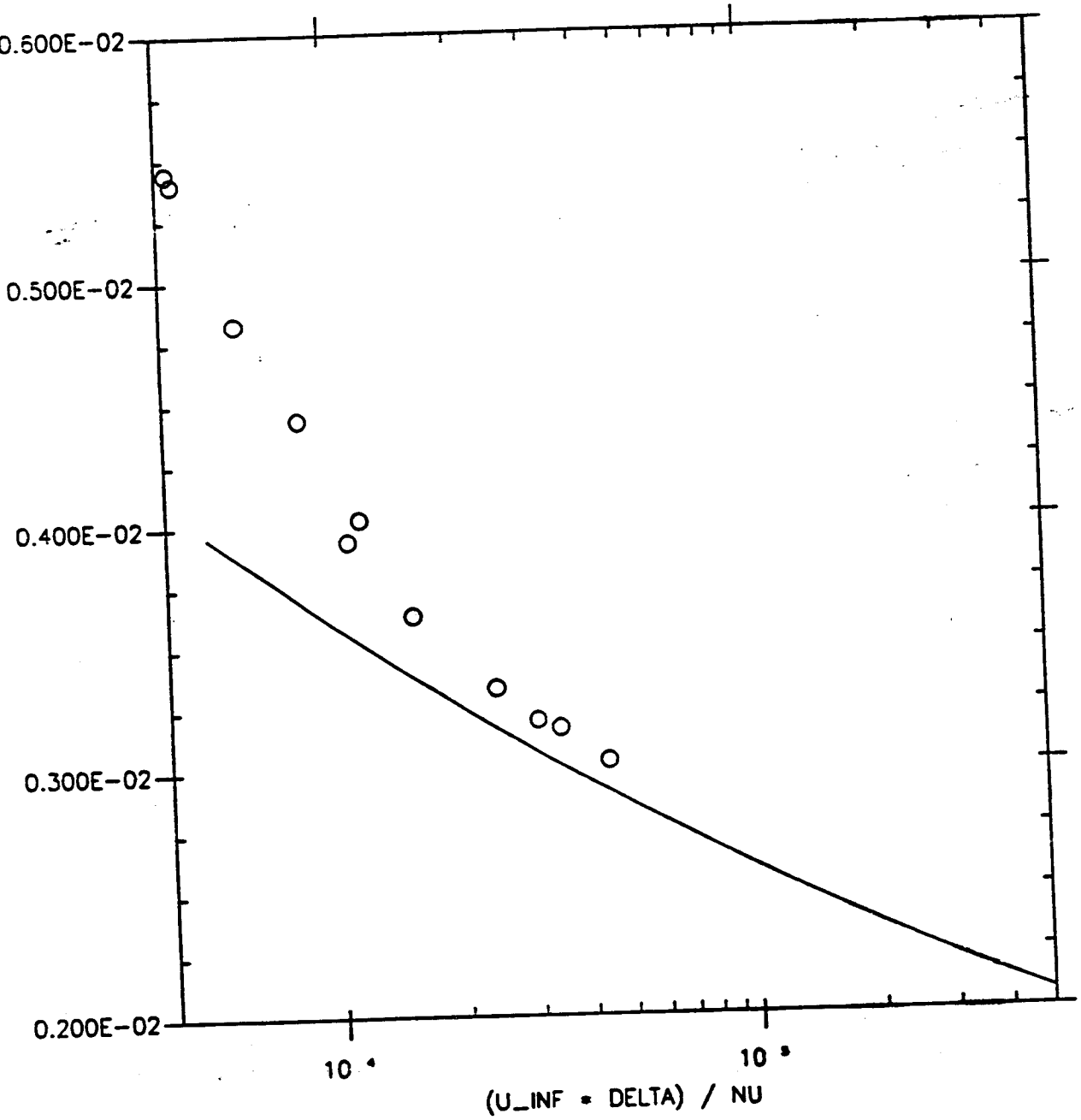

Fig. 4.4.4.4 *Friction coefficient in local variable:*
Schultz and Grunow.

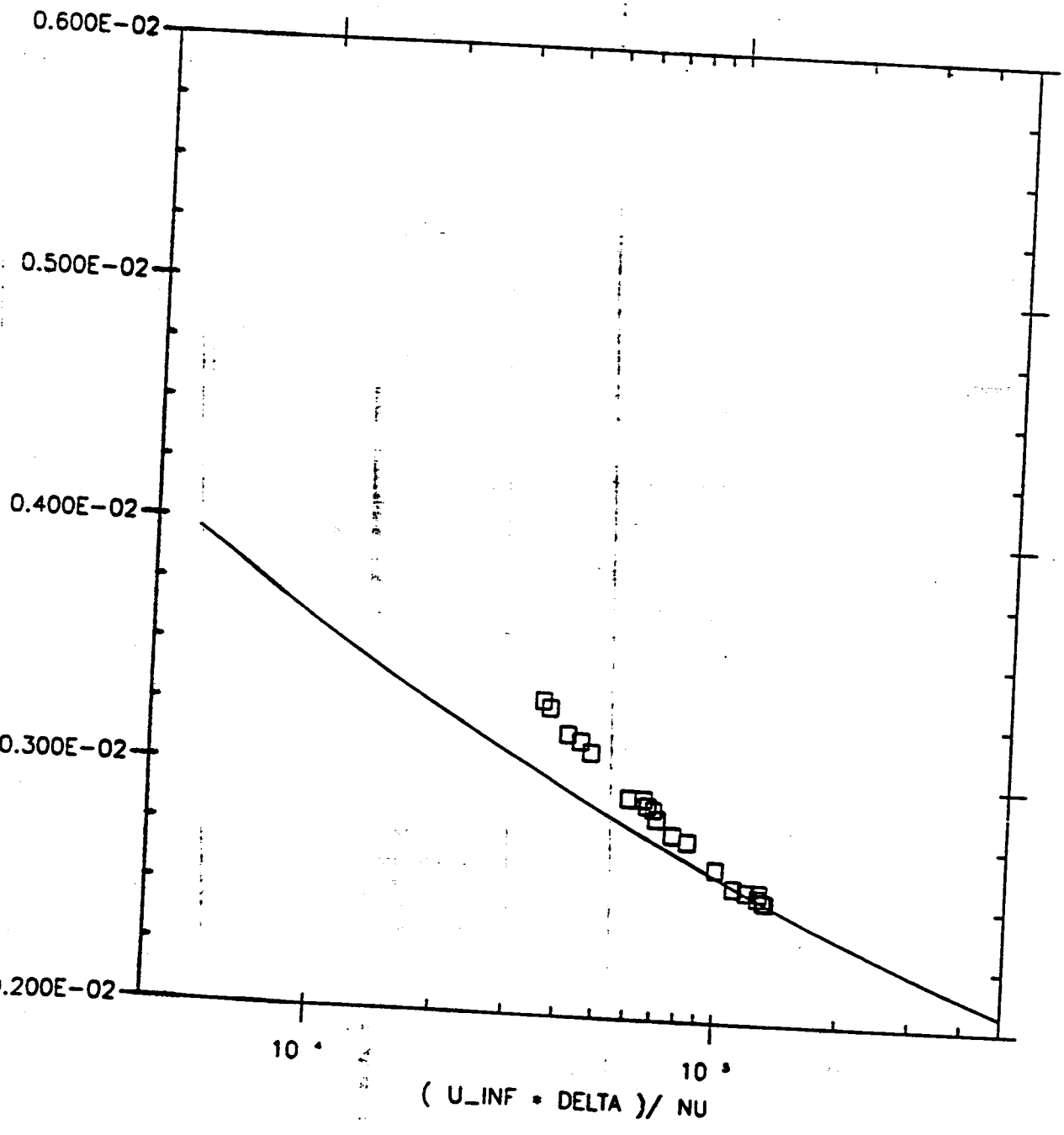

Fig. 4.4.5.1.1 *X dependence:*

Smith and Walker.

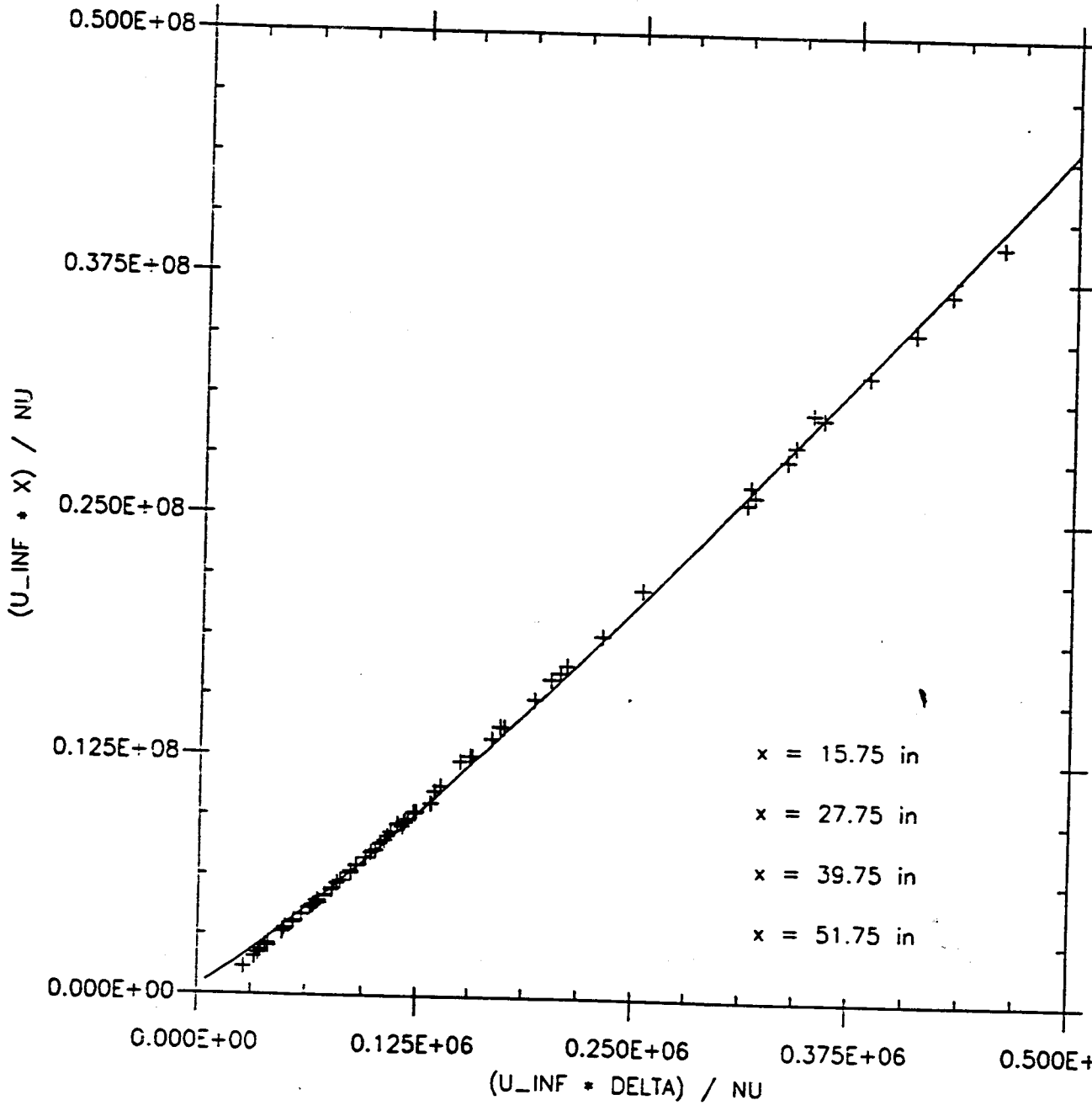

Fig. 4.4.6.1.1 *Friction coefficient as a function of x*:
Smith and Walker (53 points).